NSF/CEE-82032

PB83-101014

A STUDY OF POWER SPECTRAL DENSITY OF EARTHQUAKE ACCELEROGRAMS

by

PARVIZ MOAYYAD

and

BIJAN MOHRAZ

A Report on a Research Project

Sponsored by the

NATIONAL SCIENCE FOUNDATION

Research Grant No. PFR 8004824

CIVIL AND MECHANICAL ENGINEERING DEPARTMENT

SCHOOL OF ENGINEERING AND APPLIED SCIENCE

SOUTHERN METHODIST UNIVERSITY

DALLAS, TEXAS 75275

June 1982

INFORMATION RESOURCES
NATIONAL SCIENCE FOUNDATION

A STUDY OF POWER SPECTRAL DENSITY OF EARTHQUAKE ACCELEROGRAMS

by

PARVIZ MOAYYAD

and

BIJAN MOHRAZ

A Report on a Research Project
Sponsored by the

NATIONAL SCIENCE FOUNDATION
Research Grant No. PFR 8004824

CIVIL AND MECHANICAL ENGINEERING DEPARTMENT

School of Engineering and Applied Science
Southern Methodist University
Dallas, Texas 75275

June 1982

ACKNOWLEDGMENTS

This report is based on a doctoral dissertation by Mr. Parviz Moayyad and was submitted to the faculty of the School of Engineering and Applied Science of Southern Methodist University in partial fulfillment of the requirements for the degree of Doctor of Philosophy in Engineering Mechanics. The dissertation was prepared under the direction of Dr. Bijan Mohraz, Professor of Civil Engineering.

The authors wish to thank Dr. Henry L. Gray, C.F. Frensley Professor of Mathematical Science, whose guidance in the early part of this study played an important role in solidifying the direction of this investigation.

The study was supported by the National Science Foundation through Grant PFR 8004824. The opinions, findings, and conclusions or recommendations expressed here are those of the authors and do not necessarily reflect the views of the National Science Foundation.

The numerical results were obtained using the CDC 6600 of the SMU Computer Center.

The authors acknowledge Mrs. Sally Hackett for her diligent work in preparation of drafts and the final manuscript.

ABSTRACT

An examination of recorded earthquake accelerograms indicates their nonstationary characteristics, that is, their statistical properties, vary with time. The nonstationary characteristic takes a special form when the strong motion part of the record is considered. It is demonstrated in this study that within the strong motion duration the short time mean square value varies with time, whereas the frequency structure of the record remains time-invarient. This conclusion leads to the assumption that the strong motion segments of accelerograms can be considered to form a locally stationary random process. The power spectral density of such a process is a function of both time and frequency.

The time-dependent power spectral density for an ensemble of accelerograms is estimated as the product of a normalized power spectral density which is a function of frequency only and describes the frequency structure of the ensemble; a normalized time-dependent scale factor which is obtained from a short time averaging of mean square acceleration; and finally the mean square acceleration itself. The mean square acceleration is obtained from correlations between RMS value and a variable which incorporates four important earthquake parameters: peak ground acceleration, earthquake magnitude, epicentral distance, and duration of strong motion.

Time-dependent power spectral densities and correlations between RMS of the records and the four earthquake parameters are obtained for horizontal and veritical components of accelerograms recorded on soft, intermediate, and hard sites. The findings are used to estimate the power spectral density for a given geology, peak ground acceleration, earthquake magnitude, epicentral distance, and duration of strong motion. The estimates are then used to predict the response of a single degree of freedom system and to compare the results with both the relative displacement, relative velocity and absolute acceleration computed directly from the record and the mean plus one standard deviation response of the ensemble.

TABLE OF CONTENTS

LIST OF FIGURES

LIST OF TABLES

CHAPTER 1

INTRODUCTION

1.1 BACKGROUND

Among the approaches used in the seismic analysis and design of structures and equipments is the response spectrum. The response spectrum introduced by Biot (1941, 1942) and Housner (1941), provides a measure of the maximum response of a single degree of freedom system to an excitation. Subjecting the system to a specific ground motion of a recorded earthquake and computing its maximum response for a given frequency and damping gives a point on the response spectrum curve. For small damping, the relative velocity and absolute acceleration of the system can be estimated from the relative displacement (Housner 1970b, Clough 1970). Such quantities are termed pseudo-velocity and pseudo-acceleration, respectively. For engineering applications the relative displacement, pseudo-velocity, and pseudo-acceleration are plotted as a function of the period or frequency of the system on a tripartite paper (four-way log paper). In seismic analysis such plots are made for a specific recorded ground motion. To obtain a design spectrum, the response spectra from individual records are normalized and averaged at various frequencies or periods. The mean plus one standard deviation response has been generally used as a basis for design spectrum (Blume et al., 1972; Mohraz et al., 1972; Newmark et al., 1973; Mohraz 1976).

After 1971, studies were carried out to correlate the shape and magnitude of response spectra to site geology, earthquake magnitude, duration of strong motion, epicentral distance, and maximum ground acceleration. Seed et al. (1976) and Mohraz (1976) independently studied the influence of site geology on response spectra, and some of their conclusions were incorporated in a joint report by the Applied Technology Council, the National Bureau of Standards and the National Science Foundation (1978) for the development of seismic regulations for buildings. In a statistical study, McGuire (1974) showed that long epicentral distances tend to decrease the response at high frequencies. Later Trifunac and Brady (1975) correlated the duration of strong motion with the Modified Mercalli Intensity Scale, earthquake magnitude, epicentral distance and site geology. Finally, Mohraz (1978a,b) showed that the earthquake magnitude, peak ground acceleration and duration of strong motion influence response spectra, and consequently the design spectra.

A different approach in seismic analysis and design of structure is the use of random vibration theory. The simulation of earthquake records by a random process has received a great deal of attention. Both stationary and nonstationary random processes have been used to model earthquake ground motion. Housner (1947, 1955), Thompson (1959), Barstein (1960), Bycroft (1960), Tajimi (1960), Rosenblueth and Bustamente (1962), and Housner and Jennings (1964) used a stationary random process while Cornell (1960), Bolotin (1960), Bogdanoff et al. (1961), Shinozuka and Sato (1967), Amin and Ang (1968), Jennings et al. (1969), Iyengar and Iyengar (1969), Liu (1970), and Trifunac (1971a) employed a nonstationary process. A special form of the nonstationary random process

in which an earthquake record is assumed to be a member of a stationary random process modulated by a time-dependent intensity function has been widely used by many investigators, for example, Amin and Ang (1968), Jennings et al. (1968), Goto and Toki (1969), Ruiz and Penzien (1969), Murakami and Penzien (1975), and Hsu and Bernard (1978). A nonstationary random process in which the frequency structure of the records is assumed to be time-dependent has been used by Trifunac (1971b), Saragoni and Hart (1972), Kubo and Penzien (1976), and Wong and Trifunac (1979).

The majority of studies in earthquake motion simulation use either a stationary or nonstationary random process has been to obtain a response spectrum from artifically generated accelerograms. For example, Bycroft (1960) used "white noise" to model earthquake ground motion and related his result to Housner's (1959) standard velocity spectra. Later Housner and Jennings (1964) used a stationary Gaussian random process to generate artificial accelerograms from which they computed response spectra. They demonstrated that the velocity spectra of the real and artificially generated earthquake motion are similar in shape and statistical properties. Using Rosenblueth and Bustamente's (1962) approximate theory based on diffusion analysis and Kanai's (1957) and Tajami's (1960) semi-empirical equation for power spectral density, Housner and Jennings presented expressions for damped and undamped velocity spectra in terms of power spectral density.

Although the use of random vibration theory in seismic analysis and design is straightforward (see for example Hurty and Rubinstein, 1964; Lin, 1967; and Penzien, 1970), this theory has not received the wide attention that the response spectrum has. A random phenomenon,

such as an earthquake and its damage potential to a structure, may best be described by probability statements. Once the ground motion is characterized through its power spectral density, the mean square response of the system can be computed and probability statements regarding the response exceeding a specified value be made by either the use of Chebychve's inquality or a normal distribution function, if the process can be assumed to be normal. Such probability statements provide useful information regarding the susceptibility of a design to failure as well as the means for improving it. A designer currently lacks such information when using a response spectrum approach since it is a collection of the peak responses and any probability statement based on a statistical analysis of response spectra provides statements on peak rather than on the response.

The difficulty in using the random vibration theory in seismic analysis and design is the lack of a sufficient number of useful recorded ground motion and the remote possibility of having them in the near future. Hence there is a need for a methodology based on the available information which one can use with reasonable confidence. Parameters such as earthquake magnitude, peak ground motion, epicentral distance, duration of strong motion, energy release, etc., are random variables which characterize an earthquake and therefore should be considered in the application of the random vibration to seismic design. Motion recorded at different stations during the same event or at the same station during different events differ in characteristics; nevertheless, they should be considered as different realizations of the same random process with some common underlying features.

The first phase in seismic design is to determine the probability of occurrence of an earthquake at a given site for a specified set of parameters, such as peak ground acceleration, earthquake magnitude, epicentral distance, duration of strong motion, etc. The second phase is to formulate an appropriate statistical description of the ground motion. The response of a structure to a seismic disturbance can then be obtained when the above two phases are completed. The determination of the probability of occurrence of an earthquake has received the attention of many investigators (see Esteva, 1976; Burridge and Knopoff, 1976), and is beyond the scope of this investigation. We will, therefore, restrict our attention to the formulation of statistical description of ground motions.

1.2 OBJECTIVE AND SCOPE

Power spectral density, the most useful statistical description of a random process, is an essential part of seismic design of structures through the use of random vibration theory. As noted previously, a number of parameters such as site geology, earthquake magnitude, epicentral distance, duration of strong motion, and peak ground acceleration influence earthquake ground motion and response spectra. It is believed that these parameters would also influence the power spectral density of the recorded ground motion.

The objective of this investigation is to study the power spectral densities of a number of recorded earthquake accelerograms. The study considers the influence of earthquake parameters such as site geology, earthquake magnitude, epicentral distance, duration of strong

motion, and peak ground acceleration on power spectral density. Relationships between the root mean square acceleration of the records and an expression characterising the various earthquake parameters are established. These relationships are used to estimate the power spectral density of the motion for a set of specified earthquake parameters at a site. Finally, the estimated power spectral density is used to obtain the response of a single degree of freedom system and the results are compared with the response computed from the records directly. The study includes horizontal as well as vertical ground motion.

Chapter 2 describes some preliminary concepts of random vibration and the input-output relationship for a single degree of freedom system subjected to ground motion which is used in this study. Chapter 3, in a pilot study, shows that with an appropriate selected duration of strong motion, most earthquake records may be classified as locally stationary. Procedures for generating a time-dependent power spectral density from a selected group of records and the feasibility of using it to compute the response of a single degree of freedom system are also discussed in that chapter. In Chapter 4 the correlation between the RMS value of the record and a variable reflecting the effects of earthquake magnitude, epicentral distance, peak ground acceleration and duration of strong motion is investigated. Chapter 5 presents the power spectral densities for the horizontal and vertical components of earthquake records for three geological classifications. In addition the findings in Chapters 4 and 5 are used to compute the response of a single degree of freedom system and the results are compared to those obtained from the records directly. Summary and conclusions and the recommendations for further studies are presented in Chapter 6.

1.3 NOMENCLATURE

The symbols are defined where they first appear. The majority are summarized below for ease of reference:

a	maximum ground acceleration
AA	absolute acceleration of the mass in a SDOF system [Eq. (3.5)]
A, B	constants
B_e	resolution bandwidth
C_i	constants
D	epicentral distance
E[ ]	expected value of [ ]
f	cyclic frequency
F(t)	forcing function
G(f)	one-sided power spectral density function
G(f)	raw estimate of power spectral density function
G(f)	estimate power spectral density function
h	sampling interval
H(f)	frequency response function
$\|H(f)\|$	Transmissibility function, gain factor
$\|H_d(f)\|$	Transmissibility function--base accelerations as input, relative displacement of the mass as output
$\|H_v(f)\|$	Transmissibility function--base acceleration as input, relative velocity of the mass as output
$\|H_a(f)\|$	Transmissibility function--base acceleration as input, absolute acceleration of the mass as output
j	$\sqrt{-1}$, index
k	index, constant

K	spring constant, number of records
ℓ	number of consecutive frequency components
m	mass of a SDOF system
M	earthquake magnitude
n	degrees-of-freedom associated with a random variable
N	number of data points in a record
N_0	number of added zeros to a record
P_1, P_2, P_3, P_4	constants
$Pr(\ )$	probability that ( )
r	correlation coefficient
$R_x(\tau)$, $R_{1x}(\tau)$	autocorrelation function
$R(t_1, t_2)$	nonstationary autocorrelation function
RD	relative displacement of the mass in a SDOF system [Eq. (3.3)]
RV	relative velocity of the mass in a SDOF system [Eq. (3.4)]
$S_x(f)$	two-sided power spectral density function
$S(t)$	scale factor
t_1, t_2	arbitrary times
T_1, T_2	initial and final times in selecting duration of strong motion
T	observation time
T_r	record length
u	relative displacement of the mass in a SDOF system [Eq. (2.53)]
v	absolute displacement of the mass in a SDOF system [Eq. (2.54)]
$x(t)$, $y(t)$	input and output random variable respectively
$X(f)$	Fourier Transform of $x(t)$

z	absolute base acceleration of a SDOF system [Eq. (2.53)]
α	a small probability, level of significance
ΔT	duration of strong motion
ε_r	random error
ξ	damping ratio
μ	mean value
σ	standard deviation
σ_y	standard deviation of relative displacement response of the mass of a SDOF system
$\sigma_{\dot{y}}$	standard deviation of relative velocity response of the mass of a SDOF system
σ_a	standard deviation of absolute acceleration response of the mass of a SDOF system
σ^2	variance
τ	time lag
χ^2	Chi-Square variable
ψ	root mean square
ψ^2	mean square
	variable reflecting the combined effects of earthquake earthquake parameters

CHAPTER 2

SOME PRELIMINARY CONCEPTS IN RANDOM VIBRATION

2.1 INTRODUCTORY REMARKS

This chapter presents a brief review and summary of some of the concepts in random process which are used in this study. They can be found in a number of texts, such as Crandall (1963), Lin (1967), Bendat and Piersol (1971), and Clough and Penzien (1975). The definitions of ergodic, stationary and locally stationary random processes are given and means for describing a random process are outlined. The power spectral density function, the most important descriptive characteristic of a stationary random process, is given special attention. The use of the Fast Fourier Transform (FFT) procedure in computing the power spectral density is presented, and the errors in estimating it are discussed.

2.2 RANDOM PROCESS

A collection of data representing a physical random phenomenon cannot be described by an explicit mathematical relationship because each observation is unique and any observation is only one of the many possible outcomes. A single time history representing a random phenomenon is called a sample record, and a collection of sample records constitutes a random process.

The properties of a random process can be estimated at any time by computing average values over the collection of sample records. Mean value and the autocorrelation function are usually the quantities first calculated to study the stationary characteristics of a random process. For the random process $\{x(t)\}$, where $\{\ \}$ denotes an ensemble of sample records, the mean value $\mu_x(t_1)$ and the autocorrelation function $R_x(t_1, t_1 + \tau)$ at time t_1 are computed as:

$$\mu_x(t_1) = \lim_{k\to\infty} \frac{1}{k} \sum_{k=1}^{K} x_k(t_1) \tag{2.1}$$

$$R_x(t_1, t_1 + \tau) = \lim_{k\to\infty} \frac{1}{k} \sum_{k=1}^{K} x_k(t_1)\, x_k(t_1 + \tau) \tag{2.2}$$

where the subscript k indicates the k^{th} sample record of the ensemble and τ is a time lag. The random process $\{x(t)\}$ is said to be nonstationary if $\mu_x(t_1)$ and $R_x(t_1, t_1 + \tau)$ vary as time t_1 varies. For the special case where the mean value is constant and the autocorrelation is only a function of the time lag, that is, $\mu_x(t_1) = \mu$ and $R_x(t_1, t_1 + \tau) = R_x(\tau)$, the random process $\{x(t)\}$ is said to be weakly stationary or stationary in the wide sense. The mean value and the autocorrelation function are consequences of first and second order probability distributions. If all possible probability distributions are independent of time translation, the process is called strongly stationary. For a Gaussian random process, where all possible distributions may be derived from the mean value and the autocorrelation function, stationary in a wide sense implies strong stationary character-

istics.

When the time-averaged mean value and the autocorrelation function of the k^{th} sample record as defined by

$$\mu_x(k) = \lim_{T\to\infty} \frac{1}{T} \int_0^T x_k(t)\, dt \tag{2.3}$$

$$R_x(k,\tau) = \lim_{T\to\infty} \frac{1}{T} \int_0^T x_k(t+\tau)\, dt \tag{2.4}$$

where T is the duration of the record, do not differ when computed over different sample records, and are equal to those computed over the ensemble, then the stationary random process $\{x(t)\}$ is said to be ergodic. Therefore, the statistical properties of an ergodic random process can be obtained from a single sample record.

Even though the stationary concept applies to a random process, it is sometimes used to describe a single sample record. A different interpretation of stationary characteristic is implied when a single record is being described. In such cases it is generally meant that the statistical properties computed over a short interval do not vary significantly from one interval to another.

2.3 STATIONARY RANDOM PROCESS

The following are used to describe the properties of random data: (a) mean square values, (b) probability density function, (c) autocorrelation function, and (d) power spectral density function. The mean square value describes the intensity of the data. The probability density function describes the amplitude properties of the data. The auto-

correlation and power spectral density functions, which are Fourier transform pairs, provide the same information in time and frequency domains, respectively. The autocorrelation function of a stationary random process describes the general dependency of the data on each other at different times and is defined as:

$$R_x(\tau) = E[x(t) \times (t + \tau)] \tag{2.5}$$

The autocorrelation function is always a real-valued even function with a maximum at $\tau = 0$, that is,

$$R_x(\tau) = R_x(-\tau) \tag{2.6}$$

$$R_x(0) \geq |R_x(\tau)| \text{ for all } \tau \tag{2.7}$$

The autocorrelation function at time $\tau = 0$ is equal to the mean square value, whereas at $t = \infty$ it approaches the square of the mean. In equation form

$$R_x(0) = \psi_x^2 \tag{2.8}$$

$$R_x(\infty) = \mu_x^2 \tag{2.9}$$

Perhaps the most important single descriptive characteristic of a stationary data is the power spectral density function, which describes the frequency composition of the data in terms of its mean square value. For linear systems with constant parameters (mass, stiffness and damping) the output power spectrum is equal to the product of the input power spectrum and the response function of the system. The mean square value

of the data in a frequency range of interest is determined by the area under the power spectrum in that range (note that ψ^2 is the total area under the power spectrum). The square root of the power spectrum at zero frequency represents the mean value, μ, of the data. The mean and mean square values are expressed as:

$$\psi_x^2 = \int_{-\infty}^{\infty} S_x(f)\, df \tag{2.10}$$

$$\mu_x = \left[\int_{0-}^{0+} S_x(f)\, df\right]^{1/2} \tag{2.11}$$

where the two sided power spectral density function $S_x(f)$, is defined as the Fourier transform of the autocorrelation function

$$S_x(f) = \int_{-\infty}^{\infty} R_x(\tau)\, e^{-j2\pi f\tau}\, d\tau \tag{2.12}$$

From the symmetric property of the autocorrelation function, Eq. (2.6), it follows that

$$S_x(f) = S_x(-f) \tag{2.13}$$

Using Eq. (2.13), Eq. (2.12) can be simplified to

$$S_x(f) = 2\int_0^{\infty} R_x(\tau)\, \cos 2\pi f\tau\, d\tau \tag{2.14}$$

The use of $S_x(f)$ defined over the frequency range of $(-\infty, \infty)$ and the exponentials with imaginary components often simplify mathematical formulations. The quantity measured in practice is the one sided power spectral density $G_x(f)$, where the frequency varies over $(0,\infty)$, and is defined as

$$G_x(f) = 2S_x(f) \qquad 0 \leq f < \infty \tag{2.15}$$

Usually a finite upper limit on frequency range is imposed by the sampling rate of the data. The quantity $G_x(f)$ can be defined in terms of the autocorrelation function as

$$G_x(f) = 4\int_0^\infty R_x(\tau)\cos 2\pi f\tau d\tau \qquad 0 \leq f < \infty \tag{2.16}$$

An alternative way to define the power spectral density function is to consider a sample record $x_k(t)$ of a stationary random process in the time interval of $0 \leq t < T$ and let

$$S_x(k,f,T) = \frac{1}{T} X_k^*(f,T)\, X_k(f,T) \tag{2.17}$$

where $X_k(f,T)$ is the finite range Fourier transform of $x_k(t)$ defined by

$$X_k(f,T) = \int_0^T x_k(t)\, e^{-j2\pi ft}\, dt \tag{2.18}$$

and $X_k^*(f,t)$ is the complex conjugate of $X_k(f,t)$. It should be noted that an infinite range Fourier transform of $x_k(t)$ does not exist. However, by restricting the limits to the range of 0 to T, the finite range Fourier transform can be obtained.

Defining the power spectral density function of the process as

$$S_x(f) = \lim_{T\to\infty} E[S_x(k,f,T)] \tag{2.19}$$

where, $E[S_x(k,f,T)]$ is the expected value operation over the ensemble index k, and making use of Eq. (2.17), we obtain

$$S_x(f) = \lim_{T\to\infty} \frac{1}{T} E[|X_k(f,T)|^2] \tag{2.20}$$

In terms of the one sided power spectral density function Eq. (2.20) reduces to

$$G_x(f) = 2 \lim_{T\to\infty} \frac{1}{T} E[|X_k(f,T)|^2] \tag{2.21}$$

where $0 < f < \infty$.

2.4 LOCALLY STATIONARY RANDOM PROCESS

Nonstationary data is the class of data whose statistical properties vary with time. Time-varying mean value, time-varying mean square value, and time-varying frequency structure of the data indicate the nonstationary characteristic of the data. Such a conclusion is a negative statement denoting the lack of stationary characteristic of the data. Therefore, nonstationary random processes are defined as those which do not qualify as a stationary random process, and their time-dependent statistical properties are determined by time averaging across the ensemble of records. A particular type of nonstationary random process, whose frequency structure is time invariant is called a locally stationary process (Page, 1952; Silverman, 1957; and Bendat and Piersol, 1971) which will be discussed later in this section.

The autocorrelation for a nonstationary process is generally defined as

$$R_x(t_1, t_2) = E[x(t_1)\, x(t_2)] \tag{2.22}$$

where t_1 and t_2 are two arbitrary times. A further insight in the composition of the autocorrelation function can be gained by the following transformation:

$$\text{let} \qquad \tau = t_2 - t_1 \qquad \text{and} \qquad t = \frac{t_1 + t_2}{2} \tag{2.23}$$

$$\text{which results in} \qquad t_1 = t - \frac{\tau}{2} \qquad \text{and} \qquad t_2 = t + \frac{\tau}{2} \tag{2.24}$$

With these changes of variables, the autocorrelation function becomes

$$R_x(t,\tau) = E[x(t - \tfrac{\tau}{2})\ x(t + \tfrac{\tau}{2})] \tag{2.25}$$

In the above equation t denotes time and τ represents a time lag. It should be noted that $R_x(t,\tau)$ evaluated at $\tau = 0$, gives the time-dependent mean square value function.

$$R_x(t,0) = E[x(t)\ x\ (t)] = \psi_x{}^2(t) \tag{2.26}$$

For some processes it may be possible to decompose the autocorrelation $R_x(t,\tau)$ into a product of two functions,

$$R_x(t,\tau) = R_{1x}(\tau)\ R_{2x}(t) \tag{2.27}$$

where $R_{1x}(\tau)$ is the stationary autocorrelation function, and $R_{2x}(t)$ is a slowly varying scale factor defined within a short time interval as

$$R_{2x}(t) \tilde{=} C_i \qquad t_{i-1} \leq t < t_i \tag{2.28}$$

Nonstationary random processes whose autocorrelation is in the form of Eq. (2.27) are called locally stationary processes. When $R_{1x}(\tau)$ is normalized such that $R_{1x}(0) = 1$, then

$$R_{2x}(t) = \psi_x^2(t) \tag{2.29}$$

Therefore,

$$R_x(t,\tau) = \psi_x^2(t)\, R_{1x}(\tau) \tag{2.30}$$

The Fourier transform of Eq. (2.30) gives the two sided time-dependent power spectral density function

$$S_x(t,f) = \psi_x^2(t) \int_{-\infty}^{\infty} R_{1x}(\tau)\, e^{-2j\pi f\tau} d\tau \tag{2.31}$$

In terms of the one sided time-dependent power spectral density function, Eq. (2.31) reduces to

$$G_x(t,f) = \psi_x^2(t)\, G_x(f) \qquad 0 \leq f < \infty \tag{2.32}$$

where $\psi_x^2(t)$ is the time dependent mean square value function and $G_x(f)$ is the stationary power spectral density function of the process.

The power spectral density function given by Eq. (2.32) can be estimated by first computing the time dependent mean square value function, which is averaged across the ensemble of records, and then estimating $G_x(f)$ in the same manner as for a stationary random process. Since the total area under the power spectral density represents the

mean square which is reflected in $\psi_x^2(t)$, then one needs to normalize the total area under the stationary power spectral density function to unity.

$$\int_0^\infty G_x(f) = 1 \tag{2.33}$$

Before estimating the time-dependent power spectral density function, $G_x(t,f)$, one should demonstrate the validity of the assumption of Eq. (2.27). To show that the local stationary assumption is a reasonable one, the power spectral density estimates of different segments of a record in the ensemble should exhibit similar shapes but have different scales. In order to have confidence in the assumption, a sufficient number of records in the ensemble should be tested for similarity of their segmentally computed power spectral densities.

2.5 ESTIMATING POWER SPECTRAL DENSITY OF STATIONARY RANDOM PROCESS

Equation (2.21) defines the power spectral density of a stationary random process. A stationary random process contains many sample records with infinite duration, whereas the records of physical phenomenon are few in number and short in duration. Therefore, one can only estimate the power spectral density function. In order for the power spectral density function to reveal the characteristic of the data, the record should be long enough to include all the pertinent frequencies in the data and, further, the time interval used in the digitization of the record should be short enough to allow the computation of power spectral density with a good resolution.

An estimate of the power spectral density function is obtained

by first computing the power spectral density function of each of the sample records and then averaging the spectral components $\tilde{G}_k(f)$ at each frequency over the ensemble. This averaging or smoothing operation is intended to approximate the expected value operation in Eq. (2.21). Thus, Eq. (2.21) is replaced by the following equations:

$$\tilde{G}_k(f) = \frac{2}{T} |X_k(f,T)|^2 \tag{2.34}$$

$$\hat{G}_x(f) = \frac{1}{k} \sum_{k=1}^{k} \tilde{G}_k(f) \tag{2.35}$$

where $\tilde{G}_k(f)$ represents the raw estimate of the power spectral density of the k^{th} sample record, and $\hat{G}_x(f)$ is the estimate of the power spectral density of the process $\{x(t)\}$.

Assuming that the records contain N data points spaced h seconds apart and letting

$$x_n = x\,(nh) \qquad n = 0, 1, 2 \ldots N-1 \tag{2.36}$$

Eq. (2.18) can be expressed in discrete form as

$$X_k(f,T) = h \sum_{n=0}^{N-1} X_n\, e^{-j2\pi fnh} \tag{2.37}$$

The discrete frequencies at which the Fourier transforms $X_K(f,t)$ are computed are

$$f_p = \frac{P}{T} = \frac{P}{Nh} \qquad P = 0, 1, 2 \ldots N-1 \tag{2.38}$$

Substituting Eq. (2.38) into Eq. (2.37), one obtains

$$X_k(f_p,T) = h \sum_{n=0}^{N-1} x_n \, e^{-j\frac{2\pi pn}{N}} \qquad P = 0, 1, 2 \ldots N-1 \qquad (2.39)$$

It should be noted that when a continuous record is sampled such that the time interval between sample values is h seconds, the highest frequency which can be detected in the data is $\frac{1}{2h}$ cps. The cut off frequency

$$f_c = \frac{1}{2h} \qquad (2.40)$$

is called the Nyquist frequency. Therefore, when the N data points in the record are h seconds apart, the Nyquist frequency occurs at $P = \frac{N}{2}$. Hence the raw estimates of the power spectral density is given by

$$\tilde{G}_k(f_p) = \frac{2}{Nh} \left| X_k(f_p,T) \right|^2 \qquad k = 1, 2 \ldots K \qquad (2.41)$$

where the spectral components $X_k(f_p,T)$ are computed at the frequencies

$$f_p = \frac{P}{Nh} \qquad P = 0, 1, 2 \ldots \frac{N}{2} \qquad (2.42)$$

The smallest frequency increment for which a change in the estimate can be detected is called the resolution bandwidth which is defined as

$$B_e = \frac{1}{T} = \frac{1}{Nh} \qquad (2.43)$$

Equation (2.43) shows that the larger the number of data points in the sample record, the finer the resolution bandwidth. Because of the na-

ture of the Fast Fourier Transforms, one can add zeros to the record to obtain a finer resolution bandwidth. When padding a record with zeros, the spacing of the spectral components will be based on the augmented rather than the original record length. The resolution bandwidth is then given by

$$B_e = \frac{1}{(N + N_0)h} \tag{2.44}$$

where N_0 is the number of zeros added to the beginning or the end of the record. In such a case the area under the power spectral density is no longer equal to the mean square value of the original record, but rather to the mean square value of the augmented record.

2.5.1 RANDOM ERROR IN POWER SPECTRAL DENSITY ESTIMATE

It can be shown (see Bendat and Piersol, 1971) that each component of $\tilde{G}_k(f_p)$ is a chi-square variable with two degrees of freedom. The random error of the estimate $\tilde{G}_k(f_p)$ is the ratio of the standard deviation to the mean value of the estimate:

$$\varepsilon_r = \frac{\sigma[\tilde{G}_k(f_p)]}{G_k(f_p)} \tag{2.45}$$

The mean and variance of a chi-square variable with n degrees of freedom are n and 2n, respectively. Hence for two degrees of freedom, the random error is

$$\varepsilon_r = \frac{\sigma[\tilde{G}_k(f_p)]}{G_k(f_p)} = \frac{\sqrt{2n}}{n} = \sqrt{\frac{2}{n}} = 1 \tag{2.46}$$

which indicates that the standard deviation of the estimate is as large as the mean value which is obviously not desirable. In the next section techniques for reducing the error are briefly described.

2.5.2 SMOOTHING OF POWER SPECTRAL DENSITY ESTIMATE

The random error associated with Eq. (2.34) in estimating the power spectral density can be reduced in one of three ways. First is the frequency smoothing, in which the result of ℓ contiguous spectral components of the estimate of a single sample record are averaged. Second is the ensemble averaging, which is accomplished by computing the estimate from K sample records and then averaging the estimates at each frequency of the spectral components. The third approach uses a combination of the two.

Frequency Smoothing. When ℓ adjacent frequency components are averaged, the final spectral estimate G_i is given by

$$\hat{G}_i = \frac{1}{\ell} [\tilde{G}_i + \tilde{G}_{i+1} + \ldots \tilde{G}_{i+\ell-1}] \tag{2.47}$$

There are $N/2\ell$ such estimates which can be considered as representing the midpoint of the frequency interval between f_i and $f_{i+\ell-1}$. By the χ^2 (Chi square) addition theorem for independent variables, (see Wagpole and Myers, 1978) the quantity $\hat{G}_i$ will be a χ^2 variable with roughly $n = 2\ell$ degrees of freedom. The final effective resolution bandwidth will approximately be ℓ/T. Therefore,

$$n = 2\ell \tag{2.48a}$$

$$B_e = \frac{\ell}{T_r} \tag{2.48b}$$

$$\varepsilon_r = \sqrt{\frac{1}{\ell}} \tag{2.48c}$$

Ensemble Smoothing. Assuming that all sample records are of equal length T_r, the frequencies at which the spectral estimates for each record are computed by the Fast Fourier Transform procedure will be identical. Therefore, by averaging across the ensemble of K estimates, the final spectral estimate is given as

$$\hat{G}(f_p) = \frac{1}{K} [\tilde{G}_1(f_p) + \tilde{G}_2(f_p) + \ldots + \tilde{G}_K(f_p)] \tag{2.49}$$

The quantity $\hat{G}(f_p)$ will be a χ^2 variable with approximately $n = 2K$ degrees of freedom. The effective resolution bandwidth will still be $\frac{1}{T_r}$. Therefore,

$$n = 2K \tag{2.50a}$$

$$B_e = \frac{1}{T_r} \tag{2.50b}$$

$$\varepsilon_r = \sqrt{\frac{1}{K}} \tag{2.50c}$$

Usually the record lengths in an ensemble are not equal. In such cases, one needs to pad the records with zeros to achieve equal record lengths. The effect of adding zeros to records was discussed in section 2.5.

Combined Smoothing. For a combination of frequency smoothing and ensemble averaging, the final effective resolution bandwidth will be $\frac{\ell}{T_r}$ and the resulting estimate will be a χ^2 variable with $n = 2\ell K$ degrees of freedom. The random error in this case is given by $\varepsilon_r = \sqrt{\frac{1}{\ell K}}$.

2.5.3 EQUIVALENT POWER SPECTRAL ESTIMATES

When power spectral density estimates are obtained under different conditions, e.g. from two parts of the same record or from two independent sample records, they may be tested for equivalence. Bendat and Piersol (1971) give a procedure to determine whether two estimates are statistically equivalent over the same frequency interval. The test is based on the statistic

$$\tilde{\chi}^2 = \frac{1}{2}\left(\frac{n_1 n_2}{n_1+n_2}\right) \sum_{i=1}^{N_f} \left(\log \frac{G_1(f_i)}{G_2(f_i)}\right)^2 \qquad (2.51)$$

having a chi-square distribution with N_f degrees of freedom. The region of acceptance is

$$\tilde{\chi}^2 \leq \chi_{n;\alpha}^2 \qquad n = N_f \qquad (2.52)$$

where the two estimates $G_1(f)$ and $G_2(f)$ have the same resolution bandwidth, with n_1 and n_2 degrees of freedom, respectively; N_f is the number of bandwidths to cover the frequency range of interest and α is the level of significance of the test.

It should be noted that this test is valid for the condition when the power spectra are computed from two statistically independent records

or segments of a record. This condition is not strictly satisfied when overlapping segments of a record are used. However, when the overlap is small, the segment and the entire record may be considered statistically independent.

2.6 INPUT-OUTPUT RELATIONSHIP

For a single degree of freedom system subjected to a base motion (Figure 2.1), the governing differential equation of motion is

$$\ddot{u} + 2\omega_n \xi \dot{u} + \omega_n^2 u = -\ddot{z} \tag{2.53}$$

where

u = relative displacement of mass m,

z = absolute displacement of the base,

ω_n = natural frequency = $\sqrt{\frac{K}{m}}$,

ξ = damping ratio = $\frac{c}{2\sqrt{Km}}$

The equation of motion of a single degree of freedom whose mass is subjected to a forcing function is

$$\ddot{v} + 2\omega_n \xi \dot{v} + \omega_n^2 v = F(t) \tag{2.54}$$

where,

v = absolute displacement of the mass,

$F(t)$ = forcing function per unit mass.

Since Eq. (2.53) and (2.54) are of the same form, the study of both types of excitation can be combined into one. The base motion or the

forcing function or a combination of both will be referred to as input. Correspondingly, the induced response of the system, either absolute or relative displacement, velocity and acceleration of the system will be referred to as output.

Let us consider a single degree of freedom system with a constant mass, stiffness, and damping subjected to a Gaussian stationary input x(t) with zero mean. Since the system is linear, the output y(t) will also be Gaussian stationary with zero mean. The relationship between the input and output power spectral density is given by

$$G_y(f) = |H(f)|^2 G_x(f) \tag{2.55}$$

where $G_x(f)$ and $G_y(f)$ are the one sided power spectral density of the input and output, respectively, and the function $|H(f)|^2$ is the transmissibility function or the gain factor, which prescribes the portion of the energy to be transmitted through the system at various frequencies. It follows that the mean square value of the output is given by

$$\psi_y^2 = \int_0^\infty G_y(f)df = \int_0^\infty |H(f)|^2 G_x(f)df \tag{2.56}$$

The integration of Eq. (2.56) for obtaining the mean square response can be carried out in a closed form if a mathematical expression for $G_x(f)$ is available; however, if $G_x(f)$ is given in a tabular form, a numerical integration is necessary. When $G_x(f)$ is a smooth function with no sharp peaks, a good approximation of equation (2.56) can be obtained for small damping as follows: For small damping ratio ξ, the

transmissibility function $|H(f)|^2$ is sharply peaked around the natural frequency f_n and it reduces considerably for small changes in frequency. Therefore, the major contribution to the integral in equation (2.56) comes from the region around the natural frequency f_n. In addition if the power spectral density varies slowly in the vicinity of the natural frequency, then the contribution of $G_x(f)$ to the integral outside that vicinity is minimal. For such cases $G_x(f)$ in Eq. (2.56) can be taken outside the integral. Thus,

$$\psi_y^2 = G_x(f) \int_0^\infty |H(f)|^2 \, df \tag{2.57}$$

Considering the relationship between the mean square, variance, and the mean value

$$\psi_y^2 = \sigma_y^2 + \sigma_y^2 \tag{2.58}$$

and noting that the mean of the output is zero

$$\mu_y = 0 \tag{2.59}$$

the variance of the output can be written as

$$\sigma_2^2 = G_x(f) \int_0^\infty |H(f)|^2 \, df \tag{2.60}$$

The mean and the variance of a stationary Gaussian process are the only quantities needed to describe the probability density function of the process.

Since the excitation x(t) is random, the response y(t) is also random, and it is conceivable that it may exceed a specified level y_{max}.

Consequently, the output is described by making probability statements regarding the response exceeding y_{max}. The probability of y(t) exceeding y_{max} is

$$Pr(y > y_{max}) = \int_{y_{max}}^{\infty} \frac{1}{\sqrt{2\pi}\sigma_y} e^{-\frac{1}{2}\frac{(y-\mu_y)^2}{\sigma_y^2}} dy \qquad (2.61)$$

or

$$Pr(y > y_{max}) = \frac{1}{2}\left[1 - erf\left(\frac{y_{max}-\mu_y}{\sqrt{2}\,\sigma_y}\right)\right] \qquad (2.62)$$

where the error function is defined as

$$erf(x) = \frac{2}{\sqrt{\pi}} \int_0^x e^{-p^2} dp \qquad (2.63)$$

Since $\mu_y = 0$, we can write equation (2.62) as

$$Pr(y > y_{max}) = \frac{1}{2}\left[1 - erf\left(\frac{y_{max}}{\sqrt{2}\,\sigma_y}\right)\right] \qquad (2.64)$$

In design the sign of y(t) is unimportant. The probability that the absolute value of y(t) exceeds y_{max} is

$$Pr(|y| > y_{max}) = 1 - erf\left(\frac{y_{max}}{\sqrt{2}\,\sigma_y}\right) \qquad (2.65)$$

by allowing $y_{max} = k\sigma_y$, where k = 1, 2, 3, ..., we obtain the following

probability statements:

$$\Pr(|y| > \sigma_y) = 1 - \text{erf}\left(\frac{1}{\sqrt{2}}\right) = 31.74\%$$

$$\Pr(|y| > 2\sigma_y) = 1 - \text{erf}\left(\frac{2}{\sqrt{2}}\right) = 4.56\% \qquad (2.66)$$

$$\Pr(|y| > 3\sigma_y) = 1 - \text{erf}\left(\frac{3}{\sqrt{2}}\right) = 0.26\%$$

It should be noted that the above probability statements result when the mean and the variance of the output are known.

So far our discussion of the input-output relation has been general. If we now consider support acceleration as input and the relative displacement of the mass as output, we can formulate the transmissibility function as

$$|H_d(f)|^2 = \frac{1}{16\pi^4 f_n^4 \left\{ \left[1 - \left(\frac{f}{f_n}\right)^2 \right]^2 + \left[2\xi \left(\frac{f}{f_n}\right) \right]^2 \right\}} \qquad (2.67)$$

Upon substitution of Eq. (2.67) into Eq. (2.60) and integrating, we obtain the variance of the relative displacement as

$$\sigma_y^2 = \frac{G_{\ddot{x}}(f_n)}{64\pi^3 \xi f_n^3} \qquad (2.68)$$

where the subscript $\ddot{x}$ indicates that the power spectral density $G_{\ddot{x}}(f)$ is obtained from the input acceleration. The transmissibility function for support acceleration as input and the relative velocity as output is

$$|H_v(f)|^2 = \frac{f^2}{4\pi^2 f_n^4 \left\{ \left[1 - \left(\frac{f}{f_n} \right)^2 \right]^2 + \left[2\xi \left(\frac{f}{f_n} \right) \right]^2 \right\}} \tag{2.69}$$

Similarly from Eq. (2.60), the variance of the relative velocity is

$$\sigma_{\dot{y}}^2 = \frac{G_{\ddot{x}}(f_n)}{16\pi\xi f_n} \tag{2.70}$$

Finally the transmissibility function for support acceleration as input and the absolute acceleration as output is

$$|H_a(f)|^2 = \frac{1 + \left[2\xi \left(\frac{f}{f_n} \right) \right]^2}{\left[1 - \left(\frac{f}{f_n} \right)^2 \right]^2 + \left[2\xi \left(\frac{f}{f_n} \right) \right]^2} \tag{2.71}$$

the variance of the absolute acceleration is

$$\sigma_a^2 = \frac{\pi f_n (1 + 4\xi^2) G_{\ddot{x}}(f_n)}{4\xi} \tag{2.72}$$

Knowing the mean and the variance of the output, it is a simple matter to make probability statements such as those given by Eq. (2.66).

For a locally stationary random process the input power spectral density is time-dependent (Eq. 2.32); therefore, the variance of the output will also be time-dependent. In this case the time dependent mean square value is

$$\psi^2(t)_y = G_x(t,f) \int_0^\infty |H(f)|^2 \, df \tag{2.73}$$

and the relative displacement, velocity and the absolute acceleration of a single degree of freedom system subjected to a base motion are given by

$$\sigma^2(t)_y + \frac{G_{\ddot{x}}(t,f_n)}{64\pi^3\xi f_n^3} \tag{2.74}$$

$$\sigma^2(t)_{\dot{y}} = \frac{G_{\ddot{x}}(t,f_n)}{16\pi\xi f_n} \tag{2.75}$$

$$\sigma^2(t)_a = \frac{\pi f_n\ (1 + 4\xi^2)\ G_{\ddot{x}}(t,f_n)}{4\xi} \tag{2.76}$$

Probability statements for output are obtained from expressions similar to those of Eq. (2.66). Thus,

$$Pr(|y| > k\sigma(t)_y) = 1 - \text{erf}\left(\frac{k}{\sqrt{2}}\right) \qquad k = 1, 2, 3, \ldots \tag{2.77}$$

It is interesting to note that y and $\sigma(t)_y$ on the left side of Eq. (2.74-2.76) depend on time whereas the probability statements are not time dependent.

Equations (2.74-2.76) have been obtained under the assumption of smooth or slow varying power spectral density (ideal white noise). For cases where the power spectral density is not flat Eq. (2.56) must be utilized in which case the response takes the following form:

$$\sigma^2(t)y = \int_0^\infty |H_d(f)|^2\ G_{\ddot{x}}(t,f)\ df \tag{2.78}$$

$$\sigma^2(t)_{\dot{y}} = \int_0^\infty |H_v(f)|^2\ G_{\ddot{x}}(t,f)\ df \tag{2.79}$$

$$\sigma^2(t)_a = \int_0^\infty |H_a(f)|^2 \, G_{\ddot{x}}(t,f) \, df \tag{2.80}$$

where the functions $|H(f)|$ are given in Eq. (2.67), (2.69), and (2.71), respectively.

The materials presented in this chapter are employed in the subsequent chapters to obtain a time-dependent power spectral density, to predict the response of a single degree of freedom system to a set of base excitations, and finally, to compare the predicted response to the response of the system computed directly from the records.

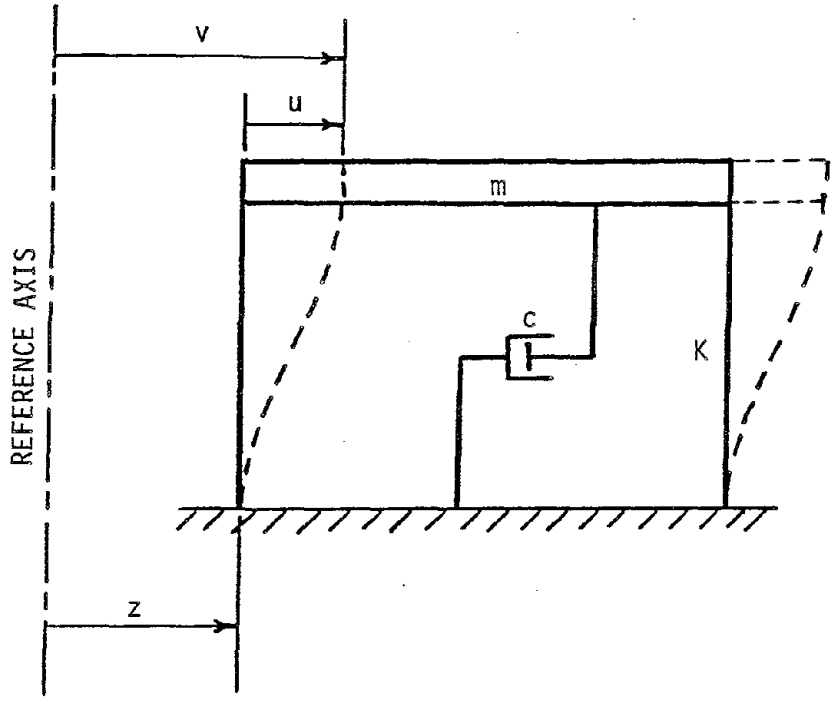

m = mass

c = damping

K = spring constant

u = relative displacement of mass m

v = absolute displacement of mass m

z = absolute motion of base

FIG. 2.1. Single degree of freedom system.

CHAPTER 3

TIME-DEPENDENT POWER SPECTRAL DENSITY OF EIGHT SELECTED RECORDS

3.1 INTRODUCTORY REMARKS

An examination of earthquake records reveals some of their general characteristics. First, due to a finite energy release at the source the resulting motion is transient. Second, this transitory phenomenon manifests itself in three distinct zones in an accelerogram: an initial build-up zone, an intermediate zone of strong motion, and a decaying zone. Third, the acceleration oscillates around a zero line. These general observations lead one to believe that earthquake records are nonstationary. In fact, Amin and Ang (1968) confirm the nonstationary characteristics of the eight earthquake records used originally by Housner (1959) to establish a standard velocity reponse spectrum.

As mentioned in Section 2.4, the nonstationary characteristic could manifest itself in the time-varying mean value, time-varying mean square value, and time-varying frequency structure of the data. For earthquake records one can readily eliminate the time-varying mean value as a contributing factor to nonstationary characteristic. Time averaging results show insignificant changes in the mean value as a function of time, whereas significant changes are observed in the mean square value and the frequency structure of the records.

Realizing that the low amplitude impulses which usually appear

toward the beginning and the end of an earthquake accelerogram have little effect on the energy content within the strong motion duration of the earthquake, we will consider only that part of an earthquake record which contains the strong motion. We further assume that no significant variation in the spectral composition occurs during the strong motion segment of the record. Under such conditions it will be justified to assume that the nonstationary earthquake random process is of locally stationary form (Page 1952, Silverman 1957, Priestley 1965, Bendat and Piersol 1971).

In this chapter, using the eight selected records considered by Housner (1959), we will show that it is possible to select a strong motion segment of earthquake records during which its frequency structure remains reasonably constant. Using such selected segments for the eight records a time-dependent power spectral density is formulated whose frequency structure remains time-invariant, whereas its magnitude (area under the power spectral density) becomes a function of time. This time-dependent magnitude is the ensemble short time mean square value of the eight records. Finally, we will show that a good correlation exists between the RMS value of the selected duration, and a parameter reflecting peak ground acceleration, duration of strong motion, earthquake magnitude and epicentral distance; thereby permitting one to estimate the average magnitude of the time-dependent power spectral density from the knowledge of the mentioned earthquake parameters.

3.2 DURATION OF STRONG MOTION

The duration of strong motion is widely recognized as an important characteristic of ground motion. Studies by Bolt (1974), Trifunac and Brady (1975b), and McCann and Shah (1979) suggest that the duration of strong motion depends on the purpose for which it is used. The intention in this study is to determine the duration of strong motion during which the frequency structure of the record remains nearly the same.

The definition proposed by Bolt (1974), which is known as the bracketed duration, is useful to find the duration of strong motion during which the structure will be subjected to a level of acceleration equal to or greater than a specified limit. Another definition, which is related to the structural response, is that of Trifunac and Brady (1975b) where they define the duration as the time interval during which a significant contribution to the integral $\int_0^t a^2 dt$ takes place. The first and last 5 percent contributions to this integral is omitted and the remaining 90 percent is defined as the significant or the strong motion contribution to the integral. The time interval between the low and the high 5 percent cut-off points (5 and 95 percent, respectively) is defined as the duration of strong motion.

The definition of strong motion suggested by McCann and Shah (1979) is related to the average energy arrival rate and is obtained by considering the cumulative root-mean square function of the record. A search is performed on the derivative of this function to identify the cut-off times. The final cut-off time, T_2, is taken as the last time at which the derivative of cumulative root-mean square function is positive.

To obtain the initial time T_1, the same procedure is repeated except the record is now considered from the "tail-end."

The method proposed here is similar to McCann and Shah's (1979), with one slight difference in the manner that the cut-off points are determined. In this case the cut-off time is selected as the last time at which the slope of the cumulative root mean square function is equal to or greater than one cm/sec^2/sec. For accelerogram spacing of .02 seconds, this corresponds to a change of .02 cm/sec^2 in the cumulative RMS function. The derivative of cumulative root mean square function, in addition to sharp peaks and valleys, exhibits flat regions. The selection of unity or any other appreciable slope instead of any positive slope (which could be extremely small) ensures that the cut-off points are determined where the contribution to the cumulative RMS function is no longer significant. Two other slopes, 0.5 and 2.0 cm/sec^2/sec, were also examined and it was determined that in general they did not result in satisfactory durations of strong motion. As will be shown later, the criteria used in this study provides durations of strong motion for which the frequency structure of data remains time-invariant more often than the methods proposed by either Trifunac and Brady (1975b) or McCann and Shah (1979).

Another procedure for determining the duration of strong motion such that the frequency structure of the data would be time-invariant is to apply the equivalent power spectral test (see Section 2.5.3) to the normalized power spectra of two different segments of the accelerograms. If the two normalized power spectral densities are equivalent, the frequency structure of the two accelerogram segments are the same;

and therefore, time-invariant. Establishing equivalency between the normalized power spectral densities of consecutive segments of an accelerogram would give a duration for which the frequency structure remains time-invariant. However, such a procedure is extremely time consuming and not economical when large number of records are to be analyzed. In addition, this method may or may not yield consecutive segments with consistent frequency structure. Therefore, this procedure was not used.

3.3 COMPARISONS OF PROPOSED DURATIONS OF STRONG MOTION

In order to determine the suitability of the proposed method of computing the duration of strong motion, the eight strong motion records used originally by Housner (1959) were used to compute the durations and compare them with those obtained using the procedures given by Trifunac and Brady (1975b) and McCann and Shah (1979). Table 3.1 lists these records and some of their properties. In Table 3.2 the initial time T_1, the final time T_2, the duration of strong motion ΔT, the root-mean square RMS, and the percent contribution to the integral $\int a^2 dt$ for different procedures are presented and compared.

Figures 3.1 through 3.8 compare the duration of strong motion for the three methods. The method proposed here consistently gives shorter duration than either of the two other methods. As suspected, for a given accelerogram, a shorter duration of strong motion results in a larger RMS value. This is attributed not only to the insignificant contribution of smaller pulses at the latter portion of the accelerogram to the total RMS value, but also to the fact that fewer number of pulses

are used in the computation as well.

It should be noted that a recomputation of the duration and the RMS values by the procedure proposed by McCann and Shah (1979) did not reproduce their reported values exactly. Their study includes six of the eight components of the records used in this chapter. The durations and RMS values as reported by them and recomputed in this study are presented in Table 3.3. Also shown are the values reported later by McCann (1980). The values for El Centro 1940 are extremely close to each other; however, large discrepencies are noted for the other two records. It should be noted that the results reported by McCann and Shah (1979) and by McCann (1980) are also slightly different from each other. Although Trifunac and Brady (1975b) did not report durations and RMS values in their study, the values computed by McCann and Shah (1979) using their procedure and those computed in this study for the six records are in close agreement. The discrepency observed in Table 3.3 may be attributed to the different methods of calculating the derivatives of the cumulative RMS function. A centeral 3-point difference formula was used in this study to obtain the derivative.

To check the durations computed by the three procedures for their consistency of frequency structure, the equivalent power spectra test of Section 2.5.3 was used. The test compares the normalized power spectral density of consecutive segments of the selected duration with the normalized power spectral density of the total selected duration. It is necessary to normalize the power spectral densities, since we compare their shapes (frequency structure) rather than their magnitudes. The normalization is accomplished by setting the area under power spectral

densities to unity. A brief description of the test procedure follows:

First, the power spectral density of the selected duration is estimated using the Fast Fourier Transform procedure (Bendat and Piersol 1971) and then it is smoothed and normalized. Next, a segment from the selected duration is padded with zeros to make its length equal to the length of the selected duration. The padding is performed in order to obtain spectral estimates at the same frequencies as those for the selected duration (see Section 2.5). The power spectral density for this augmented segment is then estimated, smoothed and normalized. The same degree of smoothing is performed on the power spectral density of the augmented segment and the power spectral density of the selected duration. The normalized power spectral density of the augmented segment is then compared with the normalized power spectral density of the selected duration in the frequency range of 0 to 25 Hertz using a Chi-square test with a 5 percent level of significance. Other consecutive segments are chosen and the procedure is repeated until the selected duration is exhausted. With the exception of the last segment, all segments are equal in length.

The above procedure was used to test the duration of the strong motion for the eight records computed by the three methods. The results of such comparisons for 2, 4, 6 and 10 second long segments are presented in Figs. 3.9 through 3.16. The plots show the ratio of computed Chi-square to the theoretical one. The two power spectral densities (for the selected duration and the segment) are accepted as being equivalent when this ratio is less than or equal to one (see Section 2.5). Two observations can be made from the result presented in Figs. 3.9 through

3.16. First, the Chi-square ratio is less than one for most of the records, regardless of the method employed in determining the duration of strong motion. Second, the Chi-square ratios for longer segments (6 and 10 seconds) are closer to zero than the ratios for shorter segments (2 and 4 seconds) indicating that for longer segments the frequency structure of the segment is closer to that of the selected duration. This is to be expected, since for longer segments more characteristics of data are taken into account in the comparison. In the limit, when the length of the segment is equal to that of the selected duration, no difference in the frequency structure can be detected and the Chi-square ratio would be zero (see Eq. 2.52) indicating identical data sets.

These figures indicate that in the majority of cases even a two second segment gives acceptable Chi-square ratios for three procedures. As mentioned previously (Section 2.5.3) the equivalent spectra test is more reliable when the segment length is short as compared to the entire duration of the record. For this reason Chi-square ratios were also computed for a one second segment of the selected duration as determined by the three procedures as well as for the entire record length. The results are shown in Figs. 3.17 through 3.24. The Chi-square ratios for the entire record length of the eight records (Figs. 3.17 to 3.24) clearly indicate that the frequency structure of the record changes with time. The change is more pronounced towards the latter portion of the records which correspond to the region of decaying activity. The figures show that in a majority of cases the ratios computed using the method proposed herein is within the acceptable limit more often

than those computed by the other two procedures. Therefore, it was decided to adopt the proposed procedure for determining the duration of strong motion in this study. Since the spectrum of one second long segments is equivalent to the spectrum of the selected duration of strong motion, the locally stationary assumption for earthquake records is justified. Consequently, a one second segment is used in the computation of the magnitude of the time-dependent power spectral density.

3.4 TIME-DEPENDENT POWER SPECTRAL DENSITY

It was shown in Section 3.3 that the power spectral density computed from one second long segments of the records remains the same for the selected duration for the eight records. This implies that the normalized power spectral density for the selected duration is a good representation of the local (one second long segment) normalized power spectral densities. Since the frequency structure of the data (the shape of power spectral density) remains time-independent, then the time dependency of the power spectral density must manifest itself in its magnitude. It should be noted that the term magnitude here is referred to the area under the power spectral density curve, which is also equal to the variance (mean square value when the mean of the record is zero) of the record (see Section 2.3).

An inspection of accelerograms indicates that the short time mean square value of the records changes with time. If one estimates the ensemble power spectral density of the eight records and normalizes its area to unity, then its time-dependent magnitude should be computed by performing a short time mean square operation on the ensemble of

the records. Therefore, we may consider the time-dependent power spectral density to be composed of the product of two functions--the normalized power spectral density representing the frequency structure of the data, and the time-dependent magnitude representing the area under the power spectral density. The normalized power spectral density is estimated from the ensemble of the records using the selected durations as if they were stationary records, and the magnitude is computed using a one-second long mean square averaging on the ensemble of the records.

When the magnitude is computed within the duration of the shortest record in the ensemble, it includes all records in the ensemble. Beyond the shortest duration, fewer records are included in the computation resulting in a larger variance as the end of the longest record is approached. To compute the time-dependent magnitude in a consistent manner for the duration of longest record, the other records are padded with zeros to make their length equal to that of the longest record in the ensemble before the mean square averaging is carried out. However, with padding the average mean square value is no longer correct and in fact, will be smaller than the average of the individual mean square values of the records in the ensemble. This problem is overcome by reducing the average value to one, and using the normalized time-dependent magnitude as a scale factor which represents the variation of the local magnitude (one second long mean square value) to an average magnitude of unity. The scale factor can now be adjusted to reflect the average mean square value of any record by multiplying the scale factor by the record's mean square value which is computed from the

selected duration of the record.

Therefore, one may consider the time-dependent power spectral density to be composed of three parts. First a normalized power spectral density which describes the frequency structure of the ensemble and remains the same for the segments of the records considered; second, a time-dependent scale factor, obtained by performing a short time averaging on the square of the acceleration and normalizing the mean of the resulting function to one, thereby describing the normalized variation of the localized mean square acceleration; and finally the mean square acceleration. Since the mean square acceleration can be computed for each record, we can obtain a time-dependent power spectral density corresponding to each of the records in the ensemble. Correlations between the mean square acceleration and earthquake parameters would enable one to estimate the time-dependent power spectral density for a given set of earthquake parameters.

The most important ground motion parameter which is widely used in design is the peak ground acceleration. As it will be shown later in Chapter 4, a good correlation exists between the peak ground acceleration and the RMS value. Nevertheless, a better correlation is obtained when a combination of peak ground acceleration, earthquake magnitude, duration of strong motion and epicentral distance is considered.

The procedure for computing the normalized power spectral density is as follows: First the durations of strong motion are determined based on the method proposed in this chapter (modified McCann and Shah's method). Then enough zeros are added to the end of each record to make their length equal to 120 seconds or 6000 data points (6000 data points

would result in a fine resolution in the spectral estimates). Power spectral density of each augmented record is then estimated and normalized (area is set equal to one). The ensemble smoothing procedure similar to one presented in Section 2.5.2 is used to smooth the power spectral density. The only difference is using a duration weighted average to take into account the unequal durations of the unpadded records. Figure 3.25(a) shows the normalized power spectral density of the ensemble of the eight records in the frequency range of 0-25 Hz. Because of a spacing of 0.02 seconds in the accelerograms, the power spectral density is estimated in the frequency range of 0-25 Hz (see Eq. 2.40); however, the dominant frequencies appear in the frequency range of 0 to 10 Hz. Since we used a small number of records in this chapter, the random error associated with the estimated power spectral density shown in Fig. 3.25(a) is quite high (ε_r = 0.35). To reduce this random error, the frequency smoothing technique of Section 2.5.2 is applied to this estimate, where every 100 neighboring spectral ordinates are averaged. Figure 3.25(b) shows the power spectral density after combined smoothing, where the random error is reduced to 0.035. The ordinates in Fig. 3.25(b) are joined by straight lines where in Fig. 3.25(c) third degree polynomial segments join them. The power spectral density in Fig. 3.25(c) was obtained by using a cubic-spline interpolation (DeBoor 1978).

The time-dependent scale factor is determined as follows: The longest duration was found to be almost 25 seconds. Therefore, the other seven records are padded with zero up to 25 seconds in order for all records to have the same length. The accelerations are then squared

and averaged across the ensemble at every 0.02 second interval. The average value of this "biased" mean square function is reduced to one. The normalized mean square function is shown in Fig. 3.26(a). Since we showed that the spectrum remained time-independent for one second long segments, we average the normalized mean square function at one second intervals. The result of this short time averaging which are joined by straight lines is shown in Fig. 3.26(b). Finally the scale factor after using a cubic spline interpolation to join the ordinates is presented in Fig. 3.26(c).

We have now determined the normalized power spectral density and the scale factor which are shown in Figs. 3.25(c) and 3.26(c), respectively. What remains is an estimate of the average magnitude of the power spectral density (mean square value) for a set of earthquake parameters generally specified in design. As will be discussed later in Chapter 4, relationships between RMS values and earthquake parameters such as peak ground acceleration, earthquake magnitude, duration of strong motion, and epicentral distance can be established which enables one to estimate the RMS value or the mean square acceleration for a given set of earthquake parameters. Such a relationship was established for the eight earthquake records used in this chapter and the equation of the regression line is given below:

$$\psi(a,M,T,D) = 10^{1.9468} \left[a \left(\frac{M^{1.3}}{D^{.066} T^{.31}} \right)^{.41} \right]^{.5510} \qquad (3.1)$$

where ψ is the predicted RMS value in cm/sec^2, a is the peak ground acceleration in g, M is the earthquake magnitude, T is the duration

of strong motion in seconds, and D is the epicentral distance in kilometers.

Table 3.4 lists the properties of the eight records used in this pilot study as well as their actual and predicted RMS values using Eq. (3.1). The actual and predicted RMS values are also shown in Fig. 3.27. The correlation coefficient for the fit is 0.9278 which indicates that nearly 86 percent of the variation in RMS values can be accounted for by the above relationship. In the next chapter we will discuss in detail the correlation between RMS values and the ground motion parameters for several larger groups of records with common site geology.

The time dependent power spectral density is formulated as:

$$G(a,M,T,D,t,f) = \psi^2 (a,M,T,D)\ S(t)\ G(f) \qquad (3.2)$$

where $\psi^2(a,M,T,D)$ is the average magnitude of the power spectral density which can be obtained from Eq. (3.1) for a given set of ground motion parameters; S(t) is the time-dependent scale factor representing the variation of localized mean square to an average mean square of one, Fig. 3.26(c); and G(f) is the normalized power spectral density, Fig. 3.25(c).

3.5 COMPARISON BETWEEN RESPONSES CALCULATED FROM THE TIME-DEPENDENT POWER SPECTRAL DENSITY AND SPECTRAL DISPLACEMENT, VELOCITY AND ACCELERATION

In Section 2.6, the mean and variance of relative displacement, relative velocity and absolute acceleration for a Gaussian stationary and a nonstationary random process were formulated. The input-output relationship presented in that section are applicable to a system which

is subjected to an earthquake ground motion under the following two assumptions: First, the individual earthquake records form a locally stationary random process (see Section 2.4); and second, the process is normal. Since we showed in Section 3.3 that the spectrum remained time invariant even for as short as a one second long segment, it is reasonable to assume that by selecting strong motion duration the earthquake records constitute a locally stationary random process. The assumption of normality is accepted since it is generally recognized that the motion recorded at a station results from the arrival of multiple waves after many reflections and refractions of the initial disturbance at the source of the earthquake.

With the above two assumptions, we can rewrite Eqs. 2.78-2.80 to describe the relative displacement RD, relative velocity RV, and absolute acceleration AA of a single degree of freedom system for a given probability that the response may exceed a specified limit. Thus,

$$RD_{k\sigma} = k\sigma_y = k\left[\psi^2(a,M,T,D)\ S(t)\ \int_0^\infty |H_d(f)|^2\ G(f)\ df\right]^{1/2} \tag{3.3}$$

$$RV_{k\sigma} = k\sigma_{\dot{y}} = k\left[\psi^2(a,M,T,D)\ S(t)\ \int_0^\infty |H_v(f)|^2\ G(f)\ df\right]^{1/2} \tag{3.4}$$

$$AA_{k\sigma} = k\sigma_a = k\left[\psi^2(a,M,T,D)\ S(t)\ \int_0^\infty |H_a(f)|^2\ G(f)\ df\right]^{1/2} \tag{3.5}$$

where y and $\dot{y}$ refer to relative displacement and velocity, respectively, and a refers to absolute acceleration. It should be noted that $G_{\ddot{x}}$ in Eqs. 2.78-2.80 has been replaced by its equivalent from Eq. 3.2.

Equations 3.3-3.5 were used to predict the response of a single

degree of freedom system subjected to a base motion. The results for two records (El Centro 1940, S00E Component and Taft 1952, N21E Component) at 3σ level ($k = 3$) and for damping coefficients of 2, 5, 10 and 20 percent of critical are presented in Figs. 3.28-3.35. With the knowledge of earthquake parameters (peak ground acceleration a, earthquake magnitude M, duration of strong motion T, and epicentral distance D) for each of the two records, the appropriate value of mean square acceleration $\psi^2(a,M,T,D)$ is estimated from either Eq. 3.1 or Fig. 3.27. Also shown in the figures are the corresponding spectral relative displacement, spectral relative velocity, and spectral absolute acceleration as reported by Trifunac et al., 72-75.

It should be noted that spectral response obtained from an earthquake record at a given frequency and damping is the absolute maximum value of the response regardless of the time at which it occurs. The probability that the response equals the maximum during the duration of the record is very small (one over the number of points at which the response is computed). In order to compare the results of this study with the spectral values one should select a low probability for exceeding the response and account for the maximum response in the computation. To achieve the maximum response, one should use the maximum scale factor S(t). To reduce the probability for exceeding the response one needs to compute the response at a high σ level ($k = 3$ or 4). The maximum scale factor obtained from Fig. 3.26 is 3.49. Selecting a 3σ level ($k = 3$), the probability that the maximum response will be exceeded is .0026. It should be noted a 3σ level is also suggested by Penzien (1970).

In general the responses computed from the power spectral density follow the shape of the spectral curves and for the most part envelope the curves even at higher damping ratios. In spite of the small sample size of eight, the results obtained compare well with the spectral values both in shape and magnitude. As mentioned previously, in the following chapters similar results from a large number of records with various geological classifications will be presented and discussed.

TABLE 3.1

PROPERTIES OF THE EIGHT RECORDS USED IN THE PILOT STUDY

Record	Earthquake	Date	Site	Comp.	Mag.	Strong Motion Duration* (sec)	Peak Acc. (g)	Record Length (sec)	Epicentral Distance (km)
A001	Imperial Valley	5/18/40	El Centro	S00E S90W	6.7	25-30	.348 .214	53.74 53.46	11.5
A004	Kern County	7/21/52	Taft	N21E S69E	7.7	14-17	.156 .179	54.36 54.38	41.4
B024	Lower California	12/30/34	El Centro	S00W S90W	6.5	17-25	.160 .183	90.28 90.22	66.3
B029	Western Washington	4/13/49	Olympia	N04W N86E	7.1	21-25	.165 .280	89.06 89.04	16.9

* Housner and Jennings (1964)

TABLE 3.2

COMPARISON OF DURATIONS AND ROOT MEAN SQUARE VALUES
FOR THE EIGHT RECORDS

Record	Comp.	Method*	T1 (sec)	T2 (sec)	ΔT (sec)	RMS (cm/sec^2)	$\int a^2 dt$
El Centro 1940	S00E	a	0.00	53.74	53.74	46.01	100
		b	1.68	26.10	24.42	64.75	90
		c	0.88	26.32	25.44	65.60	96
		d	1.38	26.30	24.92	65.88	95
	S90W	a	0.00	53.46	53.46	38.85	100
		b	1.66	26.20	24.54	54.39	90
		c	0.80	26.62	25.82	54.73	96
		d	1.32	26.42	24.92	55.14	94
Taft 1952	N21E	a	0.00	54.34	54.34	25.03	100
		b	3.70	34.24	30.54	31.70	90
		c	2.14	36.46	34.32	30.85	96
		d	3.46	20.66	17.20	40.19	82
	S69E	a	0.00	54.38	54.38	26.10	100
		b	3.66	32.52	28.86	33.96	90
		c	2.34	35.30	32.96	32.71	95
		d	3.18	17.34	14.16	46.20	82

TABLE 3.2 - continued

Record	Comp.	Method*	T1 (sec)	T2 (sec)	ΔT (sec)	RMS (cm/sec^2)	$\int a^2 dt$
El Centro 1934	S00W	a	0.00	90.28	90.28	19.48	100
		b	2.82	23.92	21.10	38.27	90
		c	1.92	23.88	21.96	38.38	94
		d	1.96	14.98	13.02	46.83	83
	S90W	a	0.00	90.22	90.22	20.76	100
		b	2.86	23.14	20.28	41.57	90
		c	1.62	20.10	18.48	44.26	93
		d	2.00	17.78	15.78	46.80	89
Olympia 1949	N04W	a	0.00	89.06	89.06	22.98	100
		b	1.78	27.58	25.80	40.51	90
		c	0.08	23.02	22.94	43.73	93
		d	1.06	20.18	19.12	46.59	88
	N86E	a	0.00	89.02	89.02	28.10	100
		b	4.34	22.42	18.08	59.22	90
		c	0.28	21.80	21.52	55.48	94
		d	4.34	20.46	16.12	61.50	87

* a - Entire Record
  b - Trifunac and Brady's Method
  c - McCann and Shah's Method
  d - This Study

TABLE 3.3

COMPARISON OF DURATION AND ROOT MEAN SQUARE
BY DIFFERENT METHODS

Record	Comp.	Method*	T1 (sec)	T2 (sec)	ΔT (sec)	RMS (cm/sec^2)
El Centro 1940	S00E	a	1.16	26.36	25.20	65.76
		b	1.36	26.20	24.84	65.63
		c	0.88	26.32	25.44	65.60
	S90W	a	0.88	26.28	25.40	54.95
		b	1.08	26.20	25.12	54.89
		c	0.80	26.62	25.82	54.73
Taft 1952	N21E	a	3.18	14.38	11.20	46.96
		b	3.38	14.40	11.02	47.15
		c	2.14	36.46	34.32	30.85
	S69E	a	3.20	15.80	12.60	48.24
		b	3.40	15.80	12.40	48.16
		c	2.34	35.30	32.96	32.71
El Centro 1934	S00W	a	2.00	15.00	13.00	46.80
		b	2.10	15.00	12.90	46.95
		c	1.92	23.88	21.96	38.38
	S90W	a	2.00	17.60	15.60	46.72
		b	2.24	17.60	15.36	46.59
		c	1.62	20.10	18.48	44.26

* a - Reported by McCann (1980)
  b - Reported by McCann and Shah (1979)
  c - Computed in this study by McCann and Shah's (1979) method

TABLE 3.4

ACTUAL AND PREDICTED RMS FOR THE EIGHT RECORDS

Record	Component	Peak Acc. (g)	Duration of Strong Motion (sec)	Epicentral Distance (km)	Mag.	RMS Value (cm/sec^2)	
						Predicted	Actual
El Centro 1940	S00E	.348	24.92	11.5	6.7	66.51	65.88
	S90W	.214	24.92			50.88	55.14
Taft 1952	N21E	.156	17.20	41.4	7.7	44.84	40.20
	S69E	.179	14.16			49.03	46.20
El Centro 1934	S00W	.160	13.02	66.3	6.5	43.80	46.83
	S90W	.183	15.78			46.54	46.80
Olympia 1949	N04W	.165	19.12	16.9	7.1	45.42	46.59
	N86E	.280	16.12			61.52	61.51

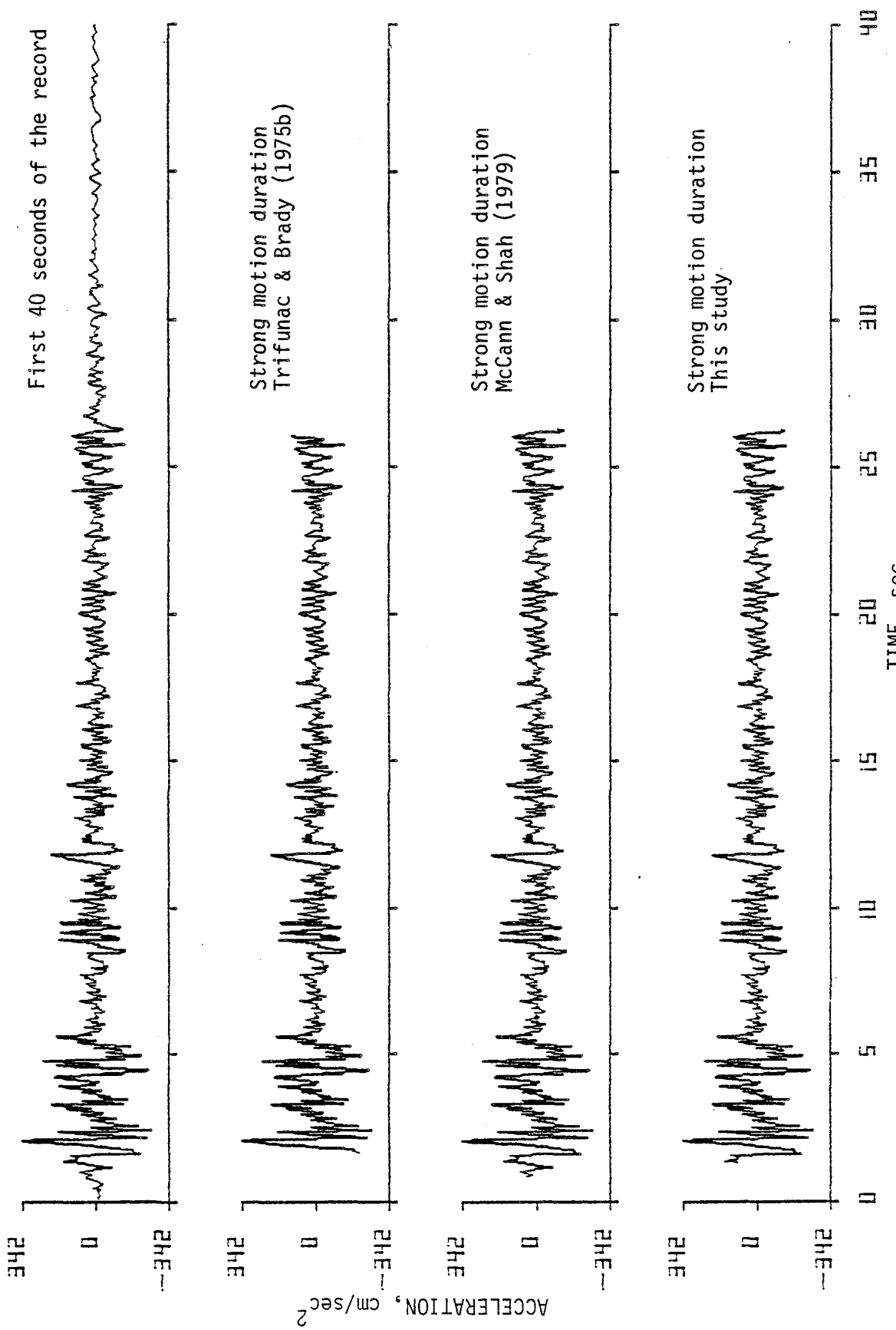

FIG. 3.1. Comparison of strong motion duration for Imperial Valley Earthquake, May 18, 1940, El Centro - component S00E.

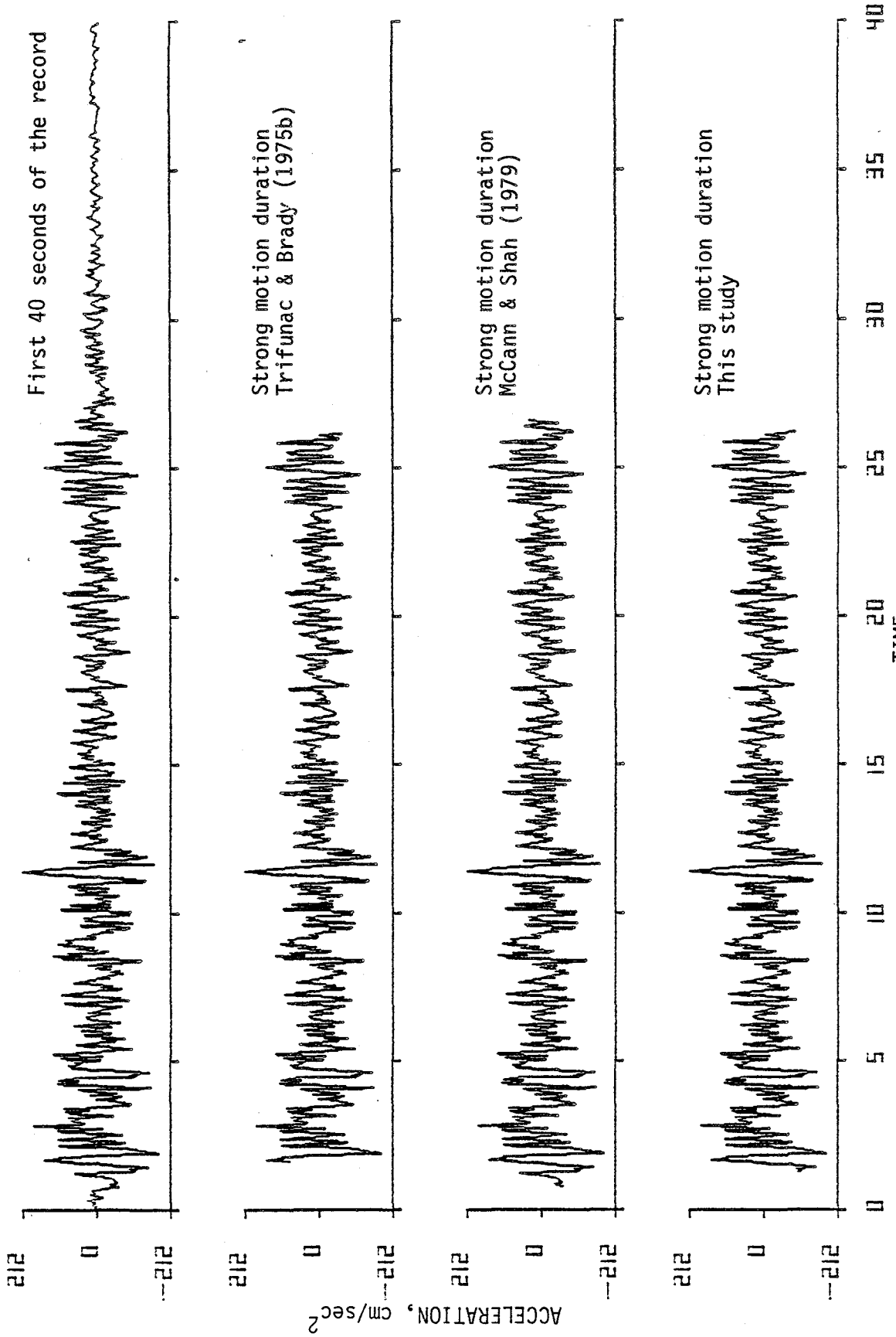

FIG. 3.2. Comparison of strong motion duration for Imperial Valley Earthquake, May 18, 1940, El Centro - component S90W.

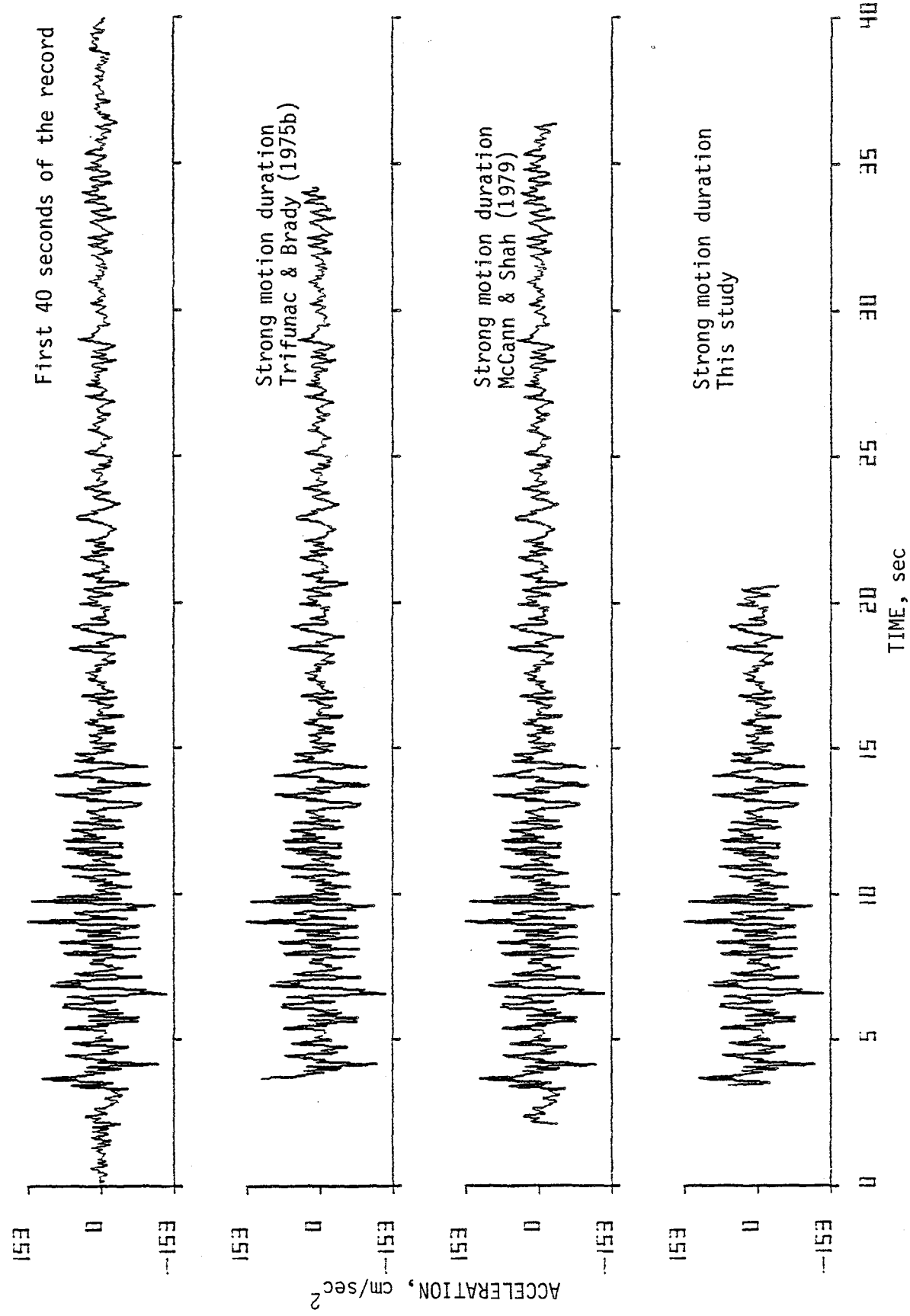

FIG. 3.3. Comparison of strong motion duration for Kern County, California Earthquake, July 21, 1952, Taft - component N21E.

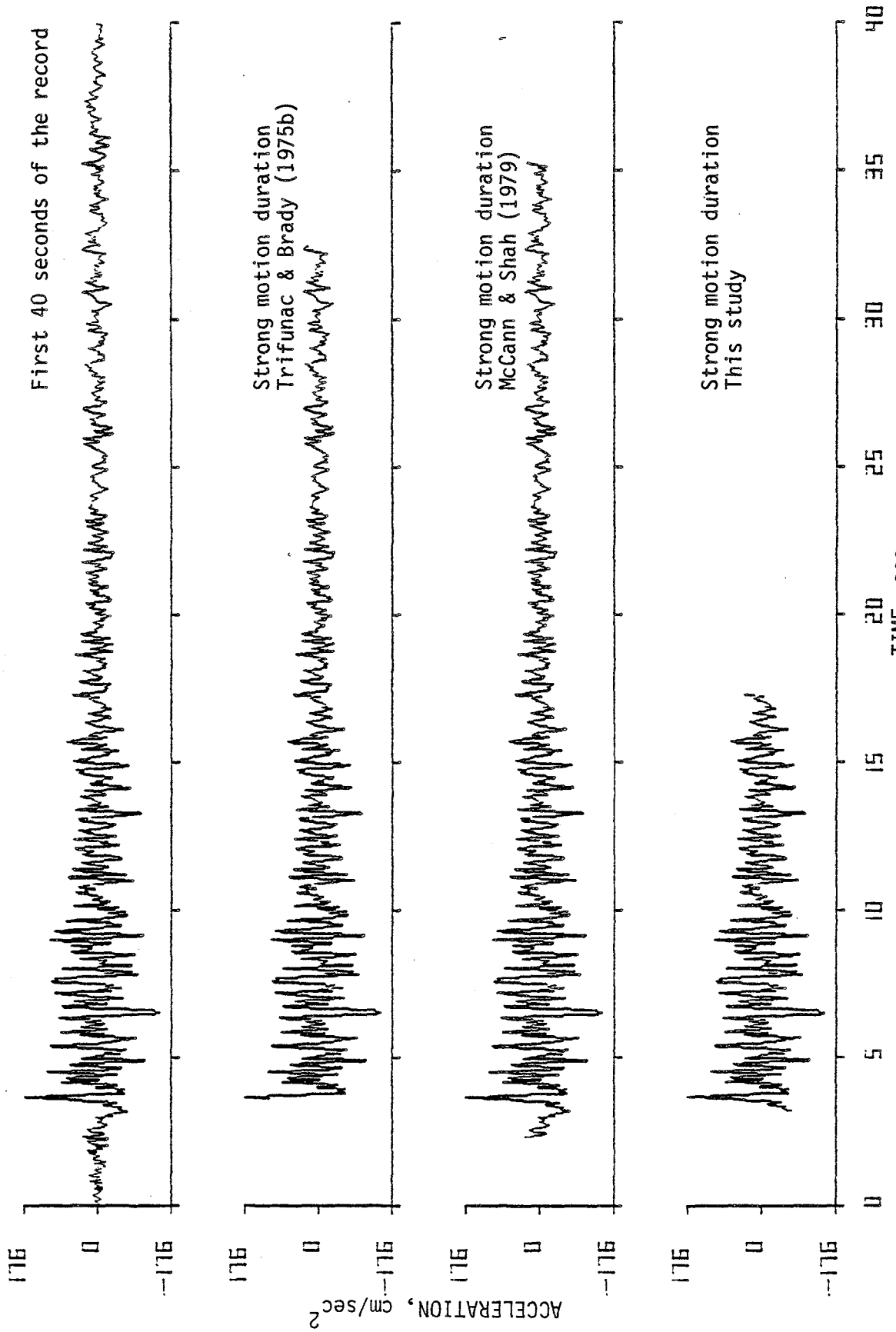

FIG. 3.4. Comparison of strong motion duration for Kern County, California Earthquake, July 21, 1952, Taft - component S69E.

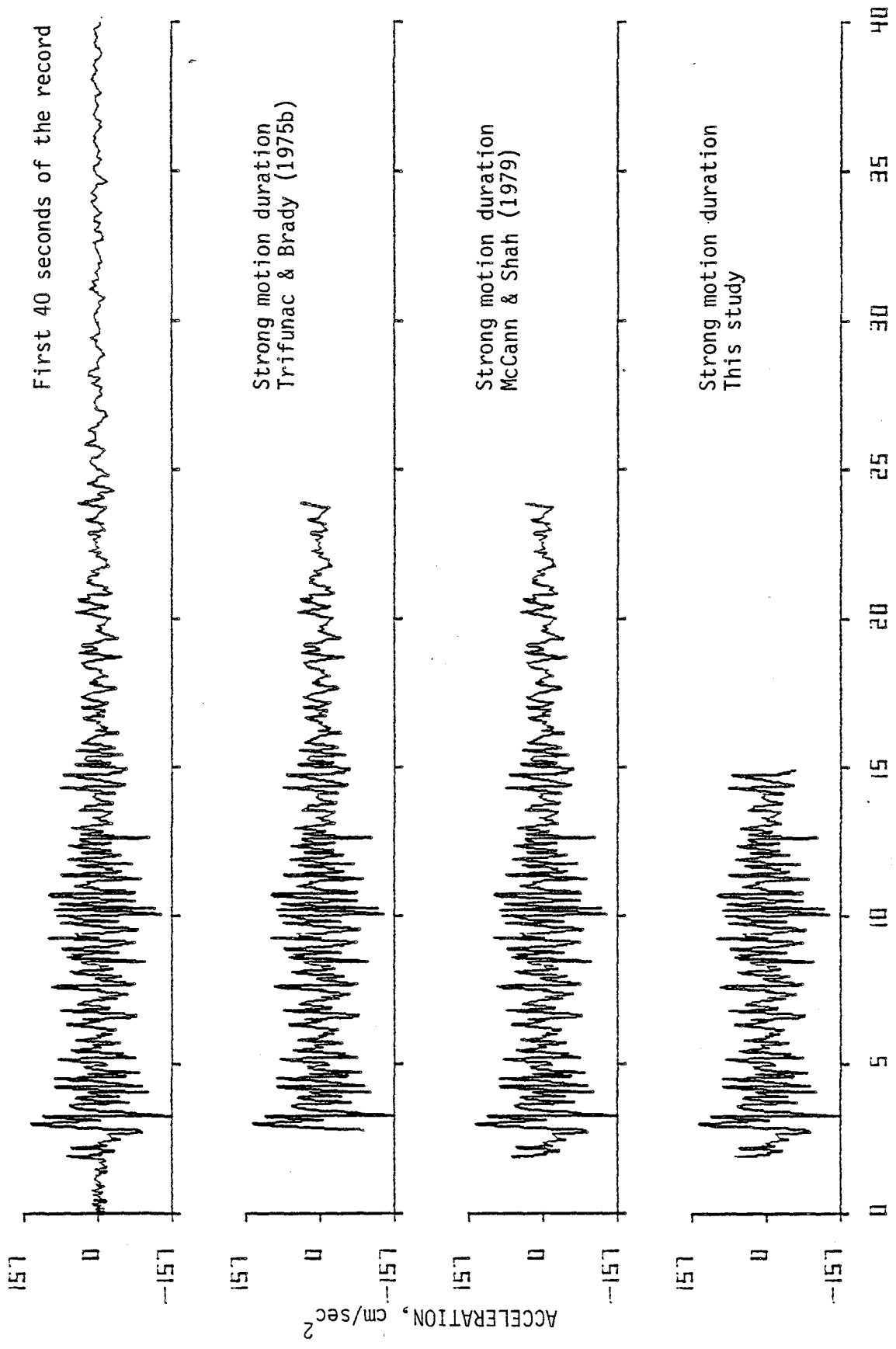

FIG. 3.5. Comparison of strong motion duration for Lower California Earthquake, December 30, 1934, El Centro - component S00W.

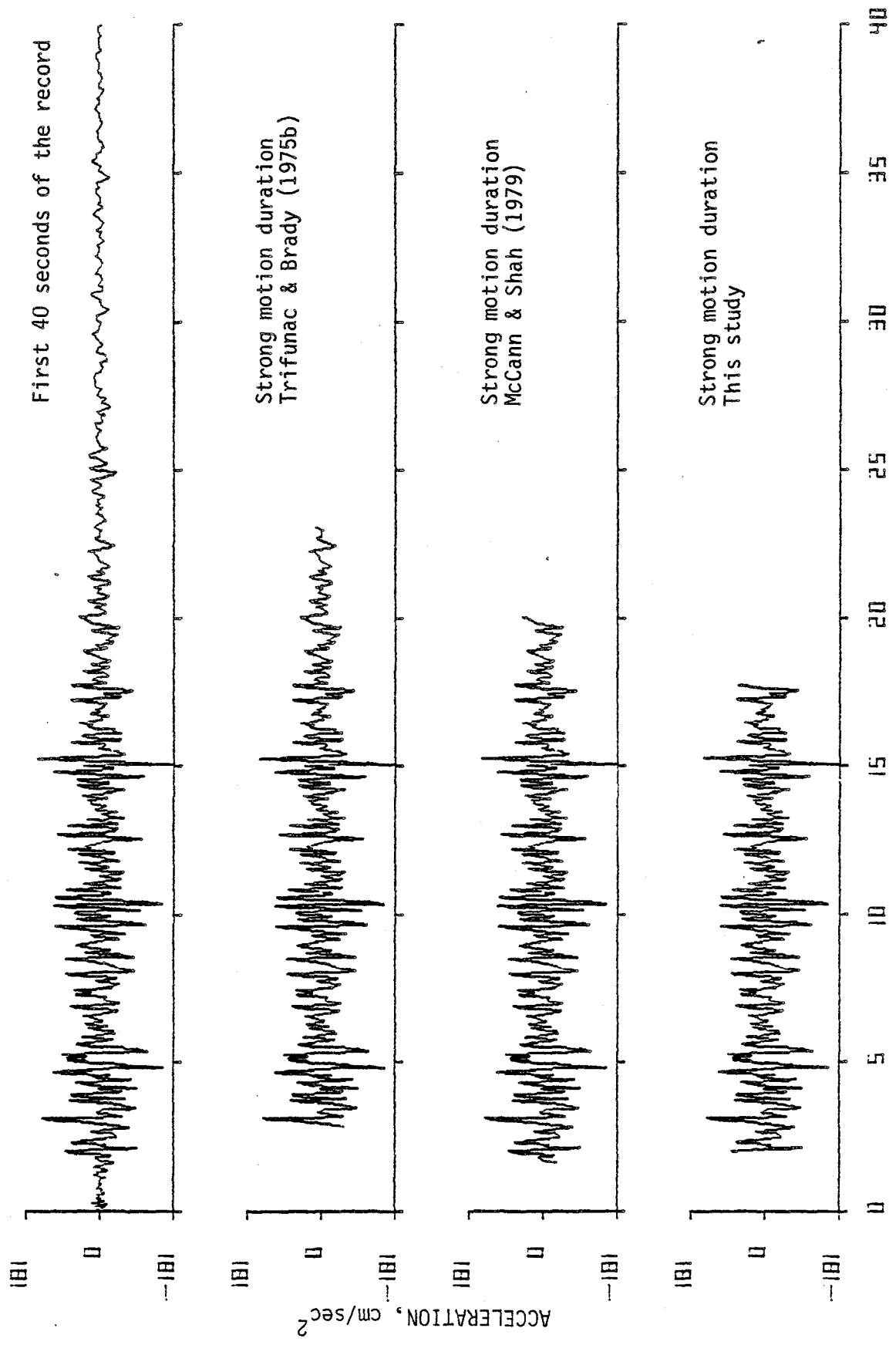

FIG. 3.6. Comparison of strong motion duration for Lower California Earthquake, December 30, 1934, El Centro - component S90W.

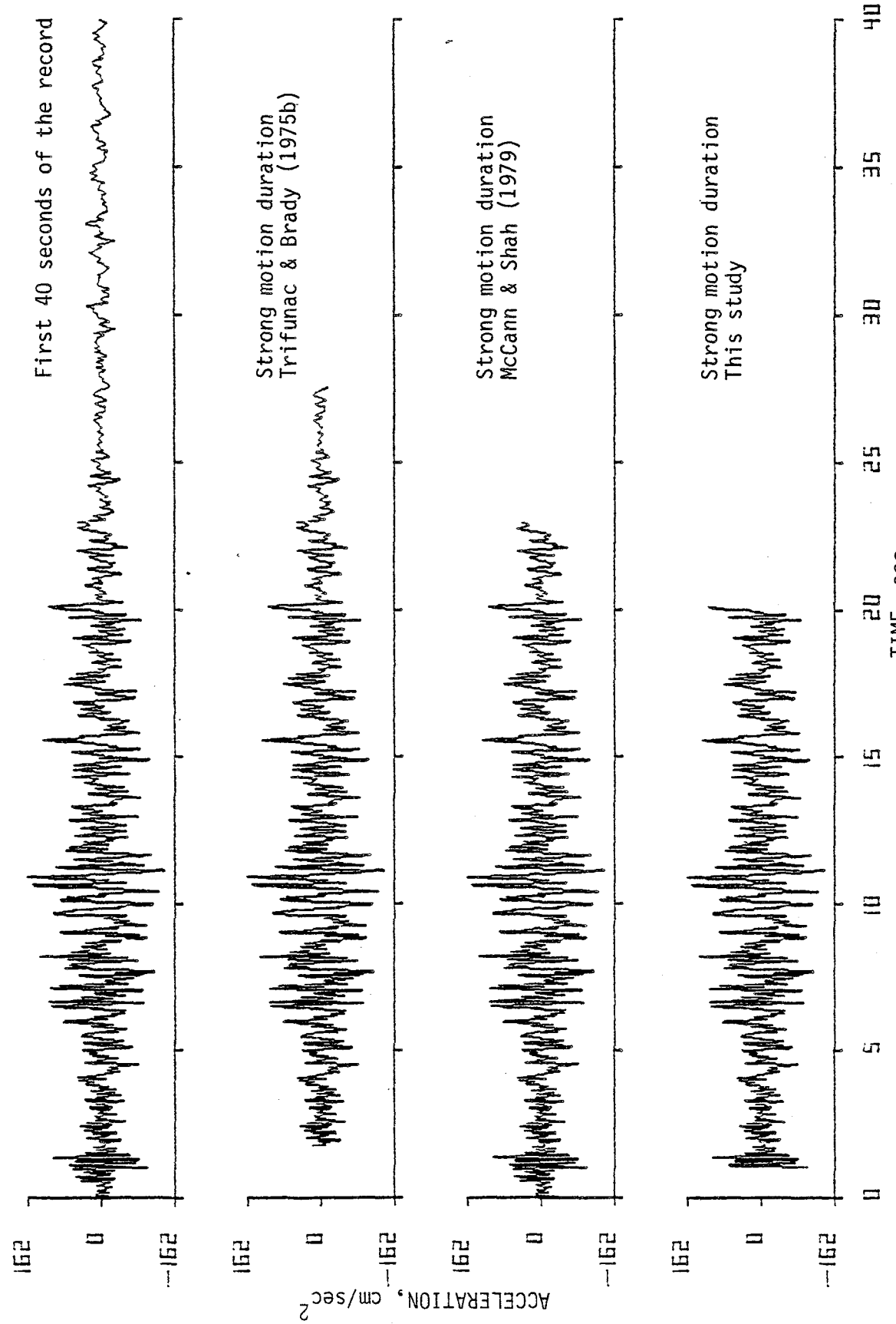

FIG. 3.7. Comparison of strong motion duration for Western Washington Earthquake, April 13, 1949, Olympia - component N04W.

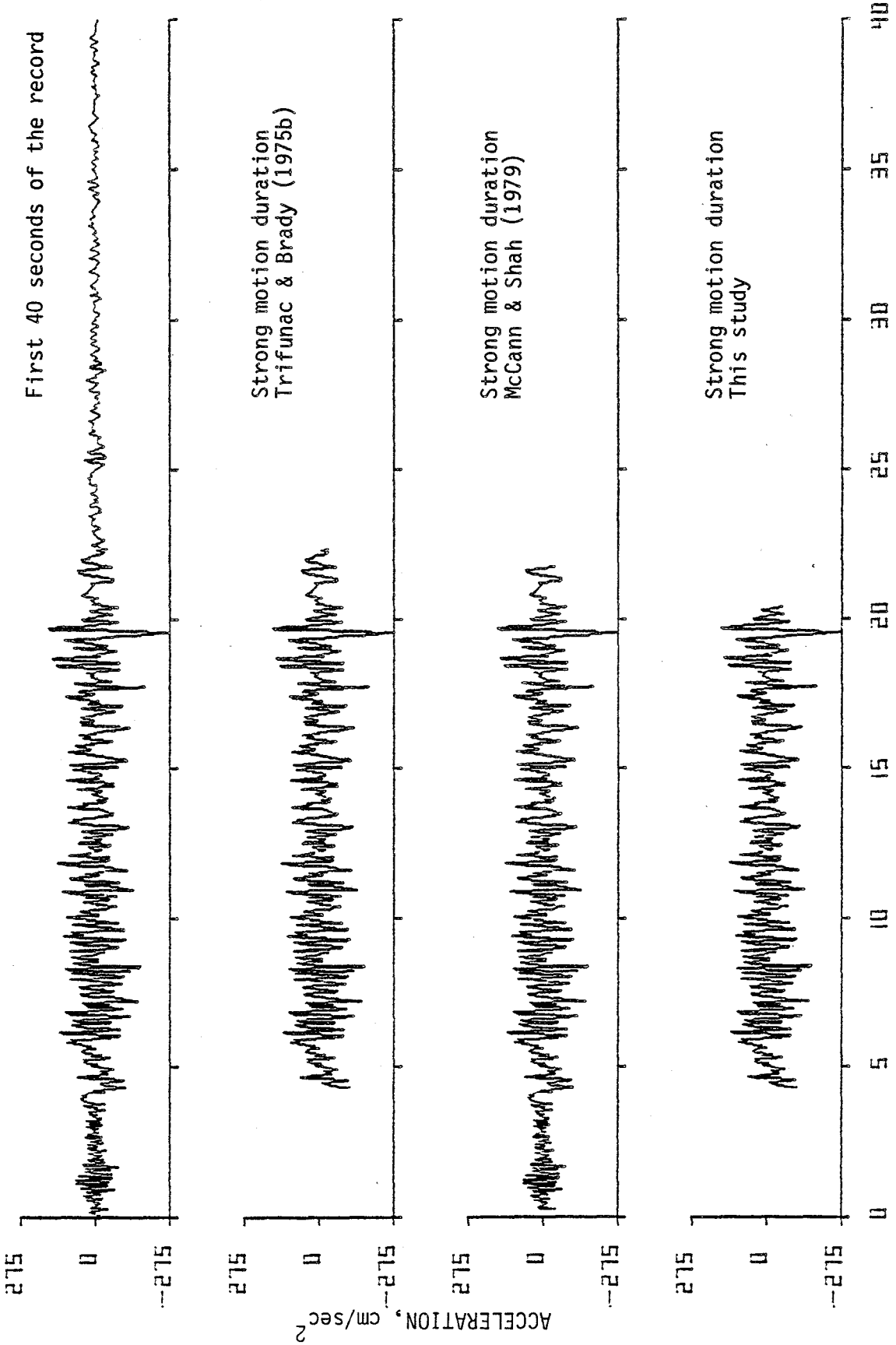

FIG. 3.8. Comparison of strong motion duration for Western Washington Earthquake, April 13, 1949, Olympia - component N86E.

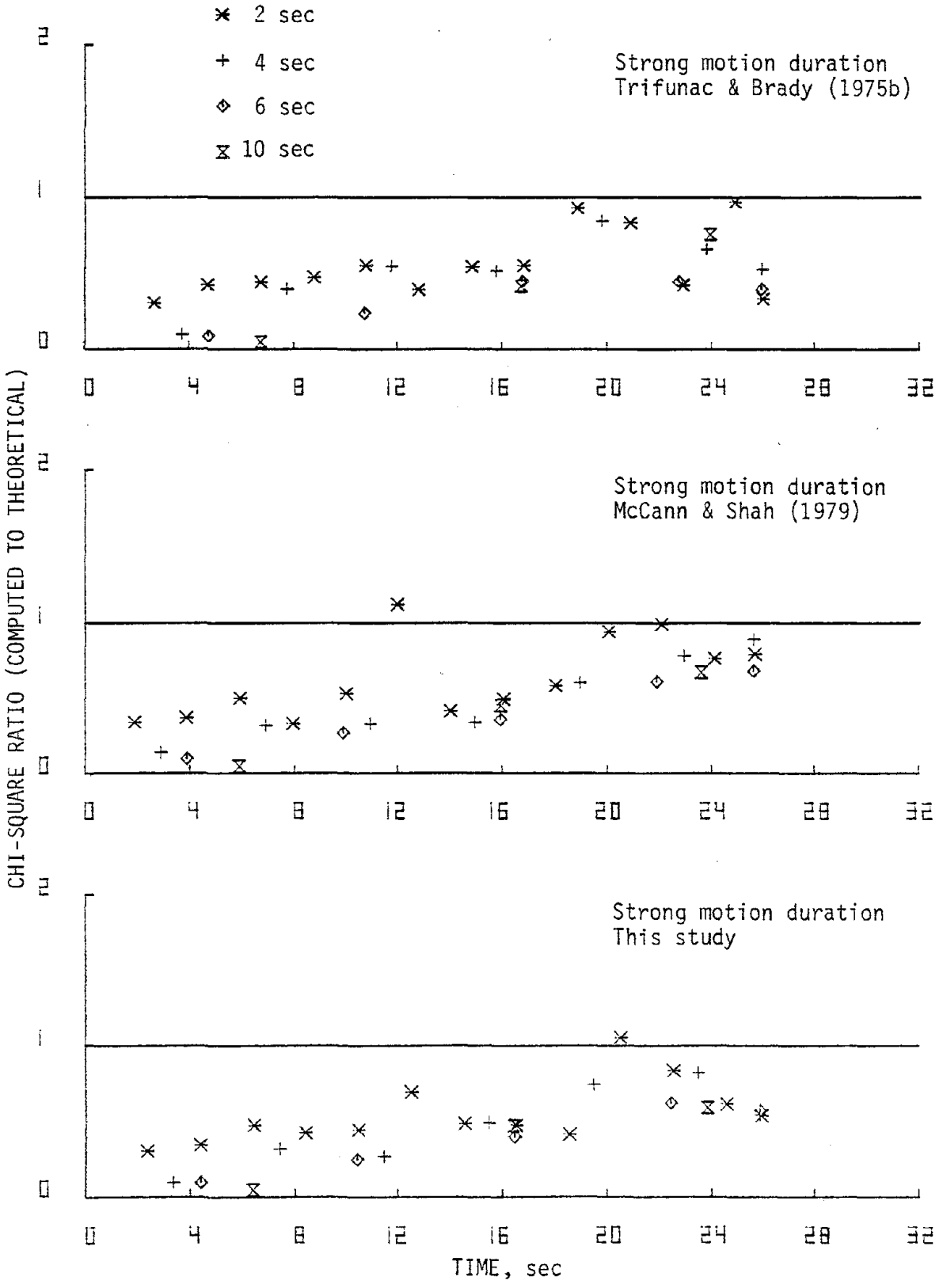

FIG. 3.9. Equivalent spectra test for 2, 4, 6 and 10 second long segments (El Centro 1940, S00E).

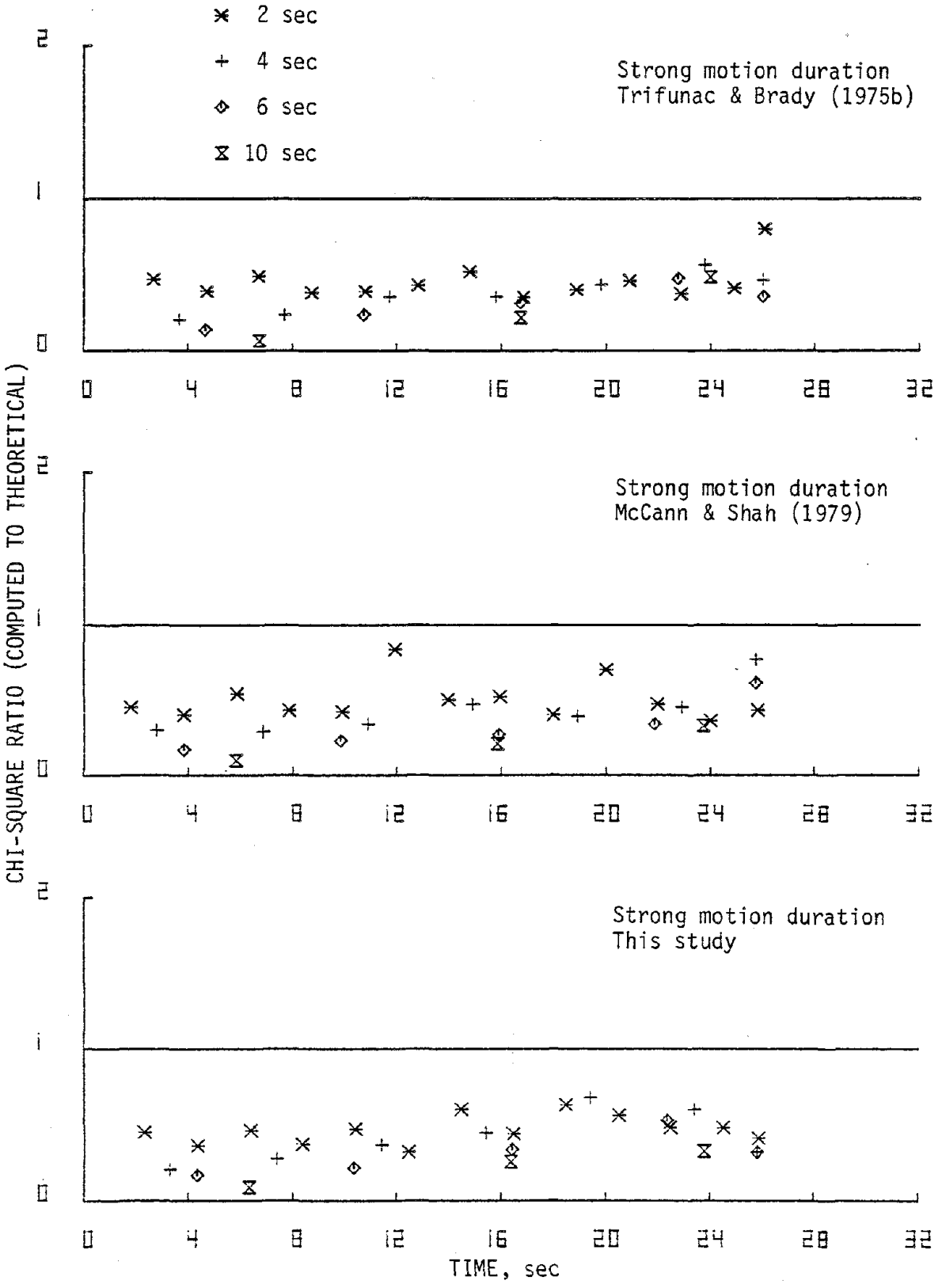

FIG. 3.10. Equivalent spectra test for 2, 4, 6 and 10 second long segments (El Centro 1940, S90W).

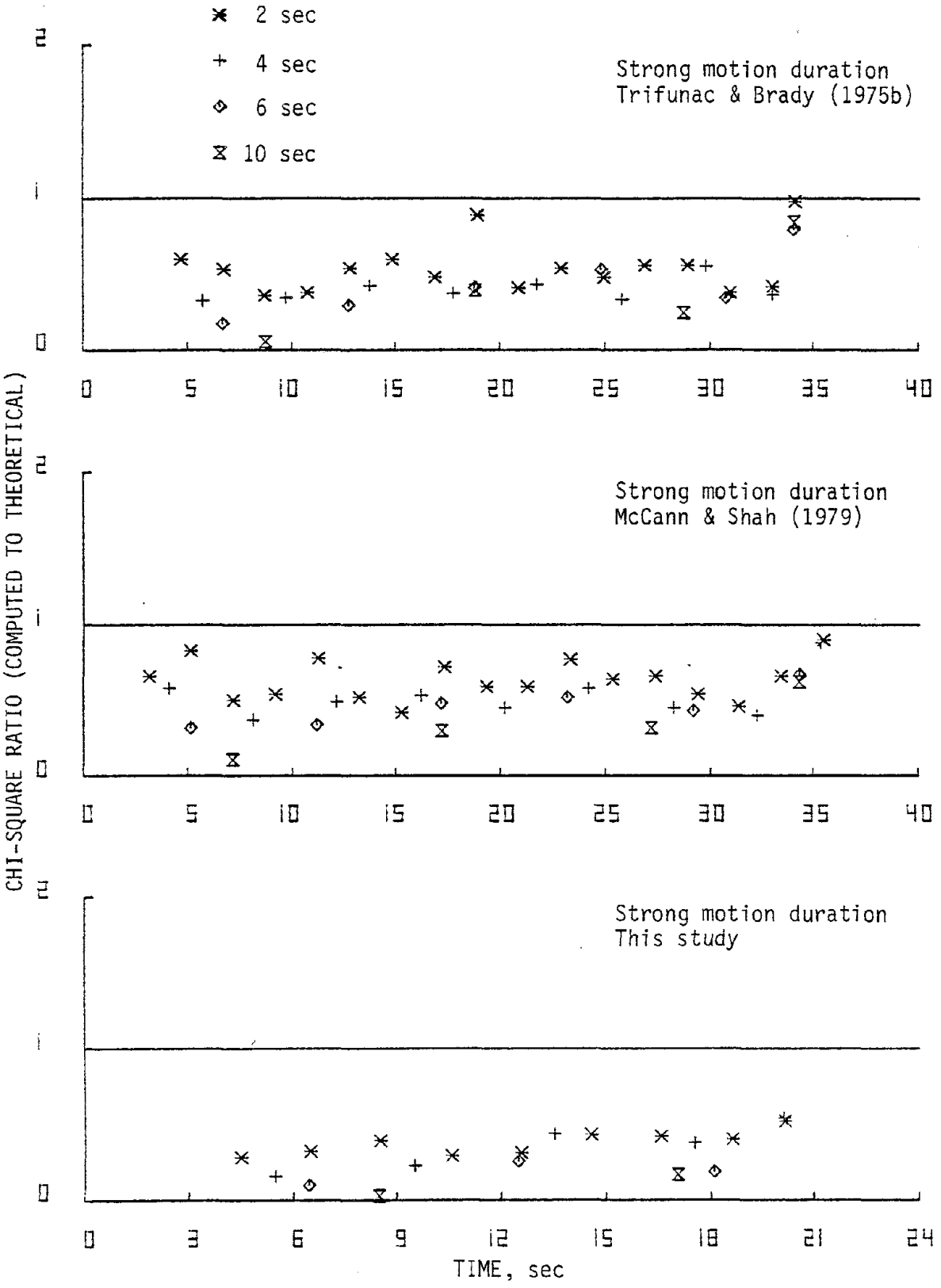

FIG. 3.11. Equivalent spectra test for 2, 4, 6 and 10 second long segments (Taft 1952, N21E).

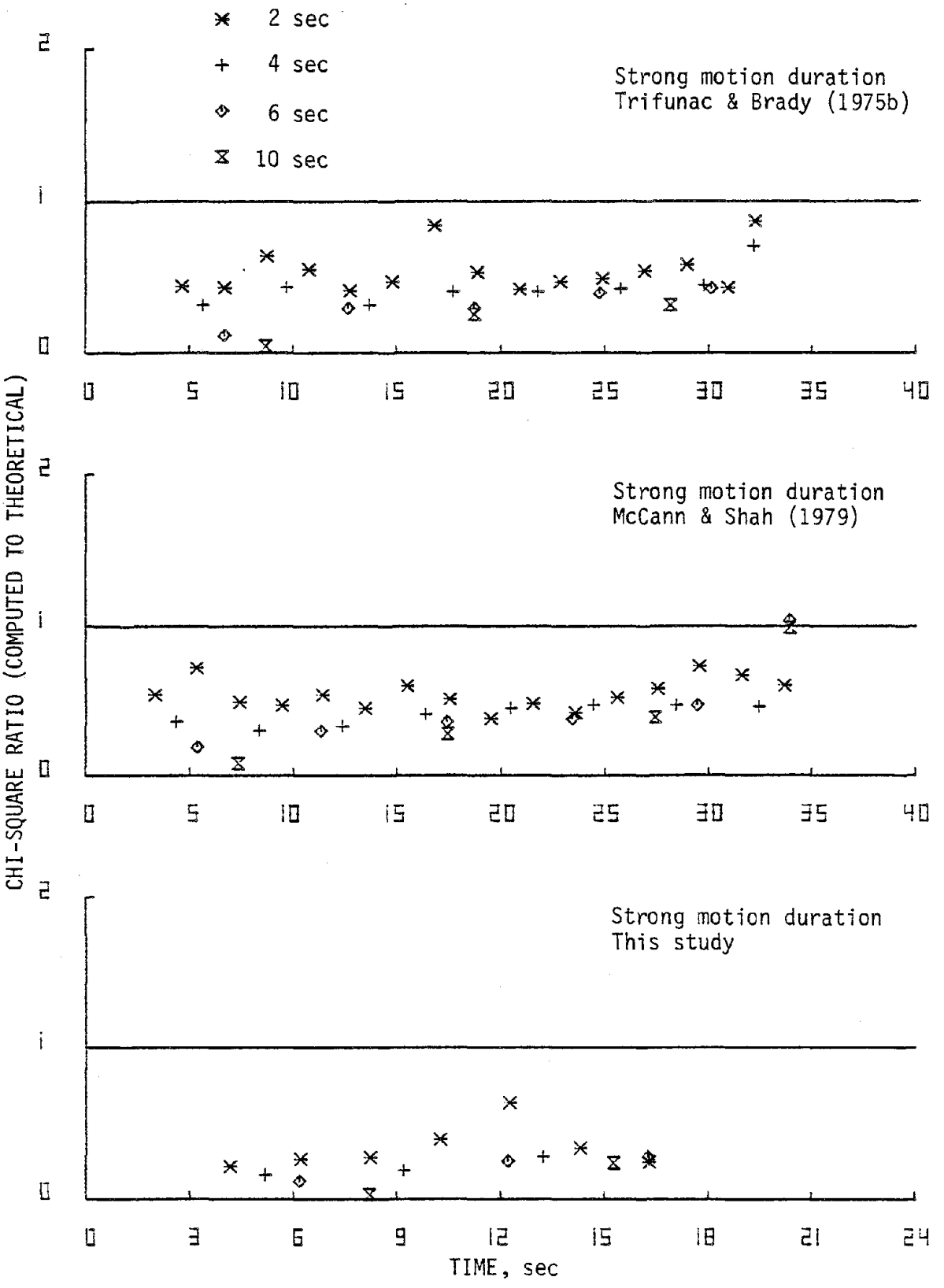

FIG. 3.12. Equivalent spectra test for 2, 4, 6 and 10 second long segments (Taft 1952, S69E).

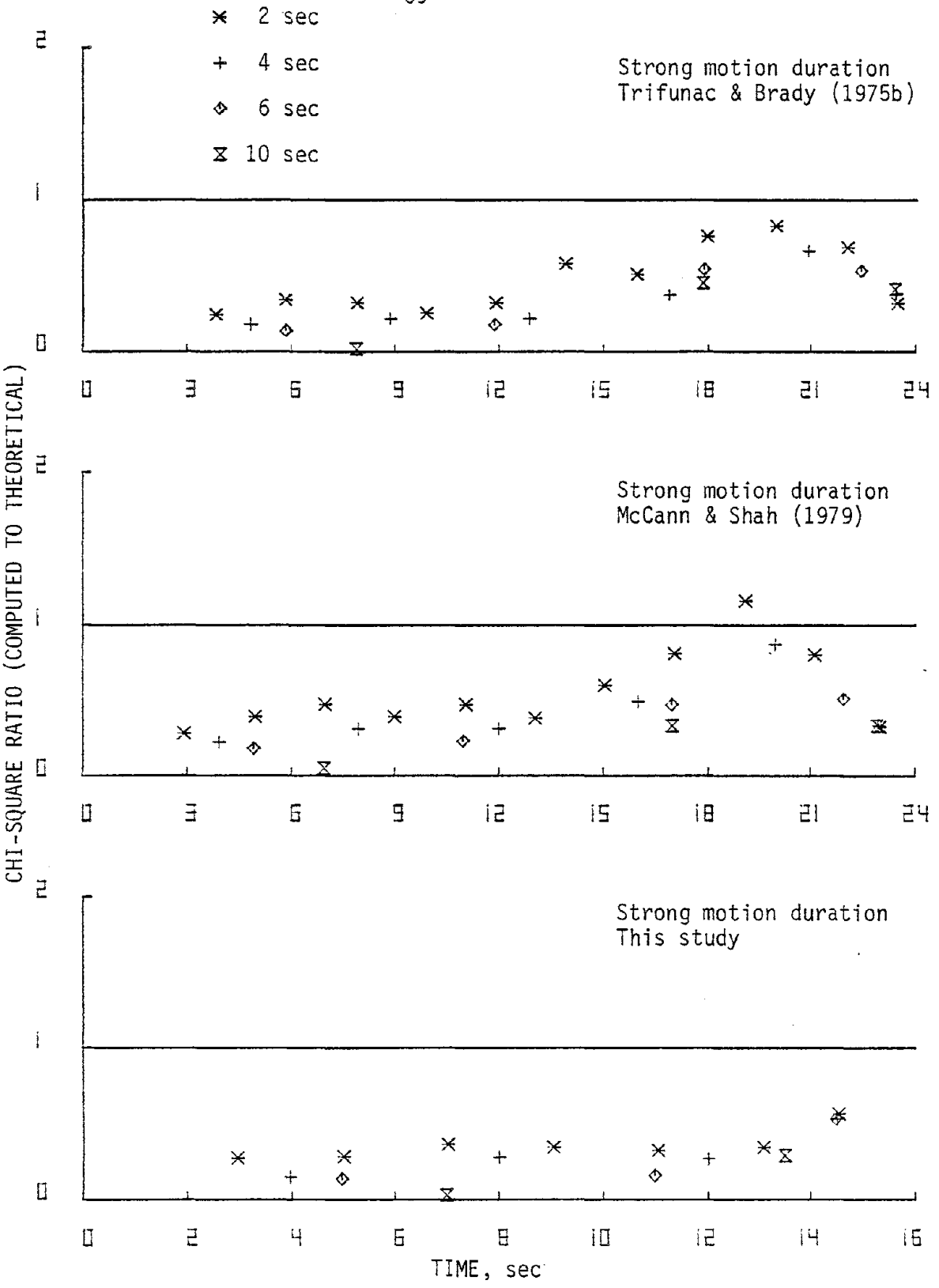

FIG. 3.13. Equivalent spectra test for 2, 4, 6 and 10 second long segments (El Centro 1934, S00W).

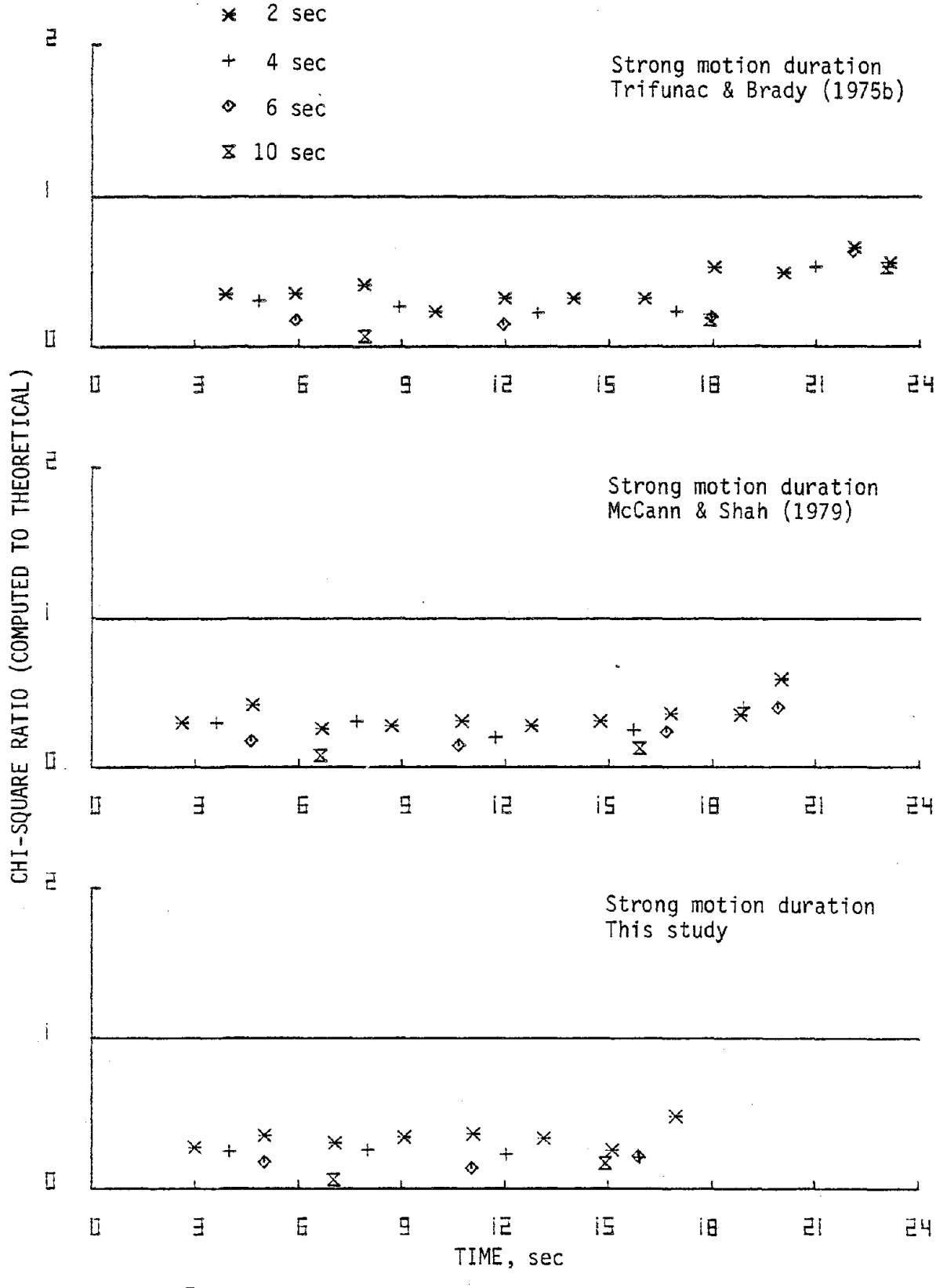

FIG. 3.14. Equivalent spectra test for 2, 4, 6 and 10 second long segments (El Centro 1934, S90W).

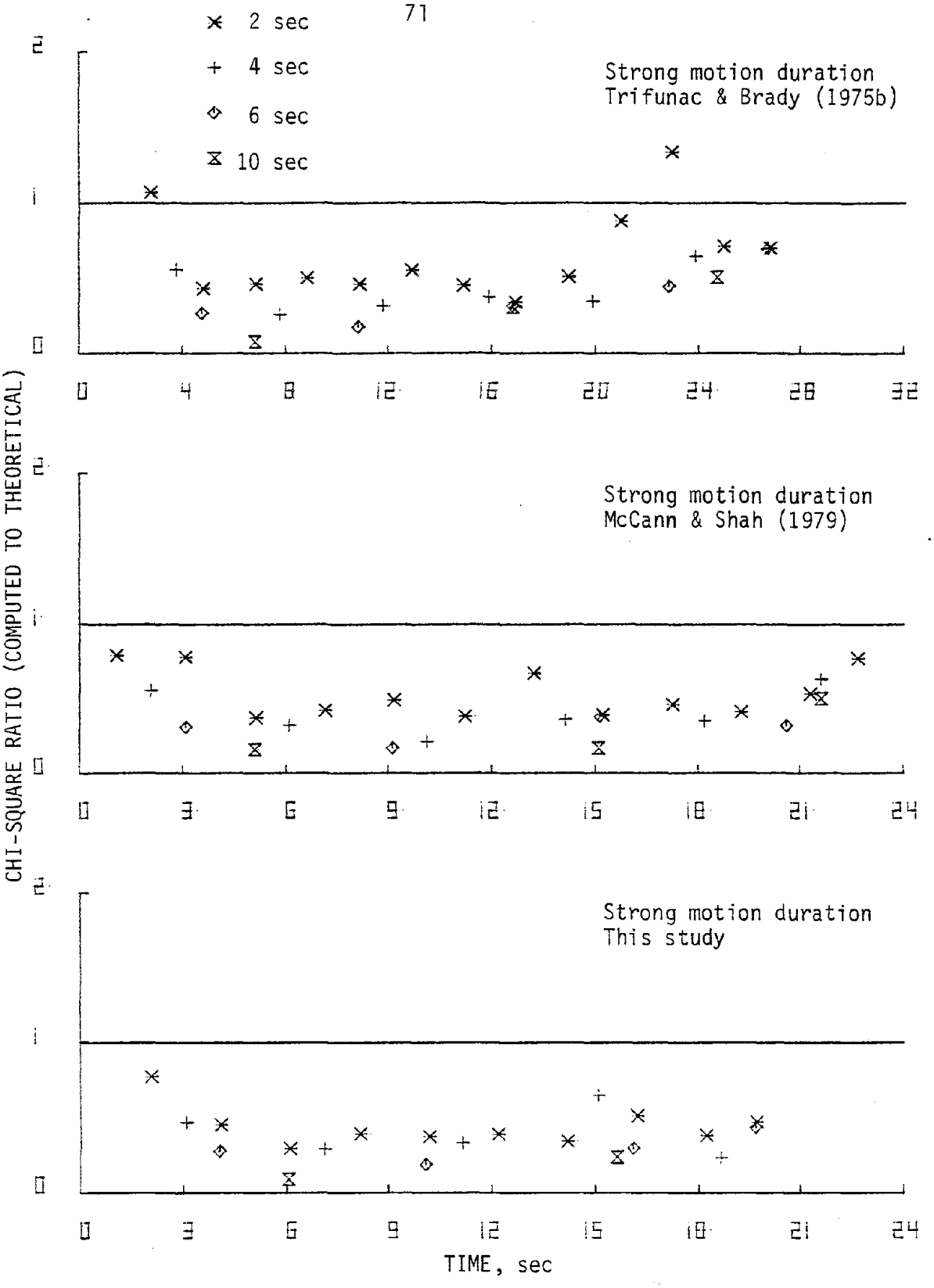

FIG. 3.15. Equivalent spectra test for 2, 4, 6 and 10 second long segments (Olympia 1949, N04W).

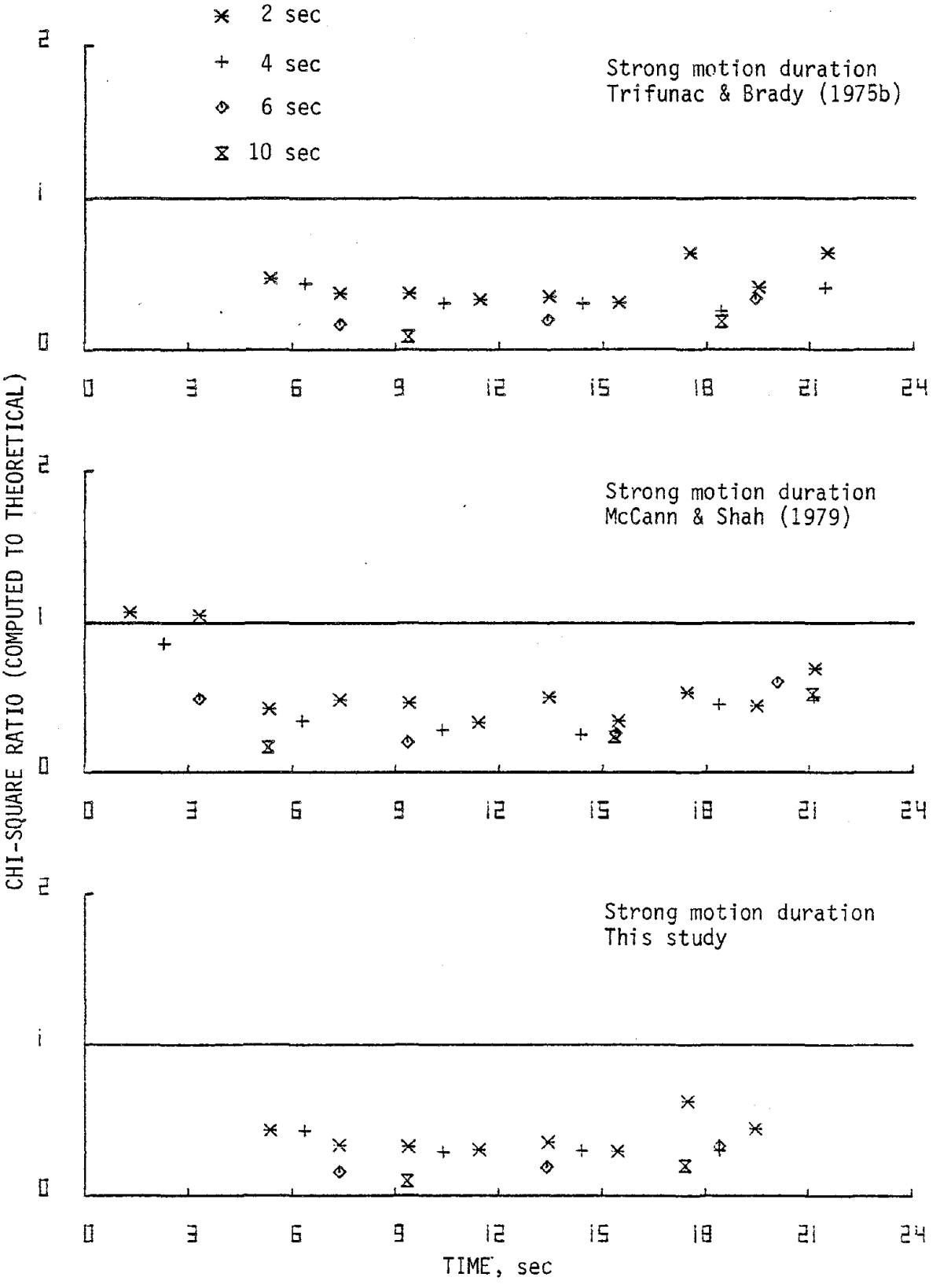

FIG. 3.16. Equivalent spectra test for 2, 4, 6 and 10 second long segments (Olympia 1949, N86E).

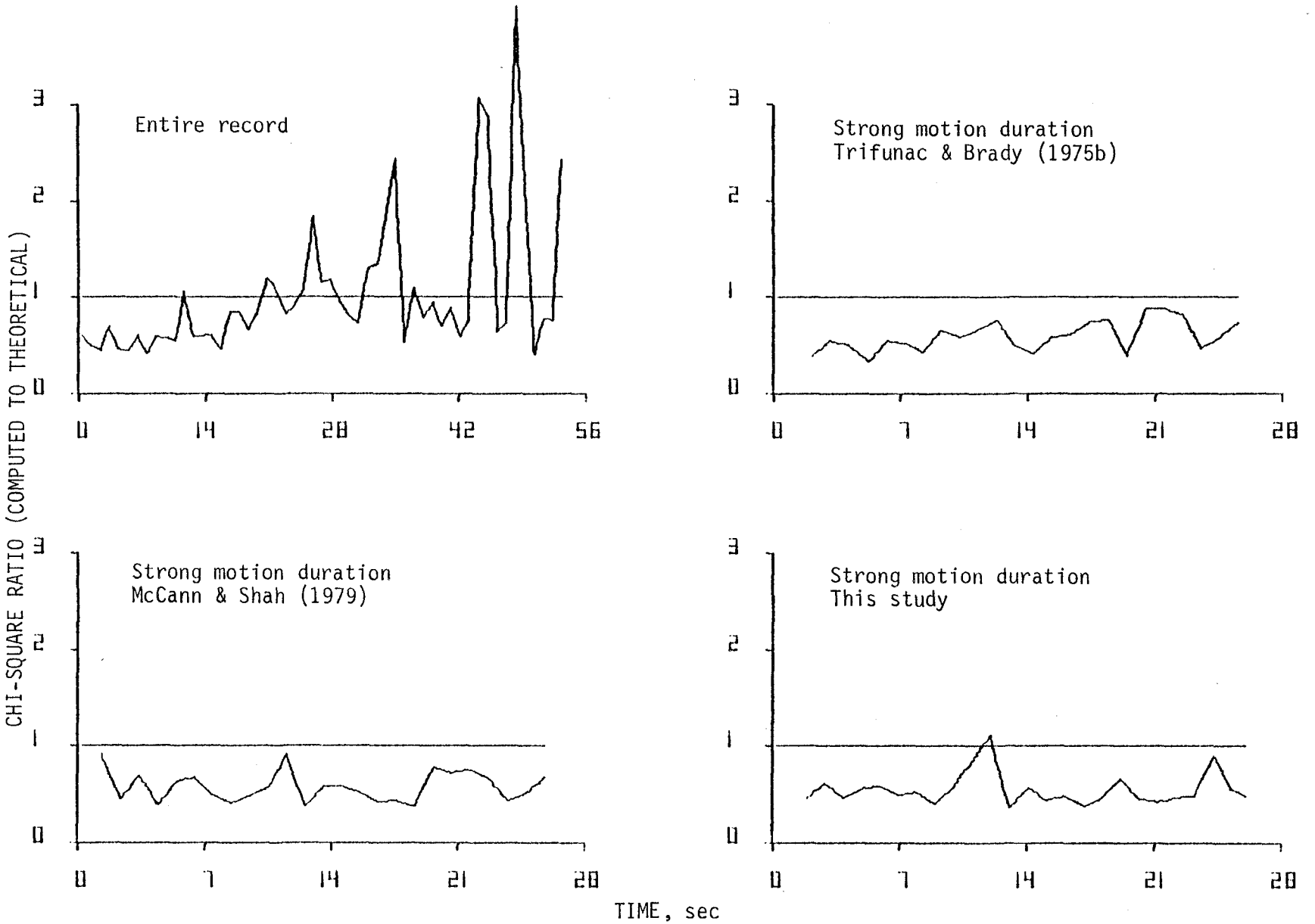

FIG. 3.17. Equivalent spectra test for 1 second long segments (El Centro 1940, S00E).

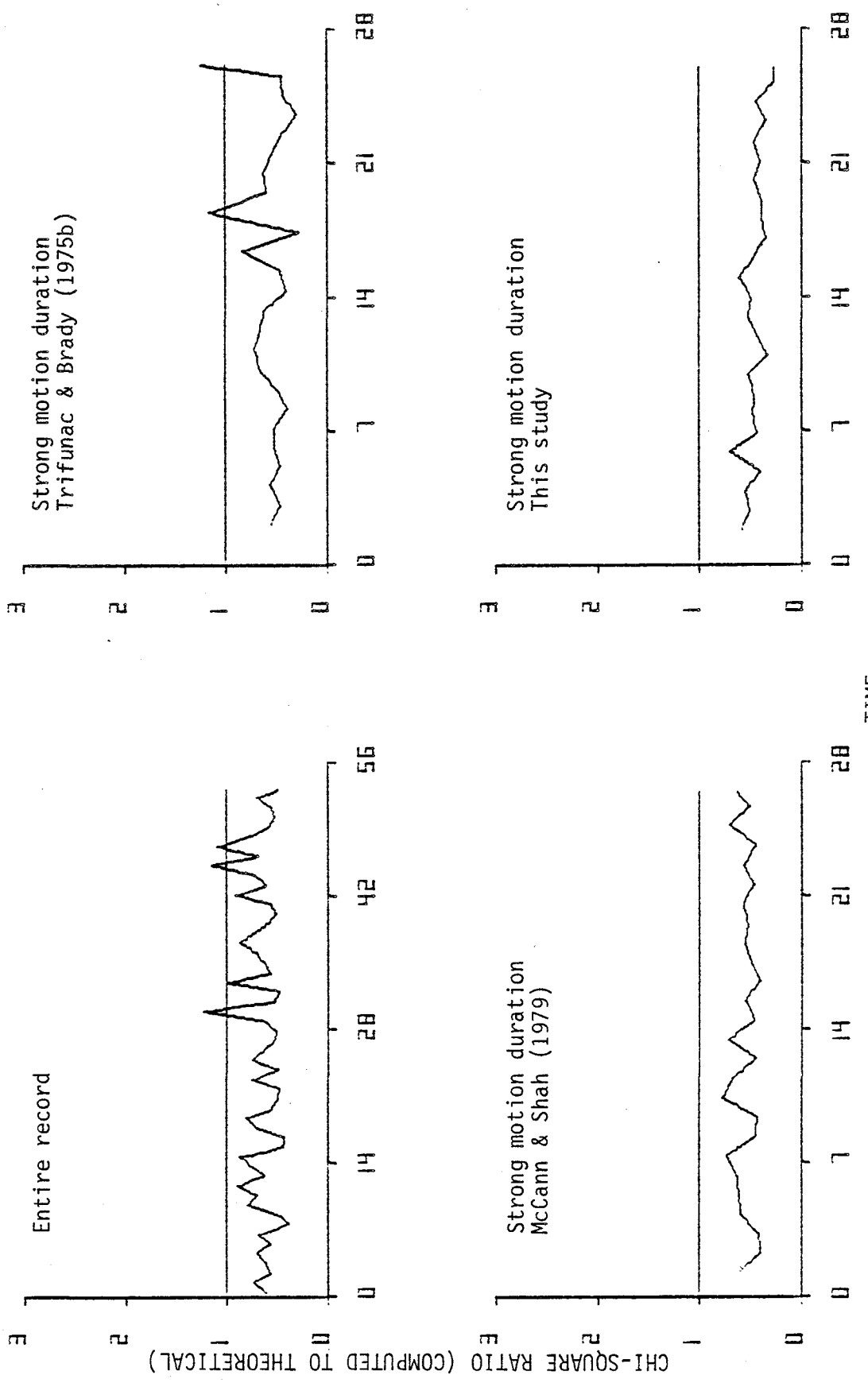

FIG. 3.18. Equivalent spectra test for 1 second long segments (El Centro 1940, S90W).

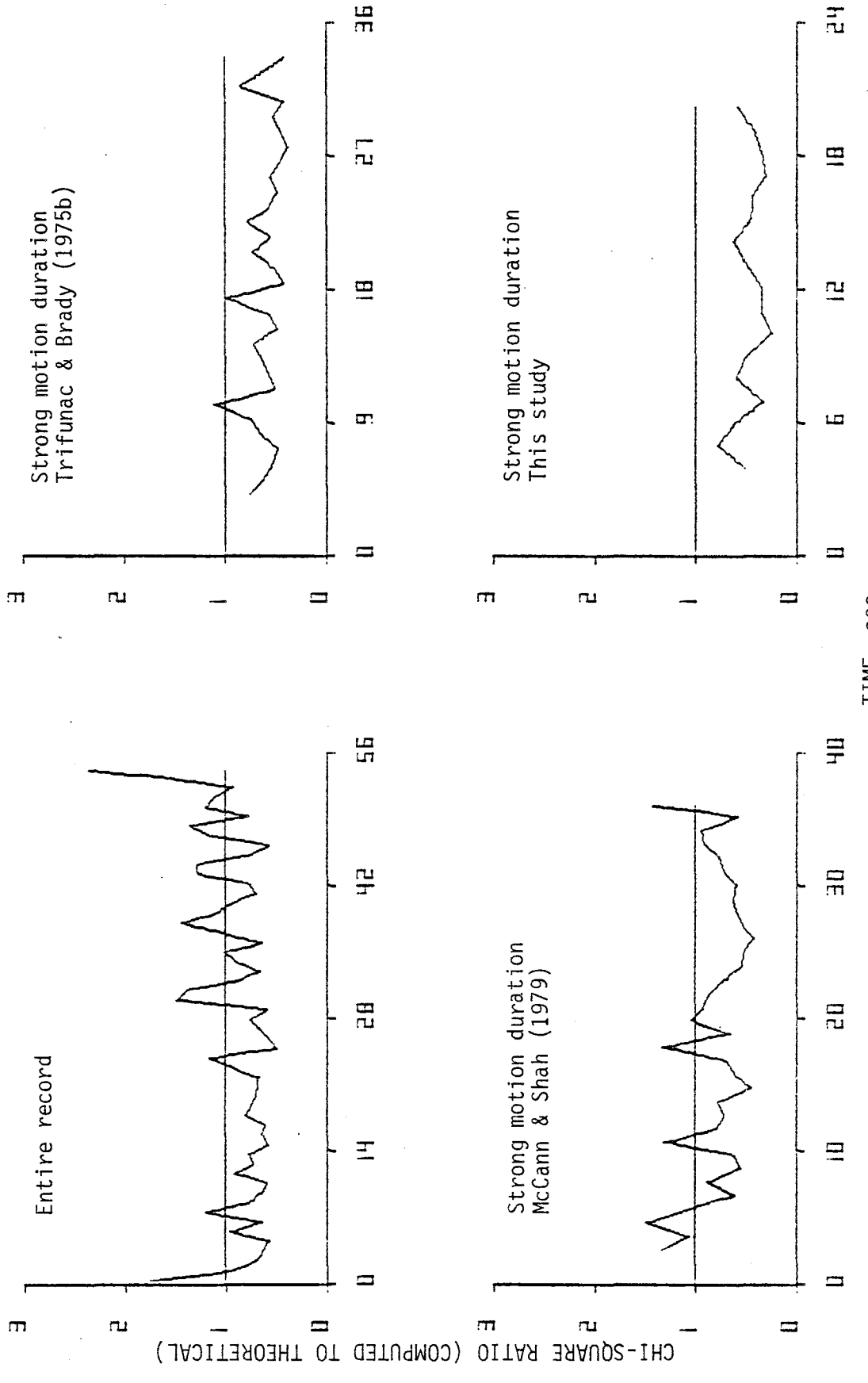

FIG. 3.19. Equivalent spectra test for 1 second long segments (Taft 1952, N21E).

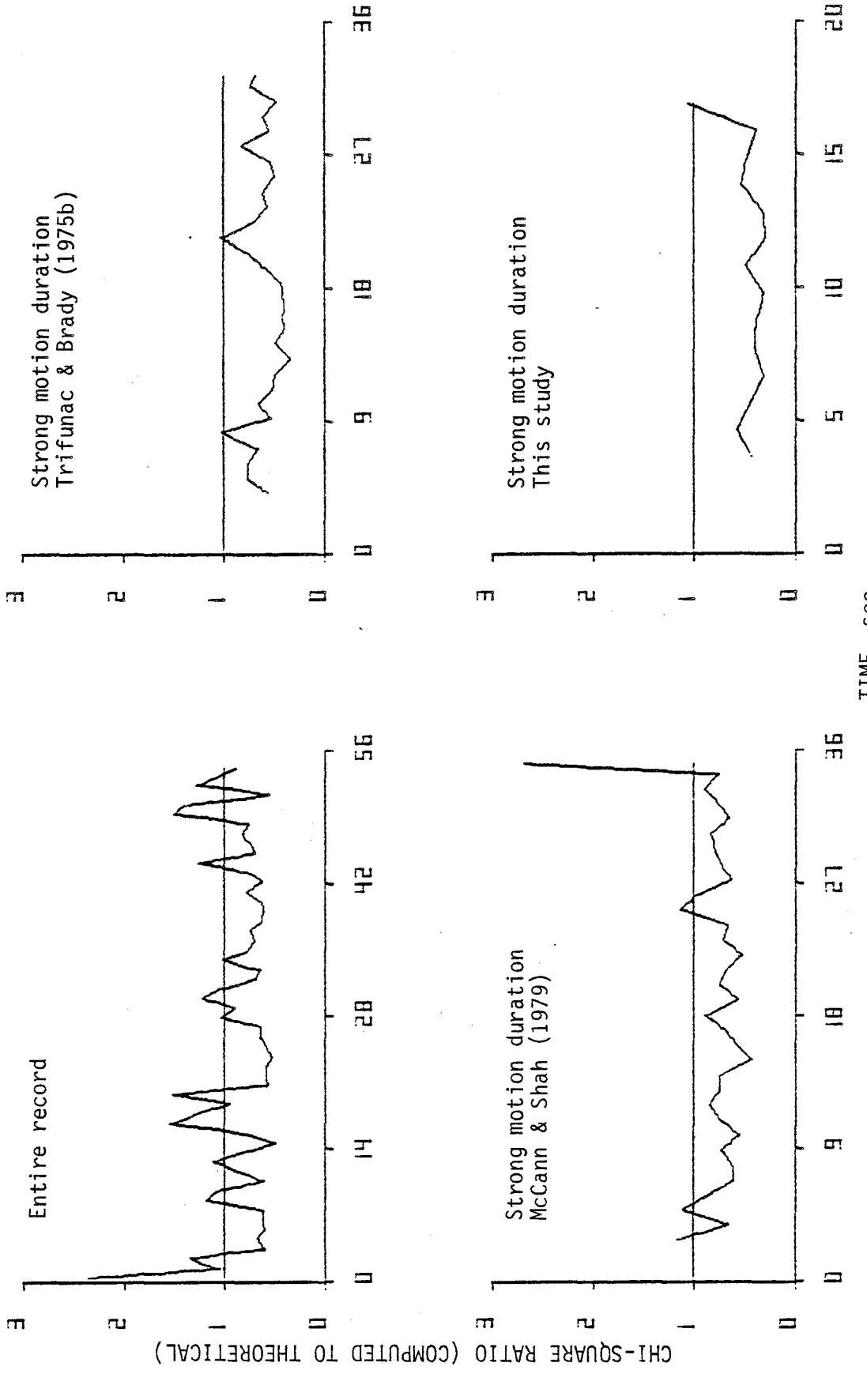

FIG. 3.20. Equivalent spectra test for 1 second long segments (Taft 1952, S69E).

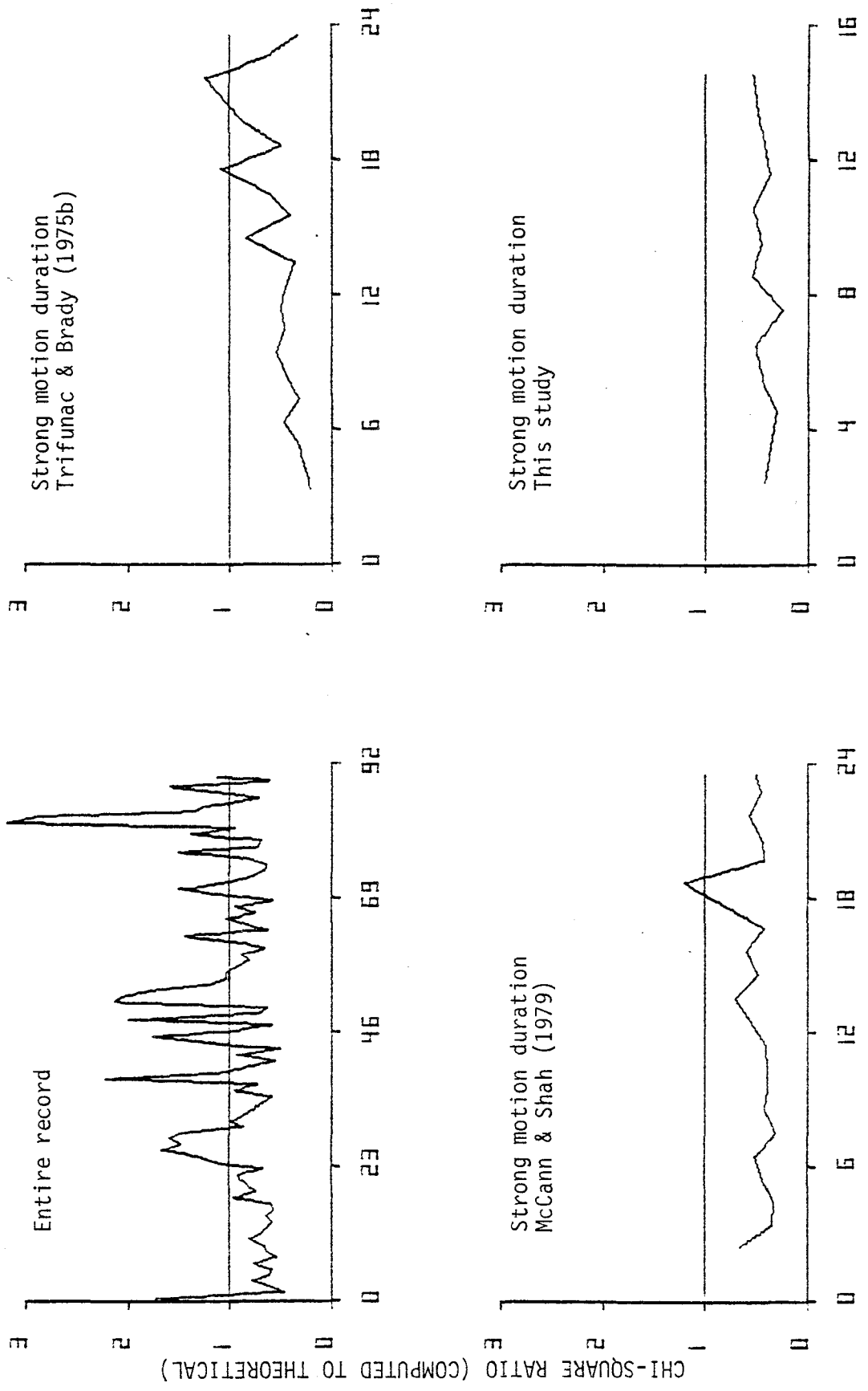

FIG. 3.21. Equivalent spectra test for 1 second long segments (El Centro 1934, S00W).

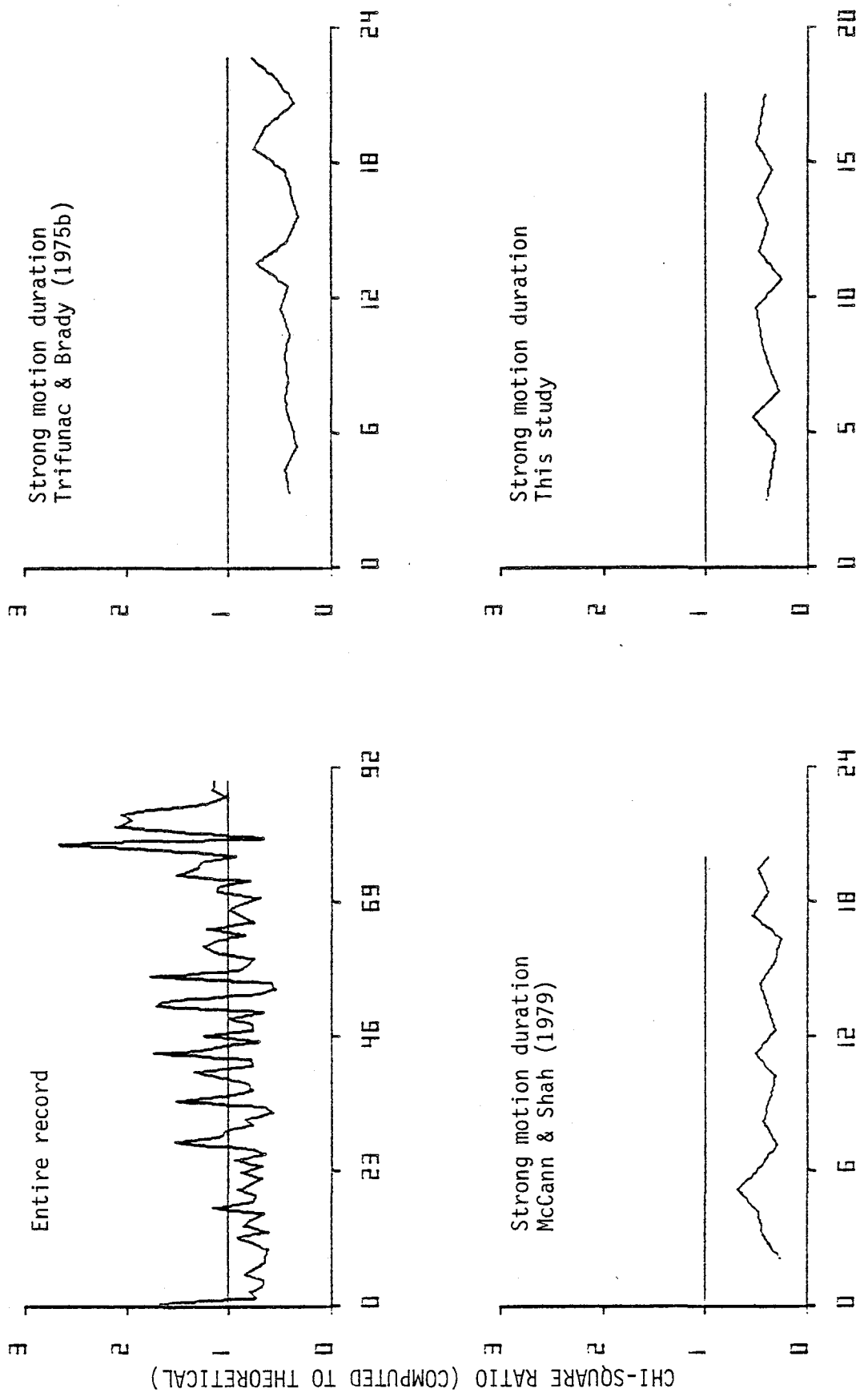

FIG. 3.22. Equivalent spectra test for 1 second long segments (El Centro 1934, S90W).

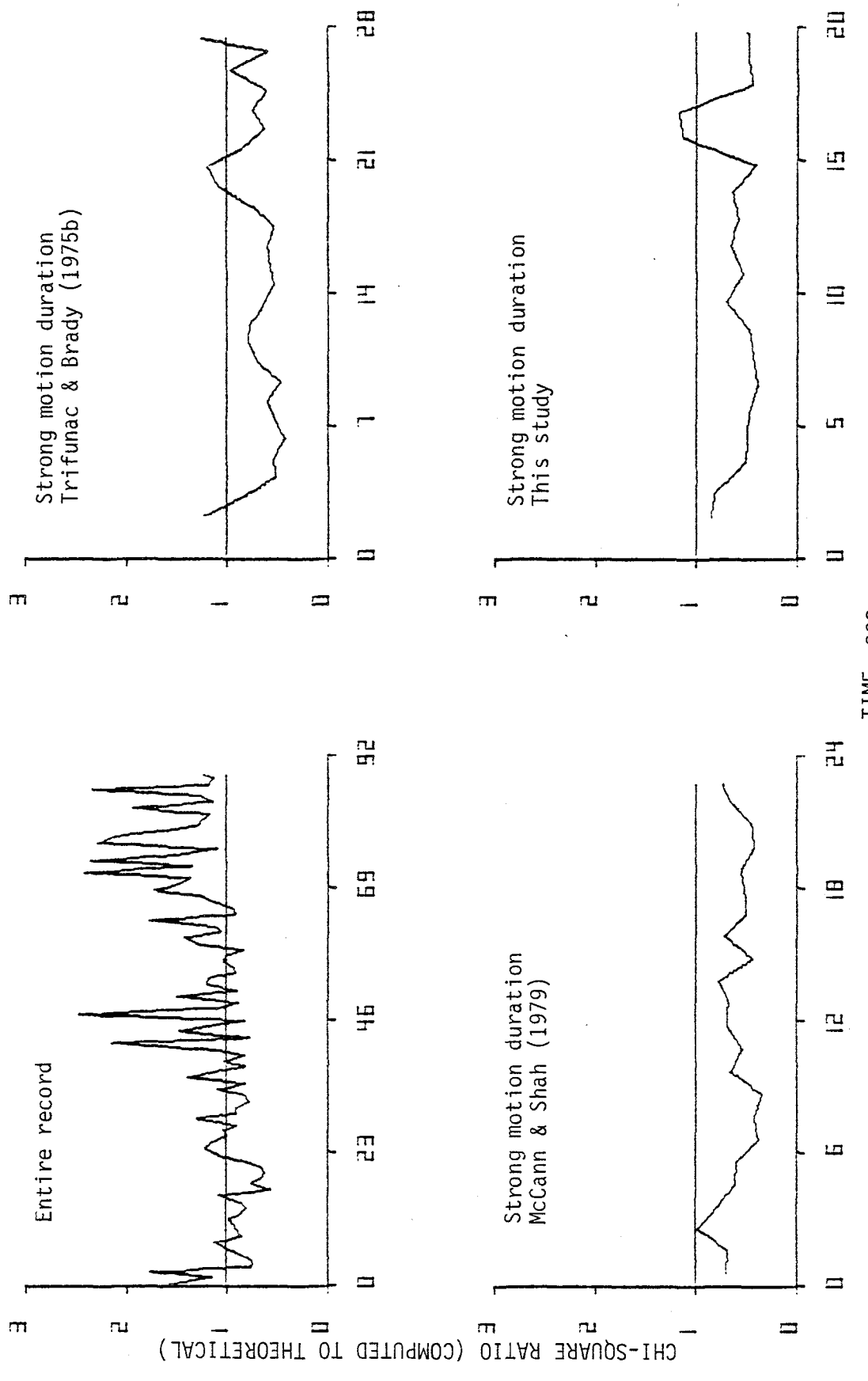

FIG. 3.23. Equivalent spectra test for 1 second long segments (Olympia 1949, N04W).

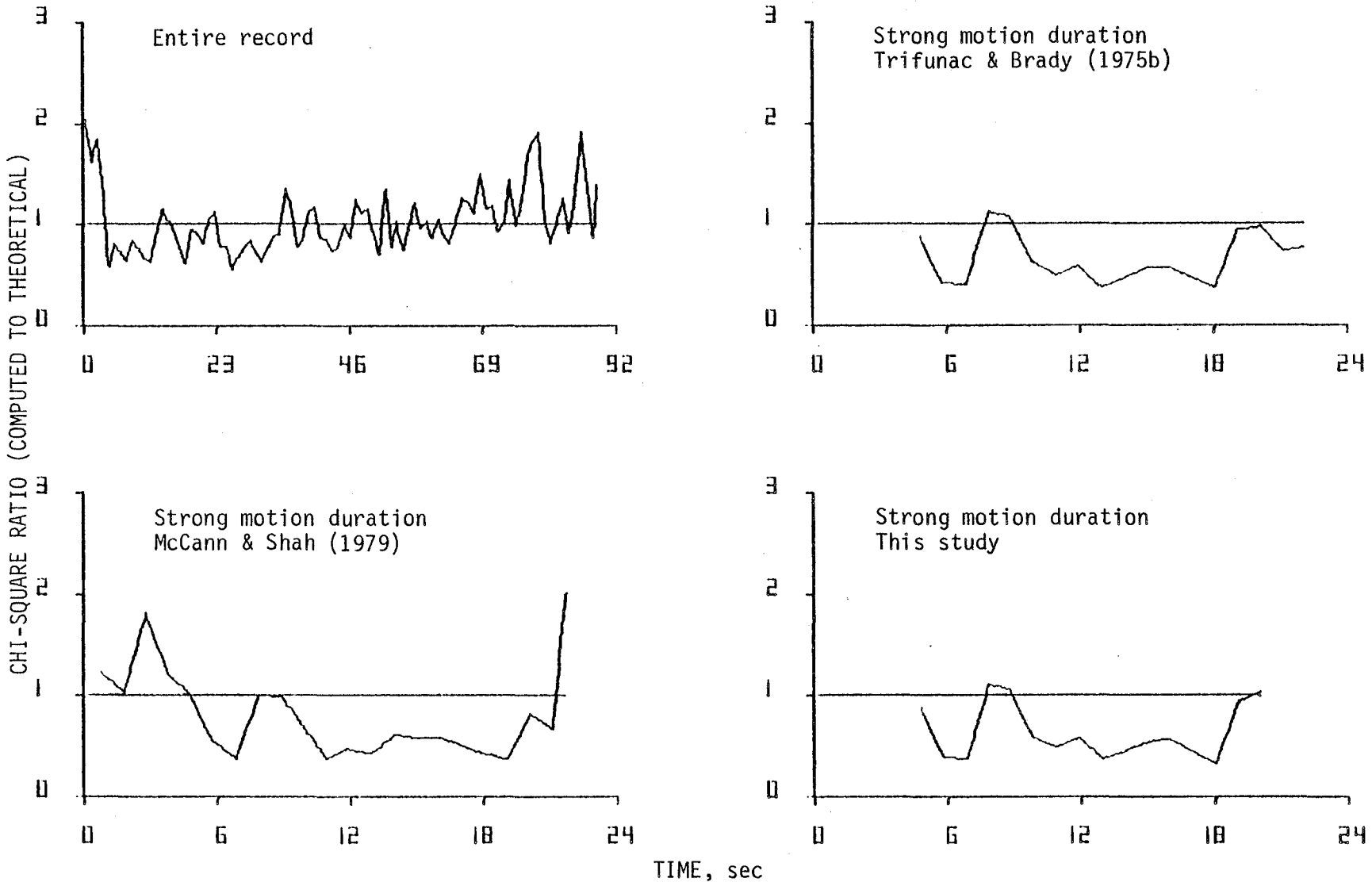

FIG. 3.24. Equivalent spectra test for 1 second long segments (Olympia 1949, N86E).

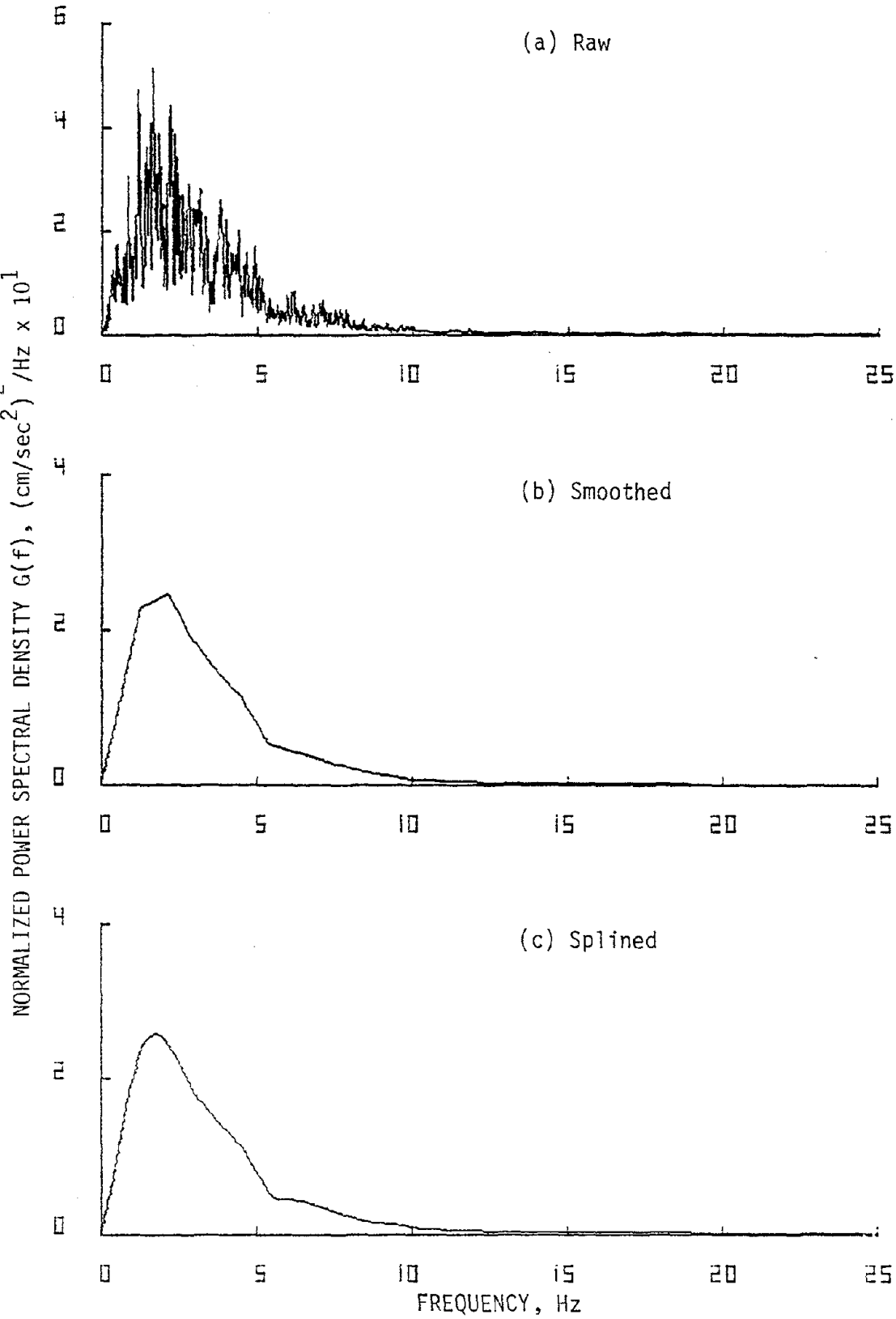

FIG. 3.25. Power spectral density for the ensemble of the eight records used in the pilot study.

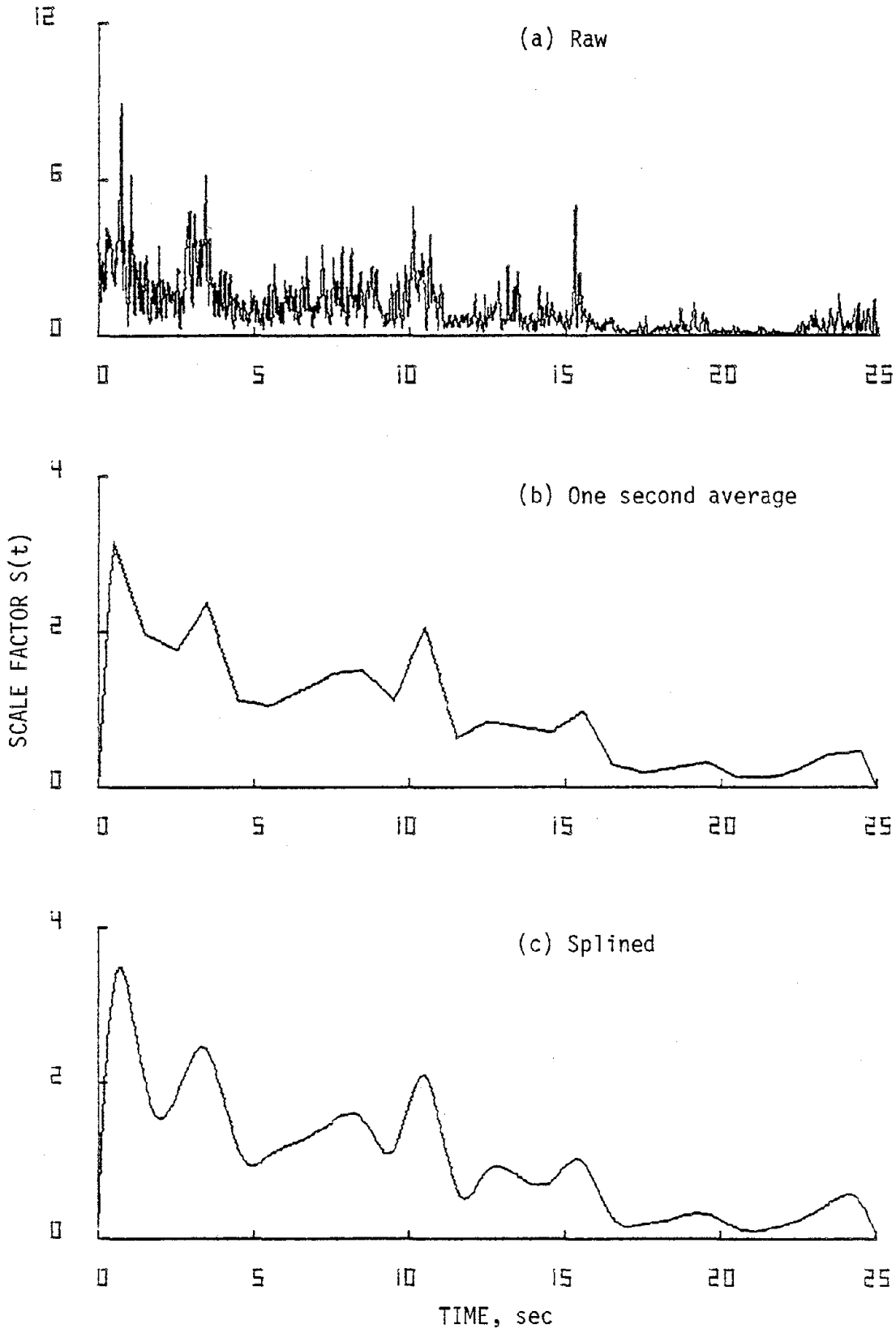

FIG. 3.26. Time variation of normalized mean square value of the ensemble of the eight records used in the pilot study.

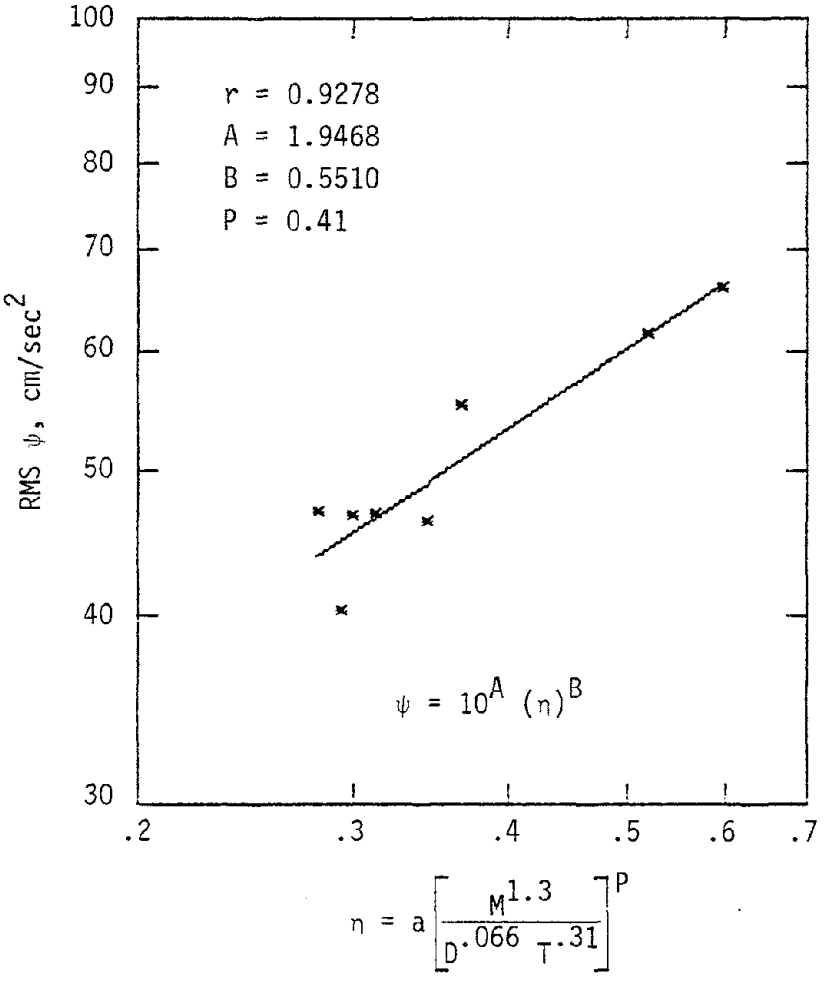

FIG. 3.27. Correlation of RMS with parameter η for eight horizontal components of recorded accelerograms.

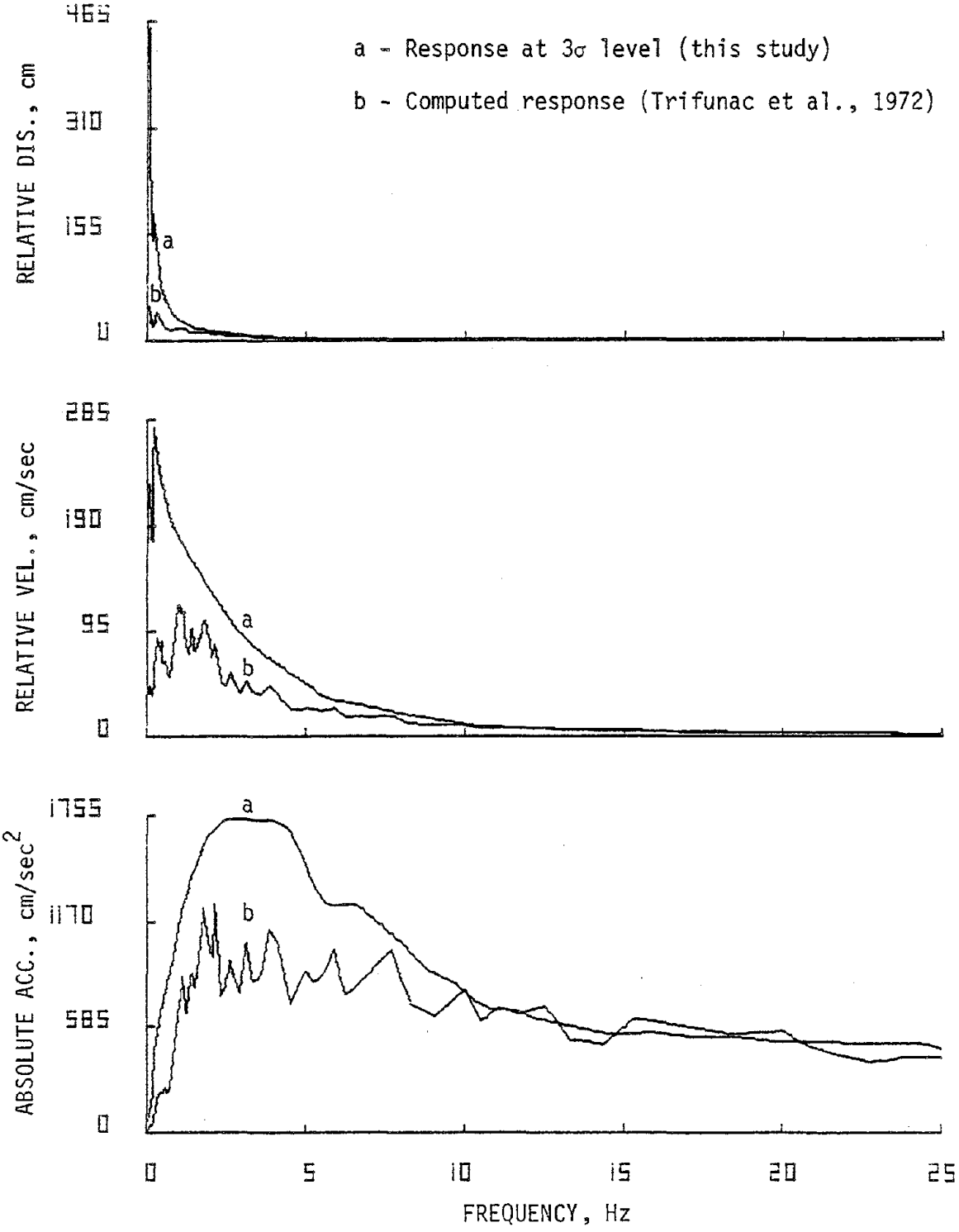

FIG. 3.28. Comparison of response for 2 percent of critical damping for S00E component of El Centro, Imperial Valley Earthquake of May 18, 1940.

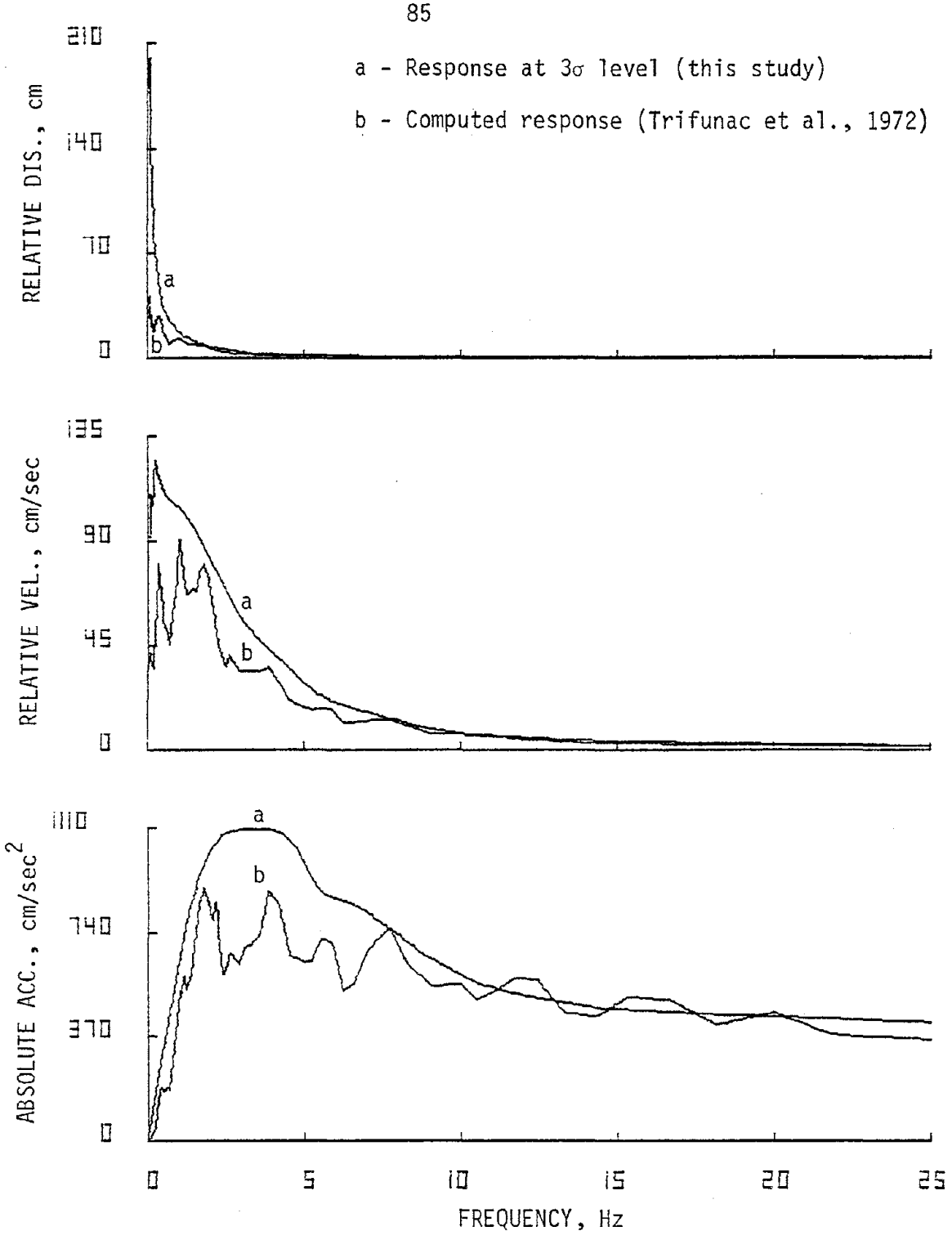

FIG. 3.29. Comparison of response for 5 percent of critical damping for S00E component of El Centro, Imperial Valley Earthquake of May 18, 1940.

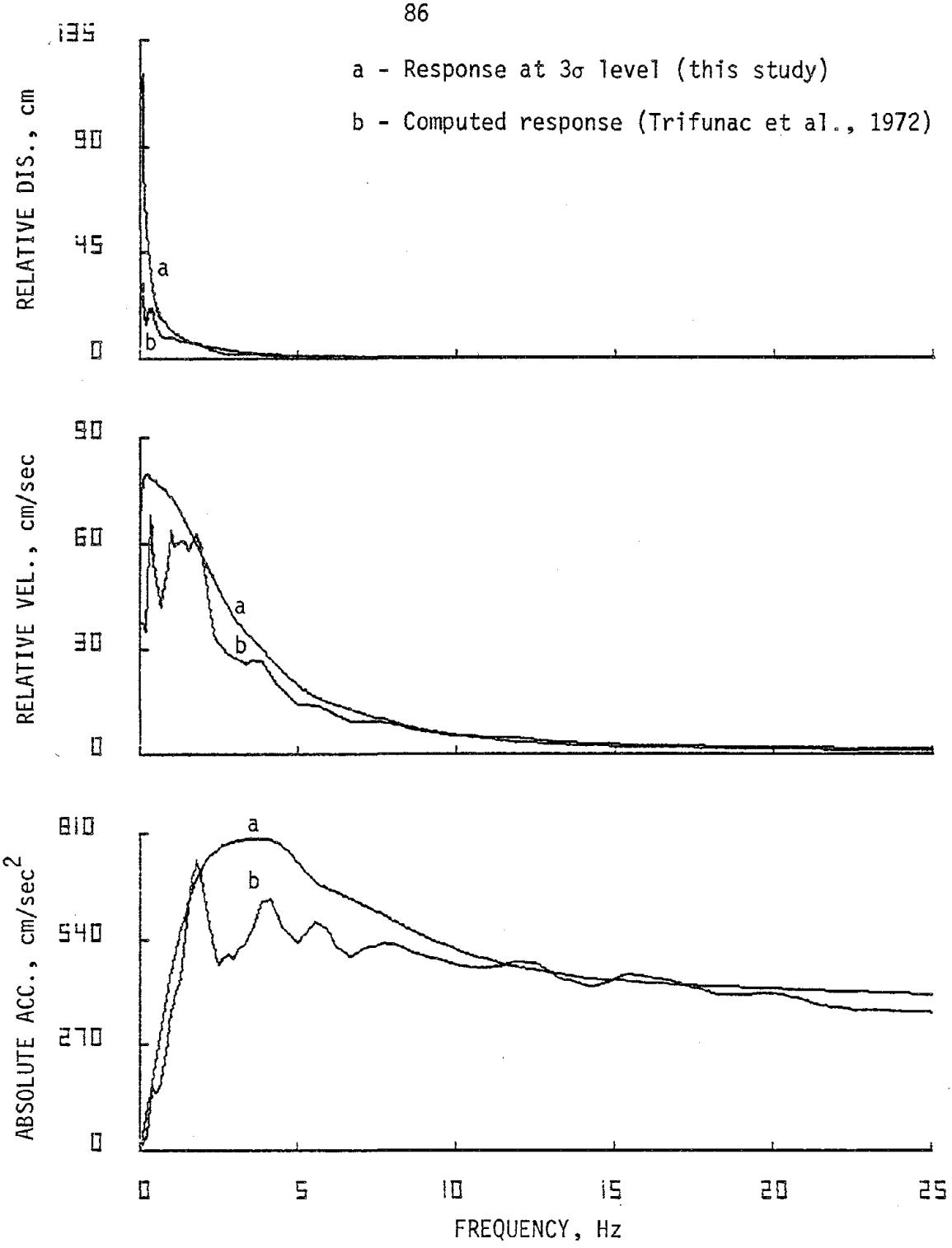

FIG. 3.30. Comparison of response for 10 percent of critical damping for S00E component of El Centro, Imperial Valley Earthquake of May 18, 1940.

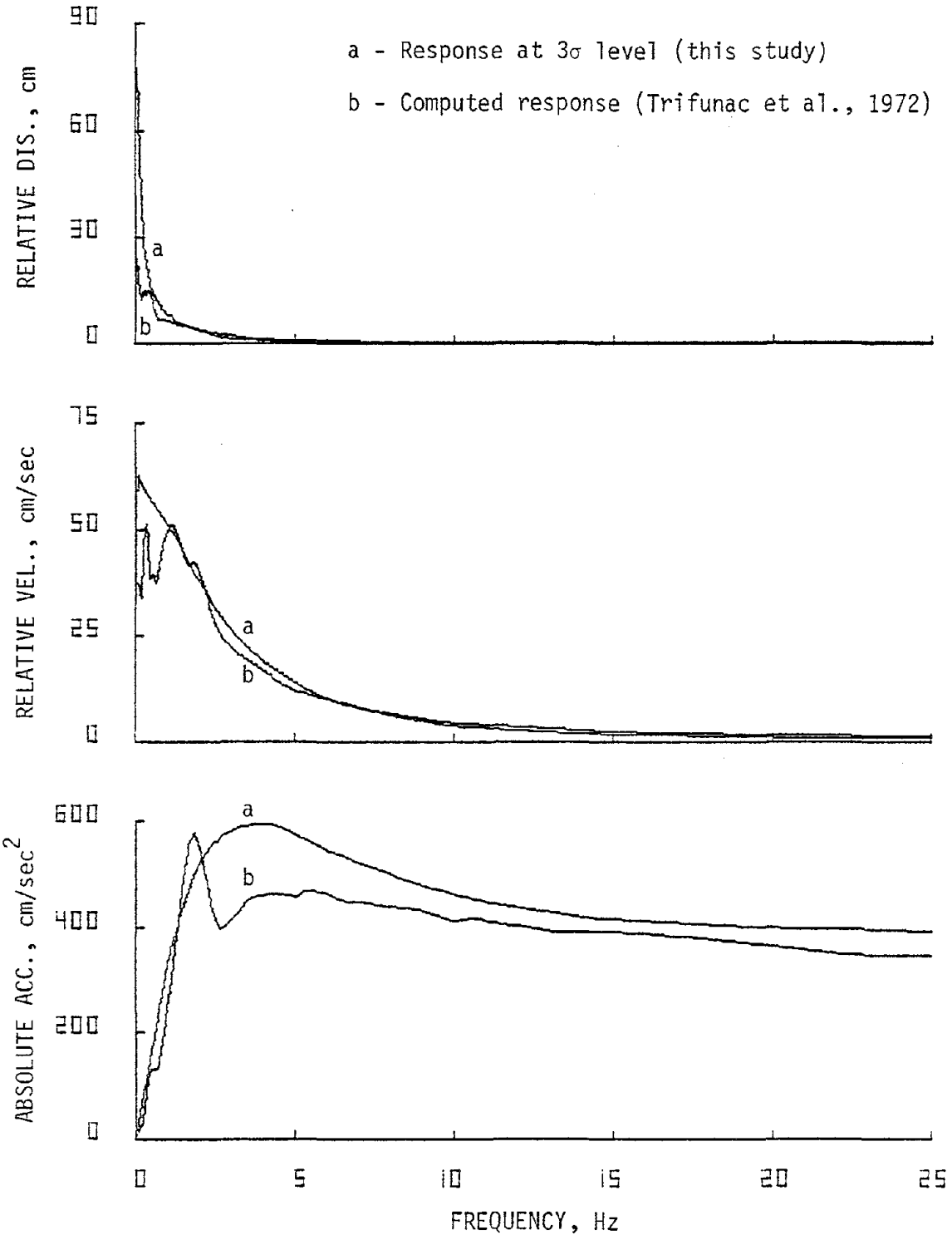

FIG. 3.31. Comparison of response for 20 percent of critical damping for S00E component of El Centro, Imperial Valley Earthquake of May 18, 1940.

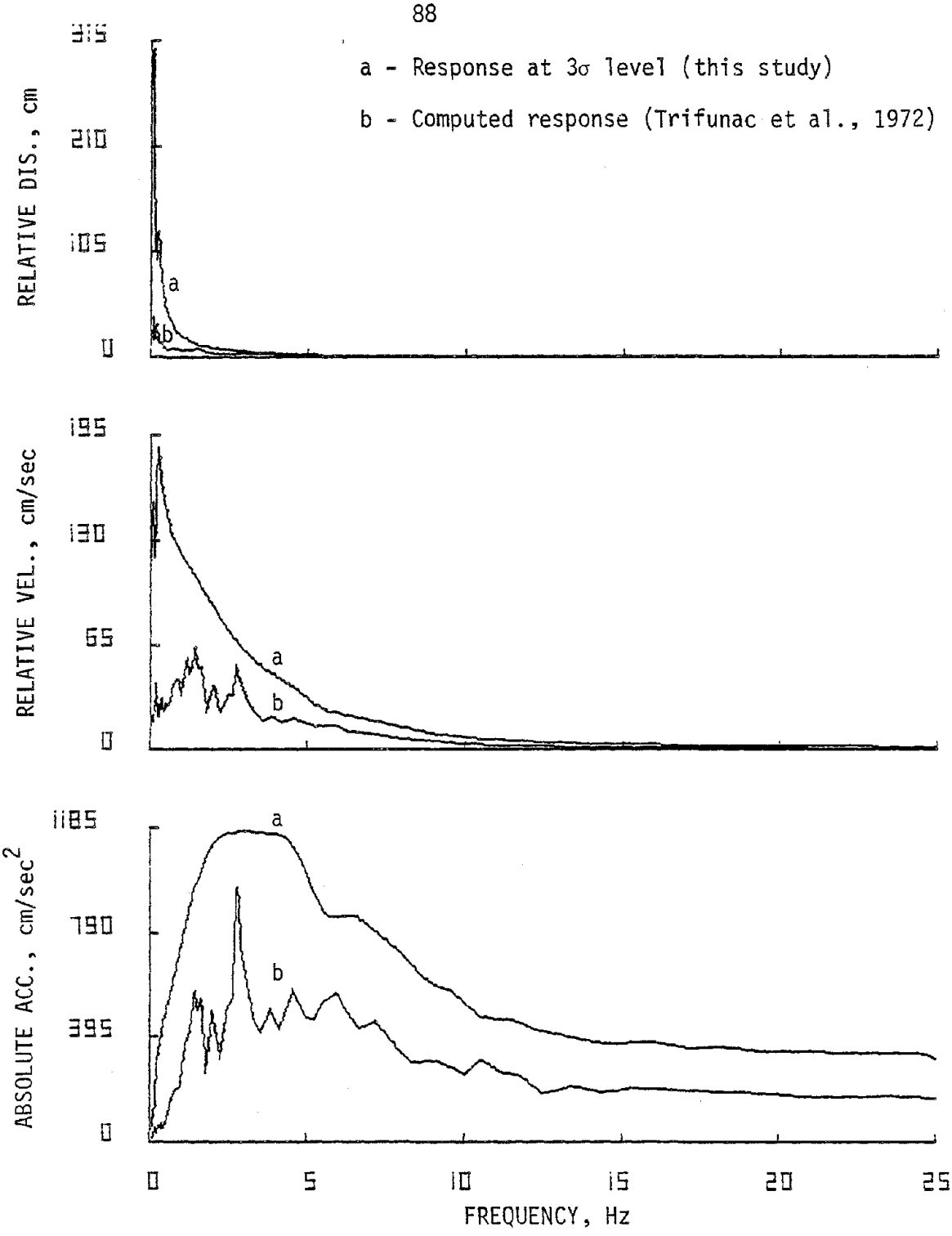

FIG. 3.32. Comparison of response for 2 percent of critical damping for N21E component of Taft, Kern County, California Earthquake of July 21, 1952.

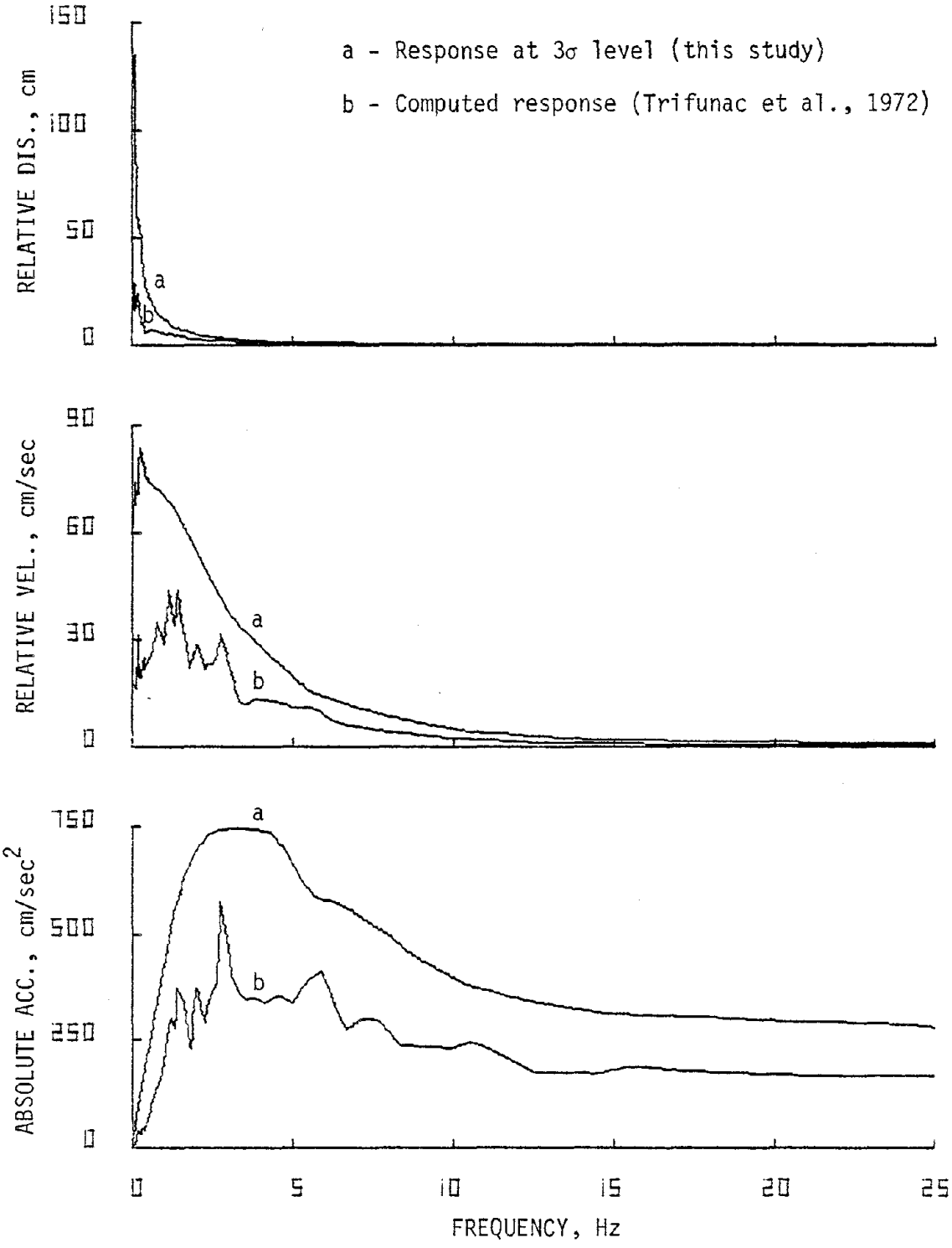

FIG. 3.33. Comparison of response for 5 percent of critical damping for N21E component of Taft, Kern County, California Earthquake of July 21, 1952.

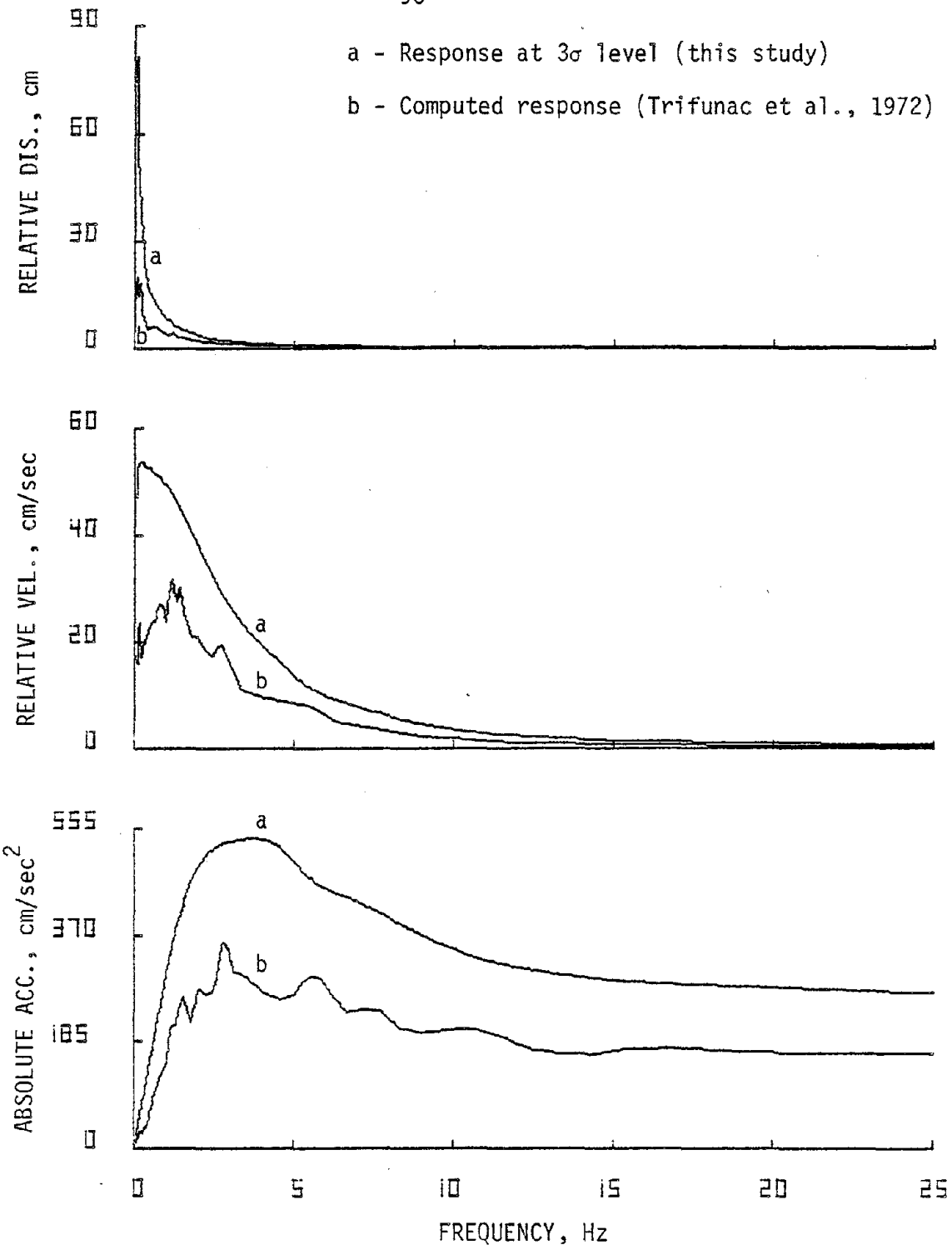

FIG. 3.34. Comparison of response for 10 percent of critical damping for N21E component of Taft, Kern County, California Earthquake of July 21, 1952.

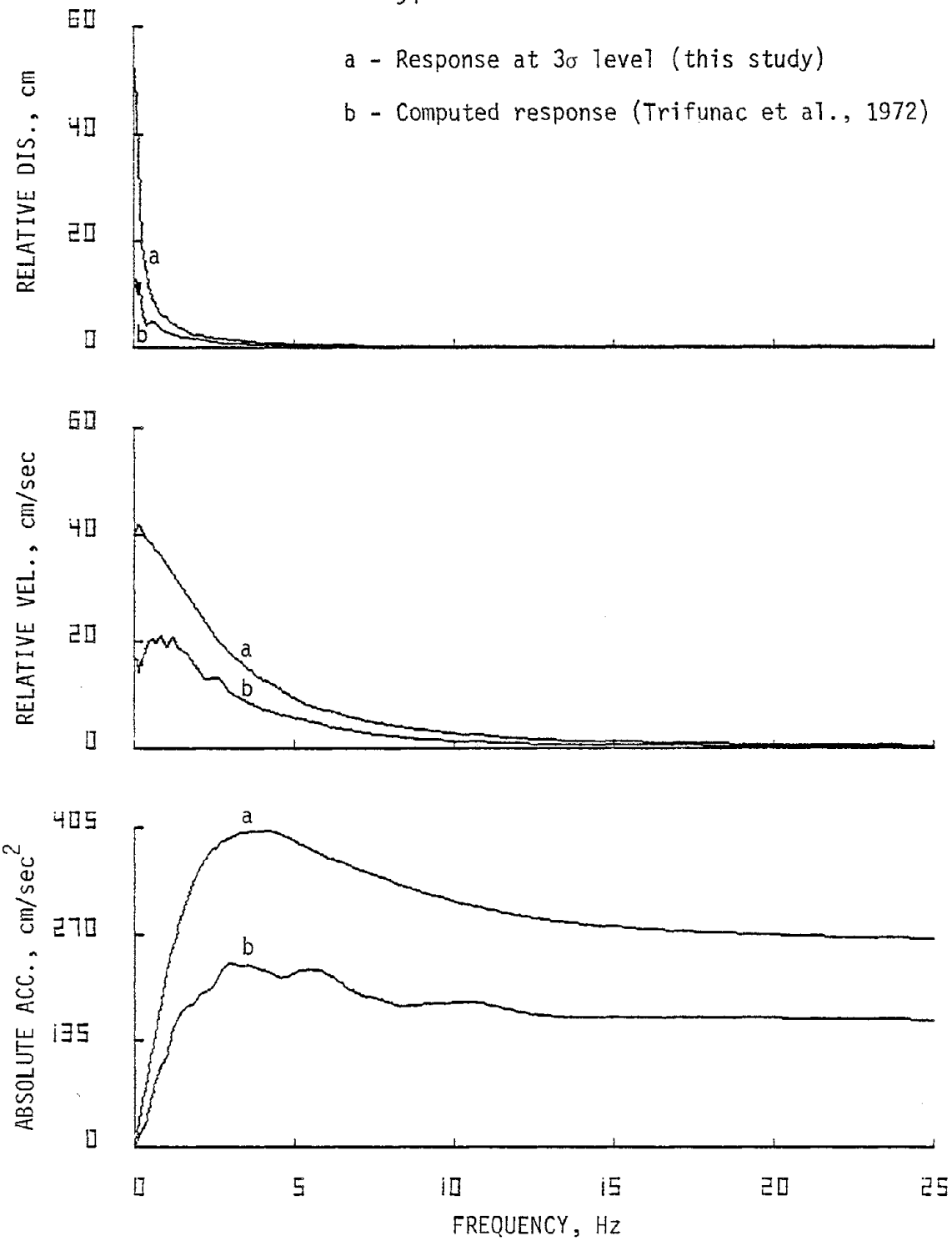

FIG. 3.35. Comparison of response for 20 percent of critical damping for N21E component of Taft, Kern County, California Earthquake of July 21, 1952.

CHAPTER 4

CORRELATION BETWEEN RMS VALUE AND EARTHQUAKE PARAMETERS

4.1 INTRODUCTORY REMARKS

In Chapter 3 a correlation between the RMS values computed for the selected duration and the combination of peak ground acceleration, earthquake magnitude, epicentral distance and the duration of strong motion was established. Even though the sample size of eight was small, the correlation was excellent. In this chapter, we will compute the duration of strong motion for a large number of records (see Section 3.2) and examine the correlation between the RMS values and the same parameters for horizontal, vertical and combined components of records with different geological classifications.

4.2 RECORD SELECTION AND CLASSIFICATION

The 987 components of the recorded earthquake accelerograms compiled by the Earthquake Engineering Research Laboratory of California Institute of Technology (Hudson, et al., 1971-1975) was used in this study. Neither the records which were identified as after shocks, nor those that were obtained from accelerographs mounted at the mid-heights or upper stories of building were considered. Among the remaining accelerograms those with at least one of the horizontal components having a peak ground acceleration equal to or greater than .05 g were chosen.

It should be noted that when one of the horizontal components had a peak ground acceleration equal to or greather than .05 g the complete set (all three components) were selected. Using the above criteria, a total of 371 components (one of the horizontal components for Parkfield California Earthquake of June 27, 1966, Cholame, Shandon Array No. 2 is not available) were selected.

It is generally recognized that the geological condition of the area near the ground surface has an important influence on the nature of the ground motion recorded there. Seed, Ugas, and Lysmer (1976) and Mohraz (1976) show that the site geology influences the response spectra to a significant degree. Therefore, it seems reasonable to suspect that the geology of the recording station would also influence the shape and the magnitude of power spectral density. For this reason, both the horizontal and vertical components of the 371 selected records were grouped according to the estimated geological condition of their sites. Table 4.1 lists the geological descriptions and the locations of the recording stations. The table has been arranged according to station number in ascending order. The descriptions were obtained from four different sources when available, namely: Trifunac and Brady (1975a), Hudson (1971), Seed, Ugas, and Lysmer (1976) and Mohraz (1976). It should be noted that if no description is listed by the author's name, his description is identical to the one given by Hudson (1971).

It is clear from Table 4.1 that it would be impossible to describe the site geology precisely. For this reason the classification was accomplished by considering the firmness of the underlying material at the recording station. The three geological groups which were selected

are soft, intermediate and hard. The geological descriptions given in Table 4.1 were examined and the underlying material at each station was identified as either soft, intermediate or hard. It should be mentioned that the boundaries between the three geological classifications are not precisely defined and there is some overlap between the soft and intermediate and the intermediate and hard classifications. Tables 4.2-4.4 list the records with their pertinent properties in chronological order of the earthquakes for the three classifications. Also listed in the tables are the Cal Tech identification number, epicentral distance, station number, peak ground acceleration and the record length.

The method of establishing the duration of strong motion discussed in Section 3.2 was applied to the 371 records selected. The method successfully determined the initial and final times and, therefore, the duration of the strong motion for 367 of the 371 records. It failed to determine the duration of strong motion for the following four records: El Alamo, Baja California Earthquake of Feb. 9, 1956 (A011); Western Washington Earthquake of April 13, 1949 (B028); Northern California Earthquake of June 5, 1960 (V308); and Torrence-Gardena Earthquake of November 14, 1941 (V316), where the initial cut-off time was greater than the final cut-off time. A possible explanation for the failure could be the stringent condition that was specified for the derivative of the cumulative RMS function (see Section 3.2). These four records were not considered in the study.

4.3 PREDICTION OF RMS VALUE

Seed, et al., (1976) and Mohraz (1976) in their statistical study showed that the site geology influences the shape and magnitude of response spectra to a significant degree. Using a regression analysis McGuire (1974) studied the effect of earthquake magnitude and epicentral distance on response spectra. The influence of earthquake magnitude, peak ground acceleration and the duration of strong motion on response spectra have also been studied by Mohraz (1978a, 1978b). The effect of earthquake magnitude, epicentral distance and site geology on Fourier amplitude spectra was first studied by Trifunac (1976). Later McGuire (1978) presented an empirical model for estimating of Fourier amplitude spectra and confirmed Trifunac's finding that site geology, earthquake magnitude and epicentral distance influence the Fourier spectra.

The above studies indicate that parameters such as earthquake magnitude, duration of strong motion, epicentral distance, site geology and peak ground acceleration are important and should be considered in design. Since these parameters influence response spectra in general and the Fourier amplitude which is directly proportional to power spectral density in particular, it is conceivable that these parameters will also influence the power spectral density of the recorded accelerograms. In addition to the five parameters mentioned above, McGuire (1974) suggests that other parameters such as stress drop, seismic moment, direction of propagation and length of rupture, etc., may be important and could be included in the study. However, at present there is not enough documented information on these parameters to include them in the analysis. The influence of site geology on the power spectral

density will be accounted for by studying the three geological groups separately. The effect of the other four parameters will be examined by considering their correlation to the RMS value. Although the relationship between the RMS value and the peak ground acceleration, duration of strong motion, epicentral distance and earthquake magnitude can individually be investigated, it will be extremely difficult to combine the individual influences. Therefore, it is desirable to correlate the RMS value with a combination of the four parameters, and to ascertain the validity of predicting the RMS value from them.

In order to gain an insight as how to combine the four parameters into one, the RMS value was correlated to each of the parameters using all 371 selected records without regard to components and site geology. Figures 4.1-4.4 show the correlation between the RMS value and each of the four parameters. The figures show the scatter of the data and regresssion line fitted to them. Also given in the figures is the correlation coefficient r. The strongest correlation is obtained with the peak ground acceleration where the correlation coefficient is .9404. For the other parameters the correlation is very weak as indicated by their correlation coefficients. Nevertheless from the sign of the correlation coefficients, one can note that the RMS value is directly proportional to peak ground acceleration and earthquake magnitude, and inversely proportional to duration of strong motion and epicentral distance. This observation led to the study of correlation between the RMS value and the parameter aM/DT. The result of this correlation is presented in Fig. 4.5. The correlation coefficient for the regression line is 0.6629 which indicates that there is a better correlation between

the RMS value and the parameter aM/DT than any of the individual parameters with the exception of the peak ground acceleration.

Each of the four parameters (a, M, D and T) is related linearly to the combined parameter aM/DT, which may not be the case for the best possible correlation. In order to obtain a correlation as good as or better than the one with acceleration, a nonlinear combination of the parameters was considered. Consequently each of the four parameters was raised to a different power as indicated in Eq. 4.1

$$\bar{n} = \frac{a^{P_1} M^{P_2}}{D^{P_3} T^{P_4}} \tag{4.1}$$

A correlation between the RMS value and $\bar{n}$ can be established for a given set of power coefficients P_1-P_4. For a given set of power coefficients the RMS values were correlated with $\bar{n}$ and the correlation coefficient computed. All possible combinations of P_1-P_4 were tried and the set of power coefficients which resulted in the best correlation was identified. The above procedure was repeated with different range and increments for P_1-P_4. The range, the increment and the selected value of each power coefficient as well as the best correlation coefficient are given in Table 4.5. It is noted from the table that all correlation coefficients for the combination of power coefficients shown are better than the one obtained when correlating with the peak ground acceleration alone. The results indicate that the best correlation is obtained for P_1 = 1.53, P_2 = 1.30, P_3 = .066, and P_4 = .31. The correlation between the RMS value and $\bar{n}$ computed using the above powers is shown in Fig. 4.6.

Different sets of coefficients P_1-P_4 can be obtained for various geological classifications as well as horizontal and vertical components of the records. Since it would be difficult to compare four different coefficients (P_1-P_4) for each category, it was decided to correlate the RMS value with a new parameter η which is obtained by rewriting Eq. 4.1 as

$$\eta = (\bar{\eta})^P = a\left[\frac{M^{P_2}}{D^{P_3} T^{P_4}}\right]^P \tag{4.2}$$

where $P = \frac{1}{P_1}$. Retaining the same P_2-P_4 of Eq. 4.1, the best correlation between the RMS value and η (Eq. 4.2) was established for P = .65 with a correlation coefficient of r = .96322 which is identical to the correlation coefficient presented in Table 4.5. The correlation with the new parameter is shown in Fig. 4.7. Since previously the best correlation between the RMS value and the individual parameters was obtained for the peak ground acceleration (r = 0.9404), the improvement (r = 0.9632) can be attributed to the quantity

$$\left[\frac{M^{P_2}}{D^{P_3} T^{P_4}}\right]^P \tag{4.3}$$

It should be noted that the expression for η presented in Eq. 4.2 is by no means the only expression that can be correlated with the RMS value. The RMS value was also correlated with the following two parameters:

$$\eta' = \frac{a^P M^{P-.23}}{D^{P-1.46} T^{P-1.22}} \tag{4.4}$$

$$\eta'' = \frac{(aM)^P}{(D+200)^{.45P} T^{.4(2-P)}} \tag{4.5}$$

The results are compared in Table 4.6. The table presents the power coefficient P and the correlation coefficient r for each of the three parameters η, η', η'' for horizontal, vertical, and combined components of the three geological classifications. The table indicates that in general (Eq. 4.2) gives slightly better correlation with RMS than η' and η''. It is interesting to note that would also give a better correlation coefficient than η' and η'' for the eight records considered in Chapter 2. The results of this comparison are given in Table 4.7.

The result of correlation between the RMS value and parameter η (Eq. 4.2) for the twelve categories (soft, intermediate, hard and combined geological classifications; horizontal, vertical and combined components are presented in Table 4.8. Also shown are the number of components of records used in the correlation N, the coefficient P, the slope A, the intercept B and the percent variation of the RMS value accounted for by η. The equation for the regression line can be expressed in arithmatic scale as $\psi = 10^A (\eta)^B$. Table 4.8 indicates that best correlations are obtained for the hard sites followed by the group containing all 367 records. Figures 4.8-4.11 show the correlation for the horizontal components of the records for soft, intermediate, hard and combined geological classification. Shown in Figs. 4.12-4.15 are

similar correlations for vertical components. The correlation for the combination of horizontal and vertical components for the three geological classifications and for all 367 records are presented in Figs. 4.16-4.19. In Figs. 4.8-4.19 in addition to the regression line the 95% interval on the future observation (see Walpole and Myers, 1978) are also presented. The RMS values predicted from the appropriate regression line as well as the actual RMS (computed using the strong motion duration--see Chapter 3) for the horizontal components of the three geological classifications are given in Tables 4.9-4.11. Also presented in the tables are the initial and final times, the duration of strong motion, the peak ground acceleration, the epicentral distance and the earthquake magnitude. Similar information for the vertical components are presented in Tables 4.12-4.14.

Comparisons of the slope A and the intercept B of the regression line given in Table 4.8 indicate that for large values of η, the predicted RMS value for the vertical components are greater than those for the horizontal components for each geological classification. The correlation coefficient given in Table 4.8 and repeated in Figs. 4.8-4.19 indicate that the RMS values can reliably be predicted from the parameter η. The correlation coefficient r indicates that $100r^2$ percent (see Walpole and Myers, 1978) of the variation of the RMS value is accounted for by the combined seismic parameter η. The values of r listed in this table are extremely close to unity (between .9453 to .9880) indicating that between 89 to 96 percent of the variation of RMS is accounted for by the relationship with parameter η. It is also observed from Table 4.8 that in general better correlations are obtained for

the "hard" geological classification than the other two geological classifications. The RMS value for any of the 12 categories listed in Table 4.8 can be predicted using the corresponding regression line for that category. However, the last category which includes all 367 records considered in the study results in a correlation coefficient which is just as good or better than most other categories and it is recommended for predicting RMS values as it covers the largest range of data. It should be noted that the plots presented in Figs. 4.8-4.19 should be used for the range of η presented.

TABLE 4.1

GEOLOGICAL CLASSIFICATION OF THE RECORDS

Station Number	Location	Reference	Group*	Geological Description
0	Seattle, Wash. District Engineers Office at Army Base	Trifunac[a]	TO	Sand, silt, and gravel over blue clay hardpan
13	Cholame, Shandon, California Array No. 2	Hudson[b]		Alluvium
		Trifunac	TO	
		Seed[c]	S2	Stiff soil 150 ft. deep
14	Cholame, Shandon, California Array No. 5	Hudson		Alluvium
		Trifunac	TO	Unconsolidated shallow soil and alluvium, overlying plio-pleistocene loosly consolidated sand, gravel, silt and clay
		Seed	S2	Stiff soil 100 ft. deep
		Mohraz[d]	MO	

TABLE 4.1 - continued

Station Number	Location	Reference	Group*	Geological Description
15	Cholame, Shandon, California Array No. 6	Hudson		Alluvium
		Trifunac	TO	
		Mohraz	MO	
16	Cholame, Shandon, California Array No. 12	Hudson		Alluvium
		Trifunac	TO	Unconsolidated shallow soil and alluvium, overlying plio-pleistocene loosly consolidated sand, gravel silt, and clay
		Mohraz	MO	
22	Eureka Federal Building	Seed	S1	Deep cohesionless soil 250 ft. deep
23	Ferndale City Hall	Trifunac	T1	1500 ft. of plio-pleistocene loosly consolidated massive conglomerate, sand stone, and clay stone
		Seed	S1	Deep cohesionless soil 500 ft. deep

TABLE 4.1 - continued

Station Number	Location	Reference	Group*	Geological Description
		Mohraz	M2	40-80 ft. of alluvium over 1000 ft. of sandstone over siltstone
28	Hollister City Hall	Trifunac	T0	Recent unconsolidated alluvium over partly consolidated gravels, and well consolidated marine sandstone and shale. Water table from 85-95 ft.
		Mohraz	M0	500 ft. of alluvium over cenozoic rock. Water table at 50 ft.
52	OSO Pumping Plant, Gorman, California	Hudson		Alluvium
		Trifunac	T1	
77	San Francisco Golden Gate Park	Trifunac	T1	Outcropping of Franciscan chert and thin interbedded shale
		Seed	S3	Rock
		Mohraz	M3	Siliceous sandstone

TABLE 4.1 - continued

Station Number	Location	Reference	Group*	Geological Description
80	San Francisco State Bldg. Basement	Trifunac	T1	Dune sand over clay, sand and gravel, 200 ft. to Franciscan bedrock - shale interbedded with fine-grained sandstone
		Seed	S2	Still soil 200 ft. deep
81	San Jose Bank of America Basement	Trifunac	TO	Unconsolidated alluvium and estuarine deposits
83	City Recreation Building, San Luis Obispo, Cal.	Hudson		5 ft. of clay loam over Franciscan shale
95	Taft Lincoln School Tunnel	Hudson		40 ft. of alluvium over poorly cemented sandstone
		Trifunac	TO	Quaternary alluvium, sand, and gravel veneer over 2000 ft. Consolidated gravel, sand and clay.
		Seed	S3	Rock
		Mohraz	M2	

TABLE 4.1 - continued

Station Number	Location	Reference	Group*	Geological Description
97	Temblor, California No. 2	Trifunac	T3	Indeterminate age serpentine and hard, severely fractured ultrabasic complex
		Seed	S3	Rock
104	Santa Anita Reservoir, Arcadia, California	Hudson		Granite diorite complex
		Trifunac	T3	
		Seed	S3	Rock
		Mohraz	M3	
108	Carbon Canyon Dam, Cal.	Hudson		Thin alluvium over poorly cemented siltstone
		Trifunac	T1	
		Mohraz	M1	
110	Castaic Old Ridge Route, California	Hudson		Sandstone
		Trifunac	T1	

TABLE 4.1 - continued

Station Number	Location	Reference	Group*	Geological Description
		Seed	S2	Stiff soil 60 ft. deep
		Mohraz	M3	
111	Allen Ranch, CWR Site, Cedar Springs, California	Hudson		Granitic
		Trifunac	T3	
112	Right Abutment, CWR Site, Cedar Springs, California	Hudson		Shallow gravelly alluvium
		Trifunac	T1	
117	El Centro Valley Irrigation District	Hudson		Alluvium - several 1000 ft.
		Trifunac	T0	
		Seed	S2	Stiff soil 100 ft. deep
		Mohraz	M0	
121	Reservoir, Fairmont Reservoir, California	Hudson		Granitic

TABLE 4.1 - continued

Station Number	Location	Reference	Group*	Geological Description
		Trifunac	T3	
		Mohraz	M3	
122	633 East Broadway, Municipal Service Bldg., Glendale, California	Hudson		Alluvium
		Trifunac	T1	
		Mohraz	M0	
125	Lake Hughes, Array Station 1, California	Hudson		Granitic
		Trifunac	T3	
		Mohraz	M3	
126	Lake Hughes, Array Station 4, California	Hudson		Weathered granitic
		Trifunac	T3	
		Seed	S3	Rock
		Mohraz	M3	

TABLE 4.1 - continued

Station Number	Location	Reference	Group*	Geological Description
127	Lake Hughes, Array Station 9, California	Hudson		Gneiss
		Trifunac	T3	
		Mohraz	M3	
128	Lake Hughes, Array Station 12, California	Hudson		Eocene sandstone below a shallow (10 ft.) layer of alluvium
		Trifunac	T1	
		Seed	S3	Rock
		Mohraz	M1	
131	Public Utilities Bldg., Long Beach, California	Hudson		Alluvium. Water table at 15 ft.
		Trifunac	T0	
133	Hollywood Storage Basement	Hudson		700 ft. of alluvium
		Trifunac	T0	

TABLE 4.1 - continued

Station Number	Location	Reference	Group*	Geological Description
		Mohraz	M0	
135	Hollywood Storage P.E. Lot	Hudson		700 ft. of alluvium
		Trifunac	T0	
		Seed	S2	Stiff soil 200 ft. deep
		Mohraz	M0	
136	L.A. Subway Terminal Sub-basement, Los Angeles, California	Trifunac	T0	Alluvium veneer over late tertiary marine sediments
137	Water and Power Building, Basement, Los Angeles, California	Hudson		Miocene siltstone
		Trifunac	T1	
		Mohraz	M3	
140	UCLA Reactor Laboratory, Los Angeles, Cal.	Hudson		70 ft. of alluvium over 5000 ft. of sedimentary rock

TABLE 4.1 - continued

Station Number	Location	Reference	Group*	Geological Description
		Trifunac	TO	
		Mohraz	M2	
141	Griffith Park Observatory, Moon Room, Los Angeles, California	Hudson		Granitic
		Trifunac	T3	
		Seed	S3	Rock
		Mohraz	M3	
143	120 North Robertson Blvd., Sub-basement, Los Angeles, California	Hudson		Alluvium
		Trifunac	TO	
		Mohraz	MO	
145	222 Figueroa Street, 1st Floor, Los Angeles, Cal.	Hudson		25 ft. of alluvium over shale, water at 20 ft.
		Trifunac	T1	

TABLE 4.1 - continued

Station Number	Location	Reference	Group*	Geological Description
148	234 Figueroa Street, Basement, Los Angeles, California	Hudson		25 ft. of alluvium over shale. Water at 20 ft.
		Trifunac	T1	
151	250 E. First Street Basement, Los Angeles, Cal.	Hudson		Alluvium
		Trifunac	TO	
		Mohraz	MO	
157	445 Figueroa Street, Subbasement, Los Angeles, California	Hudson		Shale
		Trifunac	TO	
160	535 S. Fremont Avenue, Basement, Los Angeles, California	Hudson		Alluvium
		Trifunac	TO	
163	611 West Sixth Street, Basement, Los Angeles, California	Hudson		Alluvium
		Trifunac		

TABLE 4.1 - continued

Station Number	Location	Reference	Group*	Geological Description
166	646 South Olive Avenue, Basement, Los Angeles, California	Hudson		Alluvium
		Trifunac	T0	
172	800 W. First Street, 1st Floor, Los Angeles, Cal.	Hudson		Pliocene siltstone
		Trifunac	T1	
175	808 South Olive Street, Street Level, Los Angeles, California	Hudson		Alluvium
		Trifunac	T0	
		Mohraz	M0	
181	1640 S. Marengo St., 1st Floor, Los Angeles, Cal.	Hudson		Pleistocene alluvium. Water level at 35 ft.
		Trifunac	T0	
		Mohraz	M0	

TABLE 4.1 - continued

Station Number	Location	Reference	Group*	Geological Description
184	1900 Avenue of the Stars, Basement, Los Angeles, California	Hudson		Silt and sand layers. Water table at 70 ft.
		Trifunac	TO	
187	1901 Avenue of the Stars, Sub-basement, Los Angeles, California	Hudson		Silt and sand layers. Water table at 70-80 ft.
		Trifunac	TO	
190	2011 Zonal Avenue, Basement, Los Angeles, Cal.	Hudson		Shale at east end of building. 8 ft. of fill at west end
		Trifunac	T1	
196	3345 Wilshire Boulevard, Basement, Los Angeles, California	Hudson		Alluvium
		Trifunac	TO	
199	3407 6th Street, Basement, Los Angeles, California	Hudson		Alluvium
		Trifunac	TO	

TABLE 4.1 - continued

Station Number	Location	Reference	Group*	Geological Description
		Seed	S2	Stiff soil 40 ft. deep
		Mohraz	M0	
202	3411 Wilshire Boulevard, 5th Basement, Los Angeles, California	Hudson		Siltstone. Water table at basement level.
		Trifunac	T1	
205	3440 University Avenue, Basement, Los Angeles, California	Hudson		400 ft. of alluvium over clay and shale. Water table at 275 ft.
		Trifunac	T0	
208	3470 Wilshire Boulevard, Subbasement, Los Angeles, California	Hudson		Alluvium
		Trifunac	T0	
		Seed	S2	Still soil 45 ft. deep
		Mohraz	M0	

TABLE 4.1 - continued

Station Number	Location	Reference	Group*	Geological Description
211	3550 Wilshire Boulevard, Basement, Los Angeles, California	Hudson		Alluvium. Water table at 35 ft.
		Trifunac	TO	
		Seed	S2	Stiff soil 100 ft. deep
217	3710 Wilshire Boulevard, Basement, Los Angeles, California	Hudson		Alluvium
		Trifunac	T1	
		Mohraz	MO	
220	3838 Lankershim Boulevard, Basement, Los Angeles, California	Hudson		Interlayered soft sandstone and shale
		Trifunac	T1	
		Seed	S3	Rock
223	4680 Wilshire Boulevard, Basement, Los Angeles, California	Hudson		Alluvium
		Trifunac	T1	
		Mohraz	MO	

TABLE 4.1 - continued

Station Number	Location	Reference	Group*	Geological Description
226	4867 Sunset Boulevard, Basement, Los Angeles, California	Hudson		Shallow alluvium over miocene siltstone
		Trifunac	T1	
		Mohraz	M1	
229	5260 Centuary Boulevard, 1st Floor, Los Angeles, California	Hudson		Alluvium
		Trifunac	T0	
232	6430 Sunset Boulevard, 1st Floor, Los Angeles, California	Hudson		Alluvium. Water table at 55 ft.
		Trifunac	T0	
235	6464 Sunset Boulevard, Basement, Los Angeles, California	Hudson		Alluvium. Water table at 55 ft.
		Trifunac	T0	
238	7080 Hollywood Blvd., Basement, Los Angeles, California	Hudson		Alluvium
		Trifunac	T0	

TABLE 4.1 - continued

Station Number	Location	Reference	Group*	Geological Description
		Mohraz	MO	
241	8244 Orion Blvd., 1st Floor, Los Angeles, Cal.	Hudson		Alluvium
		Trifunac	TO	
		Seed	S1	Deep cohesionless soil 550 ft. deep
		Mohraz	MO	
253	14724 Ventura Boulevard, 1st Floor, Los Angeles, California	Hudson		Alluvium
		Trifunac	TO	
		Seed	S2	Stiff soil 70 ft. deep
262	Palmdale Fire Station, Storage Room, Palmdale, California	Hudson		Alluvium
		Trifunac	TO	

TABLE 4.1 - continued

Station Number	Location	Reference	Group*	Geological Description
264	Cal Tech Millikan Library, Basement, Pasadena, Cal.	Hudson		Approximately 1000 ft. of alluvium upon granite
		Trifunac	T0	
		Seed	S1	Deep cohesionless soil 350 ft. deep
266	Cal Tech Seismological Lab., Pasadena, Cal.	Hudson		Weathered granitic
		Trifunac	T3	
		Seed	S3	Rock
		Mohraz	M3	
267	Jet Propulsion Lab., Basement, Pasadena, Cal.	Hudson		Sandy - gravel
		Trifunac	T1	
		Seed	S1	Deep cohesionless soil 450 ft. deep
269	Pumping Plant, Pearblossom, Cal.	Hudson		400 ft. of alluvium over 14,000 ft. of sedimentary rock

TABLE 4.1 - continued

Station Number	Location	Reference	Group*	Geological Description
		Trifunac	TO	
272	Navy Research Evaluation Lab., Port Hueneme, Cal.	Hudson		Alluvium greater than 1000 ft.
		Trifunac	TO	
274	Hall of Records, San Bernardino, Cal.	Hudson		Alluvium - 1000 ft. Water table at 30 ft.
		Trifunac	TO	
278	Puddingstone Reservoir, San Dimas, California	Hudson		Volcanic clastics and intrusions with associated shales
		Trifunac	T3	
279	Pacoima Dam, California	Hudson		Highly jointed diorite gneiss
		Trifunac	T3	
		Seed	S3	Rock
		Mohraz	M3	

TABLE 4.1 - continued

Station Number	Location	Reference	Group*	Geological Description
283	Santa Barbara Court House	Hudson		Boulder alluvium - 700 ft. deep
		Trifunac	TO	Approx. 600 ft. of pleistocene cemented alluvium over sand, silt and clay
		Mohraz	MO	
284	Santa Felicia Dam, Cal., Outlet Works	Hudson		Sandstone shale complex
		Trifunac	T1	
		Seed	S3	Rock
		Mohraz	M3	
287	San Antonio Dam, Upland, California	Hudson		Up to 150 ft. of alluvium over granitics
		Trifunac	TO	
		Mohraz	M2	
288	Vernon CMD Building	Hudson		Greater than 1000 ft. of alluvium. Water table greater than 300 ft.

TABLE 4.1 - continued

Station Number	Location	Reference	Group*	Geological Description
		Trifunac	TO	
		Mohraz	MO	
289	Whittier Narrows Dam, Cal.	Hudson		More than 1000 ft. of alluvium
		Trifunac	TO	
290	6074 Park Drive, Ground Level, Wrightwood, Cal.	Hudson		Alluvium veneer on igneous metamorphic complex
		Trifunac	T1	
		Seed	S3	Rock
		Mohraz	M1	
323	Helena, Montana Carroll College	Mohraz	M3	Limestone bedrock
		Seed	S3	Rock

TABLE 4.1 - continued

Station Number	Location	Reference	Group*	Geological Description
325	Olympia, Washington Hwy. Test Lab	Trifunac	TO	Sand and silt fill over recent alluvium - unconsolidated clay, silt, sand, and gravel
		Seed	S1	Deep cohesionless soil 420 ft. deep
413	1177 Beverly Drive, Basement, Los Angeles, Cal.	Hudson		Alluvium
		Trifunac	TO	
416	9100 Wilshire Boulevard, Basement, Beverly Hills, California	Hudson		Alluvium. Water table at 40 ft.
		Trifunac	TO	
425	1800 Century Park East, Basement (P-3), Los Angeles, California	Hudson		Silt and sand layers. Water table at 70-80 ft.
		Trifunac	TO	
428	5900 Wilshire Boulevard, B Parking Lot, Los Angeles, California	Hudson		Alluvium-asphaltic sand

TABLE 4.1 - continued

Station Number	Location	Reference	Group*	Geological Description
		Trifunac	T1	
431	616 S. Normandie Avenue, Basement, Los Angeles, California	Hudson		Alluvium. Siltstone at 25 ft.
		Trifunac	T1	
		Mohraz	M1	
437	1150 South Hill Street, Sub-basement, Los Angeles, California	Hudson		500 ft. of gravelly sand over shale
		Trifunac	T0	
443	6200 Wilshire Boulevard, Ground Floor, Los Angeles, California	Hudson		Thin layer of alluvium over asphaltic sand
		Trifunac	T1	
446	1760 N. Orchid Avenue, Ground Floor, Hollywood, California	Hudson		Alluvium
		Trifunac	T0	

TABLE 4.1 - continued

Station Number	Location	Reference	Group*	Geological Description
449	2500 Wilshire Boulevard, Basement, Los Angeles, California	Hudson		Alluvium. Siltstone at 20-30 ft. Water table at 35 ft.
		Trifunac	T1	
		Mohraz	M1	
452	435 North Oakhurst Avenue, Basement, Beverly Hills, California	Hudson		Alluvium. Water table at 22 ft.
		Trifunac	TO	
455	450 North Roxbury Drive, First Floor, Beverly Hills, California	Hudson		Alluvium
		Trifunac	TO	
458	15107 Vanowen Street, Basement, Los Angeles, California	Hudson		Alluvium 500 ft. Water table at 70 ft.
		Trifunac	TO	
		Seed	S1	Deep cohesionless soil 550 ft. deep

TABLE 4.1 - continued

Station Number	Location	Reference	Group*	Geological Description
461	15910 Ventura Boulevard, Basement, Los Angeles, California	Hudson		Alluvium. Water table at 35 ft.
		Trifunac	TO	
466	15250 Ventura Boulevard, Basement, Los Angeles, California	Hudson		Alluvium. Water table at 55 ft.
		Trifunac	TO	
		Seed	S2	Stiff soil 70 ft. deep
469	1625 Olympic Boulevard, Ground Floor, Los Angeles, California	Hudson		Alluvium
		Trifunac	TO	
475	Pasadena - Cal Tech Athenaeum	Hudson		Approximately 1000 ft. of alluvium upon granite
		Trifunac	TO	
		Seed	S1	Deep cohesionless soil 350 ft. deep
		Mohraz	MO	

TABLE 4.1 - continued

Station Number	Location	Reference	Group*	Geological Description
482	900 South Fremont Avenue, Basement, Alhambra, Cal.	Hudson		Few 100 ft. of alluvium over siltstone
		Trifunac	TO	
		Mohraz	M2	
1023**				

* Key to classifications

T0 = Trifunac's soft alluvium classification
T1 = Trifunac's hard sedimentary classification
T2 = Trifunac's basement/crystalline rock classification

S0 = Seed's soft to medium clay and sand classification
S1 = Seed's deep cohesionless soil classification
S2 = Seed's stiff soil classification
S3 = Seed's rock site classification

M0 = Mohraz's alluvium deposit classification
M1 = Mohraz's < 30' of alluvium over rock classification
M2 = Mohraz's 30-200' of alluvium over rock classification
M3 = Mohraz's rock classification

** Same as Station Number 23

a - Trifunac and Brady (1975a)
b - Hudson (1971)
c - Seed, Ugas and Lysmer (1976)
d - Mohraz (1976)

TABLE 4.2

EARTHQUAKE RECORDS AND DATA - SOFT

Record	Earthquake	Date	Mag.	Epicentral Distance (km)	Station Number	Comp.	Peak Acc. (g)	Record Length (sec)
B021	Long Beach	3/10/33	6.3	50.4	288	S08W N82W DOWN	.133 .154 .152	98.76 98.42 98.66
V314				57.4	136	N39E N51W UP	.064 .097 .065	98.86 98.90 98.94
V315				28.4	131	SOUTH WEST UP	.196 .159 .285	98.96 98.96 98.90
B024	Lower California	12/30/34	6.5	66.3	117	S00W S90W VERT	.160 .183 .069	90.28 90.22 90.22
T274	Imperial Valley	4/12/38	3.0	12.6	117	NORTH EAST UP	.029 .050 .022	76.60 76.56 76.54

TABLE 4.2 - continued

Record	Earthquake	Date	Mag.	Epicentral Distance (km)	Station Number	Comp.	Peak Acc. (g)	Record Length (sec)
A001	Imperial Valley	5/18/40	6.7	11.5	117	S00E S90W VERT	.348 .214 .210	53.74 53.46 53.78
U299	Santa Barbara	6/30/41	5.9	36.4	283	N45E S45E UP	.238 .176 .070	61.82 61.80 61.88
V316	Torrance-Gardena	11/14/41	5.4	3.4	131	NORTH EAST UP	.040 .055 .009	66.62 66.60 66.64
T286	Borrego Valley	10/21/42	6.5	46.2	117	NORTH EAST UP	.060 .047 .026	71.34 71.32 71.30
U301	Northern California	3/ 9/49	5.3	19.9	28	N89W S01W UP	.197 .122 .071	56.28 56.32 56.38

TABLE 4.2 - continued

Record	Earthquake	Date	Mag.	Epicentral Distance (km)	Station Number	Comp.	Peak Acc. (g)	Record Length (sec)
B028	Western Washington	4/13/49	7.1	57.7	0	S02W N88W VERT	.068 .067 .022	66.70 66.68 66.54
B029				16.9	325	N04W N86E DOWN	.165 .280 .092	89.06 89.04 88.88
A003	Kern County, California	7/21/52	7.7	126.9	475	S00E S90W VERT	.047 .053 .030	77.26 77.36 77.28
A004				41.4	95	N21E S69E VERT	.156 .179 .105	54.36 54.38 54.26
A005				88.4	283	N42E S48E VERT	.090 .131 .044	75.48 75.46 75.56
A006				120.3	133	S00W N90E VERT	.055 .044 .023	82.42 82.48 82.60

TABLE 4.2 - continued

Record	Earthquake	Date	Mag.	Epicentral Distance (km)	Station Number	Comp.	Peak Acc. (g)	Record Length (sec)
A007				120.3	135	S00W N90E VERT	.059 .042 .021	78.62 78.62 78.58
B031	Wheeler Ridge, California	1/12/54	5.9	42.8	95	N21E S69E VERT	.065 .068 .036	65.38 65.34 65.56
U305	Central California	4/25/54	5.3	26.8	28	N89W S01W UP	.053 .050 .024	57.28 57.38 57.46
A008	Eureka	12/21/54	6.5	24.0	22	N11W N79E VERT	.168 .258 .083	77.96 79.56 69.98
A010	San Jose	9/ 4/55	5.8	9.6	81	N31W N59E VERT	.102 .108 .045	49.56 51.74 51.74

TABLE 4.2 - continued

Record	Earthquake	Date	Mag.	Epicentral Distance (km)	Station Number	Comp.	Peak Acc. (g)	Record Length (sec)
T292	Imperial County	12/16/55	5.4	23.2	117	NORTH EAST UP	.064 .072 .058	41.30 43.82 43.58
A011	El Alamo, Baja California	2/ 9/56	6.8	121.2	117	S00W S90W VERT	.033 .051 .013	90.02 89.96 89.56
V329	Southern California	3/18/57	4.7	6.3	272	SOUTH WEST UP	.167 .089 .025	68.94 68.86 68.94
U307	Central California	1/19/60	5.0	8.0	28	N89W S01W UP	.057 .036 .024	76.70 76.70 76.68
A018	Hollister	4/ 8/61	5.7	22.2	28	S01W N89W VERT	.065 .179 .050	40.46 40.48 40.62

TABLE 4.2 - continued

Record	Earthquake	Date	Mag.	Epicentral Distance (km)	Station Number	Comp.	Peak Acc. (g)	Record Length (sec)
B032	Puget Sound, Washington	4/29/65	6.5	60.9	325	S04E S86W VERT	.137 .198 .061	81.84 81.94 81.80
B033	Parkfield, California	6/27/66	5.6	58.5	13	N65E DOWN	.489 .206	43.64 43.60
B034				56.1	14	N05W N85E DOWN	.355 .434 .119	43.92 43.94 43.86
B035				25.4	15	N50E N40W DOWN	.237 .275 .079	26.18 26.14 26.12
B036				53.5	16	N50E N40W DOWN	.053 .064 .046	44.24 44.16 44.20
A019	Borrego Mountain	4/ 8/68	6.4	67.3	117	S00W S90W VERT	.130 .057 .030	87.40 87.20 87.12

TABLE 4.2 - continued

Record	Earthquake	Date	Mag.	Epicentral Distance (km)	Station Number	Comp.	Peak Acc. (g)	Record Length (sec)
W338	Lytle Creek	9/12/70	5.4	29.8	274	NORTH EAST DOWN	.116 .059 .054	29.52 29.50 29.52
C048	San Fernando	2/ 9/71	6.4	21.1	241	N00W S90W DOWN	.255 .134 .171	59.48 59.58 59.46
C051				41.4	151	N36E N54W DOWN	.100 .125 .049	52.32 52.28 52.30
D057				35.6	133	S00W N90E UP	.106 .151 .051	82.12 82.10 82.10
D058				35.6	135	S00W N90E UP	.171 .211 .089	79.46 79.46 79.44
D059				38.5	187	N46W S44W DOWN	.136 .150 .068	57.24 57.28 57.28

TABLE 4.2 - continued

Record	Earthquake	Date	Mag.	Epicentral Distance (km)	Station Number	Comp.	Peak Acc. (g)	Record Length (sec)
D062				41.3	181	N38W S52W DOWN	.120 .133 .076	54.06 54.12 53.98
D065				38.5	217	S00W S90W DOWN	.150 .159 .074	41.04 41.02 41.04
D068				33.5	238	N00E N90E DOWN	.083 .100 .058	36.94 36.90 36.90
E072				38.1	223	N75W N15E DOWN	.084 .117 .066	53.76 53.68 53.72
E075				38.7	208	N00E S90W DOWN	.136 .114 .048	43.60 43.58 43.64
E083				38.6	199	S00W N90E DOWN	.161 .165 .057	62.60 62.56 62.54

TABLE 4.2 - continued

Record	Earthquake	Date	Mag.	Epicentral Distance (km)	Station Number	Comp.	Peak Acc. (g)	Record Length (sec)
F086				47.9	288	N83W S07W UP	.107 .082 .043	78.06 77.94 77.86
F088				32.6	122	S70E S20W DOWN	.271 .213 .134	54.44 54.46 54.50
F089				42.6	175	S53E S37W DOWN	.134 .142 .077	59.16 59.28 59.40
F095				36.1	143	S88E S02W DOWN	.098 .085 .027	66.58 66.54 67.00
F098				41.3	166	S53E S37W DOWN	.241 .196 .071	56.20 56.12 56.10
F103				45.0	269	N00E N90W DOWN	.093 .123 .048	27.32 27.38 27.32

TABLE 4.2 - continued

Record	Earthquake	Date	Mag.	Epicentral Distance (km)	Station Number	Comp.	Peak Acc. (g)	Record Length (sec)
F104				53.5	52	N00E N90W DOWN	.087 .105 .036	9.20 11.00 10.96
G107				38.4	475	N00E N90E DOWN	.095 .109 .095	28.56 28.58 28.58
G108				38.4	264	N00E N90E DOWN	.202 .185 .093	98.98 98.98 98.96
G112				41.1	163	N38E N52W DOWN	.104 .080 .054	52.00 51.94 51.98
G114				32.6	262	S60E S30W DOWN	.113 .139 .088	57.66 57.66 57.66
H115				28.1	466	N11E N79W DOWN	.225 .149 .096	40.30 40.26 40.32

TABLE 4.2 - continued

Record	Earthquake	Date	Mag.	Epicentral Distance (km)	Station Number	Comp.	Peak Acc. (g)	Record Length (sec)
H121				41.7	482	S90W S00W DOWN	.122 .114 .081	45.68 45.64 45.66
I128				35.8	452	N00E S90W DOWN	.062 .093 .037	27.40 27.40 27.38
I131				36.8	455	N50E N40W DOWN	.188 .164 .038	48.28 48.28 48.28
I134				37.5	425	N54E S36E DOWN	.100 .084 .064	49.44 49.44 49.44
I137				27.8	461	S81E S09W DOWN	.143 .131 .102	56.56 56.54 56.56
J145				33.4	458	S00W S90W DOWN	.116 .105 .108	98.62 98.64 98.66

TABLE 4.2 - continued

Record	Earthquake	Date	Mag.	Epicentral Distance (km)	Station Number	Comp.	Peak Acc. (g)	Record Length (sec)
M176				41.4	437	N37E S53E DOWN	.085 .118 .042	88.22 88.18 88.18
N186				52.6	289	S37E S53W DOWN	.098 .099 .060	58.68 58.70 58.70
0199				40.5	469	N28E N62W DOWN	.141 .243 .151	49.38 49.38 49.38
P217				38.6	196	S00W N90E DOWN	.110 .090 .061	41.92 41.92 41.96
Q233				28.1	253	S12W N78W UP	.248 .201 .099	36.50 36.48 36.56
Q236				33.4	446	SOUTH EAST UP	.171 .125 .075	42.24 42.24 42.24

TABLE 4.2 - continued

Record	Earthquake	Date	Mag.	Epicentral Distance (km)	Station Number	Comp.	Peak Acc. (g)	Record Length (sec)
Q239				37.0	416	SOUTH EAST UP	.121 .165 .041	44.88 44.92 44.92
R244				40.4	145	N53W S37W UP	.152 .129 .044	41.86 41.86 41.86
R246				34.1	235	SOUTH EAST UP	.118 .109 .076	43.52 43.54 43.54
R248				34.2	232	SOUTH EAST UP	.188 .178 .091	44.98 44.98 44.98
R249				37.9	184	N44E S46E UP	.081 .086 .058	41.22 41.22 41.22
R251				40.3	148	N37E S53E UP	.199 .192 .069	47.06 47.12 47.10

TABLE 4.2 - continued

Record	Earthquake	Date	Mag.	Epicentral Distance (km)	Station Number	Comp.	Peak Acc. (g)	Record Length (sec)
R253				40.6	160	N30W S60W UP	.247 .225 .083	36.36 36.36 36.36
S255				37.6	443	N08E N82W UP	.126 .131 .048	43.10 43.08 43.10
S258				43.2	205	N29E S61E UP	.057 .085 .056	48.06 48.08 48.06
S261				38.2	413	N59E N31W UP	.100 .110 .066	38.92 38.92 38.92
S262				37.7	428	N83W S07W UP	.070 .096 .034	36.06 36.10 36.04
S266				38.6	211	NORTH WEST UP	.157 .132 .055	41.92 41.94 41.94

TABLE 4.2 - continued

Record	Earthquake	Date	Mag.	Epicentral Distance (km)	Station Number	Comp.	Peak Acc. (g)	Record Length (sec)
S267				50.6	299	NORTH EAST UP	.057 .063 .026	48.86 48.70 48.80

TABLE 4.3

EARTHQUAKE RECORD AND DATA - INTERMEDIATE

Record	Earthquake	Date	Mag.	Epicentral Distance (km)	Station Number	Comp.	Peak Acc. (g)	Record Length (sec)
B026	1st Northwest California	9/11/38	5.5	55.2	23	N45E S45E DOWN	.144 .089 .032	71.36 71.36 71.36
B027	2nd Northwest California	2/ 9/41	6.4	103.7	23	N45E S45E DOWN	.062 .039 .020	67.26 67.24 67.22
U300	Northern California	10/ 3/41	6.4	64.9	1023	N45W S45W UP	.121 .116 .038	67.92 67.88 67.94
A002	Northwest California	10/ 7/51	5.8	56.2	23	S44W N46W VERT	.104 .112 .027	55.88 55.88 55.88

TABLE 4.3 - continued

Record	Earthquake	Date	Mag.	Epicentral Distance (km)	Station Number	Comp.	Peak Acc. (g)	Record Length (sec)
B030	Northern California	9/22/52	5.5	43.1	23	N44E S46E DOWN	.054 .076 .030	57.86 57.98 57.82
V319	Southern California	11/21/52	6.0	76.0	83	N36W S54W UP	.054 .036 .027	48.82 48.88 48.84
A009	Eureka	12/21/54	6.5	40.0	23	N44E N46W VERT	.159 .201 .043	42.30 42.38 42.14
A016	San Francisco	3/22/57	5.3	14.2	80	S09E S81W VERT	.085 .056 .044	40.76 40.70 40.64
U308	Northern California	6/ 5/60	5.7	60.2	23	N46W S44W UP	.059 .075 .015	82.26 82.28 82.26

TABLE 4.3 - continued

Record	Earthquake	Date	Mag.	Epicentral Distance (km)	Station Number	Comp.	Peak Acc. (g)	Record Length (sec)
U312	Ferndale, California	12/10/67	5.8	30.5	23	N46W S44W UP	.105 .237 .033	92.96 93.04 93.04
W334	Lytle Creek	9/12/70	5.4	13.2	290	S65E S25W DOWN	.142 .198 .054	16.72 16.72 16.72
W336				22.2	112	S54E S36W DOWN	.057 .071 .038	10.20 10.20 10.20
C054	San Fernando	2/ 9/71	6.4	40.6	157	N52W S38W DOWN	.150 .119 .053	57.26 57.28 57.28
D056				29.5	110	N21E N69W DOWN	.315 .271 .156	61.76 61.86 61.82
E078				41.1	137	N50W S40W DOWN	.129 .172 .068	56.82 56.96 56.84

TABLE 4.3 - continued

Record	Earthquake	Date	Mag.	Epicentral Distance (km)	Station Number	Comp.	Peak Acc. (g)	Record Length (sec)
E081				33.3	284	S08E S82W DOWN	.217 .202 .065	50.46 50.52 50.52
F092				41.6	190	S62E S28W DOWN	.065 .081 .050	33.68 33.62 33.66
F105				37.4	140	S00W N90E UP	.085 .079 .068	63.54 63.56 63.54
G110				30.1	267	S82E S08W DOWN	.212 .142 .129	97.56 97.62 97.58
J144				24.3	128	N21E N69W DOWN	.353 .283 .107	36.60 36.72 36.70
J148				38.5	431	N00E S90W DOWN	.110 .114 .053	18.58 18.58 18.60

TABLE 4.3 - continued

Record	Earthquake	Date	Mag.	Epicentral Distance (km)	Station Number	Comp.	Peak Acc. (g)	Record Length (sec)
L166				29.3	220	N00E S90W DOWN	.167 .151 .071	65.32 65.16 65.20
M183				70.0	290	N65W N25E DOWN	.043 .057 .023	19.98 19.94 19.96
M184				70.0	290	S65E S25W DOWN	.044 .058 .025	29.70 29.56 29.74
N185				74.2	108	S50E S40W DOWN	.069 .069 .042	43.50 43.50 43.54
N187				71.0	287	N15E N75W DOWN	.057 .077 .029	29.94 29.98 29.98
N192				39.3	449	N29E N61W DOWN	.099 .101 .043	25.36 25.34 25.36

TABLE 4.3 - continued

Record	Earthquake	Date	Mag.	Epicentral Distance (km)	Station Number	Comp.	Peak Acc. (g)	Record Length (sec)
P214				34.8	226	S89W S01E DOWN	.157 .159 .118	46.94 46.96 47.06
Q241				40.3	172	N37E N53W UP	.088 .141 .062	49.34 49.32 49.26
S265				38.5	202	SOUTH WEST UP	.106 .128 .055	20.84 20.84 20.82

TABLE 4.4

EARTHQUAKE RECORDS AND DATA - HARD

Record	Earthquake	Date	Mag.	Epicentral Distance (km)	Station Number	Comp.	Peak Acc. (g)	Record Length (sec)
B025	Helena, Montana	10/31/35	6.0	6.3	323	S00W S90W DOWN	.146 .145 .089	50.90 51.00 51.04
A015	San Francisco	3/22/57	5.3	11.5	77	N10E S80E VERT	.083 .105 .038	39.86 39.86 39.72
B037	Parkfield, California	6/27/66	5.6	59.6	97	N65W S25W DOWN	.269 .347 .132	30.34 30.38 30.34
W335	Lytle Creek	9/12/70	5.4	18.9	111	S85E S05W DOWN	.071 .056 .060	38.12 38.12 38.10

TABLE 4.4 - continued

Record	Earthquake	Date	Mag.	Epicentral Distance (km)	Station Number	Comp.	Peak Acc. (g)	Record Length (sec)
C041	San Fernando	2/ 9/71	6.4	7.2	279	S16E	1.170	41.80
						S74W	1.075	41.70
						DOWN	.709	41.74
G106				34.7	266	S00W	.089	98.98
						S90W	.192	98.98
						DOWN	.085	98.98
J141				30.8	125	N21E	.148	60.18
						S69E	.111	60.24
						DOWN	.095	60.20
J142				28.0	126	S69E	.172	37.00
						S21W	.146	37.00
						DOWN	.154	36.98
J143				27.7	127	N21E	.122	34.96
						N69W	.112	35.00
						DOWN	.073	34.94
0198				32.5	141	S00W	.180	42.98
						S90W	.171	43.10
						DOWN	.123	43.04

TABLE 4.4 - continued

Record	Earthquake	Date	Mag.	Epicentral Distance (km)	Station Number	Comp.	Peak Acc. (g)	Record Length (sec)
0207				34.0	121	N56E	.066	61.12
						N34W	.099	61.68
						UP	.034	61.68
P221				42.0	104	N03E	.140	29.74
						N87W	.169	29.80
						DOWN	.049	29.78
P223				63.7	278	N55E	.071	32.80
						N35W	.054	32.84
						DOWN	.039	32.82

TABLE 4.5

SUMMARY OF RANGE AND INCREMENTS USED IN SELECTING THE POWER COEFFICIENTS P_1-P_4 IN PARAMETER η

P_1				P_2				P_3				P_4				r	No. of Iterations
Range		Inc.	Select.	Range		Inc.	Select.	Range		Inc.	Select.	Range		Inc.	Select.		
0.1	0.5	.1	.5	0.1	0.5	.1	.50	0.1	0.5	.1	.1	0.1	0.5	.1	.1	.95689	625
0.4	1.	.1	1.	0.4	1.	.1	.70	-0.2	0.2	.1	0.0	-0.2	0.2	.1	.2	.96279	1225
0.80	1.5	.1	1.	1.4	1.	.1	.70	-0.2	0.2	.1	0.0	0.1	0.5	.1	.2	.96279	1400
1.1	1.2	.1	1.	0.50	0.90	.1	.70	-0.2	0.2	.1	0.0	0.1	0.5	.1	.2	.96279	250
1.3	1.5	.1	1.5	1.1	1.5	.1	1.4	-0.2	0.2	.1	.1	0.0	0.4	.1	.3	.96309	375
1.3	1.7	.1	1.5	1.3	1.7	.1	1.4	-0.2	0.2	.1	.1	0.0	0.4	.1	.3	.96309	625
1.40	1.60	.05	1.50	1.30	1.50	.05	1.30	0.06	0.14	.02	.06	0.20	0.40	.05	.30	.96320	625
1.48	1.52	.01	1.52	1.28	1.32	.01	1.29	0.058	0.062	.001	.062	0.28	0.32	.01	.31	.96322	625
1.52	1.55	.01	1.53	1.28	1.32	.01	1.3	0.062	0.067	.001	.066	0.28	0.32	.01	.31	.96322	600

TABLE 4.6

COMPARISON OF CORRELATION COEFFICIENTS FOR DIFFERENT η'S

Component	Geology Type	η		η'		η''	
		P	r	P	r	P	r
Horizontal	Soft	0.860	.9950	1.57	.9543	1.20	.9561
	Intermediate	1.320	.9475	1.66	.9413	1.14	.9438
	Hard	0.890	.9880	1.60	.9879	1.16	.9892
	All Three	0.840	.9566	1.57	.9560	1.22	.9572
Vertical	Soft	0.620	.9453	1.51	.9453	1.32	.9444
	Intermediate	0.750	.9619	1.56	.9618	1.28	.9619
	Hard	0.440	.9801	1.48	.9799	1.64	.9853
	All Three	0.620	.9527	1.50	.9529	1.34	.9525
Horizontal and Vertical	Soft	0.630	.9602	1.53	.9601	1.30	.9595
	Intermediate	0.970	.9624	1.60	.9608	1.22	.9618
	Hard	0.780	.9815	1.55	.9812	1.24	.9818
	All Three	0.650	.9632	1.53	.9632	1.30	.9613

TABLE 4.7

COMPARISON OF THE RMS PREDICTED FROM DIFFERENT η'S FOR THE EIGHT HORIZONTAL COMPONENTS OF RECORDS USED IN CHAPTER 3

Record	Component	Actual RMS	Predicted RMS From		
			η r = .9278	η' r = .9098	η'' r = .8907
El Centro 1940	S00E	65.88	66.51	64.77	65.55
	S90W	55.14	50.88	51.80	52.29
Taft 1952	N2 E	40.20	44.84	45.32	44.46
	S69E	46.20	49.03	49.58	47.30
El Centro 1934	S00W	46.83	43.80	43.00	42.29
	S90W	46.80	46.54	44.55	45.22
Olympia 1949	N04W	46.59	45.42	47.41	47.07
	N86E	61.51	61.52	61.89	59.95

TABLE 4.8

PARAMETERS USED IN DEFINING THE RMS REGRESSION LINES

Component	Geology Type	N	P	A	B	r	RMS Variation* Percent
Horizontal	Soft	161	0.86	1.8514	0.8392	0.9550	91
	Intermediate	60	1.32	1.5573	0.7890	0.9475	90
	Hard	26	0.89	1.8050	0.8728	0.9880	98
	All Three	247	0.84	1.8521	0.8413	0.9566	92
Vertical	Soft	78	0.62	1.9721	0.9067	0.9453	89
	Intermediate	29	0.75	1.9030	0.8837	0.9619	93
	Hard	13	0.44	2.0440	0.9097	0.9801	96
	All Three	120	0.62	1.9508	0.8776	0.9527	91
Horizontal and Vertical	Soft	239	0.63	2.0025	0.9170	0.9602	92
	Intermediate	89	0.97	1.7597	0.8557	0.9624	93
	Hard	39	0.78	1.8675	0.9202	0.9815	96
	All Three	367	0.65	1.9740	0.8984	0.9632	93

* RMS variation accounted for by the parameter η; computed from $100r^2$ (Walpole and Myers, 1978)

TABLE 4.9

ACTUAL AND PREDICTED RMS
FOR HORIZONTAL COMPONENTS - SOFT

Record	Comp.	Initial Time (sec) T_1	Final Time (sec) T_2	Duration (sec) T	Peak Acc. (g) a	Epicentral Distance (km) D	Richter Mag. M	RMS Value (cm/sec^2)	
								Actual ψ_a	Predicted ψ_p
A001	S00E	1.38	26.30	24.92	.348	11.5	6.7	65.88	75.64
A001	S90W	1.32	26.24	24.92	.214	11.5	6.7	55.14	50.30
A003	S00E	14.64	30.16	15.52	.047	126.9	7.7	12.92	15.93
A003	S90W	13.66	26.68	13.02	.053	126.9	7.7	19.40	18.32
A004	N21E	3.46	20.66	17.20	.156	41.4	7.7	40.20	44.93
A004	S69E	3.18	17.34	14.16	.179	41.4	7.7	46.20	52.67
A005	N42E	6.72	21.36	14.64	.090	88.4	7.7	28.57	28.32
A005	S48E	6.52	20.40	13.88	.131	88.4	7.7	31.77	39.27
A006	S00W	12.18	26.14	13.96	.055	120.3	7.7	15.97	18.65
A006	N90E	12.90	24.40	11.50	.044	120.3	7.7	16.19	16.15

TABLE 4.9 - continued

Record	Comp.	Initial Time (sec) T_1	Final Time (sec) T_2	Duration (sec) T	Peak Acc. (g) a	Epicentral Distance (km) D	Richter Mag. M	RMS Value (cm/sec^2)	
								Actual ψ_a	Predicted ψ_p
A007	S00W	11.88	26.18	14.30	.059	120.3	7.7	16.40	19.68
A007	N90E	12.92	24.46	11.54	.042	120.3	7.7	16.53	15.52
A008	N11W	2.96	6.68	3.72	.168	24.0	6.5	67.85	58.96
A008	N79E	3.06	7.00	3.94	.258	24.0	6.5	98.30	83.44
A010	N31W	.26	1.70	1.44	.102	9.6	5.8	46.30	45.03
A010	N59E	.36	5.10	4.74	.108	9.6	5.8	23.40	36.18
A011	S00W	9.88	15.58	5.70	.033	121.2	6.8	12.85	13.21
A011	S90W	4.38	23.82	19.44	.051	121.2	6.8	14.87	14.46
A018	S01W	.94	11.90	10.96	.065	22.2	5.7	24.34	18.52
A018	N89W	.82	9.98	9.16	.179	22.2	5.7	37.67	45.11
A019	S00W	7.12	21.12	14.00	.130	67.3	6.4	26.20	33.17
A019	S90W	13.56	29.46	15.90	.057	67.3	6.4	17.68	16.14

TABLE 4.9 - continued

Record	Comp.	Initial Time (sec) T_1	Final Time (sec) T_2	Duration (sec) T	Peak Acc. (g) a	Epicentral Distance (km) D	Richter Mag. M	RMS Value (cm/sec^2)	
								Actual ψ_a	Predicted ψ_p
B021	S08W	.96	12.38	11.42	.133	50.4	6.3	32.10	35.35
B021	N82W	1.26	11.42	10.16	.154	50.4	6.3	29.68	41.04
B024	S00W	1.96	14.98	13.02	.160	66.3	6.5	46.83	40.74
B024	S90W	2.00	17.78	15.78	.183	66.3	6.5	46.80	43.68
B028	S02W	10.42	31.58	21.16	.068	57.7	7.1	21.21	19.49
B028	N88W	10.76	27.64	16.88	.067	57.7	7.1	18.50	20.25
B029	N04W	1.06	20.18	19.12	.165	16.9	7.1	46.59	44.48
B029	N86E	4.34	20.46	16.12	.280	16.9	7.1	61.51	72.03
B031	N21E	5.36	11.22	5.86	.065	42.8	5.9	17.16	21.33
B031	S69E	5.52	9.94	4.42	.068	42.8	5.9	19.50	23.59
B032	S04E	5.78	12.96	7.18	.137	60.9	6.5	44.07	41.03
B032	S86W	5.24	12.48	7.24	.198	60.9	6.5	53.52	55.78

TABLE 4.9 - continued

Record	Comp.	Initial Time (sec) T_1	Final Time (sec) T_2	Duration (sec) T	Peak Acc. (g) a	Epicentral Distance (km) D	Richter Mag. M	RMS Value (cm/sec^2)	
								Actual ψ_a	Predicted ψ_p
B033	N65E	2.66	4.84	2.18	.489	58.5	5.6	207.44	135.75
B034	N05W	5.56	12.54	6.98	.355	56.1	5.6	71.02	80.13
B034	N85E	4.92	11.14	6.22	.434	56.1	5.6	87.80	97.33
B035	N50E	1.58	9.40	7.82	.237	25.4	5.6	45.54	57.80
B035	N40E	1.68	7.00	5.32	.275	25.4	5.6	59.36	71.37
B036	N50E	2.32	16.02	13.70	.053	53.5	5.6	12.87	14.00
B036	N40W	2.42	17.52	15.10	.064	53.5	5.6	13.32	16.05
C048	N00W	3.36	14.80	11.44	.255	21.1	6.4	77.45	64.54
C048	S90W	2.80	20.56	17.76	.134	21.1	6.4	45.92	34.09
C051	N36E	.18	10.36	10.18	.100	41.1	6.4	33.85	29.25
C051	N54W	.26	7.64	7.38	.125	41.4	6.4	37.99	37.90

TABLE 4.9 - continued

Record	Comp.	Initial Time (sec) T_1	Final Time (sec) T_2	Duration (sec) T	Peak Acc. (g) a	Epicentral Distance (km) D	Richter Mag. M	RMS Value (cm/sec^2)	
								Actual ψ_a	Predicted ψ_p
D057	S00W	1.50	12.64	11.14	.106	35.6	6.4	32.99	30.32
D057	N90E	1.56	9.26	7.70	.151	35.6	6.4	50.44	44.31
D058	S00W	1.52	7.54	6.02	.171	35.6	6.4	58.49	51.97
D058	N90E	1.56	9.16	7.60	.211	35.6	6.4	67.68	58.85
D059	N46W	.30	7.56	7.26	.136	38.5	6.4	35.91	40.97
D059	S44W	.38	7.66	7.28	.150	38.5	6.4	43.49	44.46
D062	N38W	4.82	14.80	9.98	.120	41.3	6.4	35.16	34.24
D062	S52W	4.50	12.40	7.90	.133	41.3	6.4	49.87	39.33
D065	S00W	.06	5.84	5.78	.150	38.5	6.4	40.30	46.81
D065	S90W	0.00	6.16	6.16	.159	38.5	6.4	53.18	48.46
D068	N00E	0.00	7.46	7.46	.083	33.5	6.4	27.91	27.09
D068	N90E	.08	7.28	7.20	.100	33.5	6.4	30.68	31.92

TABLE 4.9 - continued

Record	Comp.	Initial Time (sec) T_1	Final Time (sec) T_2	Duration (sec) T	Peak Acc. (g) a	Epicentral Distance (km) D	Richter Mag. M	RMS Value (cm/sec^2)	
								Actual ψ_a	Predicted ψ_p
E072	N75W	0.00	11.08	11.08	.084	38.1	6.4	27.73	24.89
E072	N15E	.02	12.00	11.98	.117	38.1	6.4	32.52	32.30
E075	N00E	1.76	14.24	12.48	.136	38.7	6.4	38.86	36.29
E075	S90W	1.64	12.18	10.54	.114	38.7	6.4	34.76	32.50
E083	S00W	1.44	8.64	7.20	.161	38.6	6.4	57.41	47.29
E083	N90E	1.34	10.00	8.66	.165	38.6	6.4	46.60	46.32
F086	N83W	2.02	11.36	9.34	.107	47.9	6.4	30.55	31.34
F086	S07W	2.20	13.42	11.22	.082	47.9	6.4	24.47	24.06
F088	S70E	1.30	7.06	5.76	.271	32.6	6.4	101.75	77.57
F088	S20W	1.28	9.94	8.66	.213	32.6	6.4	69.34	57.85
F089	S53E	4.82	11.34	6.52	.134	42.6	6.4	49.51	41.25
F089	S37W	4.96	14.86	9.90	.142	42.6	6.4	33.77	39.45

TABLE 4.9 - continued

Record	Comp.	Initial Time (sec) T_1	Final Time (sec) T_2	Duration (sec) T	Peak Acc. (g) a	Epicentral Distance (km) D	Richter Mag. M	RMS Value (cm/sec^2)	
								Actual ψ_a	Predicted ψ_p
F095	S88E	2.92	10.16	7.24	.098	36.1	6.4	32.37	31.24
F095	S02W	3.00	11.76	8.76	.085	36.1	6.4	31.29	26.56
F098	S53E	5.08	11.58	6.50	.241	41.3	6.4	56.75	67.66
F098	S37W	5.02	11.70	6.68	.196	41.3	6.4	53.43	56.54
F103	N00E	.48	10.26	9.78	.093	45.0	6.4	27.64	27.66
F103	N90W	.42	10.66	10.24	.123	45.0	6.4	35.20	34.61
F104	N00E	0.00	8.86	8.86	.087	53.5	6.4	20.47	26.52
F104	N90W	.12	2.88	2.76	.105	53.5	6.4	26.92	40.31
G107	N00E	5.16	14.28	9.12	.095	38.4	6.4	27.40	28.82
G107	N90E	5.34	16.86	11.52	.109	38.4	6.4	32.42	30.69
G108	N00E	4.52	14.82	10.30	.202	38.4	6.4	45.09	52.81
G108	N90E	4.68	15.40	10.72	.185	38.4	6.4	41.63	48.62

TABLE 4.9 - continued

Record	Comp.	Initial Time (sec) T_1	Final Time (sec) T_2	Duration (sec) T	Peak Acc. (g) a	Epicentral Distance (km) D	Richter Mag. M	RMS Value (cm/sec^2)	
								Actual ψ_a	Predicted ψ_p
G112	N38E	2.58	10.88	8.30	.104	41.1	6.4	30.75	31.65
G112	N52W	2.70	13.44	10.74	.080	41.1	6.4	24.87	23.97
G114	S60E	1.18	15.68	14.50	.113	32.6	6.4	35.67	30.28
G114	S30W	1.02	17.74	16.72	.139	32.6	6.4	28.96	34.90
H115	N11E	4.36	21.02	16.66	.225	28.1	6.4	55.77	52.70
H115	N79W	4.14	22.26	18.12	.149	28.1	6.4	40.81	36.59
H121	S90W	6.42	16.62	10.20	.122	41.7	6.4	36.33	34.53
H121	S00W	6.26	14.62	8.36	.114	41.7	6.4	36.90	34.11
I128	N00E	5.50	15.76	10.26	.062	35.8	6.4	21.92	19.68
I128	S90W	5.28	12.86	7.58	.093	35.8	6.4	27.40	29.60
I131	N50E	6.72	14.30	7.58	.188	36.8	6.4	52.19	53.36
I131	N40W	6.42	15.70	9.28	.164	36.8	6.4	39.29	45.48

TABLE 4.9 - continued

Record	Comp.	Initial Time (sec) T_1	Final Time (sec) T_2	Duration (sec) T	Peak Acc. (g) a	Epicentral Distance (km) D	Richter Mag. M	RMS Value (cm/sec^2)	
								Actual ψ_a	Predicted ψ_p
I134	N54E	6.56	14.54	7.98	.100	37.5	6.4	34.17	31.03
I134	S36E	6.66	14.10	7.44	.084	37.5	6.4	27.68	27.23
I137	S81E	5.44	24.92	19.48	.143	27.8	6.4	31.43	34.80
I137	S09W	5.52	21.22	15.70	.131	27.8	6.4	41.48	33.93
J145	S00W	2.82	18.14	15.32	.116	33.4	6.4	41.28	30.54
J145	S90W	1.86	18.74	16.88	.105	33.4	6.4	39.88	27.49
M176	N37E	3.48	13.34	9.86	.085	41.4	6.4	30.78	25.70
M176	S53E	2.68	15.34	12.66	.118	41.4	6.4	28.68	32.01
N186	S37E	.68	12.12	11.44	.098	52.6	6.4	23.54	27.70
N186	S53W	1.08	10.04	8.96	.099	52.6	6.4	29.91	29.50
0199	N28E	7.08	17.02	9.94	.141	40.5	6.4	38.06	39.27
0199	N62W	6.64	14.62	7.98	.243	40.5	6.4	60.51	65.13

TABLE 4.9 - continued

Record	Comp.	Initial Time (sec) T_1	Final Time (sec) T_2	Duration (sec) T	Peak Acc. (g) a	Epicentral Distance (km) D	Richter Mag. M	RMS Value (cm/sec^2)	
								Actual ψ_a	Predicted ψ_p
P217	S00W	1.68	14.06	12.38	.110	38.6	6.4	30.29	30.43
P217	N90E	1.48	11.88	10.40	.090	38.6	6.4	27.70	26.73
Q233	S12W	5.12	16.10	10.98	.248	28.1	6.4	74.12	62.77
Q233	N78W	4.84	20.06	15.22	.201	28.1	6.4	50.72	48.92
Q236	SOUT	4.94	14.44	9.50	.171	33.4	6.4	44.91	47.07
Q236	EAST	5.04	16.34	11.30	.125	33.4	6.4	29.47	34.81
Q239	SOUT	5.16	16.86	11.70	.121	37.0	6.4	38.02	33.45
Q239	EAST	5.20	13.18	7.98	.165	37.0	6.4	43.90	47.27
R244	N53W	5.70	13.86	8.16	.152	40.4	6.4	38.92	43.72
R244	S37W	5.86	15.38	9.52	.129	40.4	6.4	37.14	36.81
R246	SOUT	5.48	15.90	10.42	.118	34.1	6.4	33.25	33.74
R246	EAST	5.32	16.02	10.70	.109	34.1	6.4	37.35	31.38

TABLE 4.9 - continued

Record	Comp.	Initial Time (sec) T_1	Final Time (sec) T_2	Duration (sec) T	Peak Acc. (g) a	Epicentral Distance (km) D	Richter Mag. M	RMS Value (cm/sec^2)	
								Actual ψ_a	Predicted ψ_p
R248	SOUT	5.38	15.12	9.74	.188	34.2	6.4	50.73	50.63
R248	EAST	5.48	16.14	10.66	.178	34.2	6.4	49.58	47.39
R249	N44E	5.48	13.74	8.26	.081	37.9	6.4	28.05	25.79
R249	S46E	5.38	16.06	10.68	.086	37.9	6.4	26.24	25.60
R251	N37E	3.56	13.10	9.54	.199	40.3	6.4	55.08	52.94
R251	S53E	3.38	10.44	7.06	.192	40.3	6.4	49.84	54.95
R253	N30W	6.24	13.24	7.00	.247	40.6	6.4	60.22	67.99
R253	S60W	6.08	17.92	11.84	.225	40.6	6.4	45.75	55.89
S255	N08E	1.20	11.64	10.44	.126	37.6	6.4	38.00	35.47
S255	N82W	1.30	14.34	13.04	.131	37.6	6.4	30.40	34.87
S258	N29E	6.96	16.46	9.50	.057	43.2	6.4	23.14	18.49
S258	S61E	7.60	19.10	11.50	.085	43.2	6.4	24.10	24.78

TABLE 4.9 - continued

Record	Comp.	Initial Time (sec) T_1	Final Time (sec) T_2	Duration (sec) T	Peak Acc. (g) a	Epicentral Distance (km) D	Richter Mag. M	RMS Value (cm/sec^2)	
								Actual ψ_a	Predicted ψ_p
S261	N59E	0.00	7.36	7.36	.100	38.2	6.4	34.33	31.57
S261	N31W	0.00	7.32	7.32	.110	38.2	6.4	30.36	34.24
S262	N83W	2.58	14.76	12.18	.070	37.7	6.4	26.70	20.92
S262	S07W	3.42	17.02	13.60	.096	37.7	6.4	27.29	26.61
S266	NORT	5.88	18.52	12.64	.157	38.6	6.4	36.79	40.82
S266	WEST	5.94	17.30	11.36	.132	38.6	6.4	37.34	36.15
S267	NORT	6.66	18.18	11.52	.057	50.6	6.4	17.11	17.58
S267	EAST	7.70	21.58	13.88	.063	50.6	6.4	15.72	18.34
T274	NORT	0.00	4.02	4.02	.029	12.6	3.0	8.75	6.62
T274	EAST	.02	2.50	2.48	.050	12.6	3.0	12.13	11.66
T286	NORT	2.68	16.80	14.12	.060	46.2	6.5	15.24	17.87
T286	EAST	2.90	17.60	14.70	.047	46.2	6.5	12.59	14.43

TABLE 4.9 - continued

Record	Comp.	Initial Time (sec) T_1	Final Time (sec) T_2	Duration (sec) T	Peak Acc. (g) a	Epicentral Distance (km) D	Richter Mag. M	RMS Value (cm/sec^2)	
								Actual ψ_a	Predicted ψ_p
T292	NORT	0.00	8.56	8.56	.064	23.2	5.4	14.94	18.32
T292	EAST	0.00	8.54	8.54	.072	23.2	5.4	14.45	20.24
U299	N45E	.04	1.74	1.70	.238	36.4	5.9	97.52	84.24
U299	S45E	0.00	1.72	1.72	.176	36.4	5.9	82.03	65.22
U301	N89W	2.76	8.70	5.94	.197	19.9	5.3	40.36	50.57
U301	S01W	2.56	7.56	5.00	.122	19.9	5.3	42.79	35.15
U305	N89W	2.38	13.58	11.20	.053	26.8	5.3	13.88	14.37
U305	S01W	1.76	13.22	11.46	.050	26.8	5.3	14.61	13.62
U307	N89W	.36	7.38	7.02	.057	8.0	5.0	16.68	17.01
U307	S01W	.38	4.82	4.44	.036	8.0	5.0	13.56	12.82
V314	N39E	3.04	18.98	15.94	.064	57.4	6.3	21.08	17.65
V314	N51W	2.98	15.08	12.10	.097	57.4	6.3	30.34	26.61

TABLE 4.9 - continued

Record	Comp.	Initial Time (sec) T_1	Final Time (sec) T_2	Duration (sec) T	Peak Acc. (g) a	Epicentral Distance (km) D	Richter Mag. M	RMS Value (cm/sec^2)	
								Actual ψ_a	Predicted ψ_p
V315	SOUT	.86	6.94	6.08	.196	28.4	6.3	65.54	57.92
V315	WEST	.22	7.06	6.84	.159	28.4	6.3	56.69	47.33
V316	NORT	5.72	10.00	4.28	.040	3.4	5.4	14.99	15.80
V316	EAST	5.22	9.56	4.34	.055	3.4	5.4	20.10	20.58
V329	SOUT	0.00	4.26	4.26	.167	6.3	4.7	36.36	44.75
V329	WEST	0.00	.50	.50	.089	6.3	4.7	39.17	42.62
W338	NORT	.08	1.62	1.54	.116	29.8	5.4	44.44	43.78
W338	EAST	.08	2.36	2.28	.059	29.8	5.4	27.20	22.74

TABLE 4.10

ACTUAL AND PREDICTED RMS
FOR HORIZONTAL COMPONENTS - INTERMEDIATE

Record	Comp.	Initial Time (sec) T_1	Final Time (sec) T_2	Duration (sec) T	Peak Acc. (g) a	Epicentral Distance (km) D	Richter Mag. M	RMS Value (cm/sec^2)	
								Actual ψ_a	Predicted ψ_p
A002	S44W	1.74	9.36	7.62	.104	56.2	5.8	24.02	25.72
A002	N46W	1.98	9.46	7.48	.112	56.2	5.8	28.07	27.43
A009	N44E	6.22	16.72	10.50	.159	40.0	6.5	52.02	38.72
A009	N46W	6.10	14.60	8.50	.201	40.0	6.5	47.92	49.88
A016	S09E	.76	3.64	2.88	.085	14.2	5.3	30.01	29.22
A016	S81W	.56	4.66	4.10	.056	14.2	5.3	19.81	18.76
B026	N45E	1.80	6.54	4.74	.144	55.2	5.5	31.89	36.11
B026	S45E	2.04	7.14	5.10	.089	55.2	5.5	26.44	24.13
B027	N45E	2.70	8.78	6.08	.062	103.7	6.4	16.85	20.15
B027	S45E	.08	5.62	5.54	.039	103.7	6.4	14.70	14.40

TABLE 4.10 - continued

Record	Comp.	Initial Time (sec) T_1	Final Time (sec) T_2	Duration (sec) T	Peak Acc. (g) a	Epicentral Distance (km) D	Richter Mag. M	RMS Value (cm/sec^2)	
								Actual ψ_a	Predicted ψ_p
B030	N44E	4.66	9.70	5.04	.054	43.1	5.5	22.17	16.61
B030	S46E	4.78	9.78	5.00	.076	43.1	5.5	21.39	21.81
C054	N52W	2.16	8.86	6.70	.150	40.6	6.4	41.54	41.82
C054	S38W	2.04	12.06	10.02	.119	40.6	6.4	33.21	30.60
D056	N21E	1.02	8.02	7.00	.315	29.5	6.4	70.90	75.69
D056	N69W	1.02	14.96	13.94	.271	29.5	6.4	62.58	53.82
E078	N50W	1.62	9.08	7.46	.129	41.1	6.4	36.60	35.84
E078	S40W	1.72	10.04	8.32	.172	41.1	6.4	36.76	43.41
E081	S08E	0.00	8.52	8.52	.217	33.3	6.4	41.16	52.50
E081	S82W	.02	1.98	1.96	.202	33.3	6.4	76.38	79.74
F092	S62E	.20	7.84	7.64	.065	41.6	6.4	23.36	20.69
F092	S28W	.02	9.50	9.48	.081	41.6	6.4	24.67	22.96

TABLE 4.10 - continued

Record	Comp.	Initial Time (sec) T_1	Final Time (sec) T_2	Duration (sec) T	Peak Acc. (g) a	Epicentral Distance (km) D	Richter Mag. M	RMS Value (cm/sec^2)	
								Actual ψ_a	Predicted ψ_p
F105	S00W	2.82	8.50	5.68	.085	37.4	6.4	29.90	28.34
F105	N90E	2.80	10.60	7.80	.079	37.4	6.4	24.38	24.15
G110	S82E	2.12	7.66	5.54	.212	30.1	6.4	58.13	59.64
G110	S08W	2.32	10.40	8.08	.142	30.1	6.4	34.93	38.49
J144	N21E	.84	3.92	3.08	.353	24.3	6.4	114.37	109.39
J144	N69W	.30	3.76	3.46	.283	24.3	6.4	102.09	88.50
J148	N00E	6.10	18.46	12.36	.110	38.5	6.4	32.63	26.97
J148	S90W	5.92	16.24	10.32	.114	38.5	6.4	38.57	29.40
L166	N00E	2.02	9.38	7.36	.167	29.3	6.4	36.99	45.16
L166	S90W	1.80	7.36	5.56	.151	29.3	6.4	51.79	45.67
M183	N65W	6.78	14.68	7.90	.043	70.0	6.4	12.98	14.25
M183	N25E	7.04	15.38	8.34	.057	70.0	6.4	15.33	17.50

TABLE 4.10 - continued

Record	Comp.	Initial Time (sec) T_1	Final Time (sec) T_2	Duration (sec) T	Peak Acc. (g) a	Epicentral Distance (km) D	Richter Mag. M	RMS Value (cm/sec^2)	
								Actual ψ_a	Predicted ψ_p
M184	S65E	5.18	12.94	7.76	.044	70.0	6.4	13.18	14.60
M184	S25W	4.48	12.70	8.22	.058	70.0	6.4	15.65	17.82
N185	S50E	1.60	12.98	11.38	.069	74.2	6.4	20.61	18.33
N185	S40W	1.80	10.78	8.98	.069	74.2	6.4	24.47	19.78
N187	N15E	1.74	9.56	7.82	.057	71.0	6.4	17.83	17.85
N187	N75W	2.14	9.74	7.60	.077	71.0	6.4	26.08	22.83
N192	N29E	4.52	15.86	11.34	.099	39.3	6.4	27.83	25.48
N192	N61W	4.54	11.80	7.26	.101	39.3	6.4	36.36	29.90
P214	S89W	1.32	8.08	6.76	.157	34.8	6.4	55.86	43.69
P214	S01E	1.36	7.18	5.82	.159	34.8	6.4	61.32	46.32
Q241	N37E	6.48	16.78	10.30	.088	40.3	6.4	33.85	23.91
Q241	N53W	6.38	14.98	8.60	.141	40.3	6.4	35.46	36.77

TABLE 4.10 - continued

Record	Comp.	Initial Time (sec) T_1	Final Time (sec) T_2	Duration (sec) T	Peak Acc. (g) a	Epicentral Distance (km) D	Richter Mag. M	RMS Value (cm/sec^2)	
								Actual ψ_a	Predicted ψ_p
S265	SOUT	6.02	18.60	12.58	.106	38.5	6.4	29.60	26.04
S265	WEST	6.04	16.44	10.40	.128	38.5	6.4	32.24	32.14
U300	N45W	6.50	11.64	5.14	.121	64.9	6.4	29.86	37.24
U300	S45W	6.04	9.80	3.76	.116	64.9	6.4	35.02	39.84
U308	N46W	2.68	8.06	5.38	.059	60.2	5.7	14.77	17.89
U308	S44W	6.74	13.46	6.72	.075	60.2	5.7	14.44	20.12
U312	N46W	6.34	8.18	1.84	.105	30.5	5.8	37.90	42.76
U312	S44W	6.38	11.60	5.22	.237	30.5	5.8	31.44	58.05
V319	N36W	1.12	9.56	8.44	.054	76.0	6.0	12.29	15.22
V319	S54W	1.58	5.68	4.10	.036	76.0	6.0	14.16	13.95
W334	S65E	.06	2.36	2.30	.142	13.2	5.4	55.65	48.55
W334	S25W	.04	2.30	2.26	.198	13.2	5.4	59.67	63.47

TABLE 4.10 - continued

Record	Comp.	Initial Time (sec) T_1	Final Time (sec) T_2	Duration (sec) T	Peak Acc. (g) a	Epicentral Distance (km) D	Richter Mag. M	RMS Value (cm/sec^2)	
								Actual ψ_a	Predicted ψ_p
W336	S54E	.04	2.18	2.14	.057	22.2	5.4	24.05	23.34
W336	S36W	0.00	2.08	2.08	.071	22.2	5.4	24.81	28.01

TABLE 4.11

ACTUAL AND PREDICTED RMS
FOR HORIZONTAL COMPONENTS - HARD

Record	Comp.	Initial Time (sec) T_1	Final Time (sec) T_2	Duration (sec) T	Peak Acc. (g) a	Epicentral Distance (km) D	Richter Mag. M	RMS Value (cm/sec^2)	
								Actual ψ_a	Predicted ψ_p
A015	N10E	1.08	2.26	1.18	.083	11.5	5.3	33.94	33.20
A015	S80E	1.16	2.76	1.60	.105	11.5	5.3	40.65	37.89
B025	S00W	1.58	3.30	1.72	.146	6.3	6.0	47.98	58.03
B025	S90W	1.64	3.24	1.60	.145	6.3	6.0	63.29	58.70
B037	N65W	2.38	6.06	3.68	.269	59.6	5.6	67.40	68.47
B037	S25W	2.76	4.50	1.74	.347	59.6	5.6	117.41	102.40
C041	S15W	2.12	9.86	7.74	1.170	7.2	6.4	253.60	263.36
C041	S74W	1.18	10.50	9.32	1.075	7.2	6.4	222.72	233.90
G106	S00W	1.90	8.76	6.86	.089	34.7	6.4	28.61	26.41
G106	S90W	3.16	9.24	6.08	.192	34.7	6.4	56.15	53.18

TABLE 4.11 - continued

Record	Comp.	Initial Time (sec) T_1	Final Time (sec) T_2	Duration (sec) T	Peak Acc. (g) a	Epicentral Distance (km) D	Richter Mag. M	RMS Value (cm/sec^2)	
								Actual ψ_a	Predicted ψ_p
J141	N21E	2.14	15.24	13.10	.148	30.8	6.4	33.18	35.44
J141	S69E	2.26	15.80	13.54	.111	30.8	6.4	26.83	27.35
J142	S69E	2.06	7.94	5.88	.172	28.0	6.4	43.68	49.24
J142	S21W	2.04	6.30	4.26	.146	28.0	6.4	45.51	46.12
J143	N21E	.22	4.84	4.62	.122	27.7	6.4	36.03	38.69
J143	N69W	.08	3.52	3.44	.112	27.7	6.4	35.43	38.55
0198	S00W	3.74	9.82	6.08	.180	32.5	6.4	55.00	50.44
0198	S90W	3.56	13.12	9.56	.171	32.5	6.4	55.02	43.25
0207	N56E	.16	4.70	4.54	.066	34.0	6.4	21.23	22.49
0207	N34W	.12	2.52	2.40	.099	34.0	6.4	32.87	37.35
P221	N03E	.64	9.72	9.08	.140	42.0	6.4	38.85	36.29
P221	N87W	.26	8.62	8.36	.169	42.0	6.4	42.44	43.63

TABLE 4.11 - continued

Record	Comp.	Initial Time (sec) T_1	Final Time (sec) T_2	Duration (sec) T	Peak Acc. (g) a	Epicentral Distance (km) D	Richter Mag. M	RMS Value (cm/sec^2)	
								Actual ψ_a	Predicted ψ_p
P223	N55E	0.00	8.88	8.88	.071	63.7	6.4	17.05	19.75
P223	N35W	.66	7.44	6.78	.054	63.7	6.4	16.71	16.60
W335	S85E	.02	1.14	1.12	.071	18.9	5.4	35.12	29.15
W335	S05W	0.00	1.60	1.60	.056	18.9	5.4	21.73	21.74

TABLE 4.12

ACTUAL AND PREDICTED RMS
FOR VERTICAL COMPONENTS - SOFT

Record	Comp.	Initial Time (sec) T_1	Final Time (sec) T_2	Duration (sec) T	Peak Acc. (g) a	Epicentral Distance (km) D	Richter Mag. M	RMS Value (cm/sec^2)	
								Actual ψ_a	Predicted ψ_p
A001	VERT	.18	11.50	11.32	.210	11.5	6.7	47.40	54.74
A003	VERT	19.30	19.34	.04	.030	126.9	7.7	28.02	25.40
A004	VERT	1.08	28.00	26.92	.105	41.4	7.7	22.85	26.50
A005	VERT	8.12	19.36	11.24	.044	88.4	7.7	13.56	13.64
A006	VERT	21.96	22.02	.06	.023	120.3	7.7	21.94	18.63
A007	VERT	18.04	19.42	1.38	.021	120.3	7.7	9.07	9.94
A008	VERT	0.00	7.74	7.74	.083	24.0	6.5	20.73	23.99
A010	VERT	.54	2.90	2.38	.045	9.6	5.8	14.00	16.12
A018	VERT	1.26	14.02	12.76	.050	22.2	5.7	10.50	12.65
A019	VERT	7.46	12.20	4.74	.030	67.3	6.4	9.21	9.88

TABLE 4.12 - continued

Record	Comp.	Initial Time (sec) T_1	Final Time (sec) T_2	Duration (sec) T	Peak Acc. (g) a	Epicentral Distance (km) D	Richter Mag. M	RMS Value (cm/sec^2)	
								Actual ψ_a	Predicted ψ_p
B021	DOWN	.20	3.88	3.68	.152	50.4	6.3	30.04	44.95
B024	VERT	.86	15.34	14.48	.069	66.3	6.5	18.40	17.52
B029	DOWN	0.00	21.86	21.86	.092	16.9	7.1	21.10	23.75
B031	VERT	2.16	13.66	11.50	.036	42.8	5.9	8.72	9.57
B032	VERT	.14	10.52	10.38	.061	60.9	6.5	17.35	16.66
B033	DOWN	1.48	6.52	5.04	.206	58.5	5.6	64.87	51.15
B034	DOWN	.52	9.54	9.02	.119	56.1	5.6	31.97	28.14
B035	DOWN	.98	6.22	5.24	.079	25.4	5.6	26.76	21.97
B036	DOWN	.94	8.14	7.20	.046	53.5	5.6	16.59	12.39
C048	DOWN	0.00	21.12	21.12	.171	21.1	6.4	42.24	38.54
C051	DOWN	2.42	9.42	7.00	.049	41.4	6.4	13.41	14.67

TABLE 4.12 - continued

Record	Comp.	Initial Time (sec) T_1	Final Time (sec) T_2	Duration (sec) T	Peak Acc. (g) a	Epicentral Distance (km) D	Richter Mag. M	RMS Value (cm/sec^2)	
								Actual ψ_a	Predicted ψ_p
D057	UP	.06	9.88	9.82	.051	35.6	6.4	17.47	14.42
D058	UP	.10	9.84	9.74	.089	35.6	6.4	21.73	23.93
D059	DOWN	.54	6.80	6.26	.068	38.5	6.4	18.20	20.19
D062	DOWN	3.42	15.94	12.52	.076	41.3	6.4	15.38	19.74
D065	DOWN	.04	11.08	11.04	.074	38.5	6.4	22.20	19.74
D068	DOWN	0.00	8.26	8.26	.058	33.5	6.4	18.64	16.74
E072	DOWN	0.00	15.02	15.02	.066	38.1	6.4	14.52	16.88
E075	DOWN	1.66	13.08	11.42	.048	38.7	6.4	15.32	13.25
E083	DOWN	0.00	13.46	13.46	.057	38.6	6.4	15.31	15.05
F086	UP	1.02	12.44	11.42	.043	47.9	6.4	12.93	11.90
F088	DOWN	.72	9.78	9.06	.134	32.6	6.4	45.59	35.23

TABLE 4.12 - continued

Record	Comp.	Initial Time (sec) T_1	Final Time (sec) T_2	Duration (sec) T	Peak Acc. (g) a	Epicentral Distance (km) D	Richter Mag. M	RMS Value (cm/sec^2)	
								Actual ψ_a	Predicted ψ_p
F089	DOWN	3.30	12.62	9.32	.077	42.6	6.4	23.87	21.00
F095	DOWN	5.66	15.48	9.82	.027	36.1	6.4	8.35	8.10
F098	DOWN	3.58	12.12	8.54	.071	41.3	6.4	21.44	19.84
F103	DOWN	.64	11.68	11.04	.048	45.0	6.4	11.11	13.26
F104	DOWN	.14	8.00	7.86	.036	53.5	6.4	9.55	10.77
G107	DOWN	3.26	11.84	8.58	.095	38.4	6.4	20.06	25.88
G108	DOWN	4.28	11.54	7.26	.093	38.4	6.4	30.91	26.13
G112	DOWN	3.24	12.02	8.78	.054	41.1	6.4	15.39	15.40
G114	DOWN	.74	12.36	11.62	.088	32.6	6.4	25.50	23.04
H115	DOWN	.88	14.22	13.34	.096	28.1	6.4	25.90	24.47
H121	DOWN	1.20	16.20	15.00	.081	41.7	6.4	20.82	20.26

TABLE 4.12 - continued

Record	Comp.	Initial Time (sec) T_1	Final Time (sec) T_2	Duration (sec) T	Peak Acc. (g) a	Epicentral Distance (km) D	Richter Mag. M	RMS Value (cm/sec^2)	
								Actual ψ_a	Predicted ψ_p
I128	DOWN	3.78	16.78	13.00	.037	35.8	6.4	10.37	10.26
I131	DOWN	7.14	14.68	7.54	.038	36.8	6.4	13.92	11.55
I134	DOWN	6.52	14.40	7.88	.064	37.5	6.4	18.70	18.37
I137	DOWN	1.42	16.92	15.50	.102	27.8	6.4	25.09	25.20
J145	DOWN	1.70	24.36	22.66	.108	33.4	6.4	29.22	24.67
M176	DOWN	.96	11.70	10.74	.042	41.4	6.4	14.13	11.84
N186	DOWN	0.00	7.10	7.10	.060	52.6	6.4	9.61	17.43
O199	DOWN	5.32	13.32	8.00	.151	40.5	6.4	36.00	39.80
P217	DOWN	.86	13.58	12.72	.061	38.6	6.4	14.74	16.17
Q233	UP	1.14	14.46	13.32	.099	28.1	6.4	26.94	25.17
Q236	UP	4.96	13.76	8.80	.075	33.4	6.4	24.58	20.90

TABLE 4.12 - continued

Record	Comp.	Initial Time (sec) T_1	Final Time (sec) T_2	Duration (sec) T	Peak Acc. (g) a	Epicentral Distance (km) D	Richter Mag. M	RMS Value (cm/sec^2)	
								Actual ψ_a	Predicted ψ_p
Q239	UP	4.52	12.50	7.98	.041	37.0	6.4	13.99	12.25
R244	UP	4.30	12.58	8.28	.044	40.4	6.4	15.40	12.93
R246	UP	2.18	15.80	13.62	.076	34.1	6.4	19.81	19.59
R248	UP	2.34	14.40	12.06	.091	34.2	6.4	24.00	23.56
R249	UP	5.54	13.02	7.48	.058	37.9	6.4	16.75	16.95
R251	UP	1.38	12.44	11.06	.069	40.3	6.4	16.18	18.49
R253	UP	3.80	13.54	9.74	.083	40.6	6.4	21.34	22.35
S255	UP	.86	10.50	9.64	.048	37.6	6.4	13.19	13.67
S258	UP	3.60	16.18	12.58	.056	43.2	6.4	14.54	14.93
S261	UP	.26	5.18	4.92	.066	38.2	6.4	23.59	20.50
S262	UP	1.82	8.94	7.12	.034	37.7	6.4	13.42	10.54

TABLE 4.12 - continued

Record	Comp.	Initial Time (sec) T_1	Final Time (sec) T_2	Duration (sec) T	Peak Acc. (g) a	Epicentral Distance (km) D	Richter Mag. M	RMS Value (cm/sec^2)	
								Actual ψ_a	Predicted ψ_p
S266	UP	.44	19.02	18.58	.055	38.6	6.4	16.56	13.78
S267	UP	10.06	14.98	4.92	.026	50.6	6.4	7.15	8.72
T274	UP	.02	3.56	3.54	.022	12.6	3.0	4.29	4.80
T286	UP	4.76	7.12	2.36	.026	46.2	6.5	7.73	10.05
T292	UP	0.00	1.92	1.92	.058	23.2	5.4	12.71	19.33
U299	UP	.14	6.78	6.64	.070	36.4	5.9	15.07	19.37
U301	UP	0.00	7.24	7.24	.071	19.9	5.3	18.16	18.27
U305	UP	0.00	9.28	9.28	.024	26.8	5.3	6.89	6.47
U307	UP	1.28	5.66	4.38	.024	8.0	5.0	8.98	7.40
V314	UP	1.46	11.78	10.32	.065	57.4	6.3	18.64	17.30
V315	UP	.10	5.92	5.82	.285	28.4	6.3	82.36	74.95

TABLE 4.12 - continued

Record	Comp.	Initial Time (sec) T_1	Final Time (sec) T_2	Duration (sec) T	Peak Acc. (g) a	Epicentral Distance (km) D	Richter Mag. M	RMS Value (cm/sec^2)	
								Actual ψ_a	Predicted ψ_p
V329	UP	.74	2.92	2.18	.025	6.3	4.7	8.32	8.36
W338	DOWN	.04	1.46	1.42	.054	29.8	5.4	22.35	18.91

TABLE 4.13

ACTUAL AND PREDICTED RMS
FOR VERTICAL COMPONENTS - INTERMEDIATE

Record	Comp.	Initial Time (sec) T_1	Final Time (sec) T_2	Duration (sec) T	Peak Acc. (g) a	Epicentral Distance (km) D	Richter Mag. M	RMS Value (cm/sec^2)	
								Actual ψ_a	Predicted ψ_p
A002	VERT	3.00	9.58	6.58	.027	56.2	5.8	9.98	8.51
A009	VERT	7.96	16.56	8.60	.043	40.0	6.5	15.42	13.61
A016	VERT	1.30	3.00	1.70	.044	14.2	5.3	18.34	17.00
B026	DOWN	3.64	8.12	4.48	.032	55.2	5.5	7.68	10.23
B027	DOWN	5.96	6.92	.96	.020	103.7	6.4	11.03	10.27
B030	DOWN	5.52	8.50	2.98	.030	43.1	5.5	11.71	10.62
C054	DOWN	1.10	10.42	9.32	.053	40.6	6.4	16.33	15.87
D056	DOWN	.84	8.80	7.96	.156	29.5	6.4	41.57	43.17
E078	DOWN	.26	10.58	10.32	.068	41.1	6.4	18.36	19.37
E081	DOWN	.16	11.42	11.26	.065	33.3	6.4	14.76	18.45

TABLE 4.13 - continued

Record	Comp.	Initial Time (sec) T_1	Final Time (sec) T_2	Duration (sec) T	Peak Acc. (g) a	Epicentral Distance (km) D	Richter Mag. M	RMS Value (cm/sec^2)	
								Actual ψ_a	Predicted ψ_p
F092	DOWN	.38	7.36	6.98	.050	41.6	6.4	15.89	15.98
F105	UP	.82	9.10	8.28	.068	37.4	6.4	24.53	20.35
G110	DOWN	2.46	10.22	7.76	.129	30.1	6.4	33.12	36.66
J144	DOWN	0.00	3.54	3.54	.107	24.3	6.4	41.81	36.85
J148	DOWN	.46	15.04	14.58	.053	38.5	6.4	15.16	14.51
L166	DOWN	1.98	9.76	7.78	.071	29.3	6.4	23.81	21.64
M183	DOWN	4.38	11.28	6.90	.023	70.0	6.4	7.89	7.88
M184	DOWN	2.16	8.66	6.50	.025	70.0	6.4	7.78	8.59
N185	DOWN	1.82	10.90	9.08	.042	74.2	6.4	13.05	12.66
N187	DOWN	2.08	7.12	5.04	.029	71.0	6.4	9.90	10.32
N192	DOWN	3.62	15.64	12.02	.043	39.3	6.4	14.67	12.54

TABLE 4.13 - continued

Record	Comp.	Initial Time (sec) T_1	Final Time (sec) T_2	Duration (sec) T	Peak Acc. (g) a	Epicentral Distance (km) D	Richter Mag. M	RMS Value (cm/sec^2)	
								Actual ψ_a	Predicted ψ_p
P214	DOWN	.30	8.78	8.48	.118	34.8	6.4	28.48	33.06
Q241	UP	4.60	13.84	9.24	.062	40.3	6.4	19.49	18.27
S265	UP	.64	13.12	12.48	.055	38.5	6.4	15.26	15.48
U300	UP	7.20	11.44	4.24	.038	64.9	6.4	15.36	13.63
U312	UP	7.84	9.98	2.14	.033	30.5	5.8	11.39	13.15
V319	UP	1.98	4.40	2.42	.027	76.0	6.0	8.94	10.62
W334	DOWN	0.00	3.04	3.04	.054	13.2	5.4	20.95	18.43
W336	DOWN	0.00	1.86	1.86	.038	22.2	5.4	12.17	14.61

TABLE 4.14

ACTUAL AND PREDICTED RMS
FOR VERTICAL COMPONENTS - HARD

Record	Comp.	Initial Time (sec) T_1	Final Time (sec) T_2	Duration (sec) T	Peak Acc. (g) a	Epicentral Distance (km) D	Richter Mag. M	RMS Value (cm/sec^2)	
								Actual ψ_a	Predicted ψ_p
A015	VERT	.80	2.30	1.50	.038	11.5	5.3	11.60	12.00
B025	DOWN	.82	3.24	2.42	.089	6.3	6.0	30.14	26.58
B037	DOWN	.10	5.92	5.82	.132	59.6	5.6	22.13	31.01
C041	DOWN	.52	9.44	8.92	.709	7.2	6.4	165.49	153.87
G106	DOWN	2.12	8.24	6.12	.085	34.7	6.4	21.18	22.46
J141	DOWN	0.00	7.66	7.66	.095	30.8	6.4	30.19	24.24
J142	DOWN	.22	5.92	5.70	.154	28.0	6.4	38.69	39.12
J143	DOWN	.16	5.06	4.90	.073	27.7	6.4	21.33	20.22
0198	DOWN	.90	10.48	9.58	.123	32.5	6.4	28.62	29.78
0207	UP	.88	5.68	4.80	.034	34.0	6.4	9.42	10.06

TABLE 4.14 - continued

Record	Comp.	Initial Time (sec) T_1	Final Time (sec) T_2	Duration (sec) T	Peak Acc. (g) a	Epicentral Distance (km) D	Richter Mag. M	RMS Value (cm/sec^2)	
								Actual ψ_a	Predicted ψ_p
P221	DOWN	0.00	12.48	12.48	.049	42.0	6.4	14.37	12.39
P223	DOWN	.80	5.34	4.54	.039	63.7	6.4	12.30	11.29
W335	DOWN	.02	1.08	1.08	.060	18.9	5.4	16.12	18.91

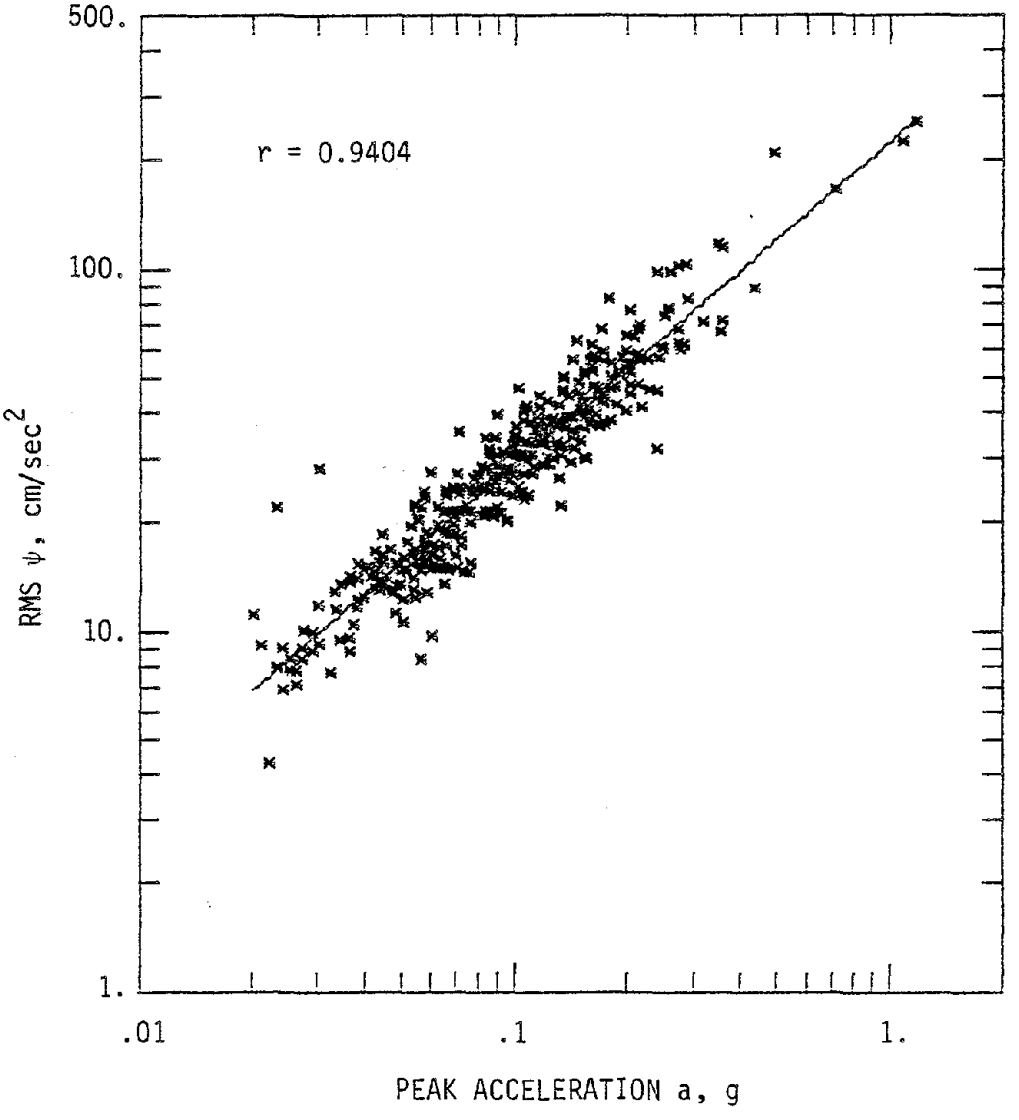

FIG. 4.1. Correlation of RMS with peak ground acceleration for 367 horizontal and vertical components of recorded accelerograms.

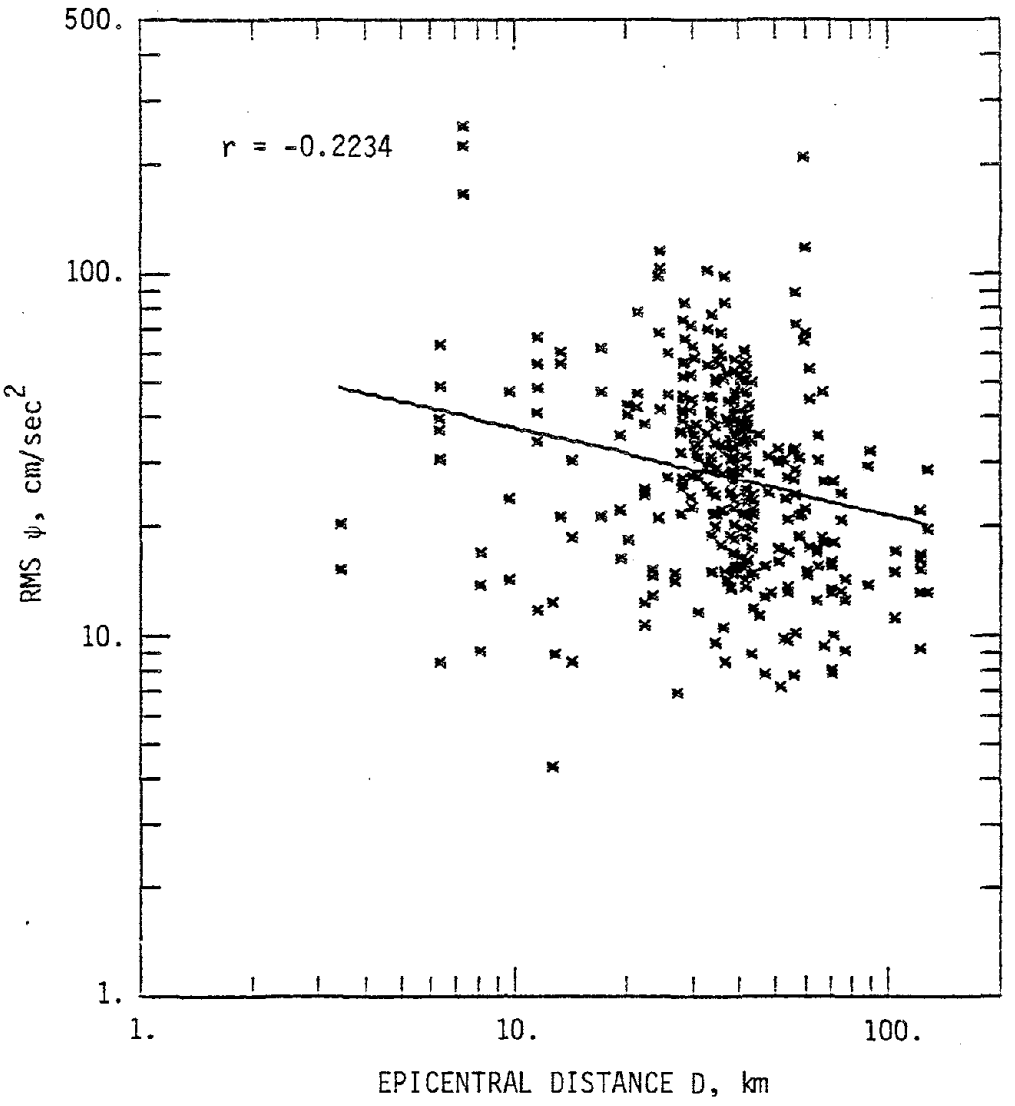

FIG. 4.2. Correlation of RMS with epicentral distance for 367 horizontal and vertical components of recorded accelerograms.

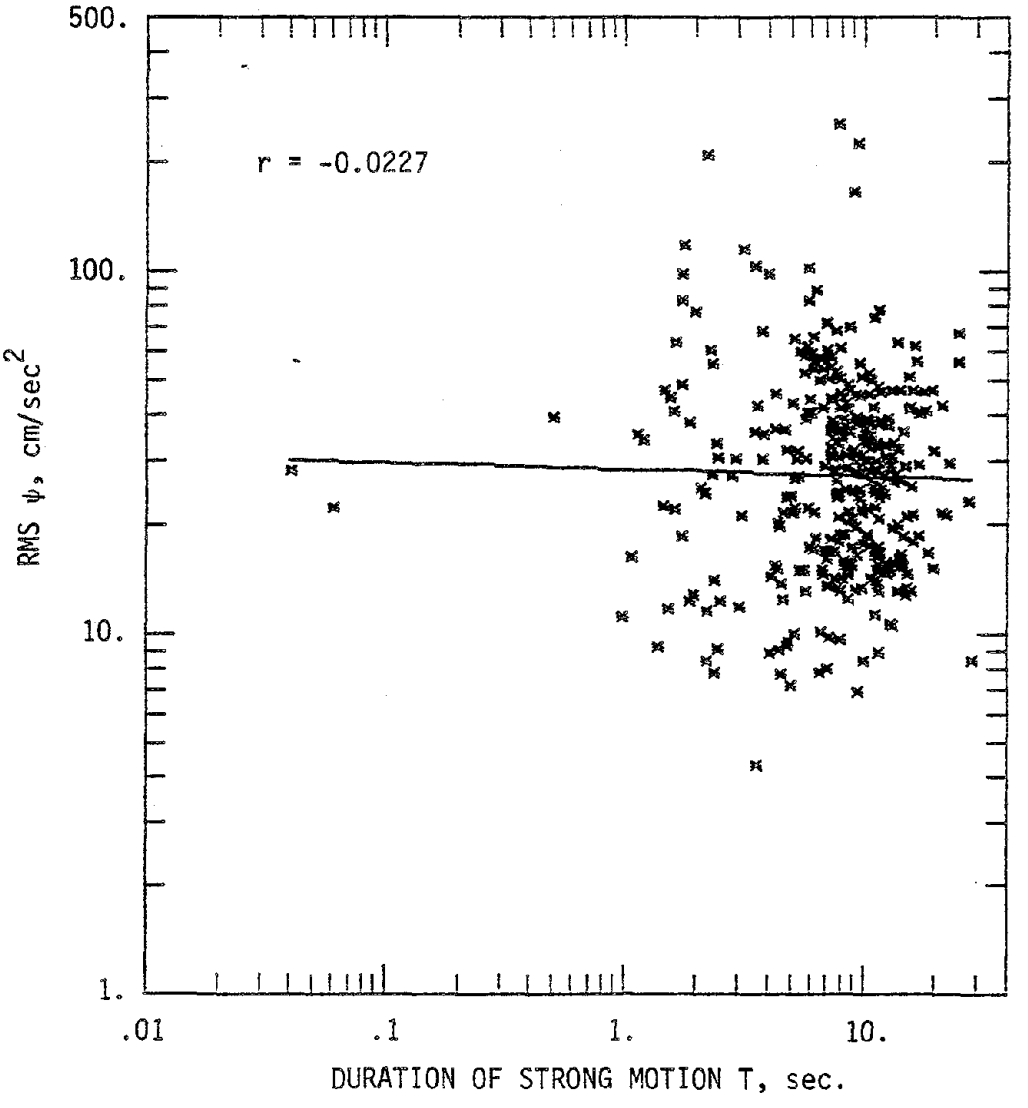

FIG. 4.3. Correlation of RMS with duration of strong motion for 367 horizontal and vertical components of recorded accelerograms.

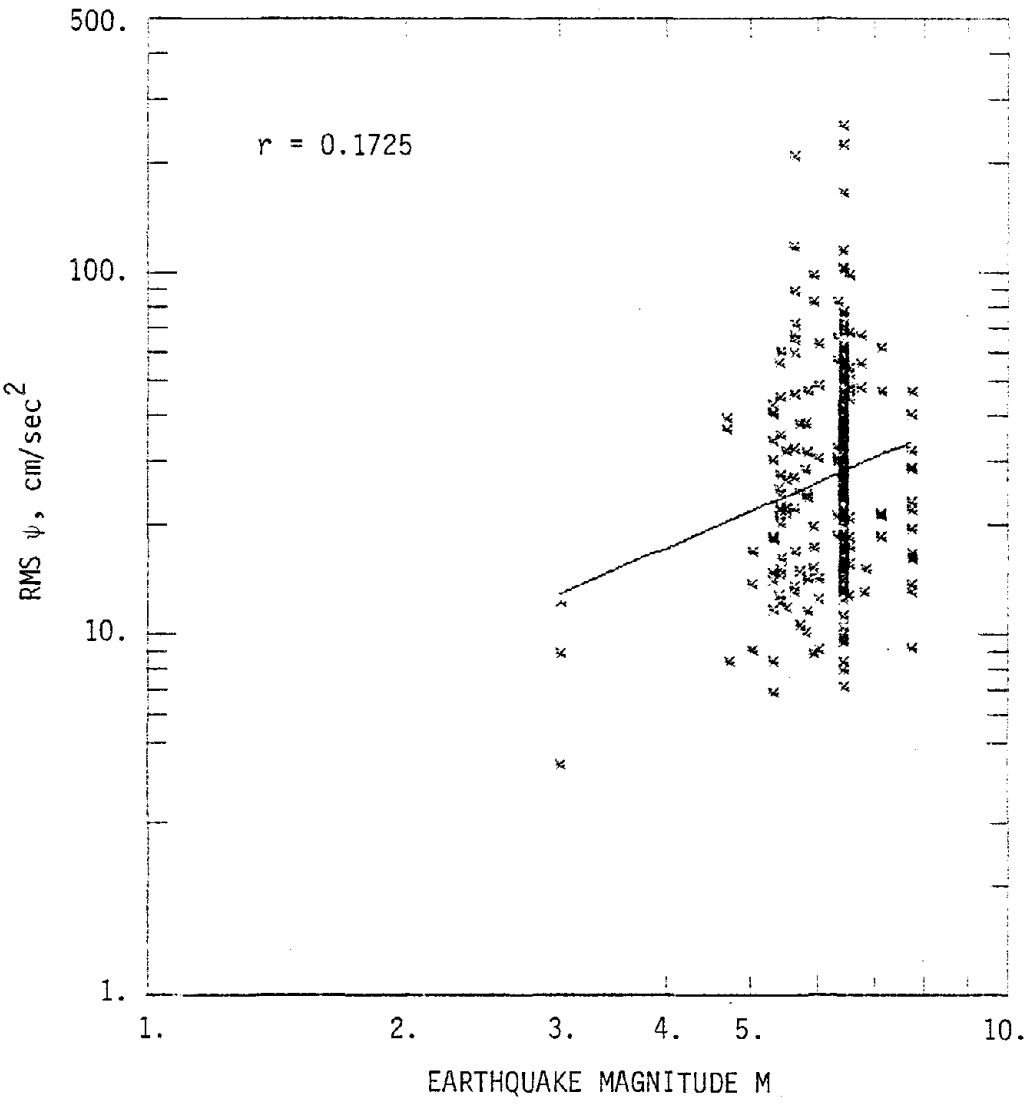

FIG. 4.4. Correlation of RMS with earthquake magnitude for 367 horizontal and vertical components of recorded accelerograms.

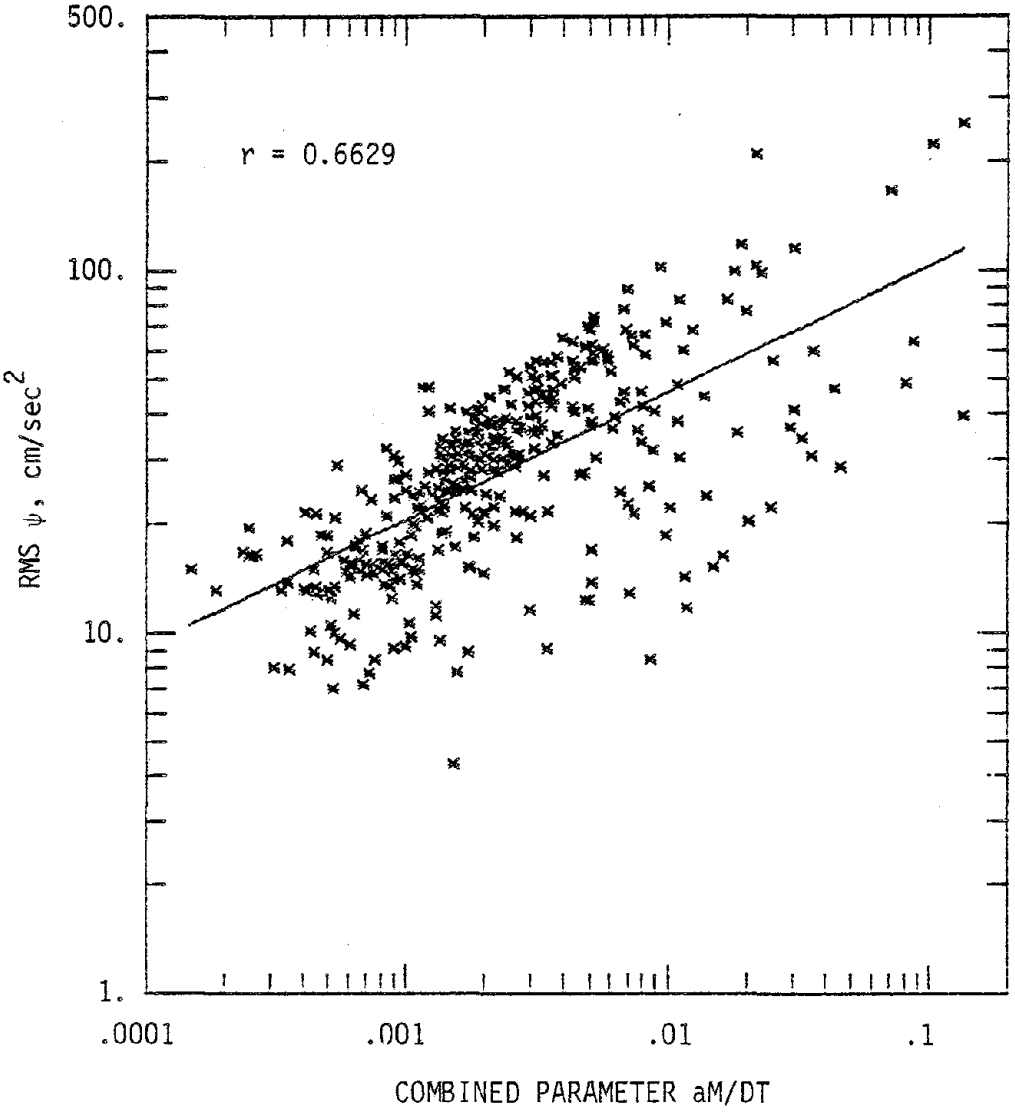

FIG. 4.5. Correlation of RMS with combined parameters for 367 horizontal and vertical components of recorded accelerograms.

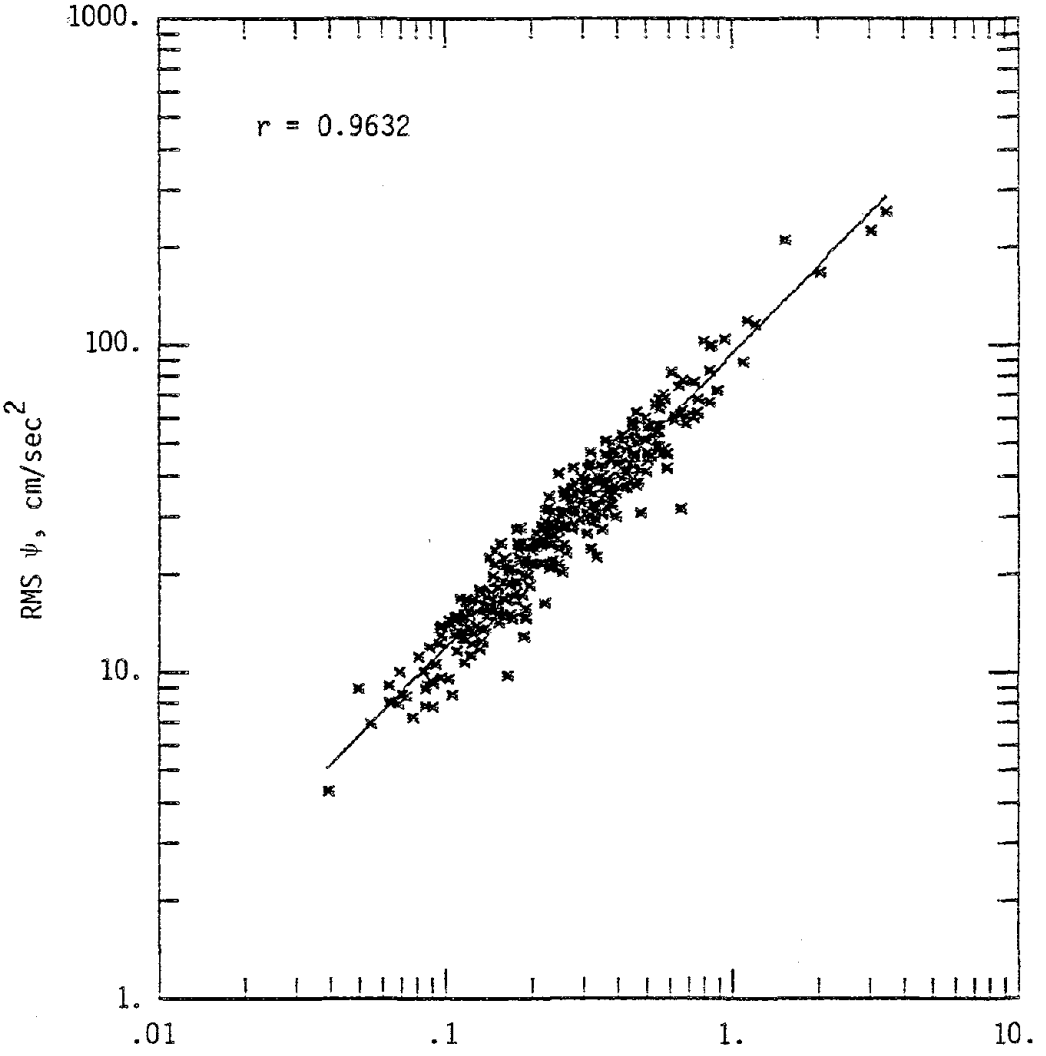

FIG. 4.7. Correlation of RMS with parameter η for 367 horizontal and vertical components of recorded accelerograms.

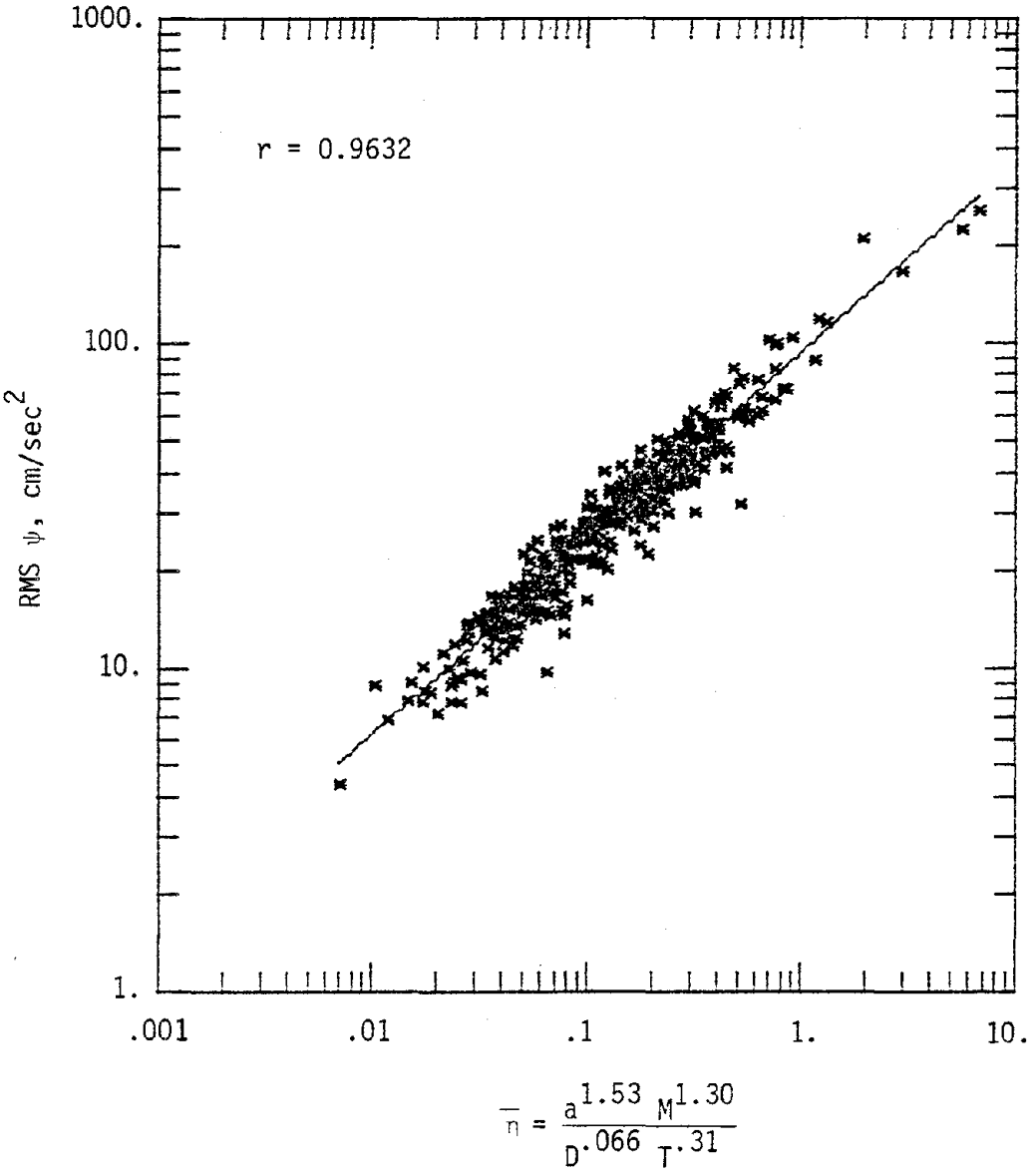

FIG. 4.6. Correlation of RMS with parameter $\bar{n}$ for 367 horizontal and vertical components of recorded accelerograms.

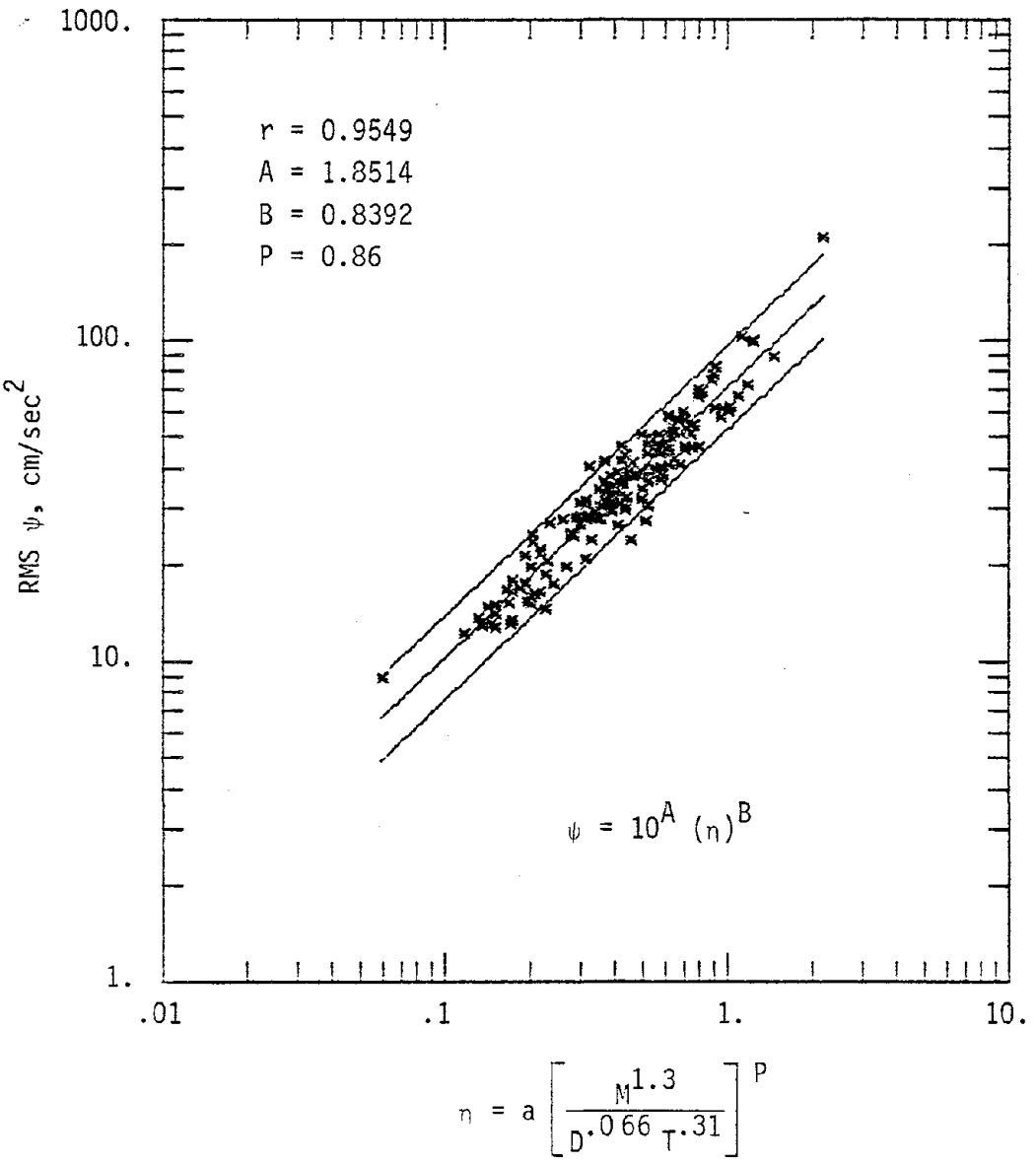

FIG. 4.8. Correlation of RMS with parameter η for 161 horizontal components of recorded accelerograms--Soft.

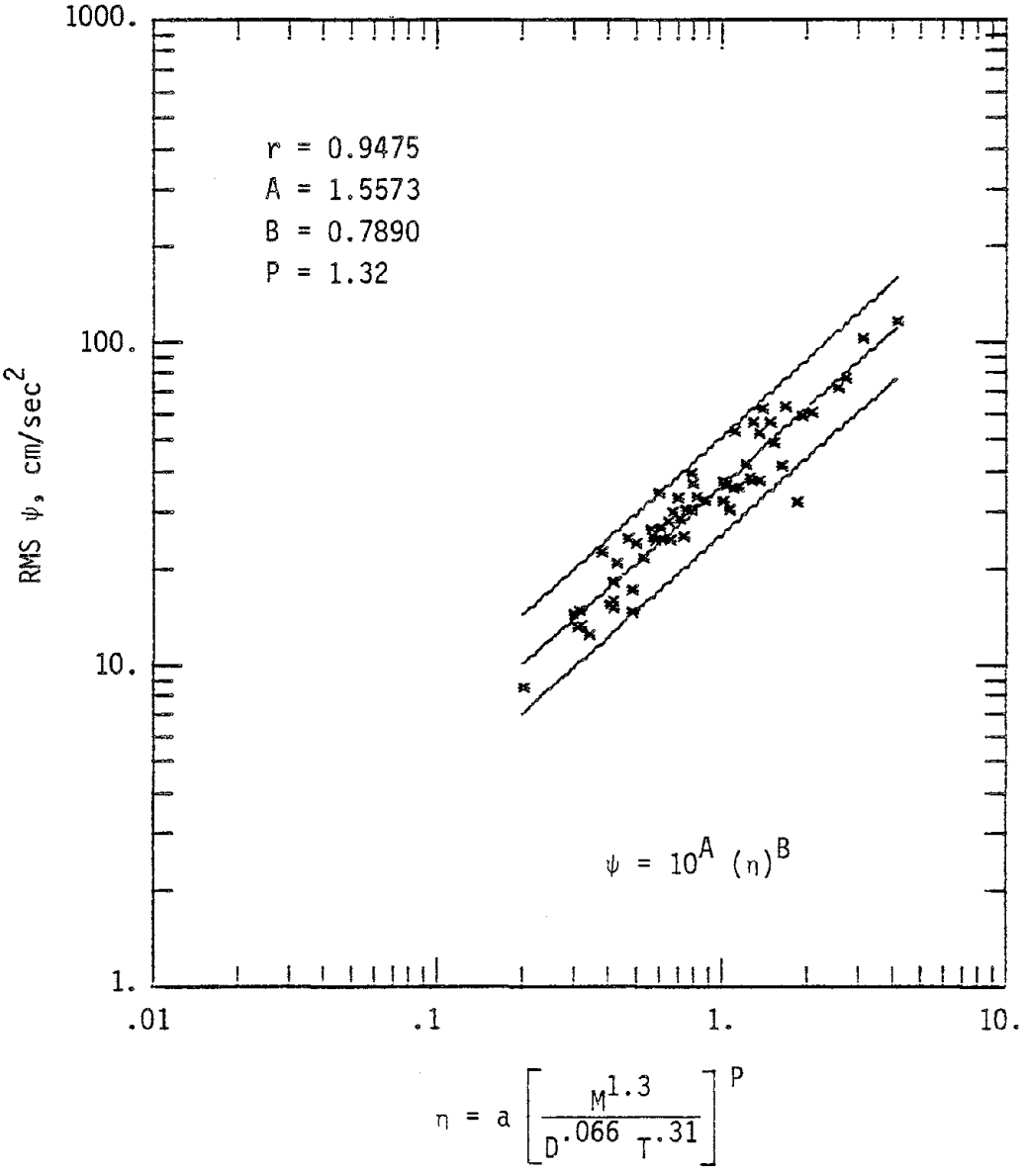

FIG. 4.9. Correlation of RMS with parameter η for 60 horizontal components of recorded accelerograms--Intermediate.

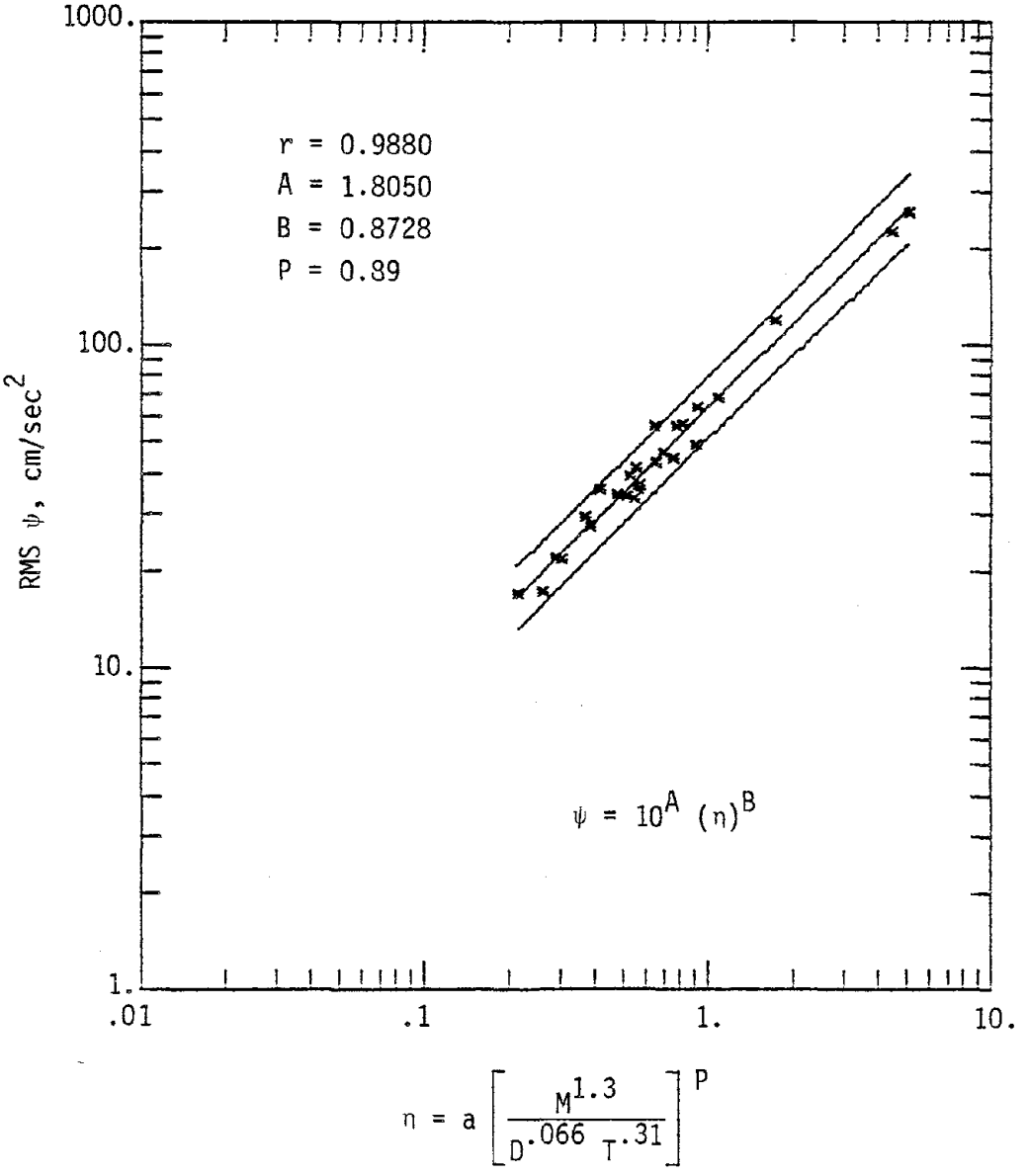

FIG. 4.10. Correlation of RMS with parameter η for 26 horizontal components of recorded accelerograms--Hard.

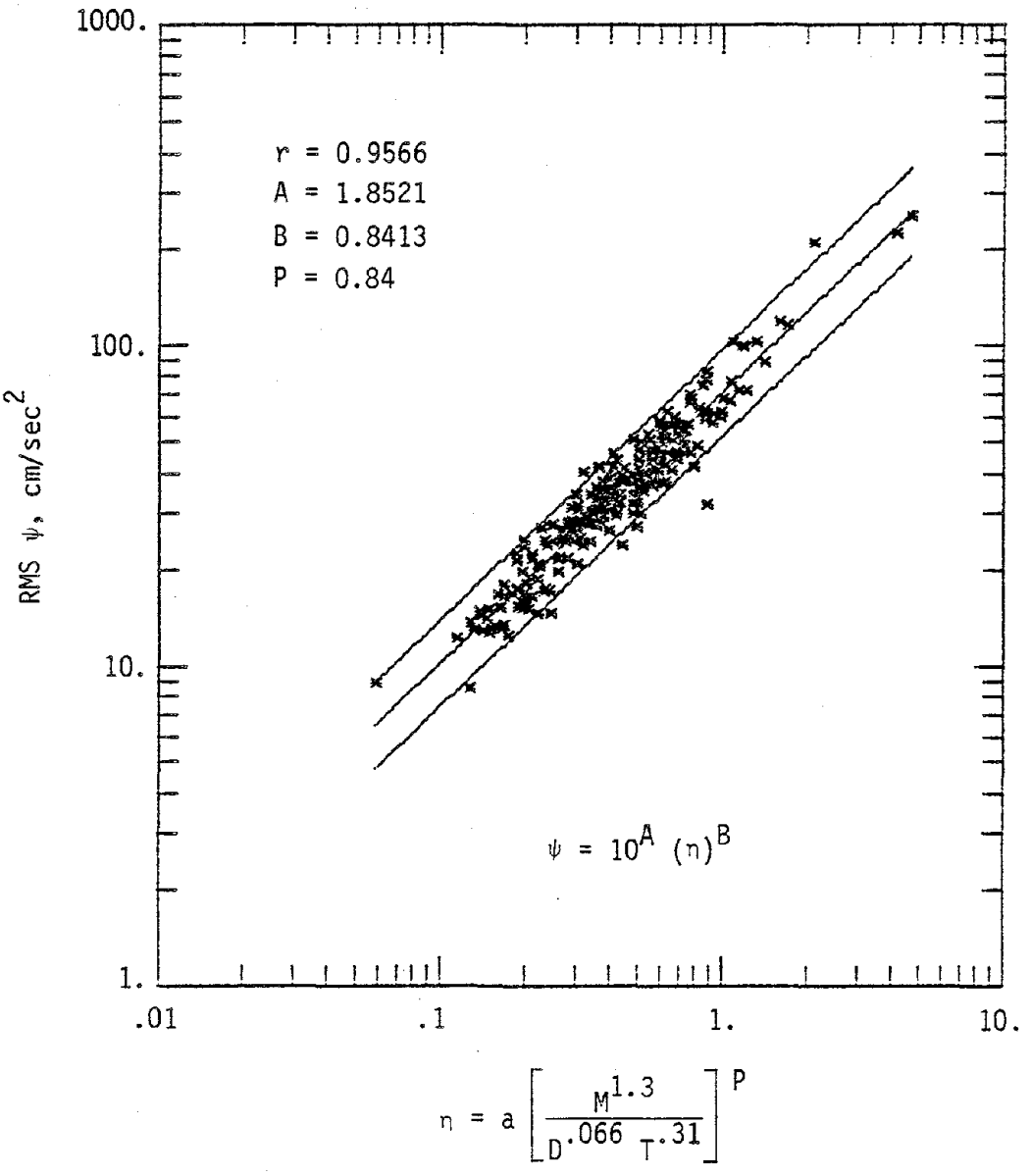

FIG. 4.11. Correlation of RMS with parameter η for 247 horizontal components of recorded accelerograms--combined Soft, Intermediate, and Hard.

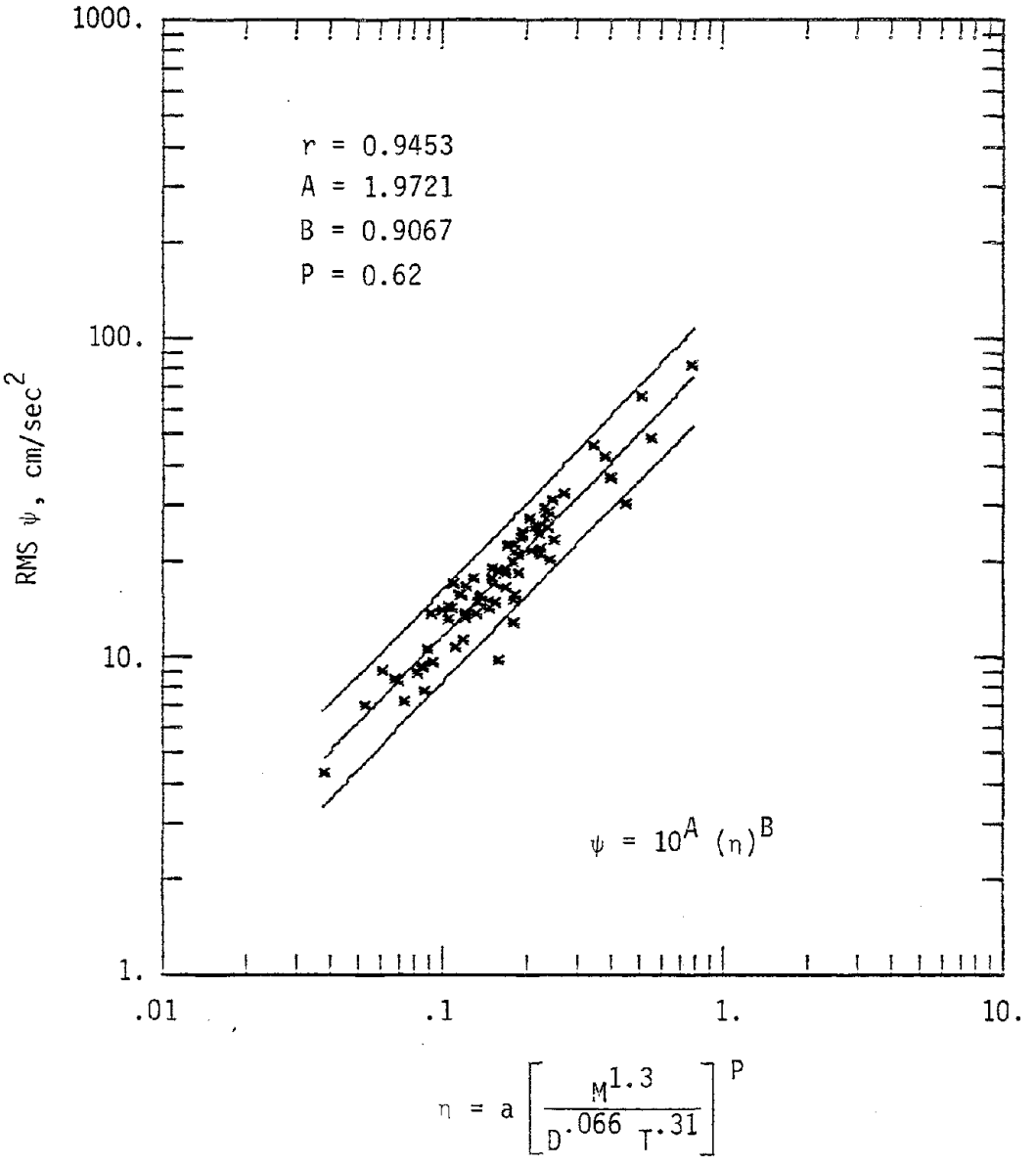

FIG. 4.12. Correlation of RMS with parameter η for 78 vertical components of recorded accelerograms--Soft.

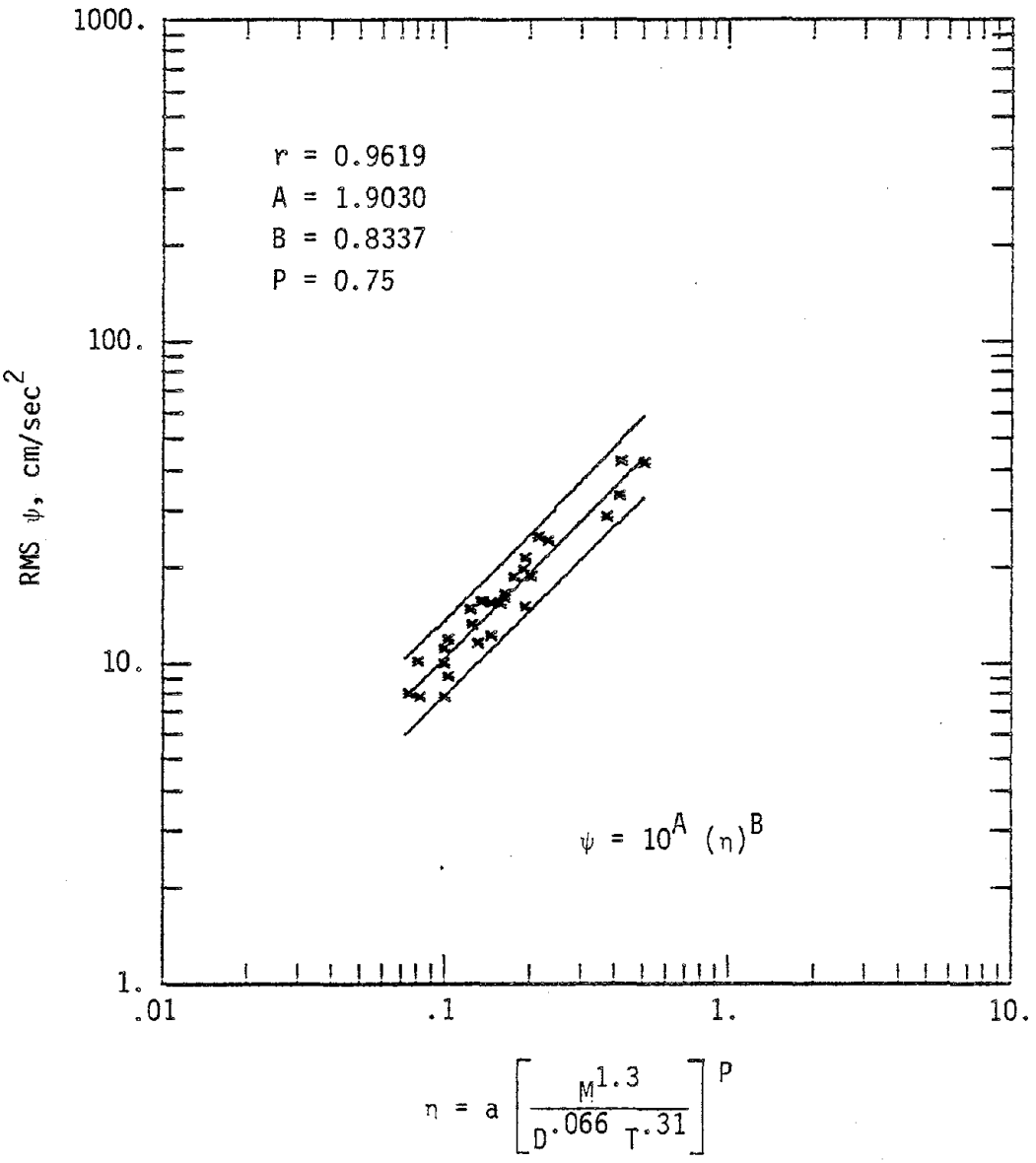

FIG. 4.13. Correlation of RMS with parameter η for 29 vertical components of recorded accelerograms--Intermediate.

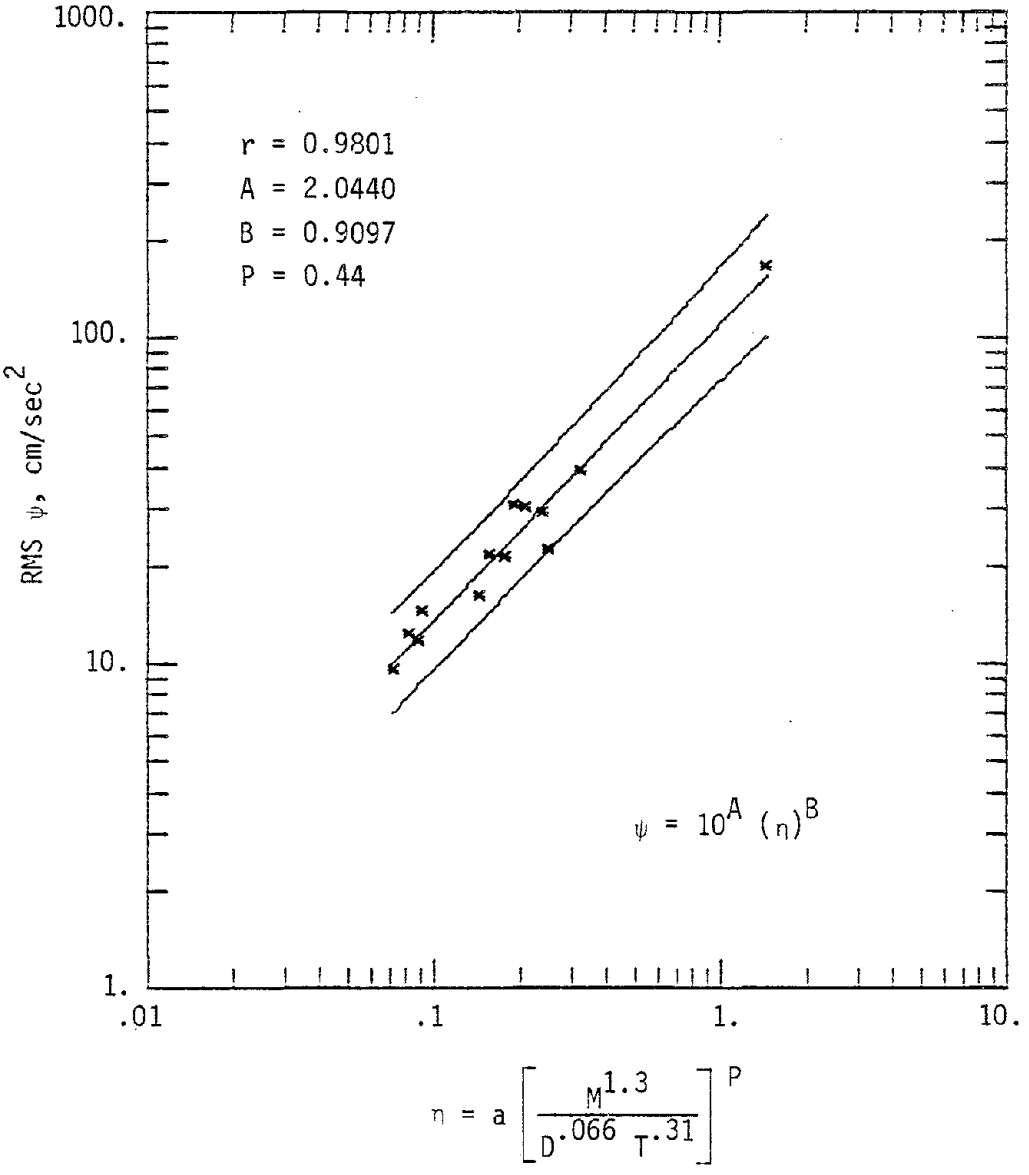

FIG. 4.14. Correlation of RMS with parameter η for 13 vertical components of recorded accelerograms--Hard.

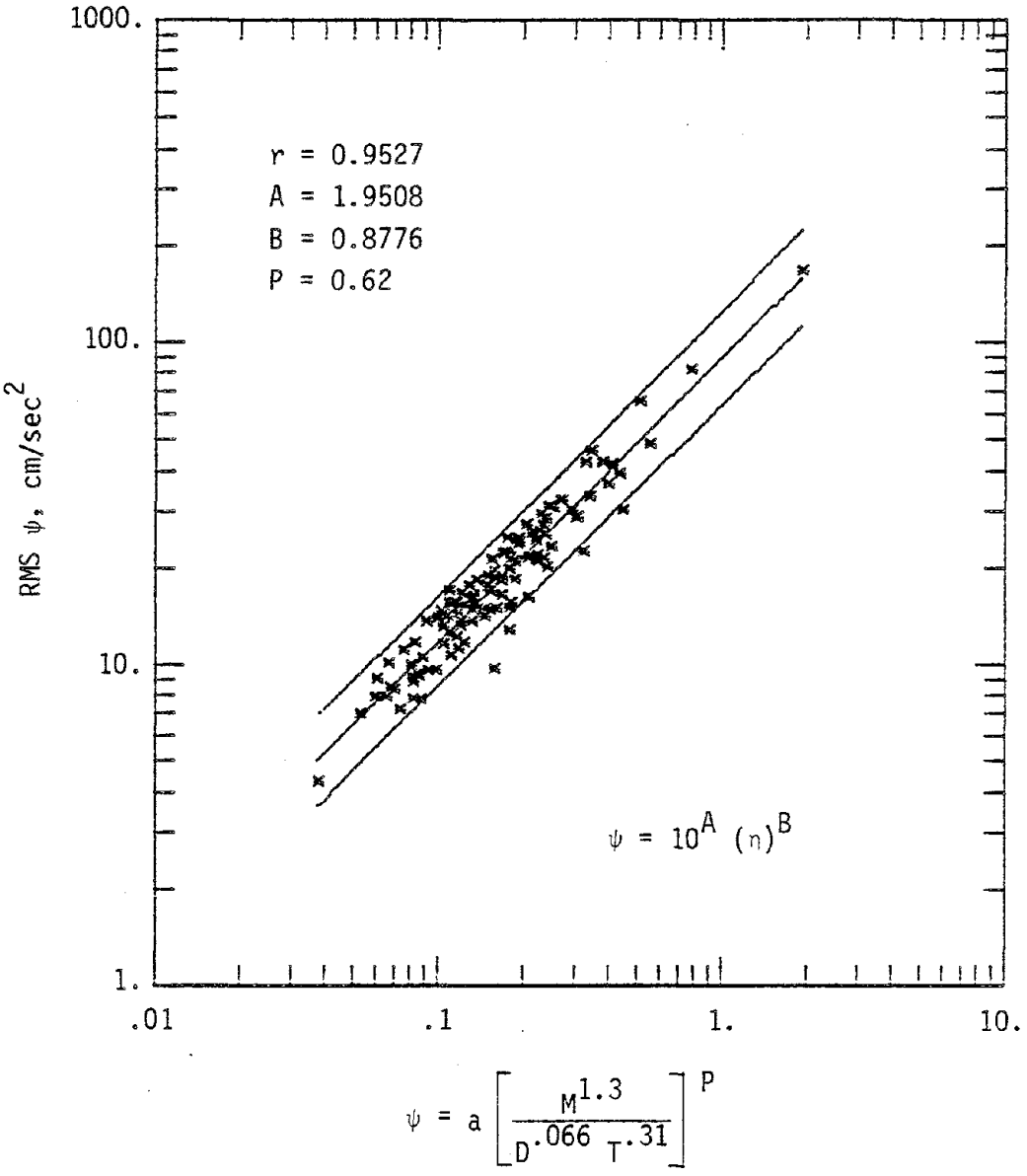

FIG. 4.15. Correlation of RMS with parameter η for 120 vertical components of recorded accelerograms--combined Soft, Intermediate and Hard.

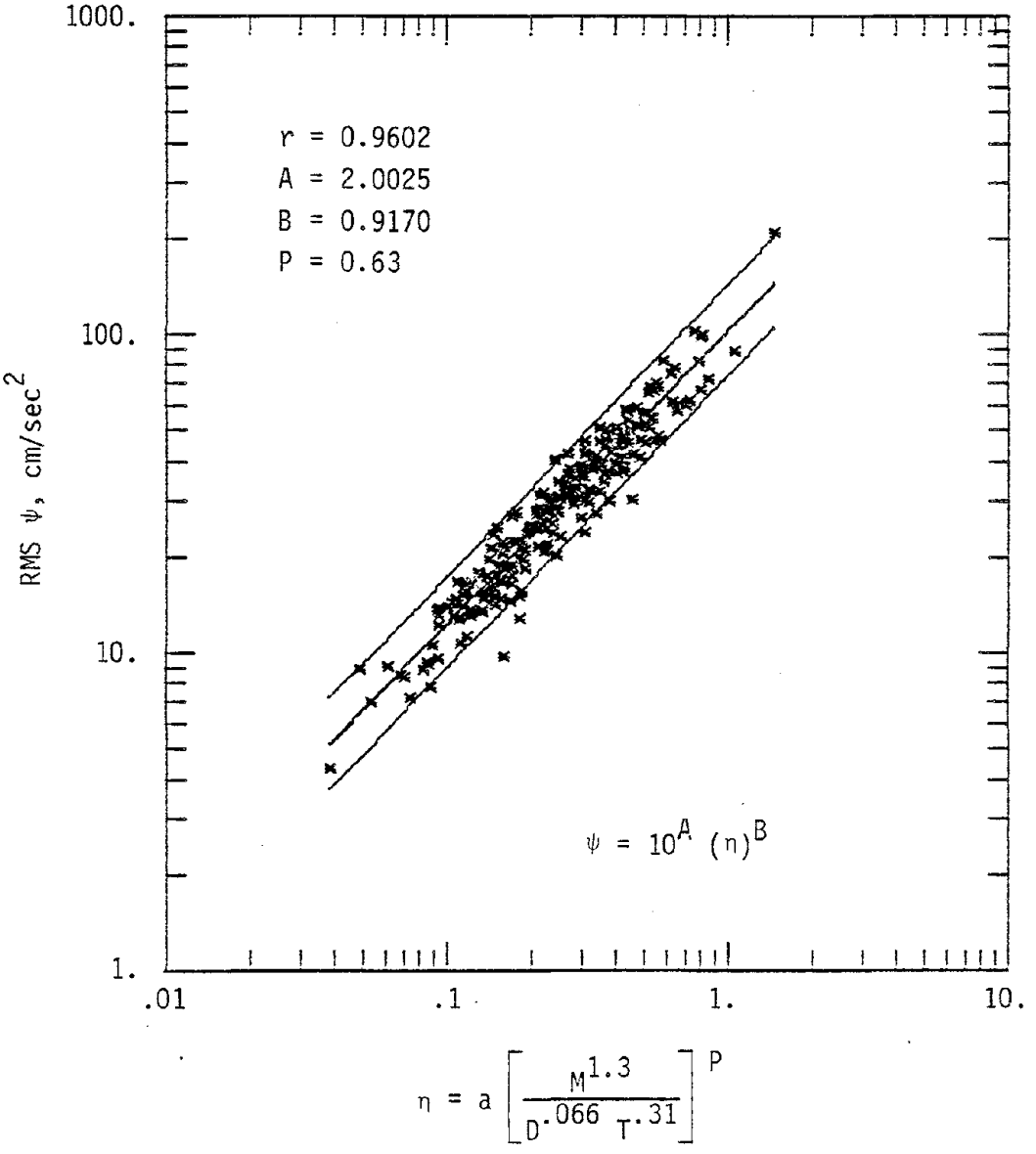

FIG. 4.16. Correlation of RMS with parameter η for 239 horizontal and vertical components of recorded accelerograms--Soft.

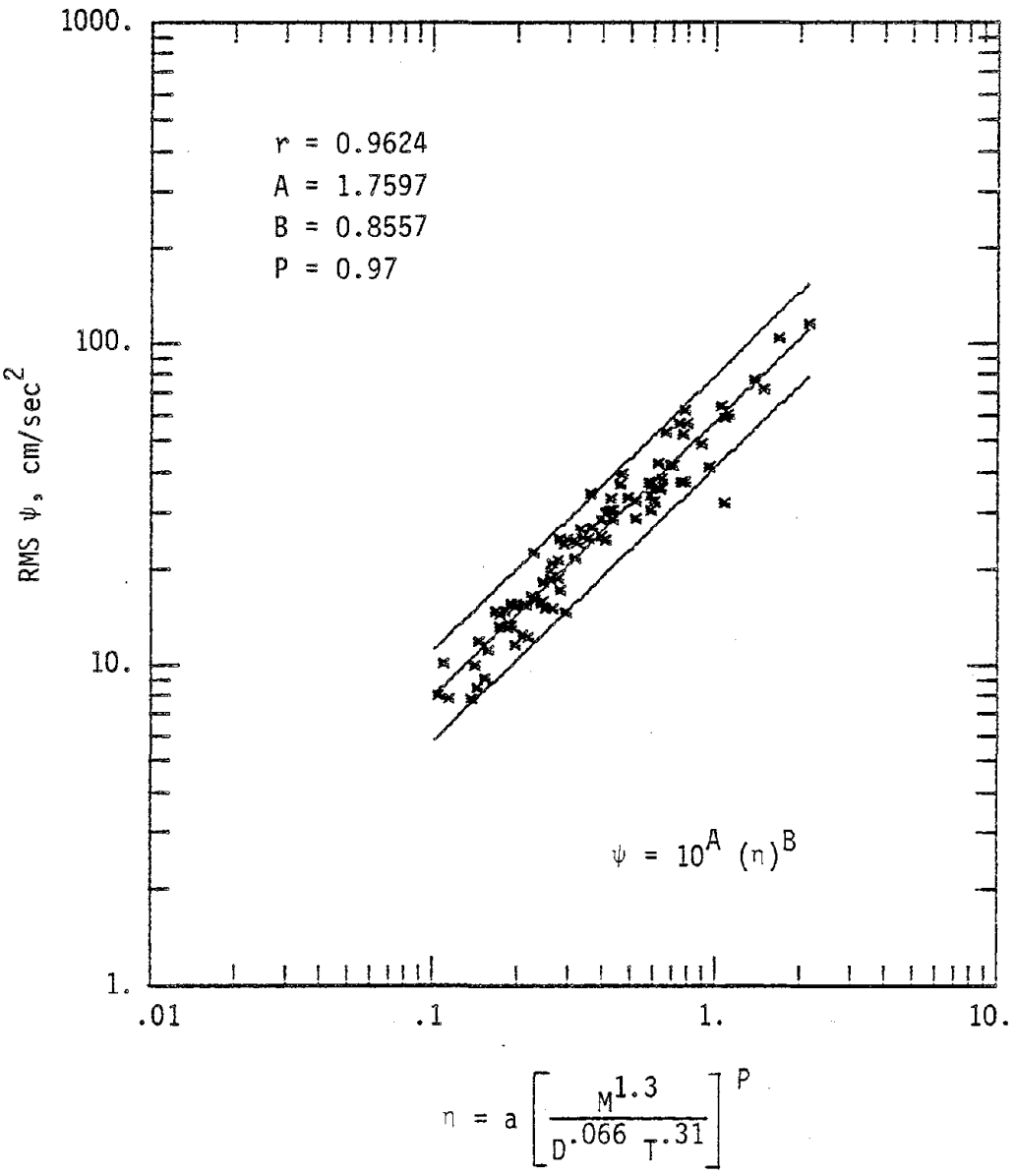

FIG. 4.17. Correlation of RMS with parameter η for 89 horizontal and vertical components of recorded accelerograms--Intermediate.

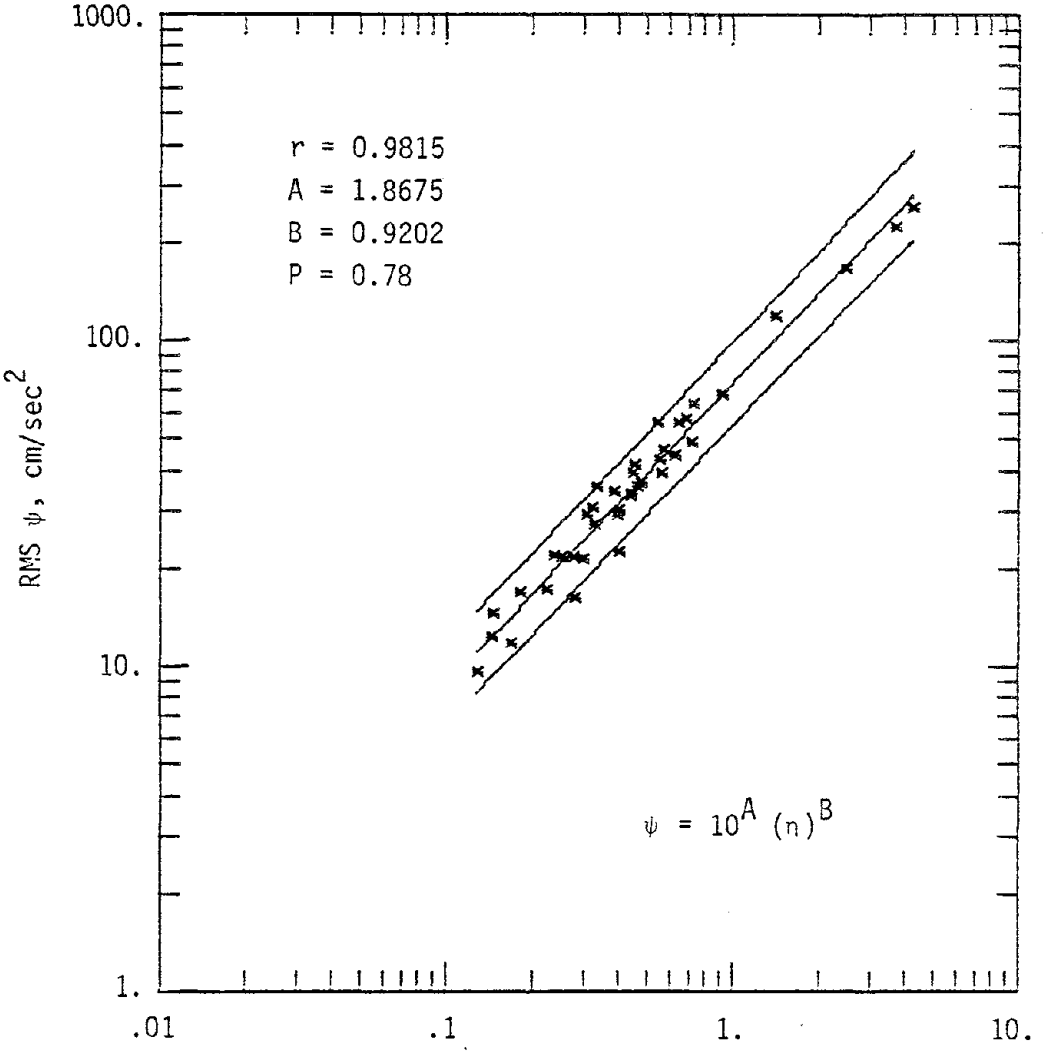

FIG. 4.18. Correlation of RMS with parameter η for 39 horizontal and vertical components of recorded accelerograms--Hard.

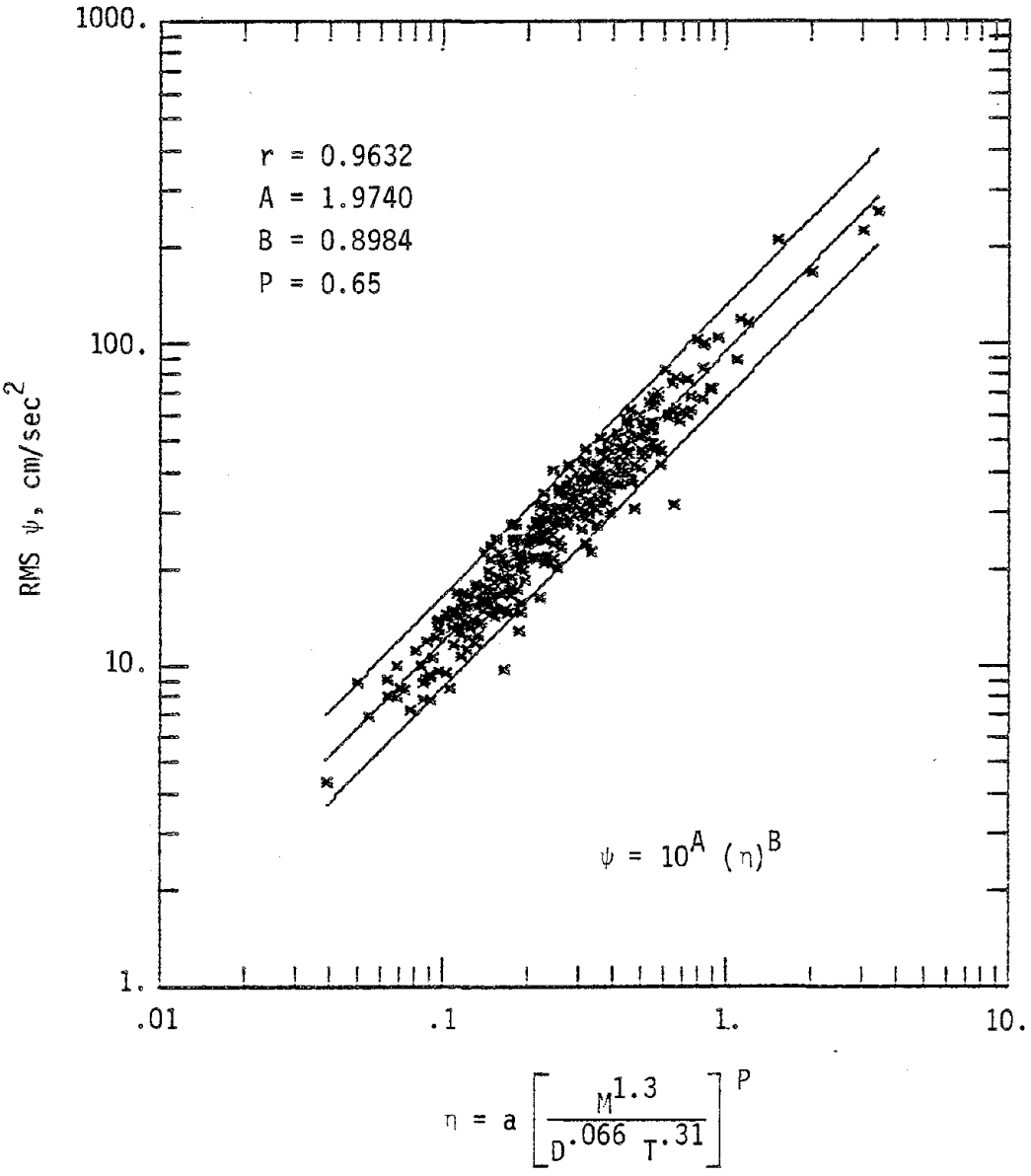

FIG. 4.19. Correlation of RMS with parameter η for 367 horizontal and vertical components of recorded accelerograms--combined Soft, Intermediate and Hard.

CHAPTER 5

POWER SPECTRAL DENSITIES AND SCALE FACTORS FOR DIFFERENT GEOLOGICAL CONDITIONS

5.1 INTRODUCTORY REMARKS

In a pilot study in Chapter 3, a power spectral density and a scale factor for an ensemble of eight strong motion accelerograms were estimated and used to compute the response of a single degree of freedom system. Using the procedure outlined in that chapter, power spectral densities and scale factors for the three geological classifications (soft, intermediate, and hard) and for both the horizontal and vertical components of a number of records are computed and presented in this chapter. In Chapter 4, relationships between the RMS of the records and a variable η reflecting the earthquake parameters were obtained for different groupings of the records including the six used in this chapter. The information presented in Chapter 4 and this chapter is used to predict the response of a single degree of freedom system and the results are compared with spectral relative displacement, relative velocity and absolute acceleration computed directly from several records.

5.2 POWER SPECTRAL DENSITIES AND SCALE FACTORS

Using the procedure outlined in Section 3.4, power spectral densities were estimated for six different classifications of records. Normalized power spectral densities for the ensemble of the horizontal

components of accelerograms recorded on soft, intermediate, and hard sites are shown in Figs. 5.1-5.3 respectively. Similar plots for the vertical components are presented in Figs. 5.4-5.6. The accumulated area under the power spectral density as a percentage of the total area for the three site classifications and for the horizontal and vertical components are given in Table 5.1. The peak ordinate for each of the six power spectral densities and their corresponding frequency is shown in Table 5.2.

From the shape of the power spectral densities in Figs. 5.1-5.6 and the rate of accumulation of areas in Table 5.1, one may make the following observations: First, power spectral densities reach their maximum values at low frequencies and practically vanish at frequencies greater than 10 Hz indicating that the dominant frequencies in earthquake accelerograms are within 0-10 Hz. Second, the power spectral densities for accelerograms recorded on softer geology display fewer peaks, whereas those recorded on harder sites show several peaks, indicating that the geology of the recording station influences the frequency structure of the data. Third, a comparison of the power spectral densities for horizontal and vertical components shows a wider range of dominant frequencies in the vertical components, indicating that the energy contained in the horizontal motion is concentrated in a narrower band than that in the vertical motion. This can also be seen from Table 5.2, where the maximum ordinates of the power spectral densities for the horizontal motion are consistently greater than those corresponding to the vertical motion. Fourth, the rate of energy accumulation (see Table 5.1) is faster for the accelerograms recorded

on softer geology and is also faster for the horizontal components than their corresponding vertical components.

The scale factors (the normalized mean square acceleration) for the six categories are computed using the procedure outlined in Section 3.4. The variation of the scale factor with time for the horizontal components of accelerograms recorded on soft, intermediate, and hard geology is presented in Figs. 5.7-5.9, respectively. Similar plots for the vertical components are presented in Figs. 5.10-5.12. Table 5.3 lists the durations of the scale factors, their maximum ordinates and the corresponding time at which they occur. Some general observations regarding the scale factors can be made. The stiffer geological classifications have shorter durations. This is true for both the horizontal and the vertical components. In transient response of a single degree of freedom, the duration of the scale factor could play an important role. For a given mean square value, the shorter duration imparts energy into the system in a shorter time than a longer one. The maximum scale factors for the soft site are generally greater than those for the stiffer sites and they occur at an earlier time.

5.3 RECORDS SELECTED FOR COMPARING THE RESPONSE

To study the application of the power spectral densities and scale factors presented in Figs. 5.1-5.2 in predicting the response of a single degree of freedom system for a given set of earthquake parameters, a total of twelve records--two records for each of the six classifications--were selected. The records and some of their properties are listed in Tables 5.4 and 5.5. The records were selected from five seismic

events (Imperial Valley 1940, Kern County 1952, Eureka 1954, Northern California 1952, and San Fernando 1971) with an earthquake magnitude between 5.5 and 7.7. The records are from six different stations with an epicentral distance ranging from 11 to 120 kilometers. For each geological classification two records were selected, one with a high peak horizontal acceleration and the other with a low peak horizontal acceleration but a high peak velocity to peak acceleration ratio. As seen from Table 5.4, the properties for the six horizontal records cover a wide range; i.e. peak ground accelerations between .05 to 1.172 g, peak ground velocities between 2.74 to 44.49 in./sec., peak ground displacements between .80 to 14.84 in., durations of strong motion between 5.04 to 24.92 sec., and actual RMS values between 16.53 to 253.6 cm/sec^2. A wide range of properties is also observed from Table 5.5 for the vertical components.

5.4 COMPARISON OF PREDICTED AND COMPUTED RESPONSE

The expressions for computing the relative displacement, relative velocity, and absolute acceleration of a single degree of freedom are presented in Eqs. 3.3-3.5. In addition, the relationships between the RMS of the records and a variable η reflecting the earthquake parameters (peak acceleration, earthquake magnitude, epicentral distance and the duration of strong motion) for different geological groupings were developed and presented in Chapter 4. Using the normalized power spectral densities and scale factors presented in this chapter and the information given in Chapters 3 and 4, the response of a single degree of freedom for several specified sets of earthquake parameters is predicted

and compared with that computed directly from the records. The mean plus one standard deviation response (normal distribution) of the ensemble, which is presently used as a basis in developing design spectrum, is also compared with the response computed directly from the records (Trifunac et al., 1972-1975).

Since a response spectrum represents the maximum response of a system, the maximum scale factor and a low probability of exceeding the maximum response (3σ level) were used in the comparisons. The results were compared for 2, 5 and 10 percent of critical damping; however only 2 and 10 percent are presented here.

A comparison between the responses predicted using the power spectral density and those computed directly from the six horizontal components of the records listed in Table 5.4 is presented in Figs. 5.13-5.36. Also shown (in separate figures) is the mean plus one standard deviation response of the appropriate ensemble. The plots are arranged in three sets. Figures 5.13-5.20 show the comparison of the response for soft sites, Figs. 5.21-5.28 for the intermediate sites, and Figs. 5.29-5.36 for the hard sites. Figures 5.37-5.60 show similar comparisons for the vertical motion. In Figs. 5.13-5.60, each comparison between the predicted and the computed response is immediately followed by a comparison of the mean plus one standard deviation and the computed response. The reason for separating the two comparisons is to provide an easier examination of the figures.

Figures 5.13-5.60 indicate that in general there is a close agreement between the shape of the predicted and the mean plus one standard deviation response. In many instances this shape closely resembles

the shape of the computed response (see for example Fig. 5.29 and 5.35). The response predicted from the power spectral density in the majority of cases envelopes the computed response over the entire frequency range of .06 to 25 Hz. This envelope seems to be closer to the computed response in the higher frequency region and is particularly evident for the horizontal components on hard geology. In the lower frequency region however, the predicted response seems to generally overestimate the computed response. This is not true for all the comparisons. For example, Fig. 5.35 shows a very good agreement between the predicted and computed response for both high and low frequency regions. The agreement is equally good for relative displacement, relative velocity and absolute acceleration. Comparison of Figs. 5.35 and 5.36 indicates that the computed response is closer to the predicted than to the mean plus one standard deviation response. Figures 5.29-5.30 show a similar comparison. Figures 5.27-5.28 and 5.49-5.50 show the comparison of the horizontal and vertical components of Ferndale City Hall 1954 in which the relative velocity predicted from PSD is much closer to the computed response than the mean plus one standard deviation. The agreement between the predicted and computed absolute acceleration is seen in Figs. 5.21-5.22 and 5.23-5.24. In general the predicted response for both horizontal and vertical components of the records for all geological classifications compare well with the computed response. The difference noted between the predicted and computed response at low frequencies, especially for low damping, indicates that 3σ level is too high for such cases. Penzien (1970) has confirmed this result. As the probability for exceeding the predicted response at 3σ level (.26%) indicates, the

computed response should seldom exceed the predicted one. This can easily be seen from the comparisons presented in Figs. 5.13-5.60. On the other hand, the mean plus one standard deviation response which represents the 84.1 percentile level is exceeded more often as expected.

The eight records used in the pilot study in Chapter 3 were classified in Chapter 4 in the soft category. It is interesting to compare Figs. 3.28 and 5.17, and Figs. 3.30 and 5.19, where the computed response for 2 and 10 percent of critical damping for El Centro 1940 NS component is compared with the predicted response. These figures indicate that not only the predicted response in Chapter 5 is higher than those of Chapter 3, but the shapes are different as well. The higher values of response are attributed to higher predicted RMS value for that record (75.64 vs. 51.56) and higher value of maximum scale factor (4.29 vs. 3.49) used in Chapter 5. Further the shape of the predicted responses are different because the power spectral densities (Fig. 3.25 and Fig. 5.1) are not the same.

TABLE 5.1

ACCUMULATED AREA AS THE PERCENTAGE OF TOTAL AREA
UNDER THE POWER SPECTRAL DENSITY

Frequency Range (Hz)	Horizontal			Vertical		
	Soft	Inter.	Hard	Soft	Inter.	Hard
0 - 1	17.94	10.75	7.22	11.75	10.10	6.58
0 - 2	41.62	30.25	26.96	26.14	24.59	15.58
0 - 3	60.32	48.81	39.49	39.89	37.59	22.53
0 - 4	73.28	64.65	52.18	52.13	49.31	32.70
0 - 5	81.85	75.91	65.93	62.29	59.29	43.73
0 - 6	87.80	83.64	76.25	70.06	66.51	54.70
0 - 7	91.57	88.10	82.09	76.15	72.27	63.35
0 - 8	94.32	91.82	87.91	82.08	76.90	70.03
0 - 9	96.15	94.67	91.83	86.09	80.82	76.58
0 - 10	97.32	96.89	94.22	89.13	85.38	82.45
0 - 11	98.13	97.94	95.59	91.74	89.63	87.34
0 - 12	98.69	98.65	96.76	93.53	92.30	90.41
0 - 13	99.09	99.09	97.68	95.01	94.31	92.79
0 - 14	99.33	99.36	98.45	96.16	95.82	94.68
0 - 15	99.49	99.52	98.84	97.11	96.84	95.91
0 - 16	99.60	99.66	99.15	97.77	97.73	97.01
0 - 17	99.69	99.74	99.39	98.33	98.38	97.80
0 - 18	99.75	99.81	99.57	98.75	98.88	98.52
0 - 19	99.81	99.86	99.69	99.03	99.18	98.93
0 - 20	99.84	99.89	99.78	99.25	99.40	99.24
0 - 21	99.88	99.92	99.85	99.46	99.56	99.52
0 - 22	99.91	99.94	99.90	99.61	99.68	99.67
0 - 23	99.94	99.96	99.93	99.74	99.80	99.76
0 - 24	99.97	99.98	99.97	99.86	99.90	99.89
0 - 25	100.00	100.00	100.00	100.00	100.00	100.00

TABLE 5.2

MAXIMUM ORDINATES OF THE POWER SPECTRAL DENSITIES
AND THEIR CORRESPONDING FREQUENCIES

Classification	Geology Type	Frequency (Hz)	Peak Value $(cm/sec^2)^2/Hz$
Horizontal	Soft	0.98	.2548
	Intermediate	1.55	.1995
	Hard	1.34	.2173
Vertical	Soft	0.90	.1587
	Intermediate	1.14	.1547
	Hard	4.76	.1118

TABLE 5.3

MAXIMUM VALUES OF SCALE FACTORS

Classification	Geology Type	Duration (sec)	Time (sec)	Peak Value
Horizontal	Soft	25	0.98	4.29
	Intermediate	14	0.84	4.07
	Hard	14	5.57	2.21
Vertical	Soft	27	0.86	3.91
	Intermediate	15	0.88	3.11
	Hard	13	5.49	3.61

TABLE 5.4

PROPERTIES OF THE SIX RECORDS USED IN
COMPARING THE PREDICTED AND COMPUTED RESPONSE--HORIZONTAL

Geology	Record	Component	Peak Acc. (g)	Peak Vel. (in/sec)	Peak Dis. (in)	v/a in/sec/g	d/a in/g	Strong Motion Duration (sec)	Magnitude	Epicentral Distance (km)	RMS Value (cm/sec^2)	
											Predicted	Actual
Soft	Hollywood 1952 (A007)*	N90E	.042	3.51	2.54	83.57	60.48	11.54	7.7	120.3	15.52	16.53
	El Centro 1940 (A001)	S00E	.348	13.15	4.29	37.79	12.33	24.92	6.7	11.5	75.64	65.88
Intermediate	Ferndale 1952 (B030)	N44E	.054	2.74	.80	50.74	14.81	5.04	5.5	43.1	16.61	22.17
	Ferndale 1954 (A009)	N46W	.201	10.24	3.79	50.94	18.86	8.50	6.5	40.0	49.88	47.92
Hard	Lake Hughes Station 1 1971 (J141)	S69E	.111	5.67	1.17	51.08	10.54	13.54	6.4	30.8	27.35	25.83
	Pacoima 1971 (C041)	S15W	1.172	44.49	14.84	37.96	12.66	7.44	6.4	7.2	263.36	253.60

* The item in parentheses refers to the Cal Tech identification number (Hudson et al., 1971)

TABLE 5.5

PROPERTIES OF THE SIX RECORDS USED IN
COMPARING THE PREDICTED AND COMPUTED RESPONSE--VERTICAL

Geology	Record	Peak Acc. (g)	Peak Vel. (in/sec)	Peak Dis. (in)	v/a in/sec/g	d/a in/g	Strong Motion Duration (sec)	Magnitude	Epicentral Distance (km)	RMS Value (cm/sec^2)	
										Predicted	Actual
Soft	Hollywood 1952 (A007)*	.021	1.20	1.34	57.14	63.81	1.38	7.7	120.3	9.93	9.07
	El Centro 1940 (A001)	.210	4.25	2.19	20.23	10.43	11.32	6.7	11.5	54.73	47.40
Intermediate	Ferndale 1952 (B030)	.030	1.19	.60	39.67	20.00	2.98	5.5	43.1	8.75	11.71
	Ferndale 1954 (A009)	.043	2.99	1.54	69.53	35.81	8.60	6.5	40.0	11.63	15.42
Hard	Lake Hughes Station 1 1971 (J141)	.095	4.61	1.12	48.53	11.79	7.66	6.4	30.8	24.24	30.19
	Pacoima 1971 (C041)	.709	22.95	7.60	32.37	10.72	8.92	6.4	7.2	153.83	165.49

* The item in parentheses refers to the Cal Tech identification number (Hudson et al., 1971)

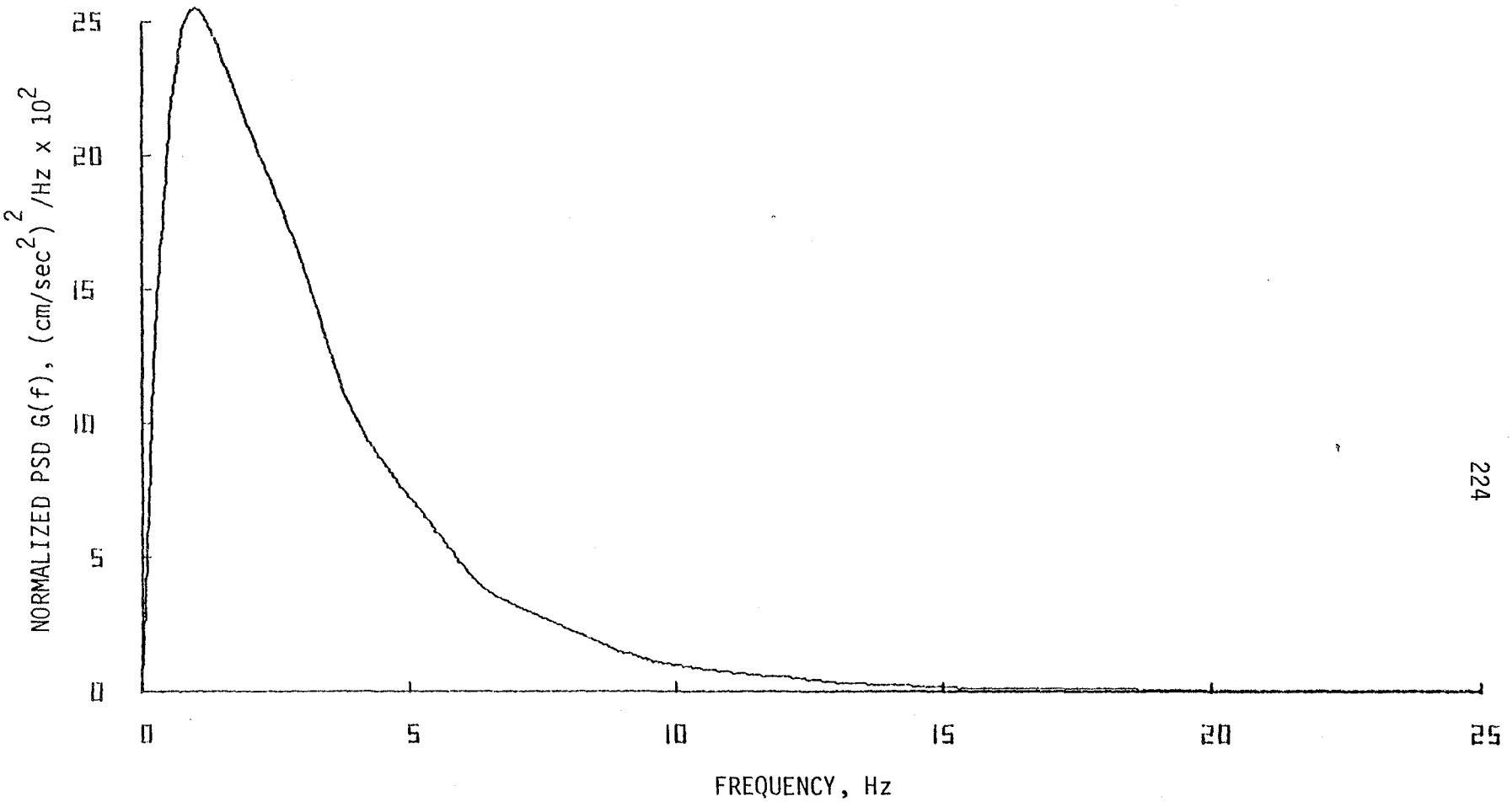

FIG. 5.1. Power spectral density of the ensemble of 161 horizontal components of recorded accelerograms--Soft.

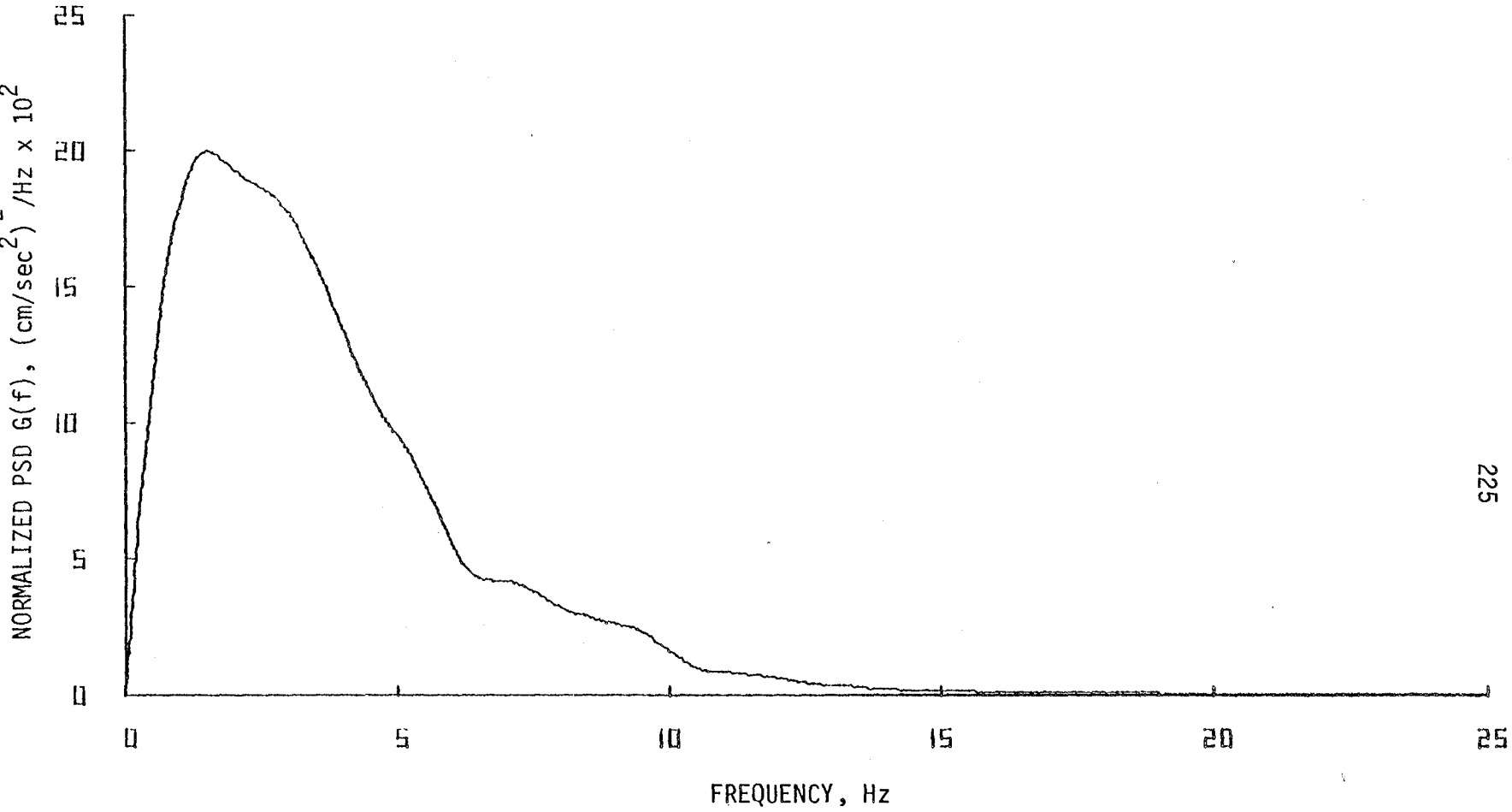

FIG. 5.2. Power spectral density of the ensemble of 60 horizontal components of recorded accelerograms--Intermediate.

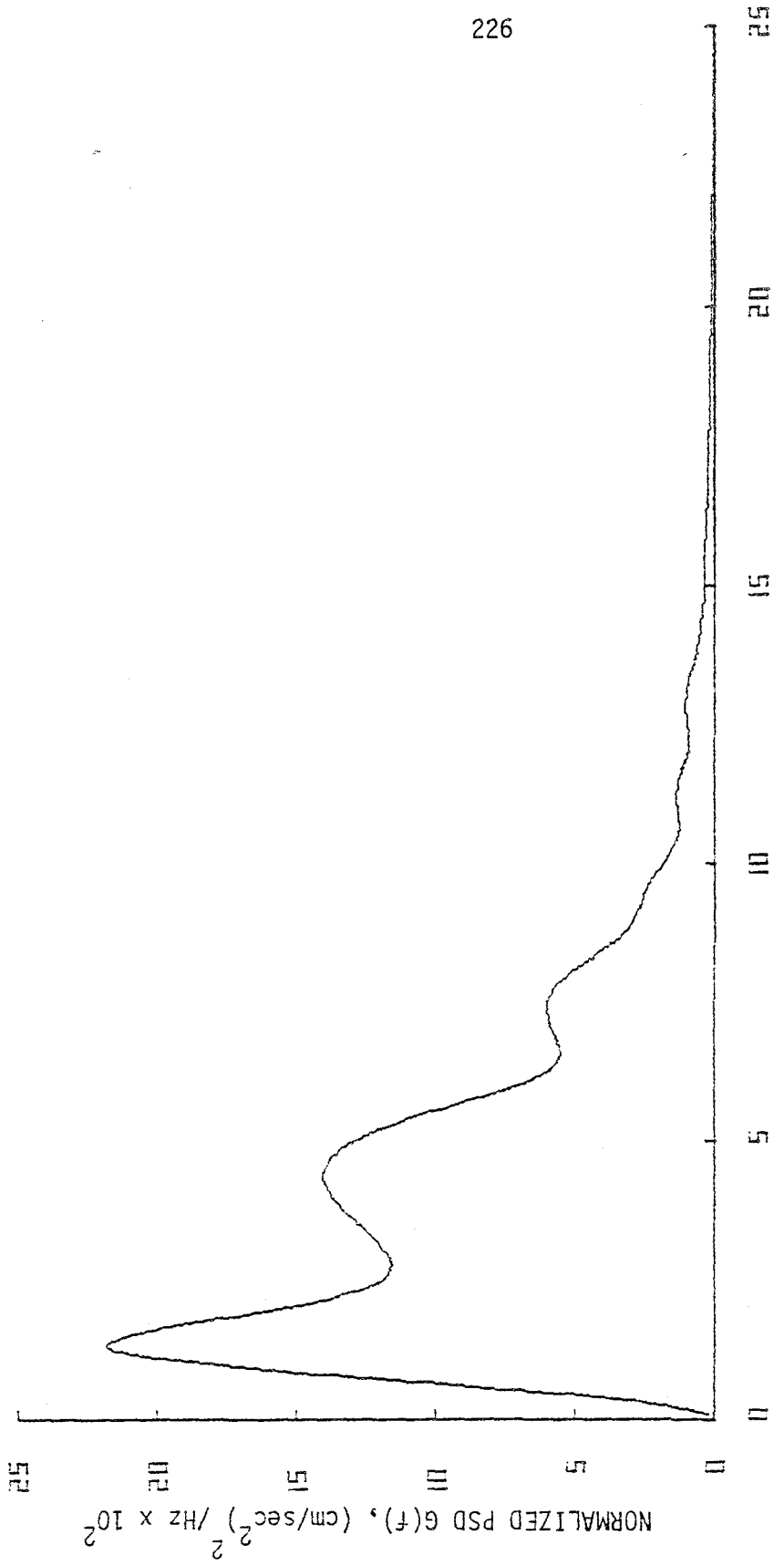

FIG. 5.3. Power spectral density of the ensemble of 26 horizontal components of recorded accelerograms--Hard.

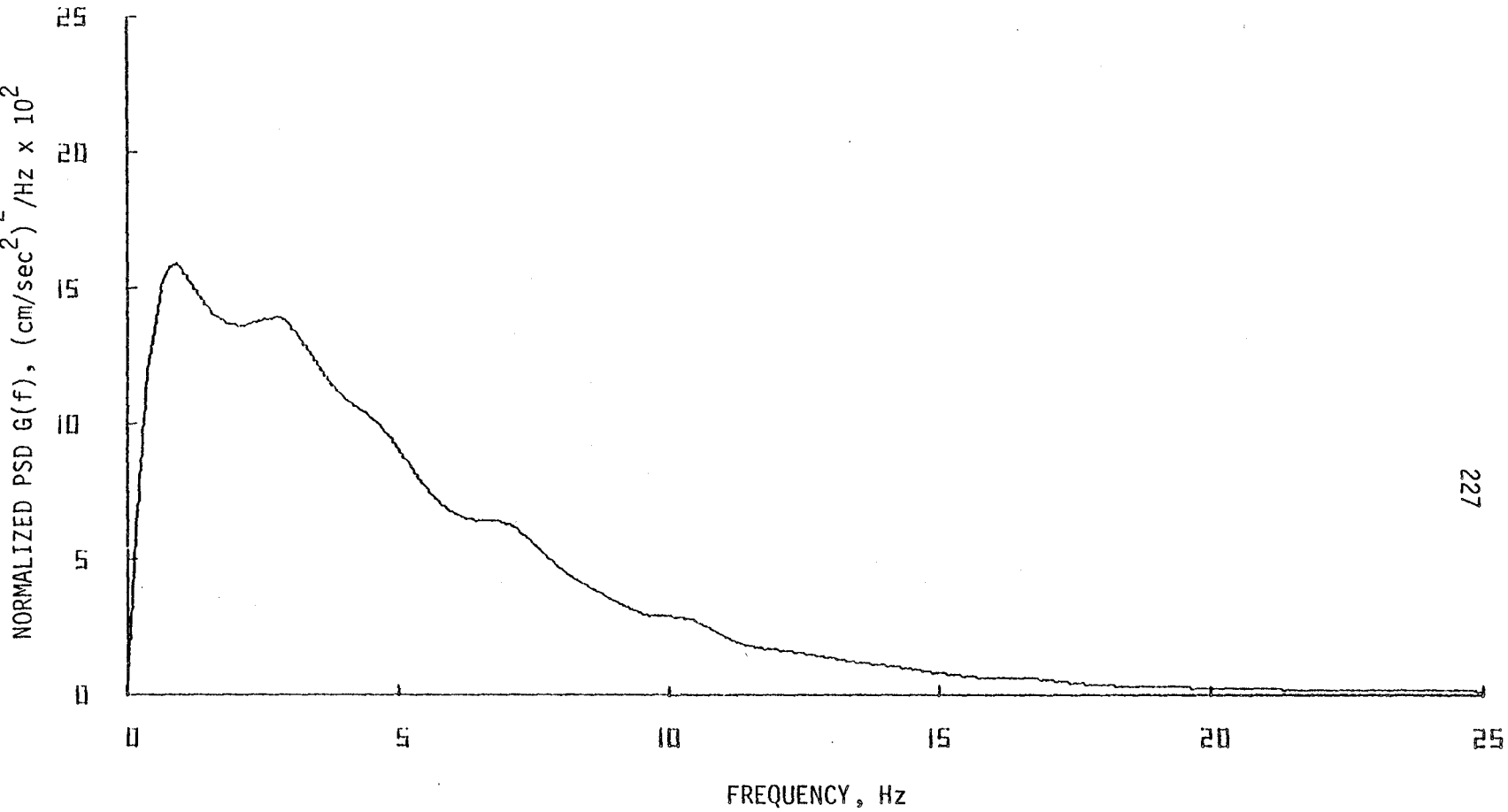

FIG. 5.4. Power spectral density of the ensemble of 78 vertical components of recorded accelerograms--Soft.

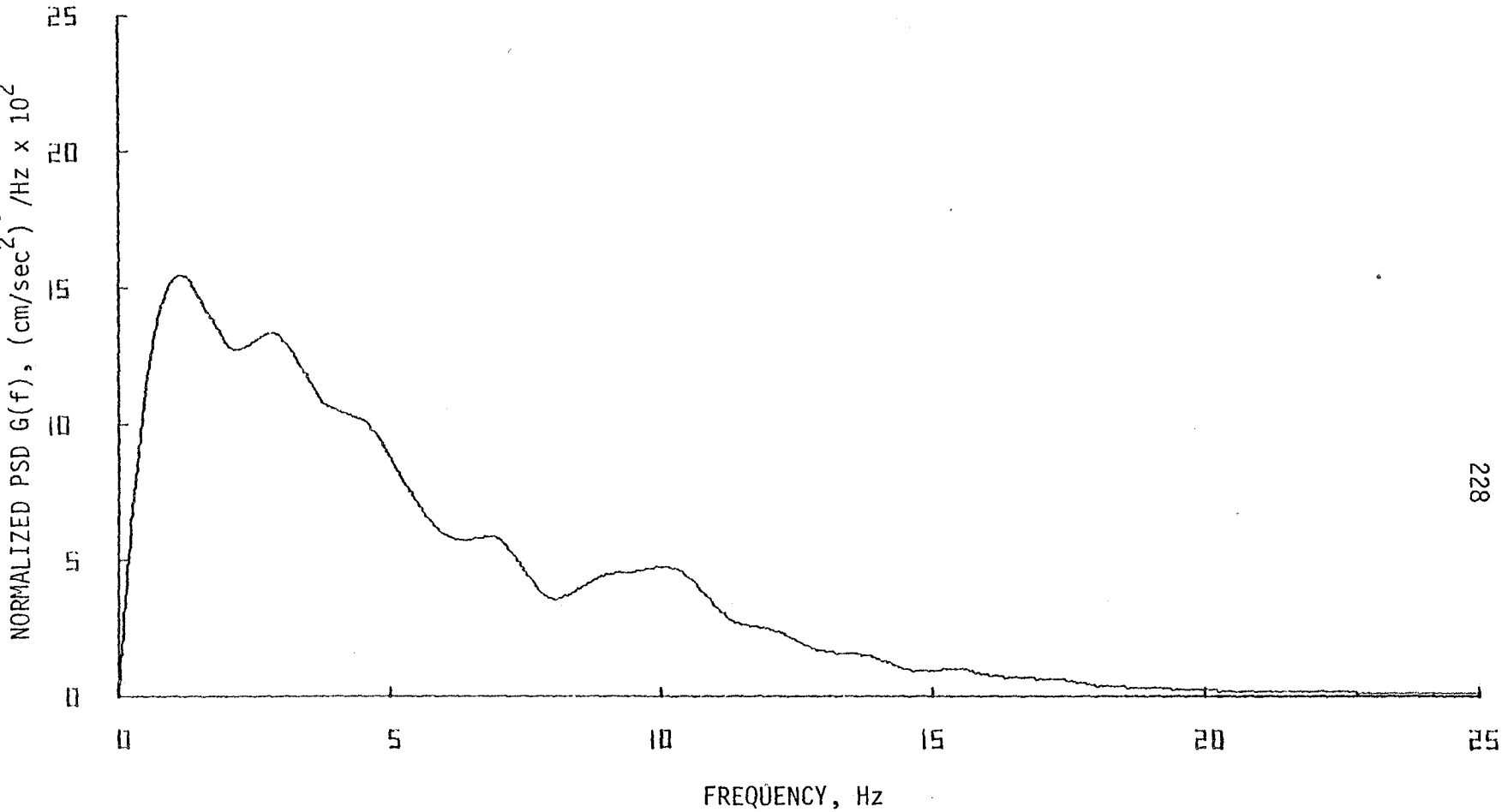

FIG. 5.5. Power spectral density of the ensemble of 29 vertical components of recorded accelerograms--Intermediate.

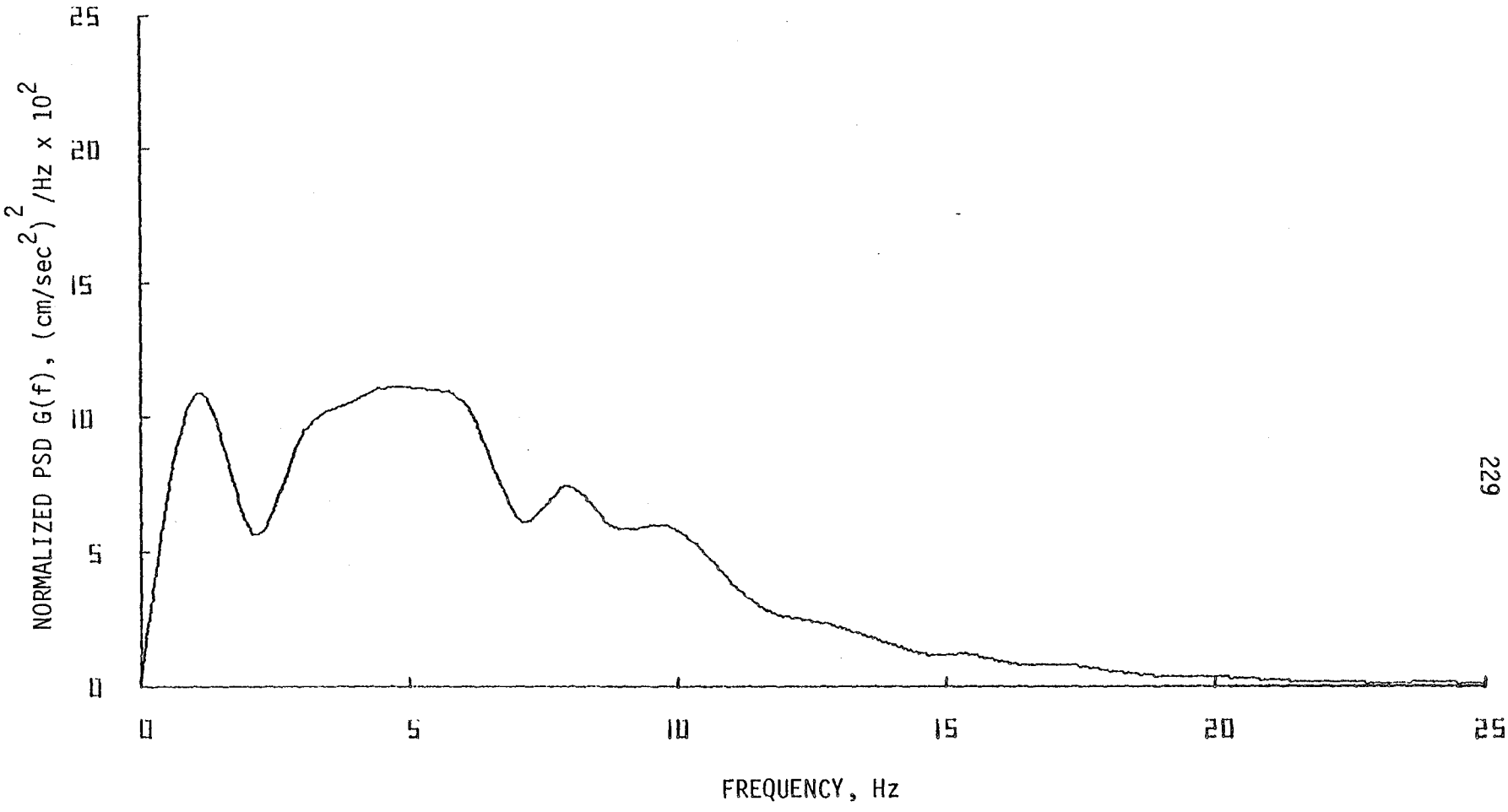

FIG. 5.6. Power spectral density of the ensemble of 13 vertical components of recorded accelerograms--Hard.

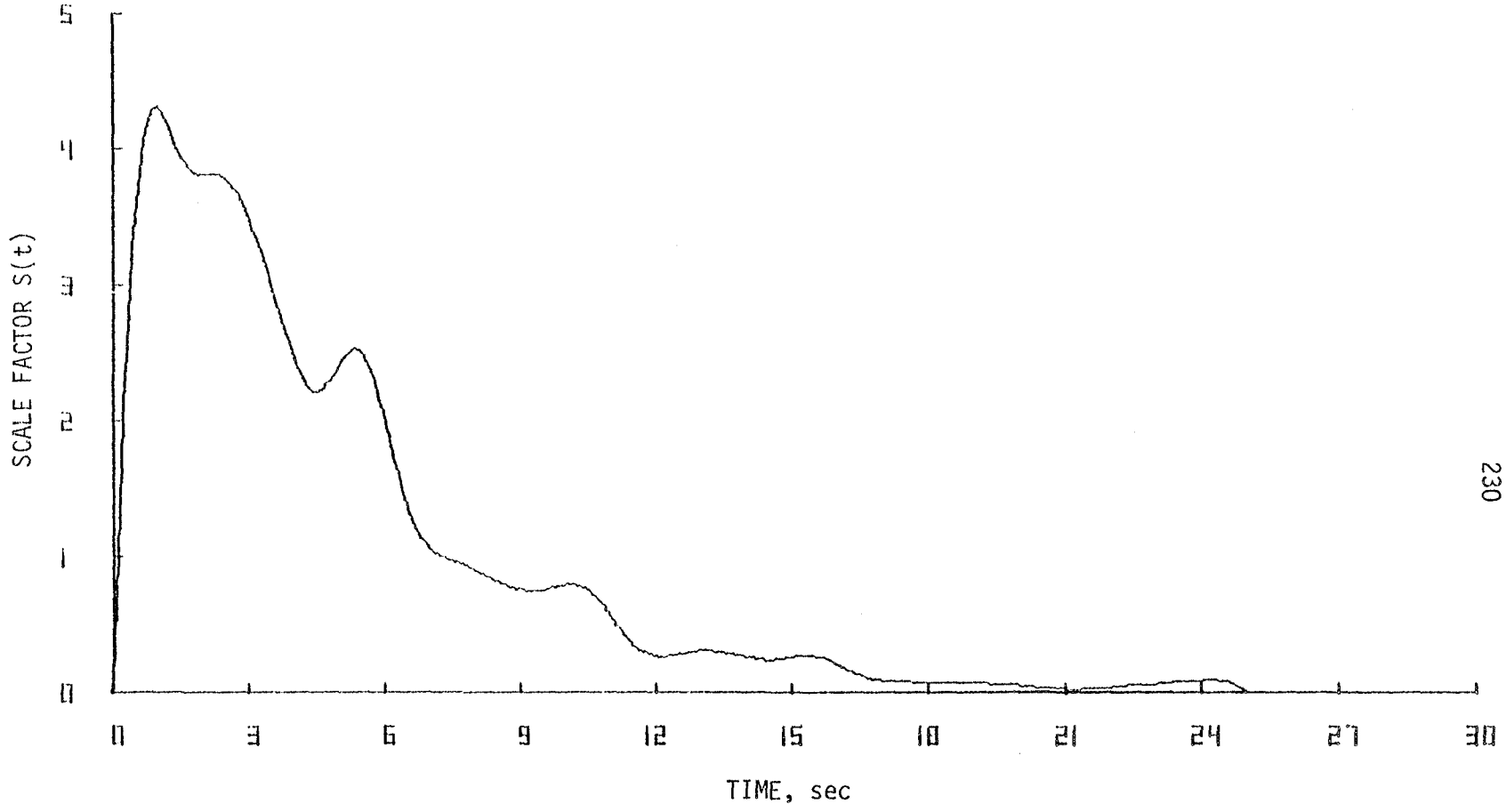

FIG. 5.7. Time variation of normalized mean square value of the ensemble of 161 horizontal components of recorded accelerograms--Soft.

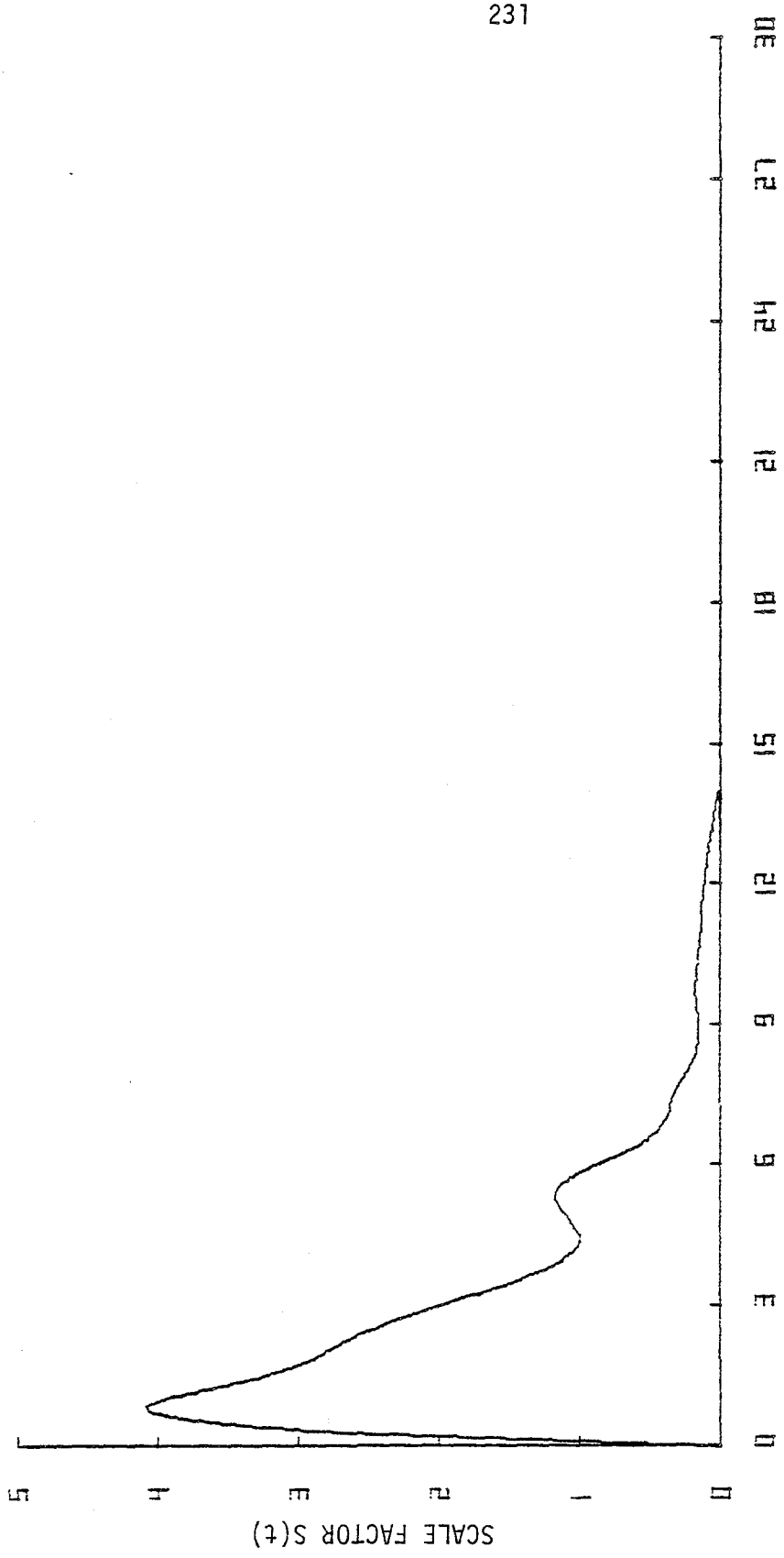

FIG. 5.8. Time variation of normalized mean square value of the ensemble of 60 horizontal components of recorded accelerograms--Intermediate.

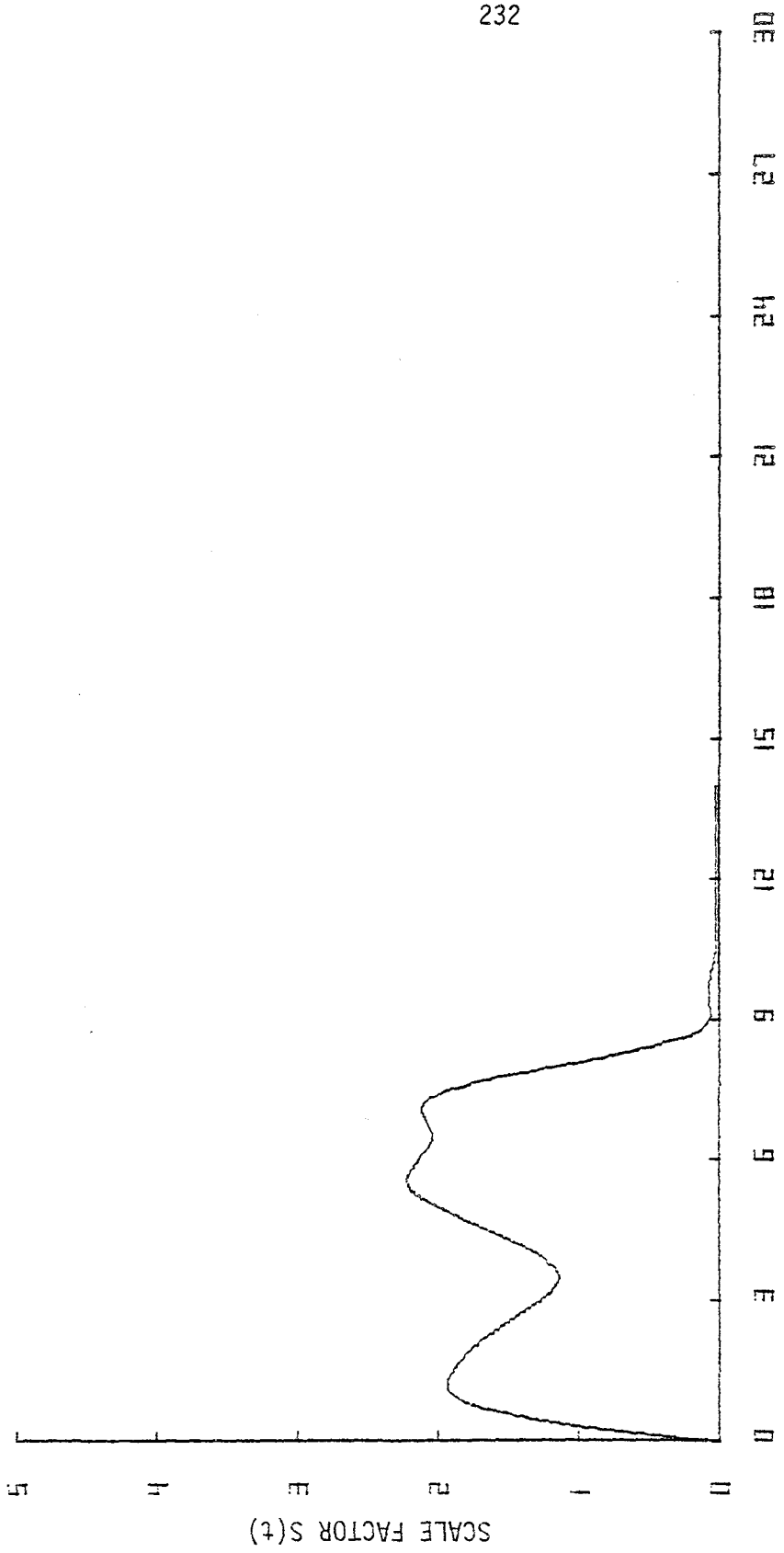

FIG. 5.9. Time variation of normalized mean square value of the ensemble of 26 horizontal components of recorded accelerograms--Hard.

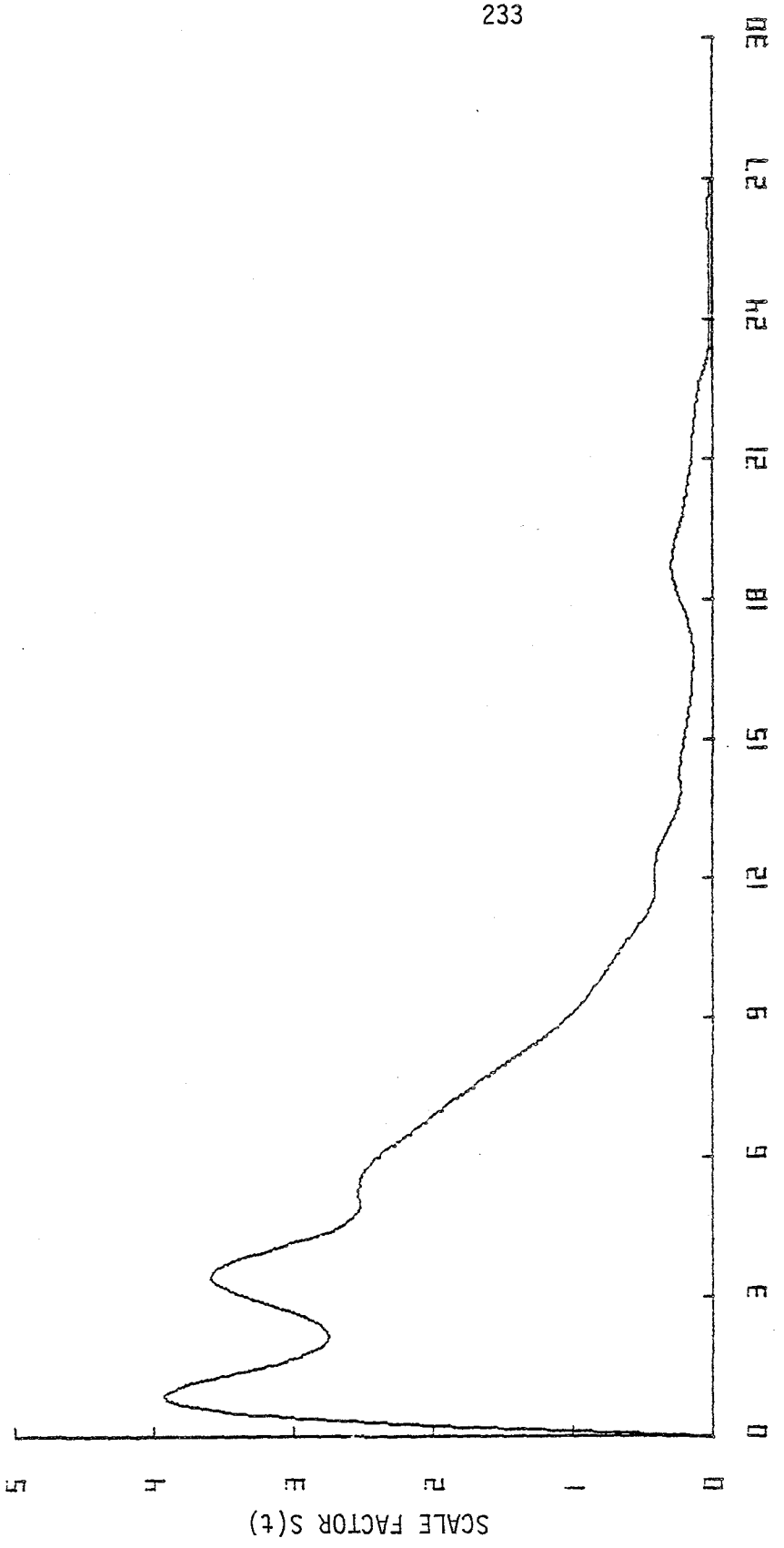

FIG. 5.10. Time variation of normalized mean square value of the ensemble of 78 vertical components of recorded accelerograms--Soft.

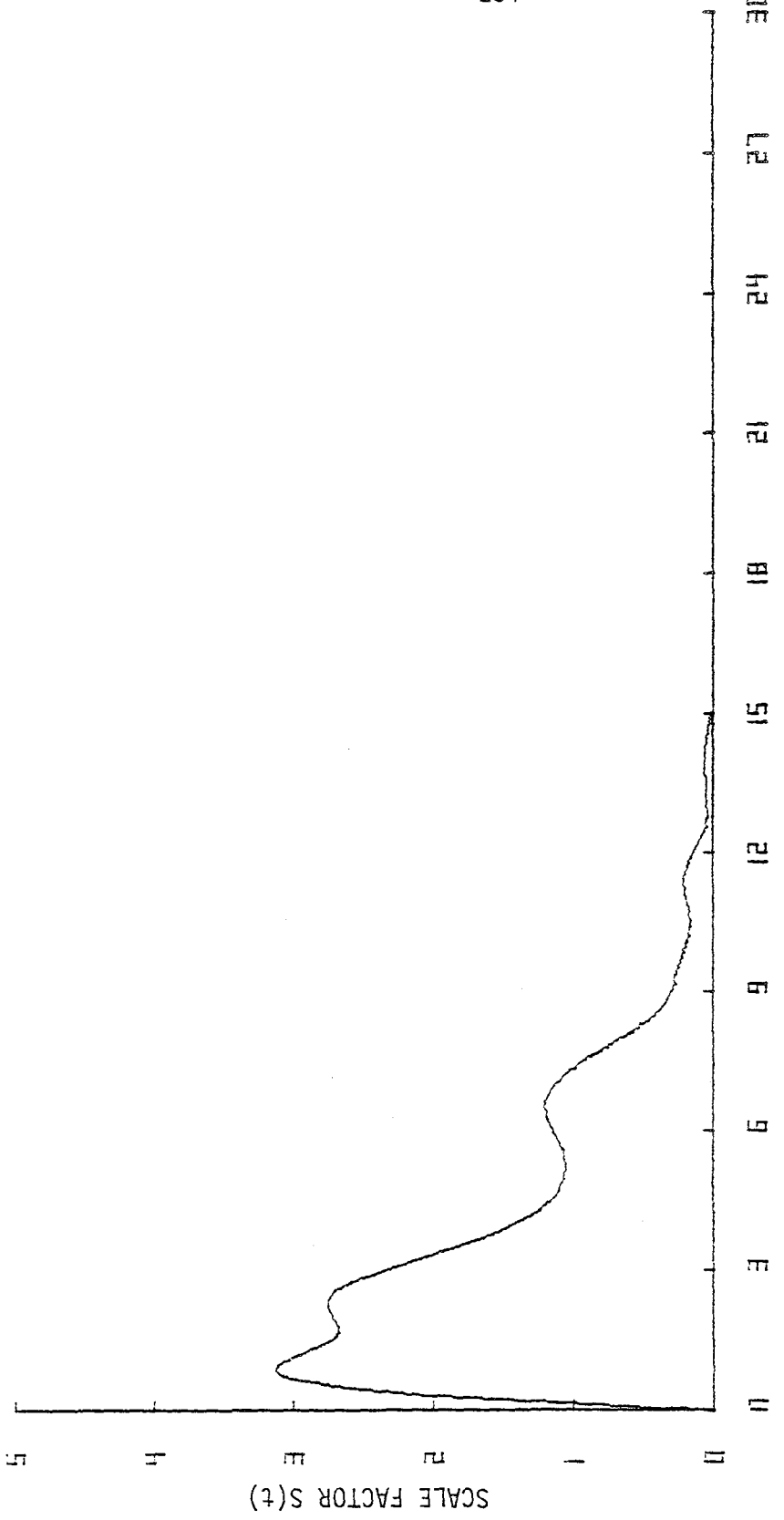

FIG. 5.11. Time variation of normalized mean square value of the ensemble of 29 vertical components of recorded accelerograms--Intermediate.

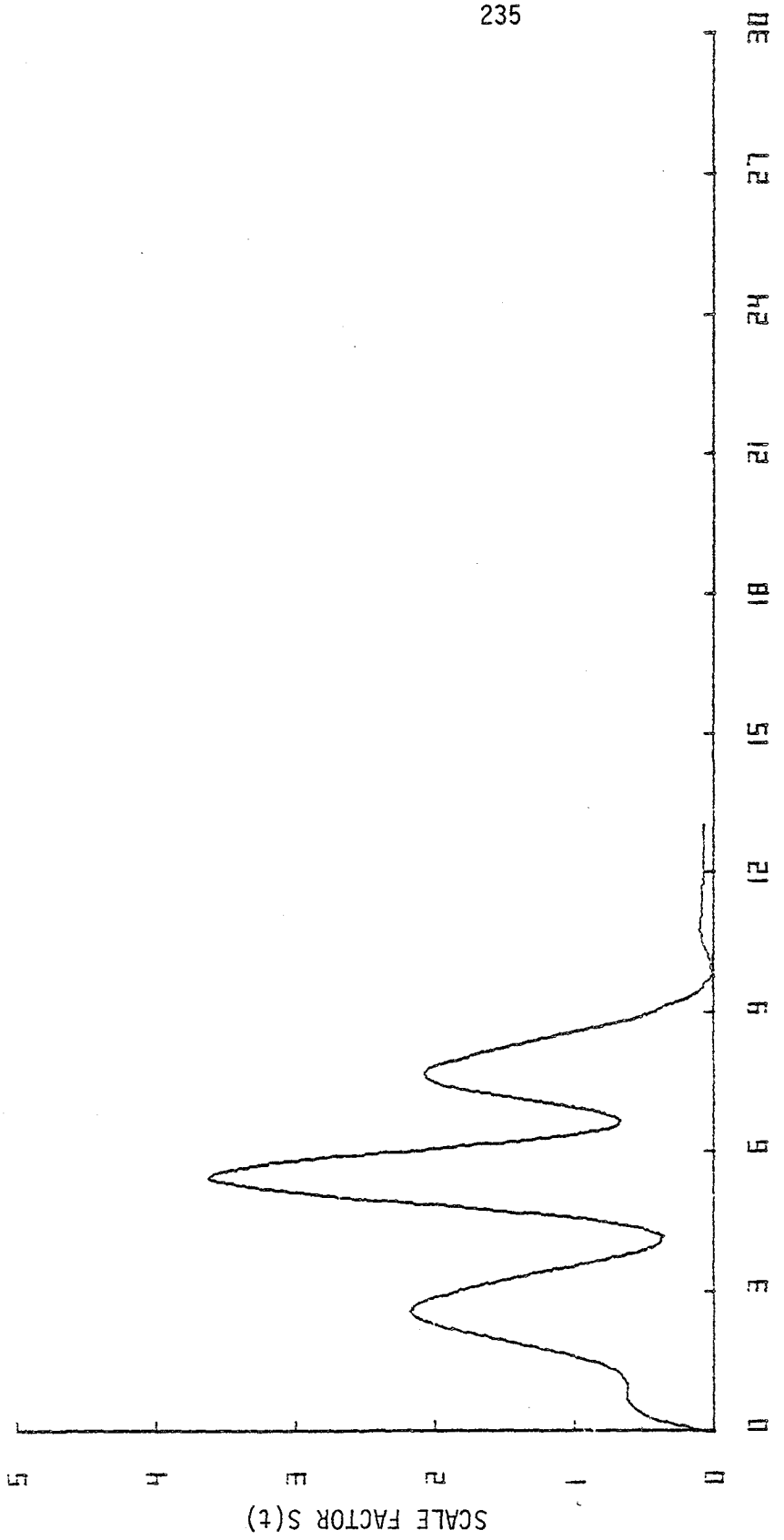

FIG. 5.12. Time variation of normalized mean square value of the ensemble of 13 vertical components of recorded accelerograms--Hard.

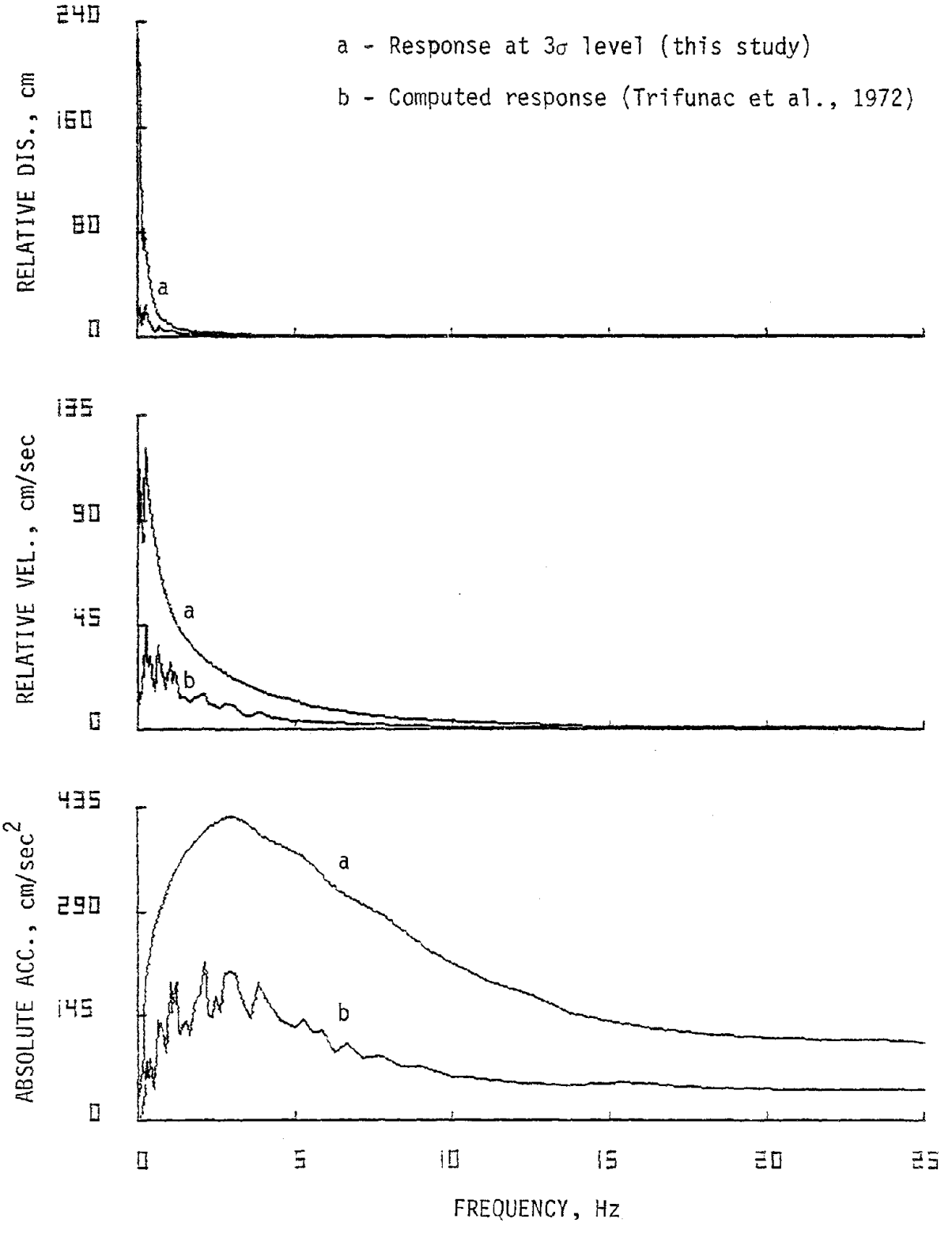

FIG. 5.13. Comparison of predicted response (soft) and computed response for 2 percent damping, Hollywood Storage P.E. lot, 1952--N90E.

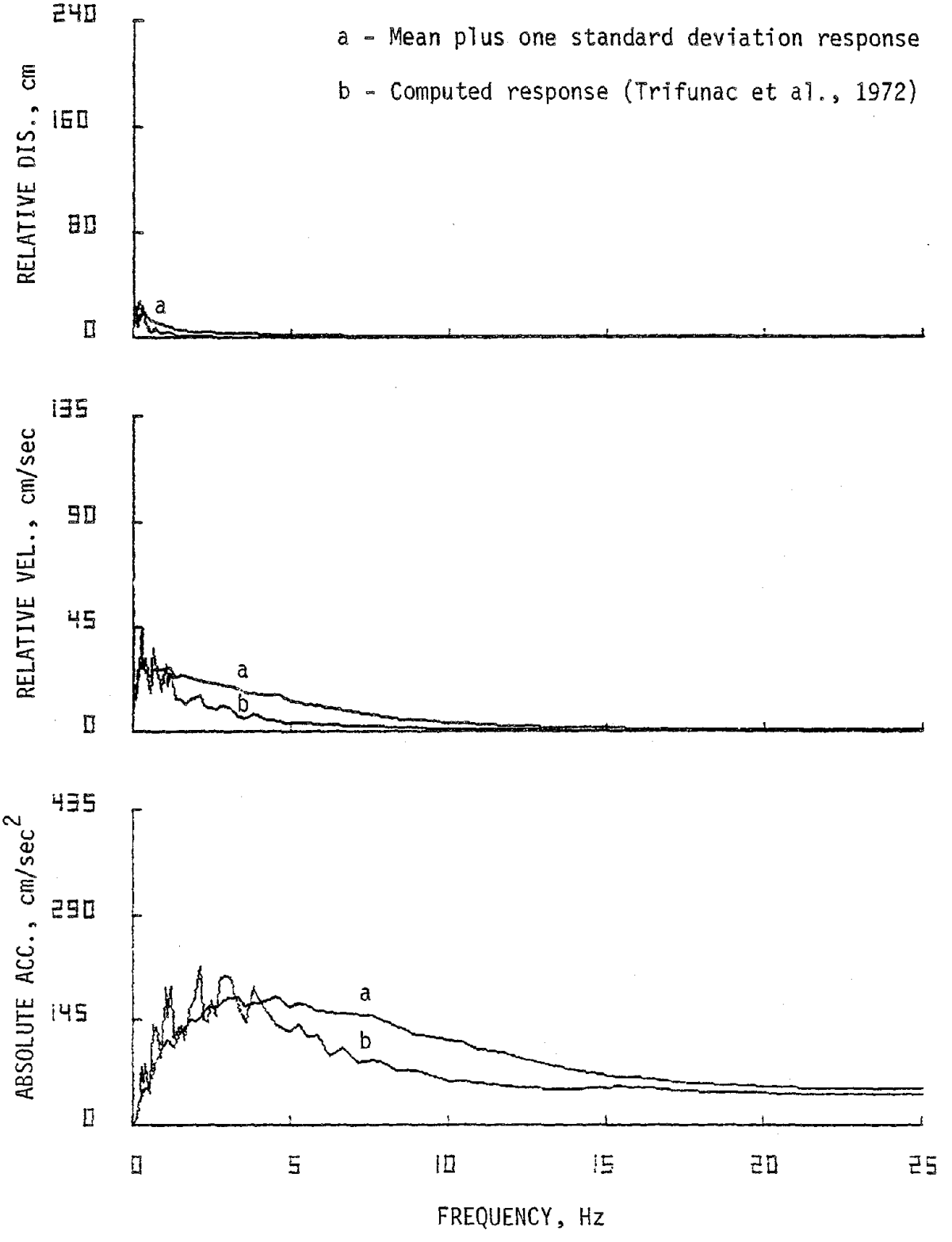

FIG. 5.14. Comparison of mean plus one standard deviation response (soft) and computed response for 2 percent damping, Hollywood Storage P.E. lot, 1952--N90E.

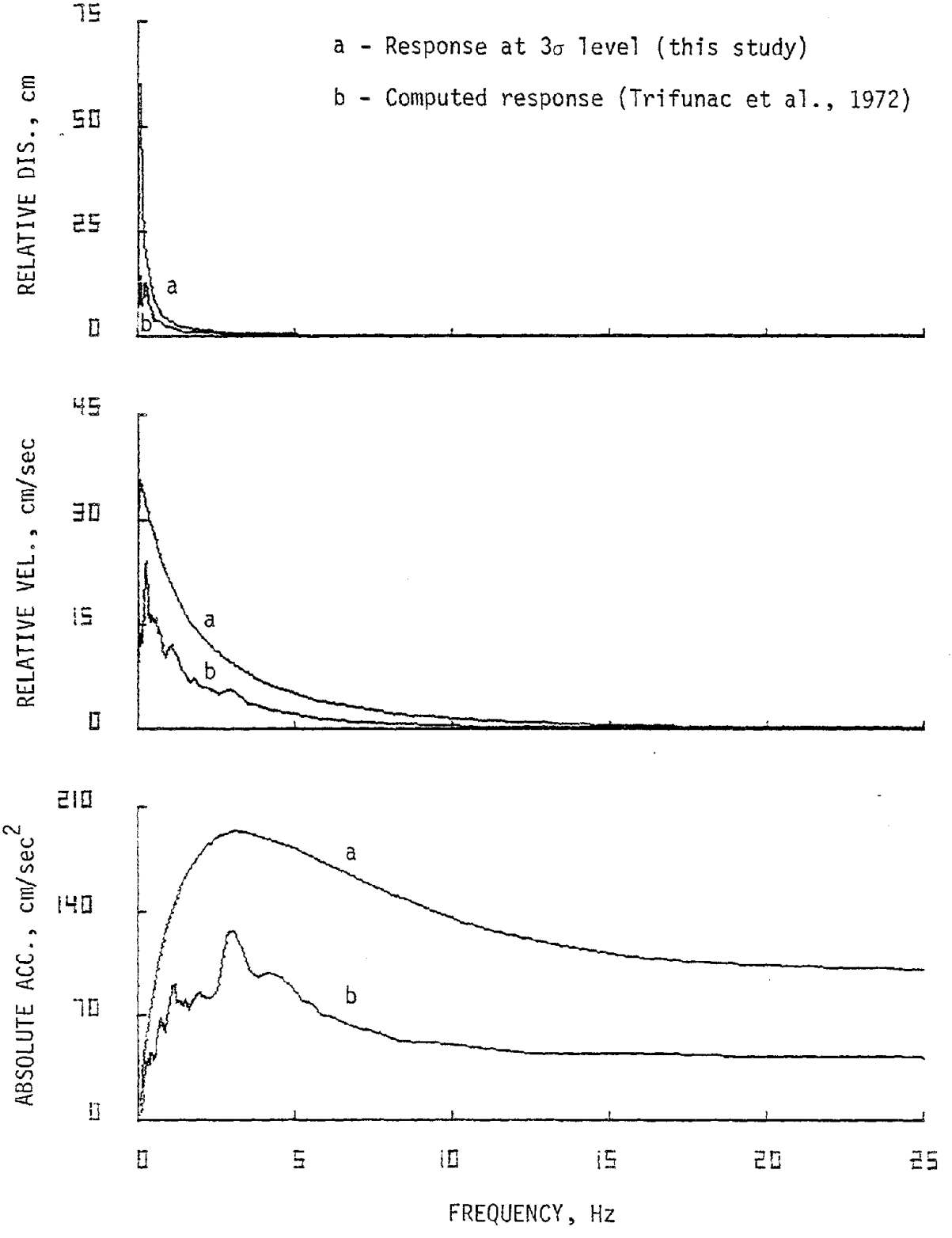

FIG. 5.15. Comparison of predicted response (soft) and computed response for 10 percent damping, Hollywood Storage P.E. lot, 1952--N90E.

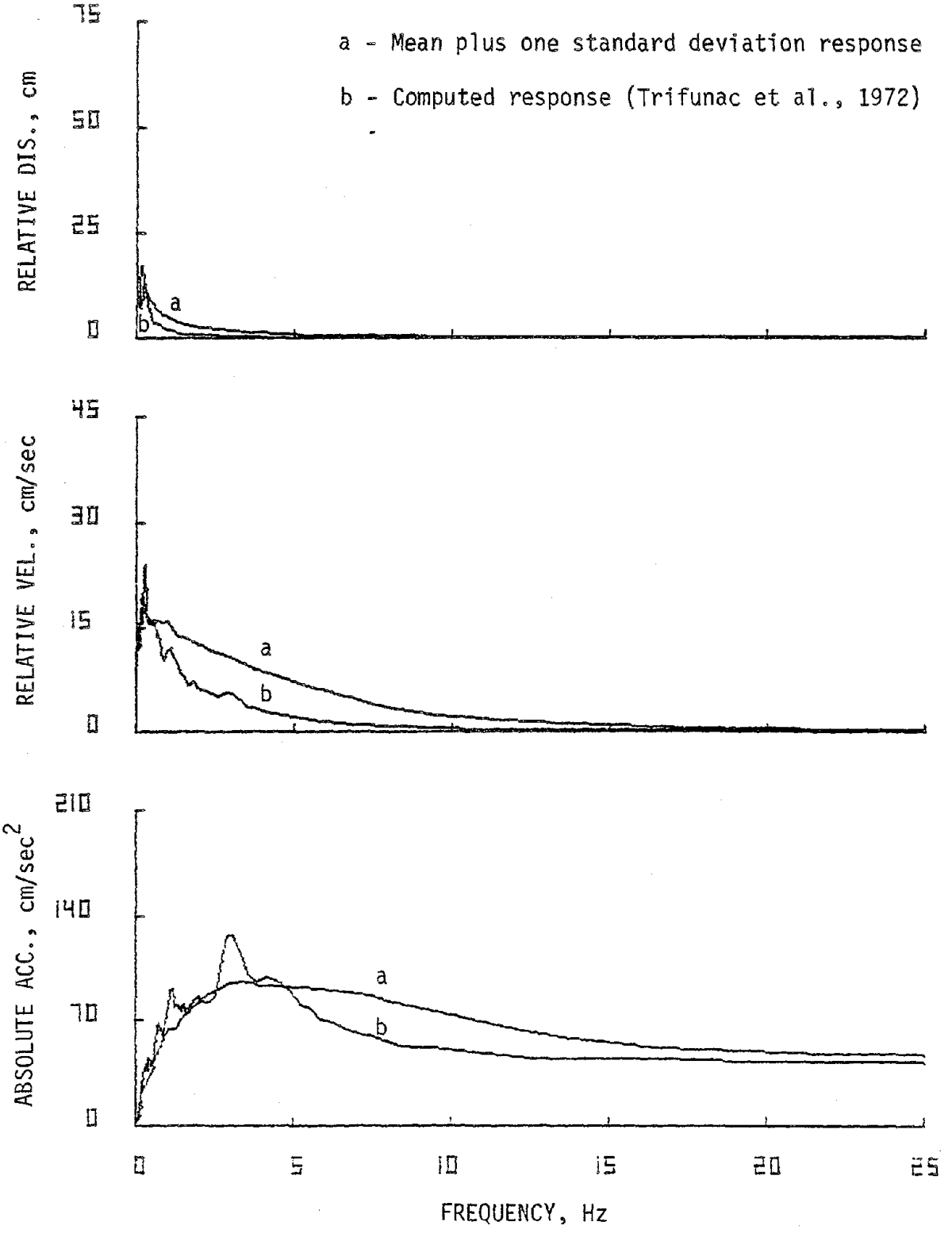

FIG. 5.16. Comparison of mean plus one standard deviation response (soft) and computed response for 10 percent damping, Hollywood Storage P.E. lot, 1952--N90E.

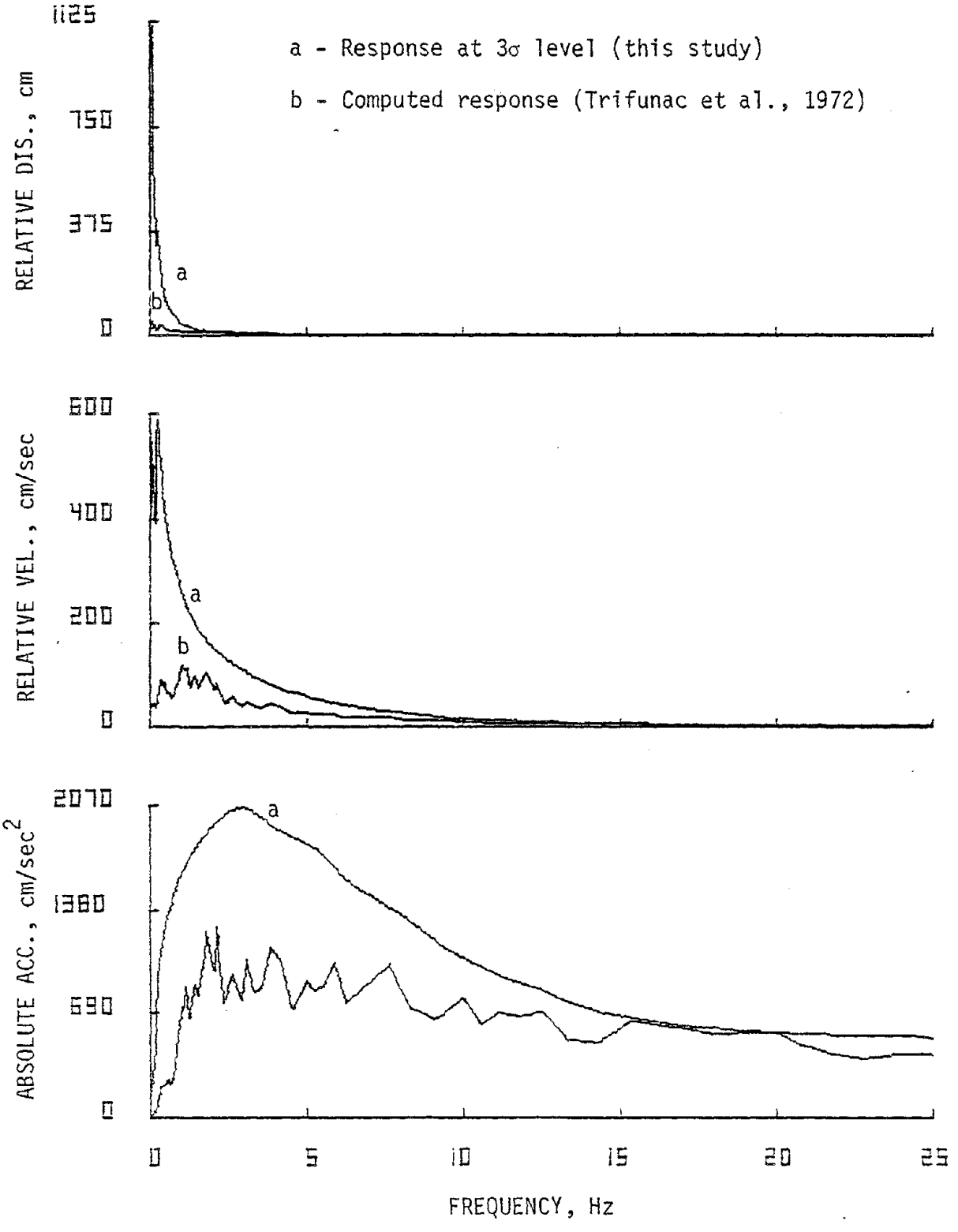

FIG. 5.17. Comparison of predicted response (soft) and computed response for 2 percent damping, El Centro, 1940--S00E.

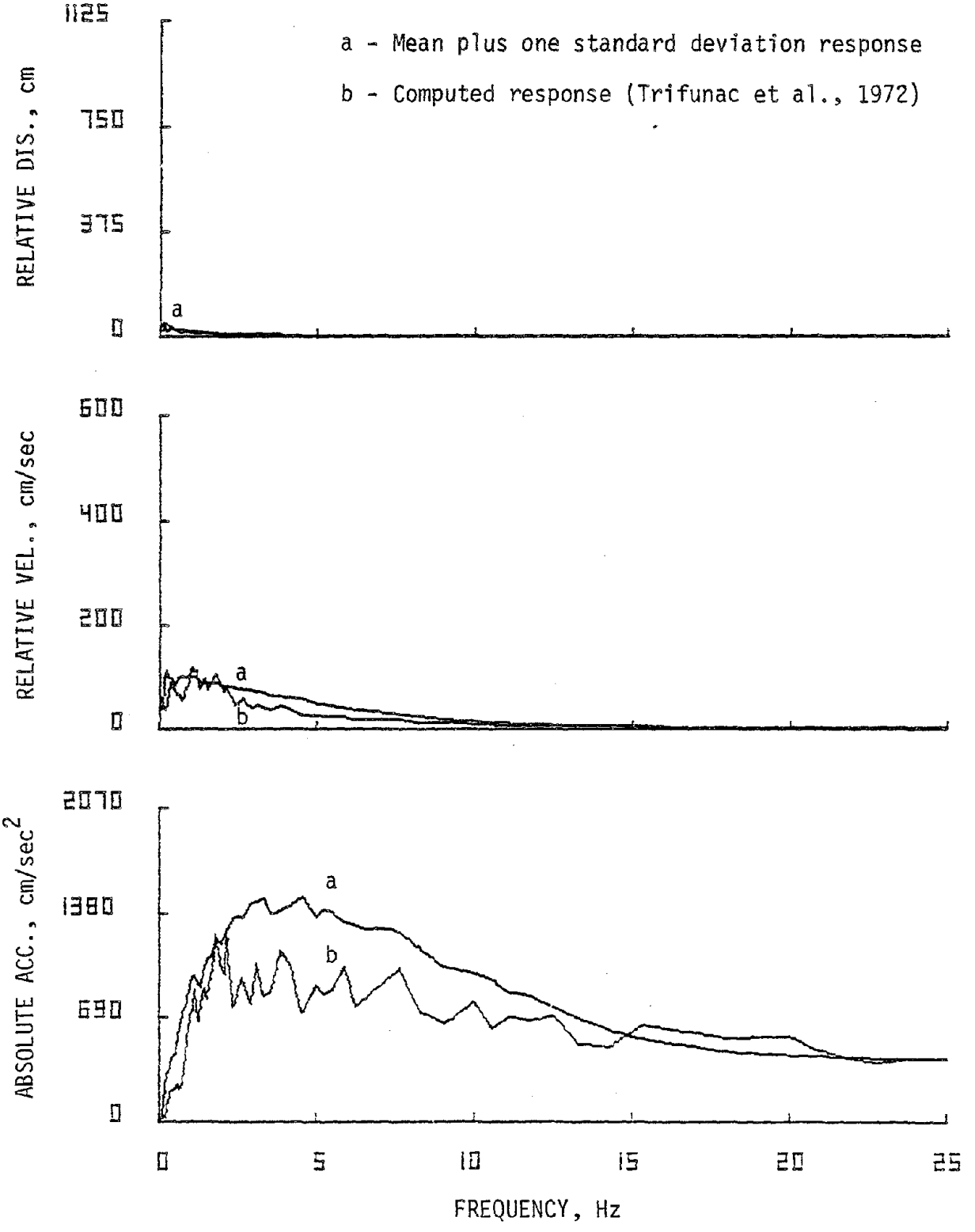

FIG. 5.18. Comparison of mean plus one standard deviation response (soft) and computed response for 2 percent damping, El Centro, 1940--S00E.

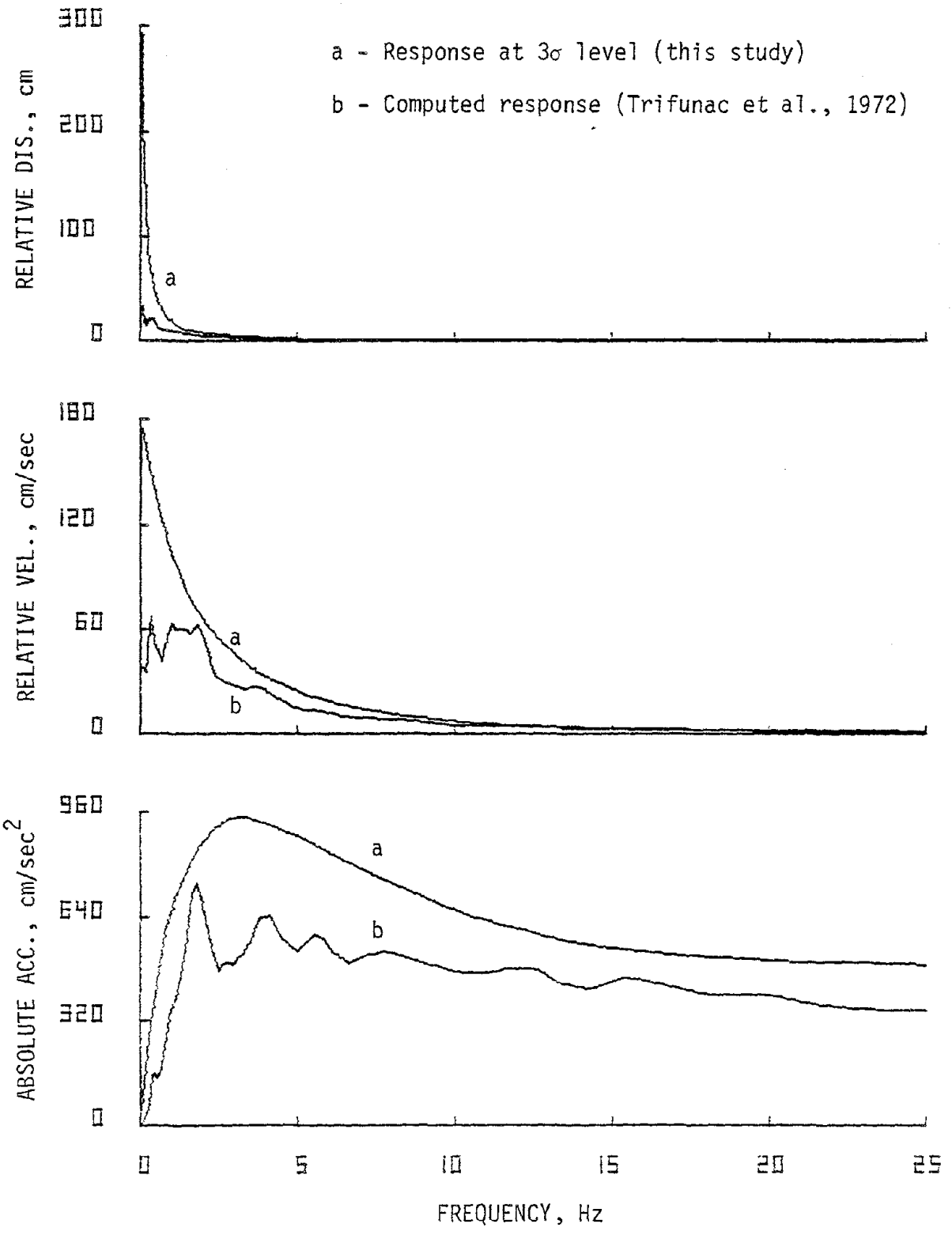

FIG. 5.19. Comparison of predicted response (soft) and computed response for 10 percent damping, El Centro, 1940--S00E.

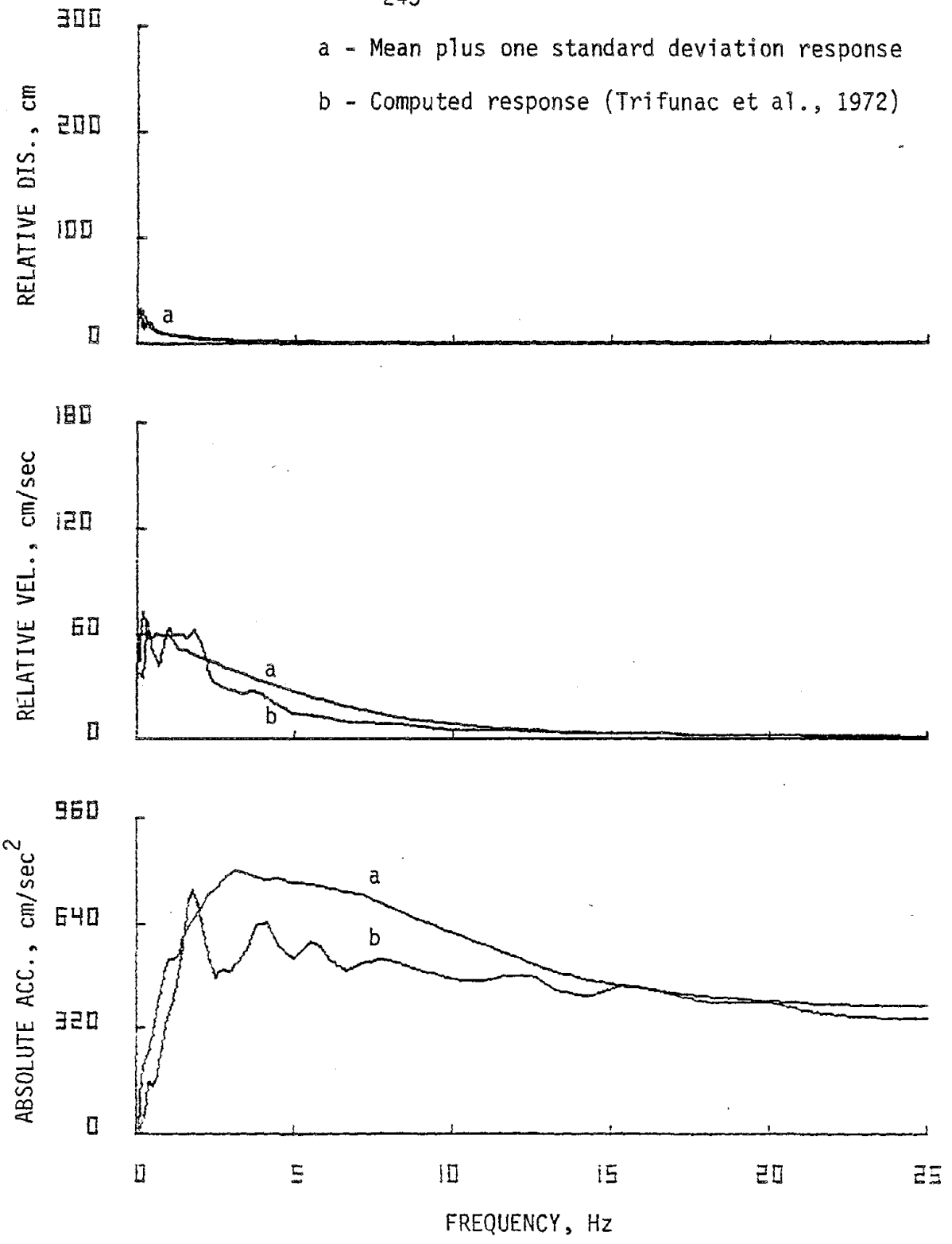

FIG. 5.20. Comparison of mean plus one standard deviation response (soft) and computed response for 10 percent damping, El Centro, 1940--S00E.

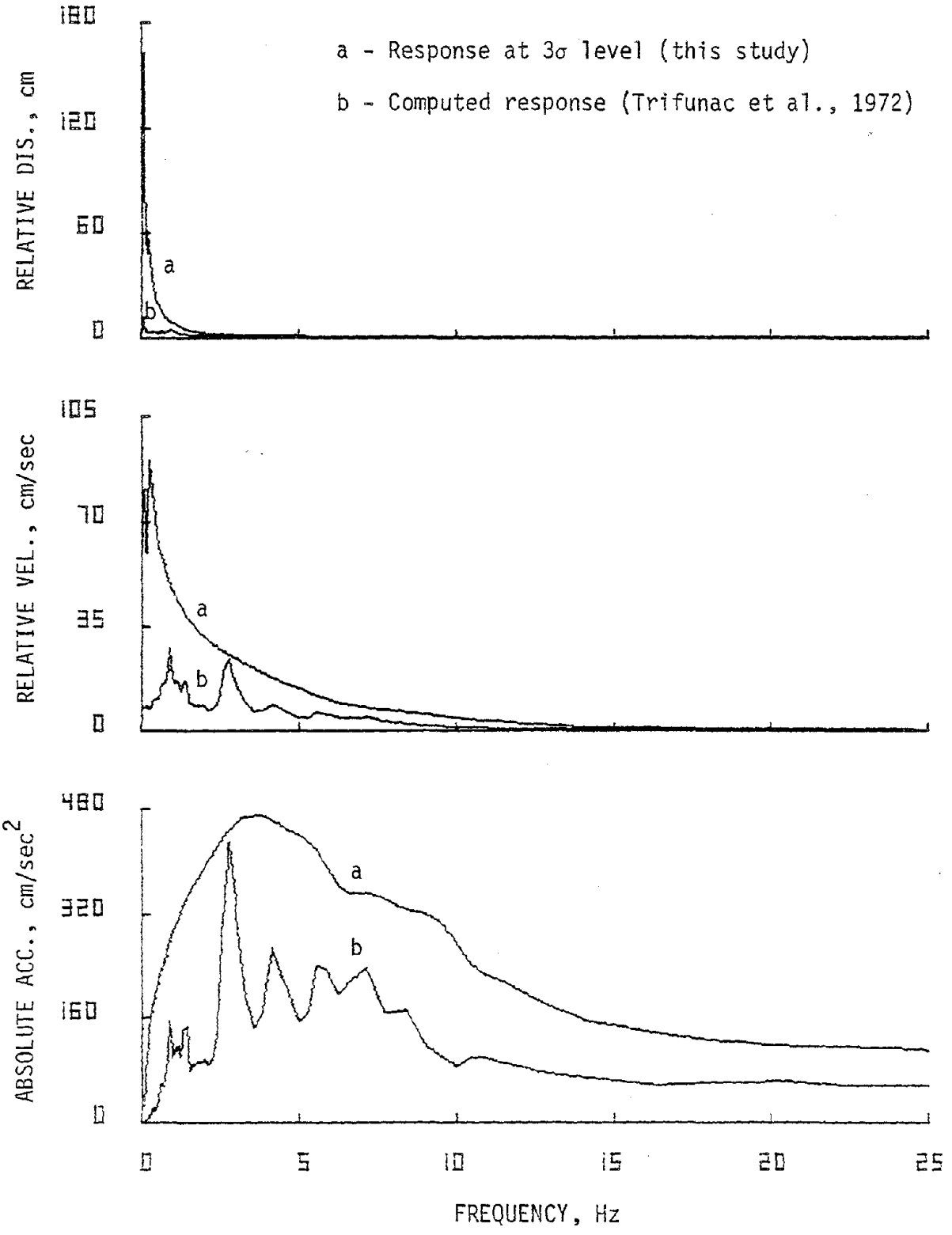

FIG. 5.21. Comparison of predicted response (intermediate) and computed response for 2 percent damping, Ferndale City Hall, 1952--N44E.

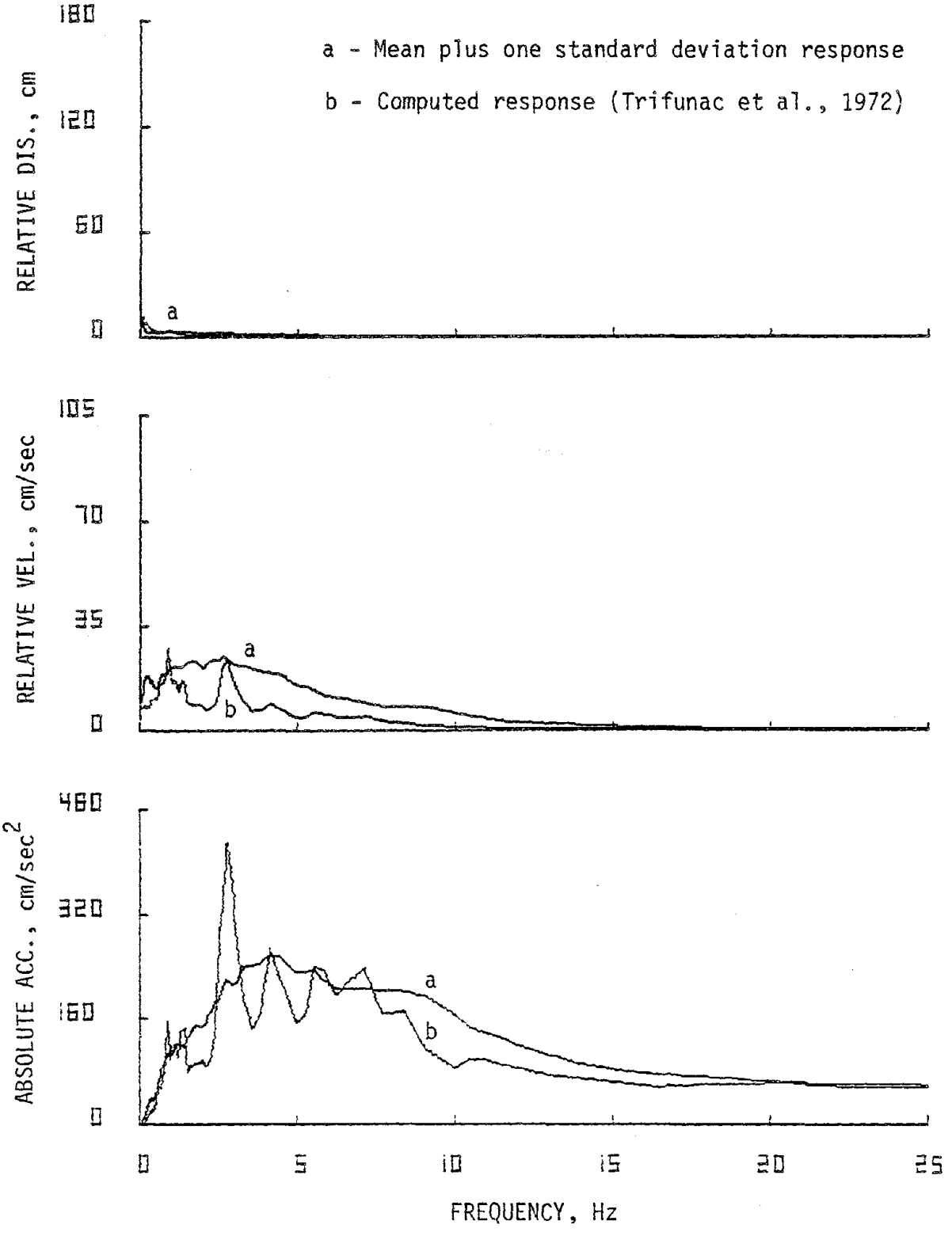

FIG. 5.22. Comparison of mean plus one standard deviation response (intermediate) and computed response for 2 percent damping, Ferndale City Hall, 1952--N44E.

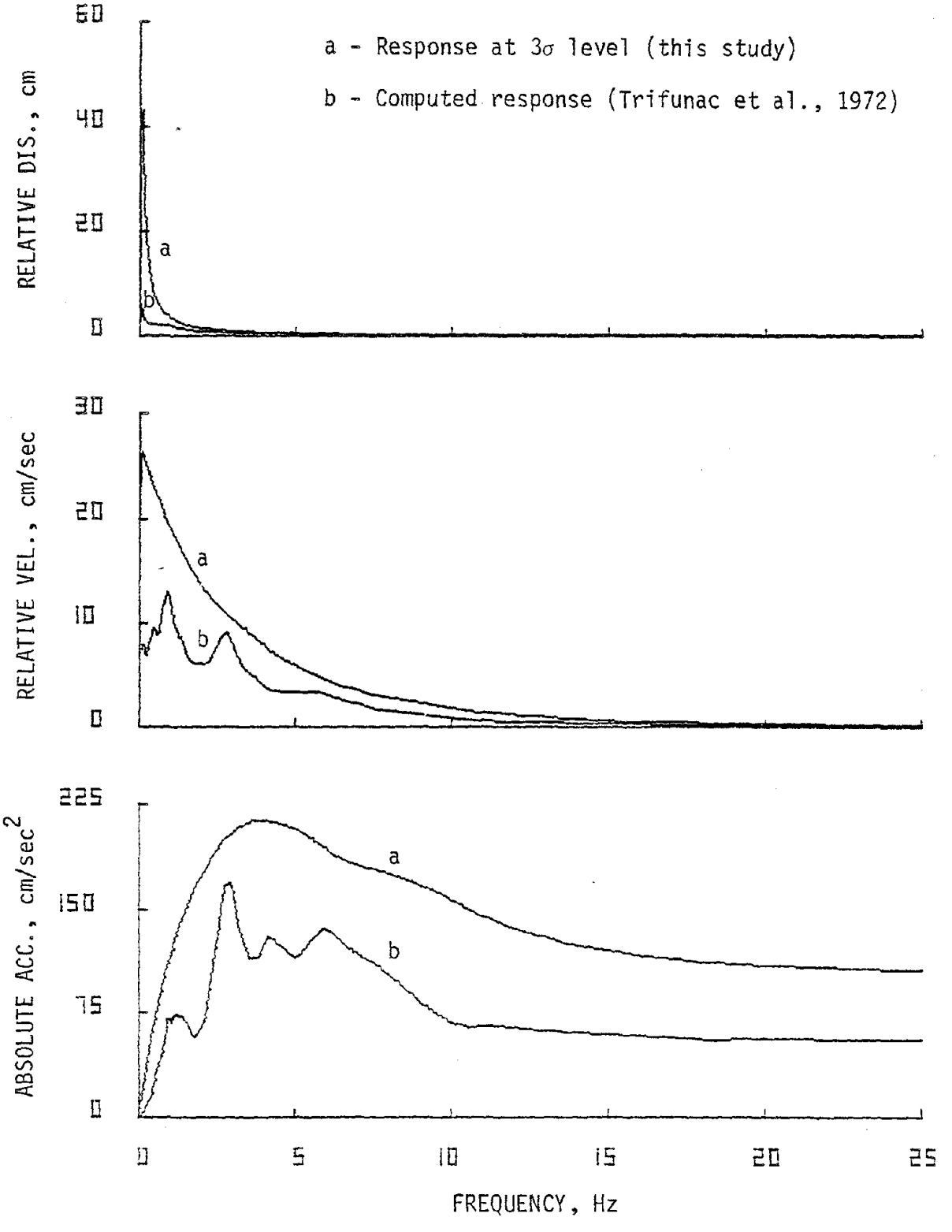

FIG. 5.23. Comparison of predicted response (intermediate) and computed response for 10 percent damping, Ferndale City Hall, 1952--N44E.

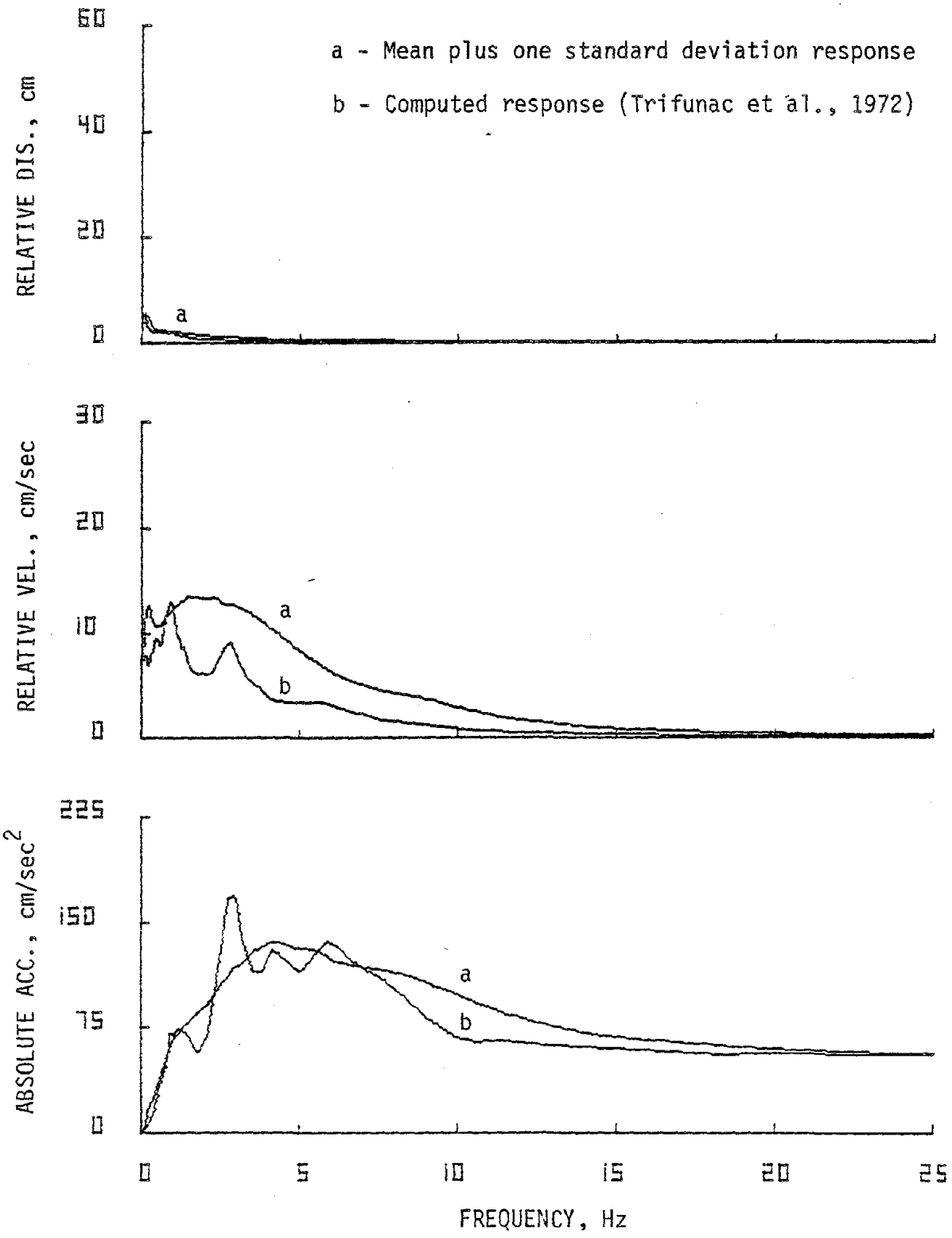

FIG. 5.24. Comparison of mean plus one standard deviation response (intermediate) and computed response for 10 percent damping, Ferndale City Hall, 1952--N44E.

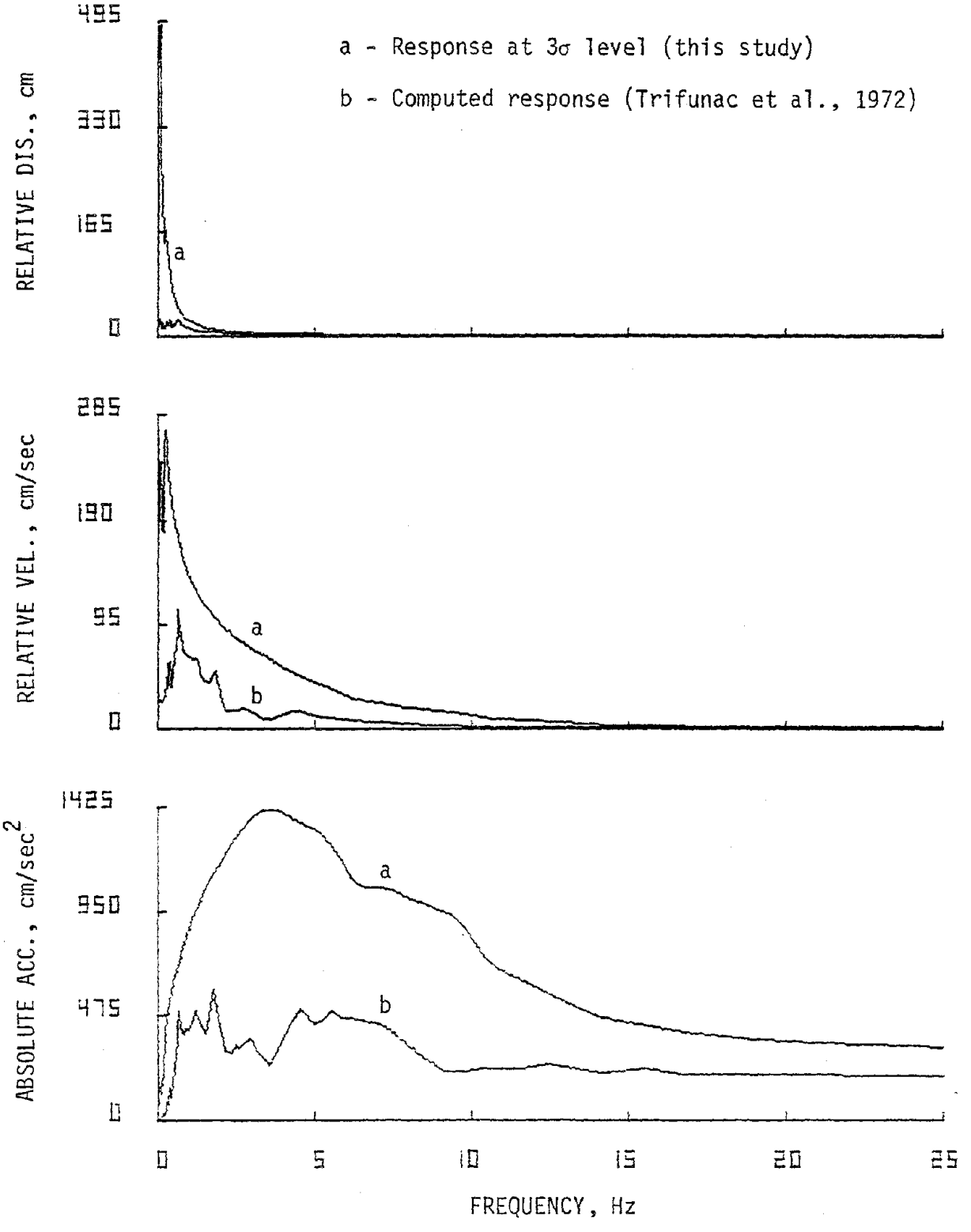

FIG. 5.25. Comparison of predicted response (intermediate) and computed response for 2 percent damping, Ferndale City Hall, 1954--N46W.

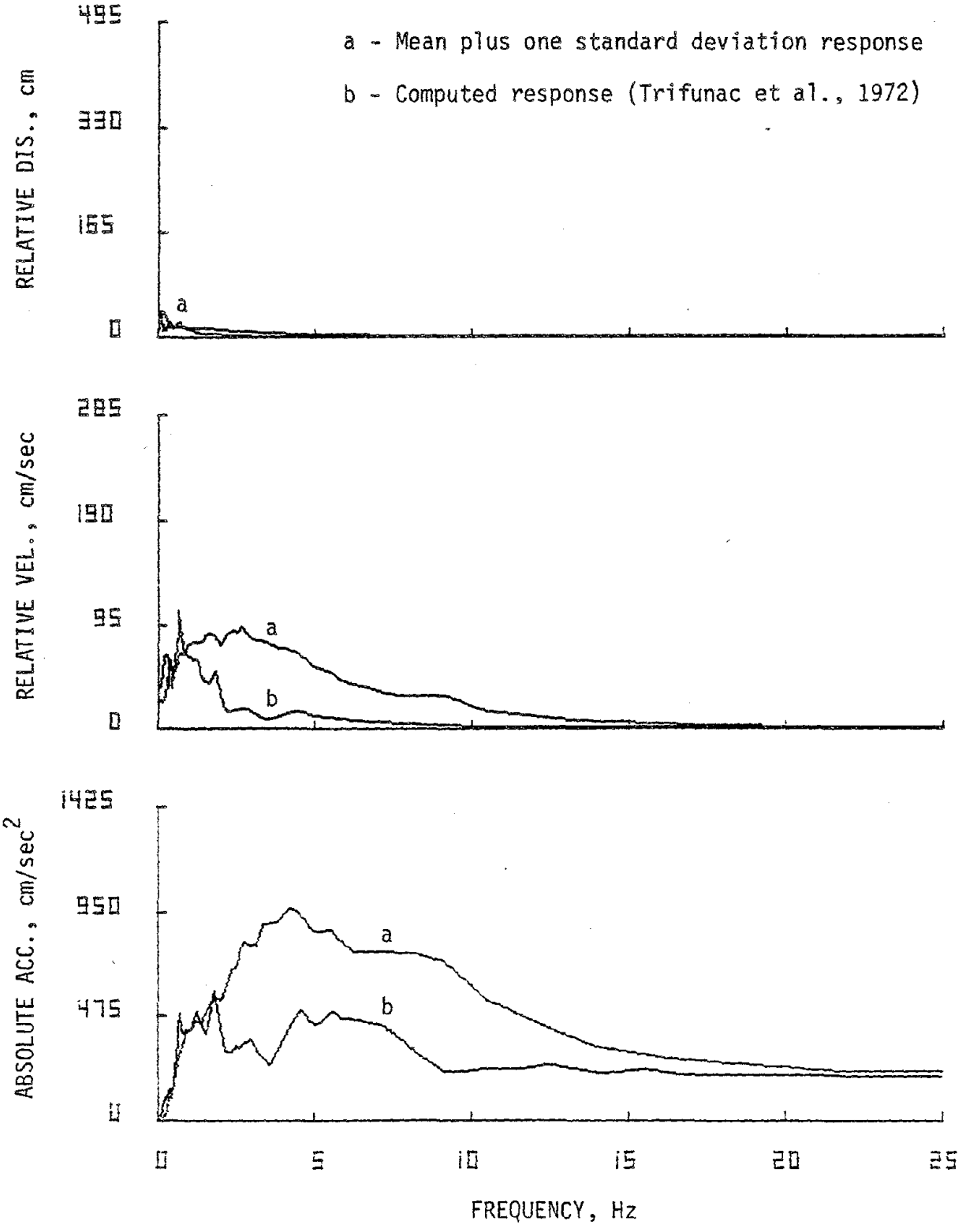

FIG. 5.26. Comparison of mean plus one standard deviation response (intermediate) and computed response for 2 percent damping, Ferndale City Hall, 1954--N46W.

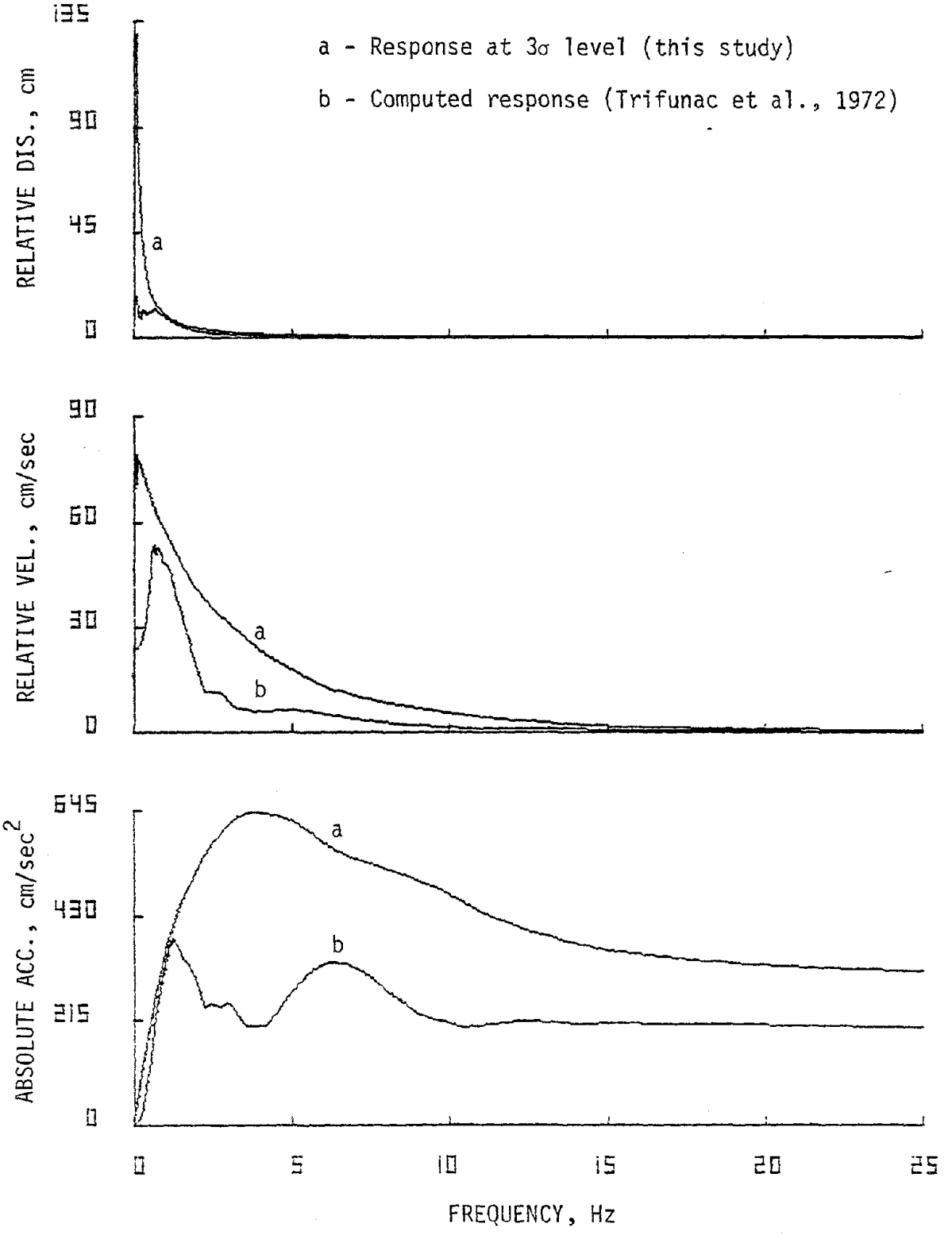

FIG. 5.27. Comparison of predicted response (intermediate) and computed response for 10 percent damping, Ferndale City Hall, 1954--N46W.

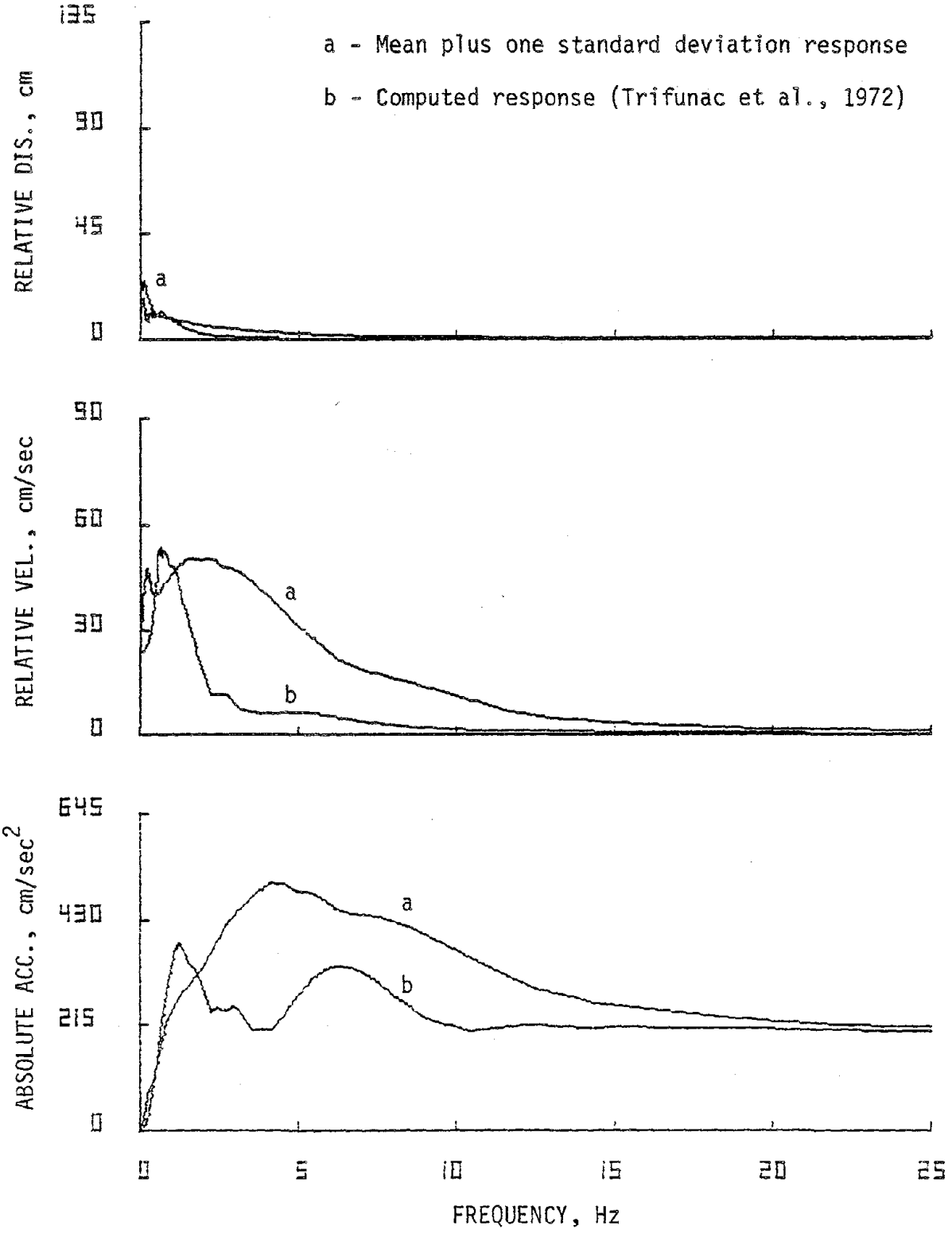

FIG. 5.28. Comparison of mean plus one standard deviation response (intermediate) and computed response for 10 percent damping, Ferndale City Hall, 1954--N46W.

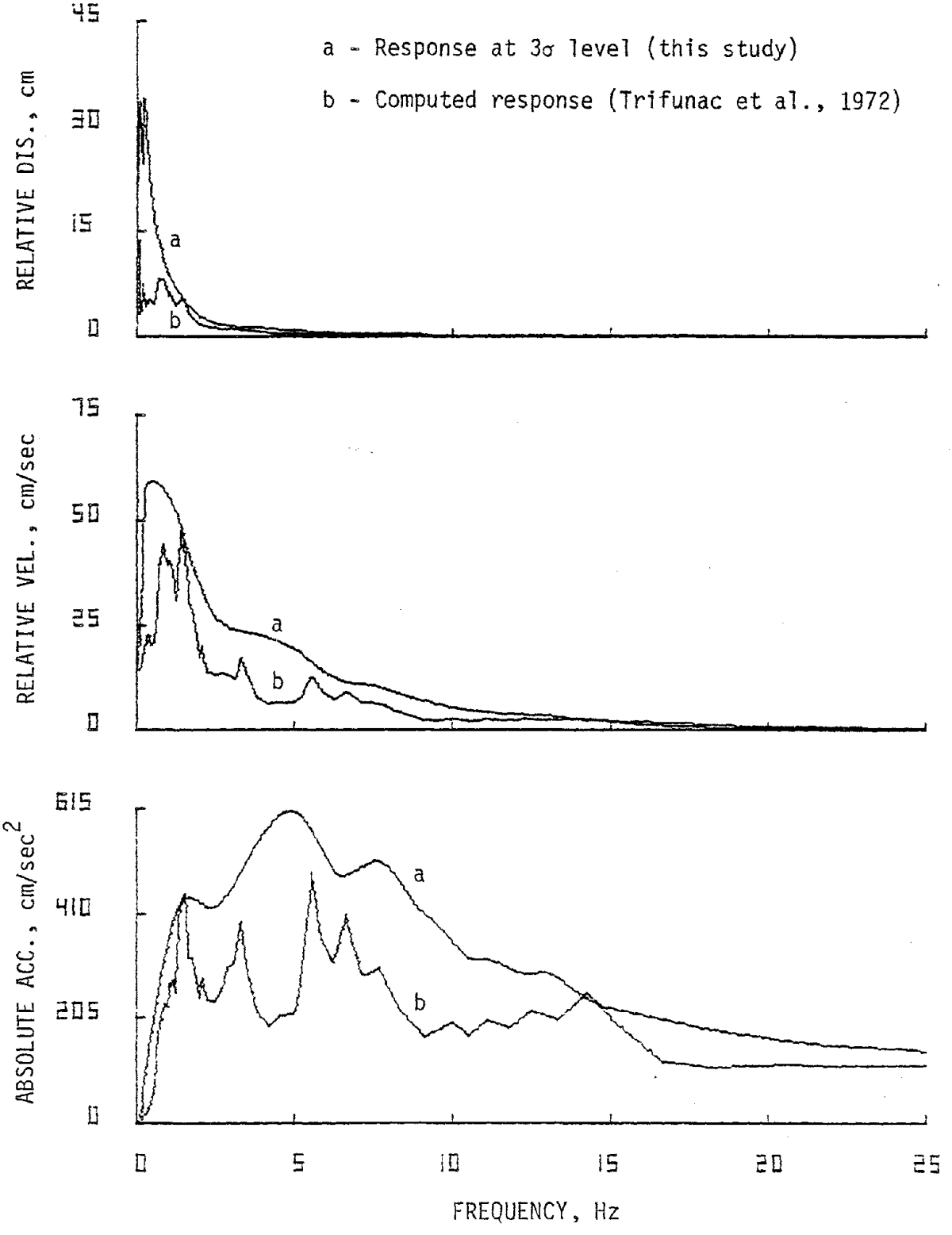

FIG. 5.29. Comparison of predicted response (hard) and computed response for 2 percent damping, Lake Hughes Station 1, 1971--S69E.

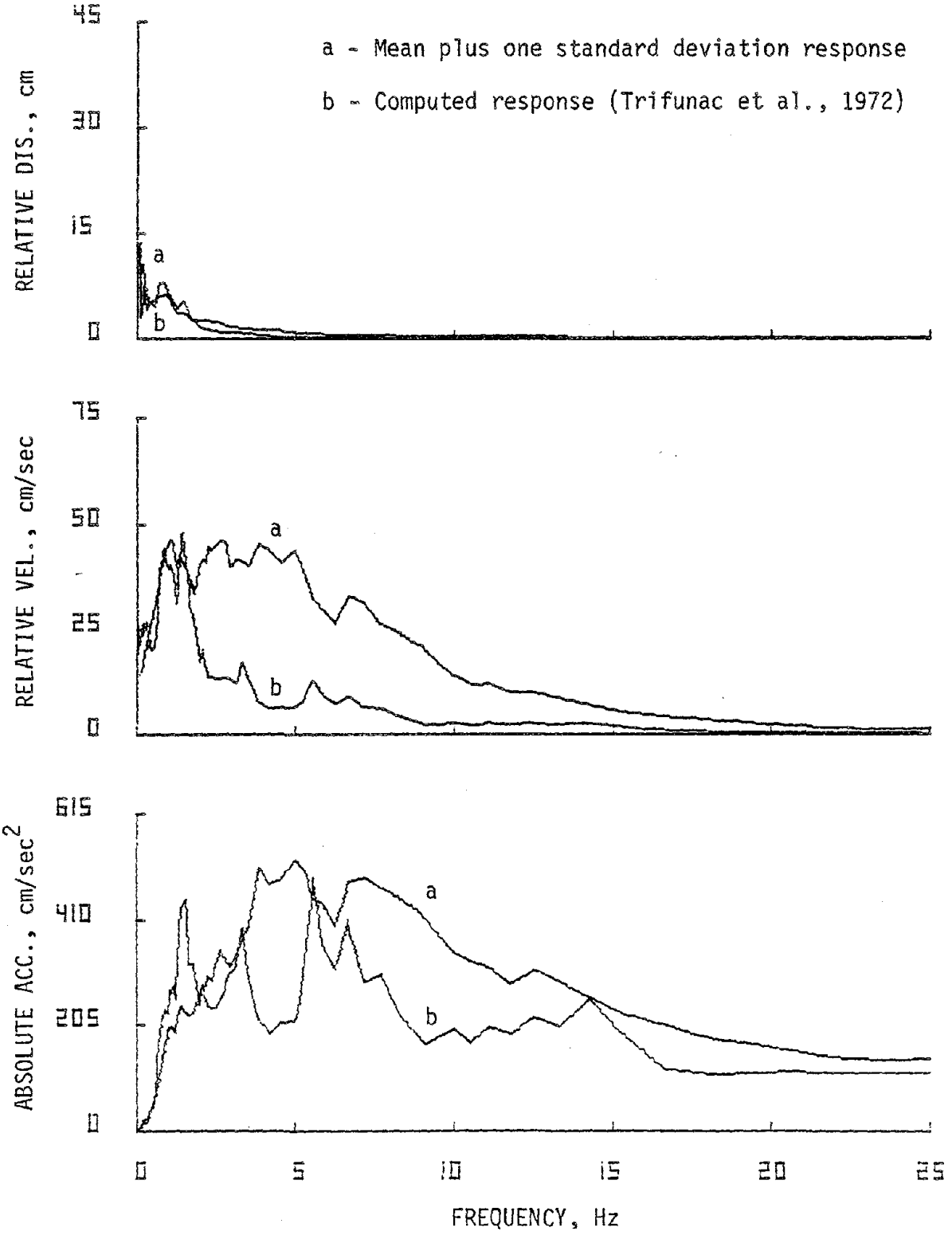

FIG. 5.30. Comparison of mean plus one standard deviation response (hard) and computed response for 2 percent damping, Lake Hughes Station 1, 1971--S69E.

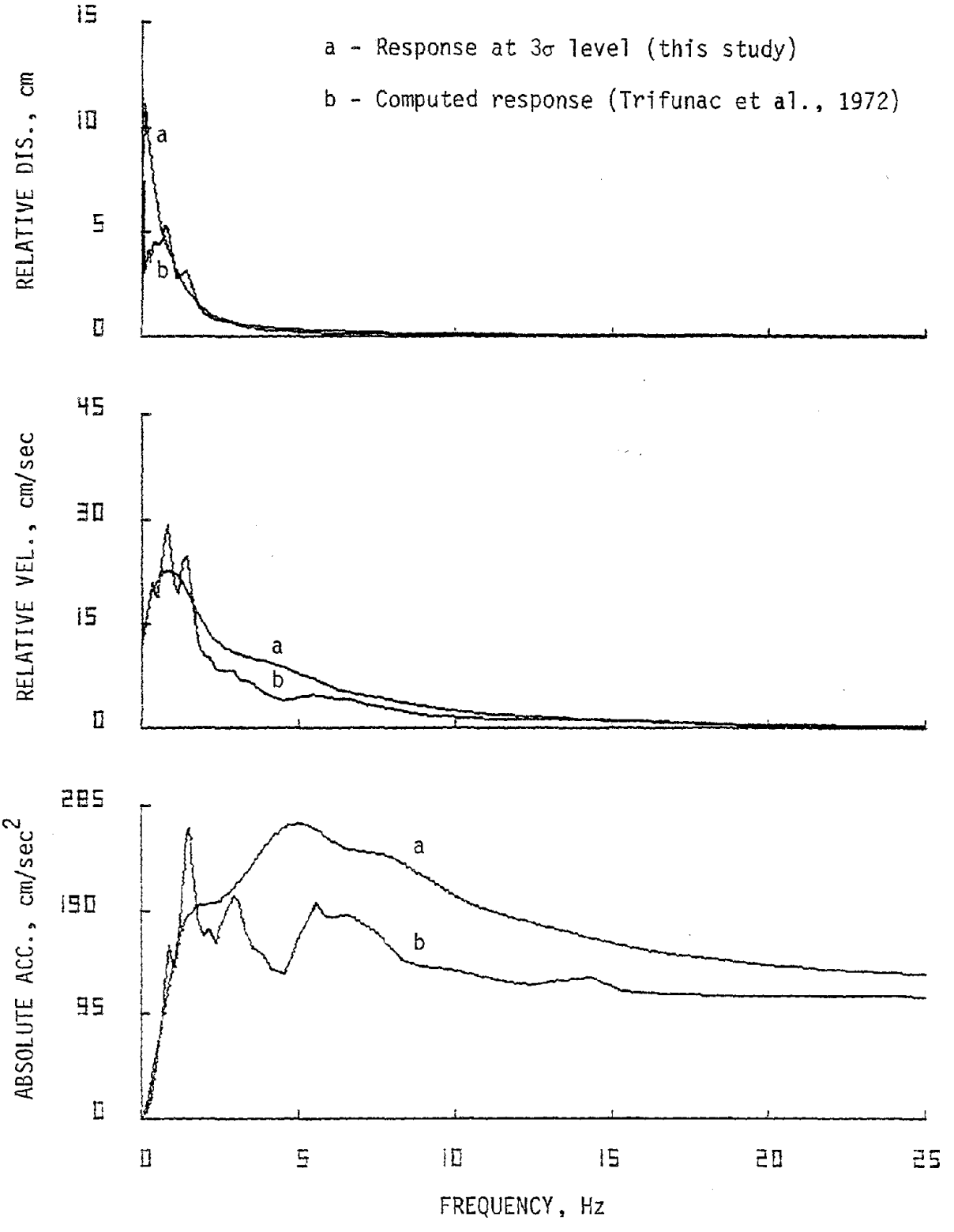

FIG. 5.31. Comparison of predicted response (hard) and computed response for 10 percent damping, Lake Hughes Station 1, 1971--S69E.

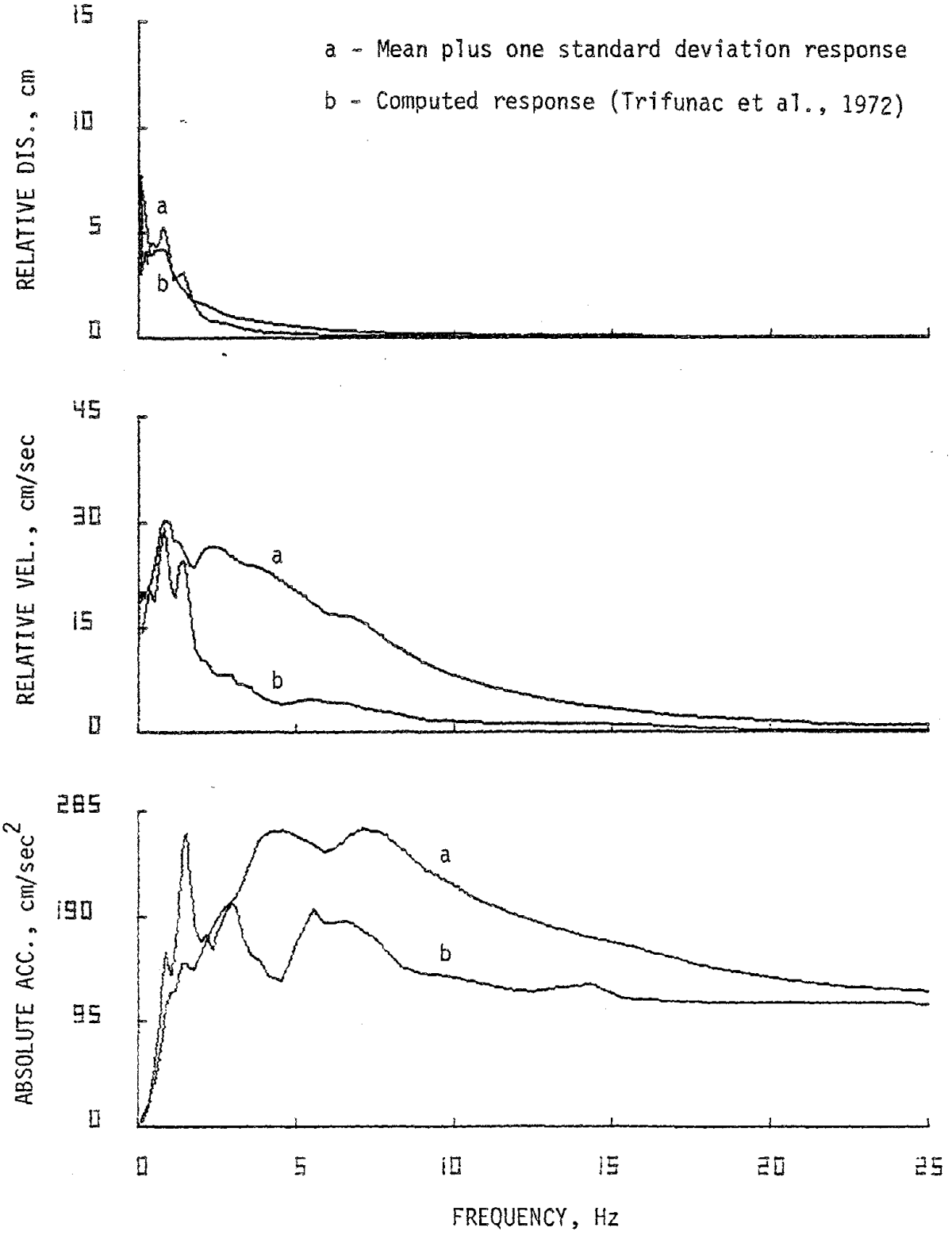

FIG. 5.32. Comparison of mean plus one standard deviation response (hard) and computed response for 10 percent damping, Lake Hughes Station 1, 1971--S69E.

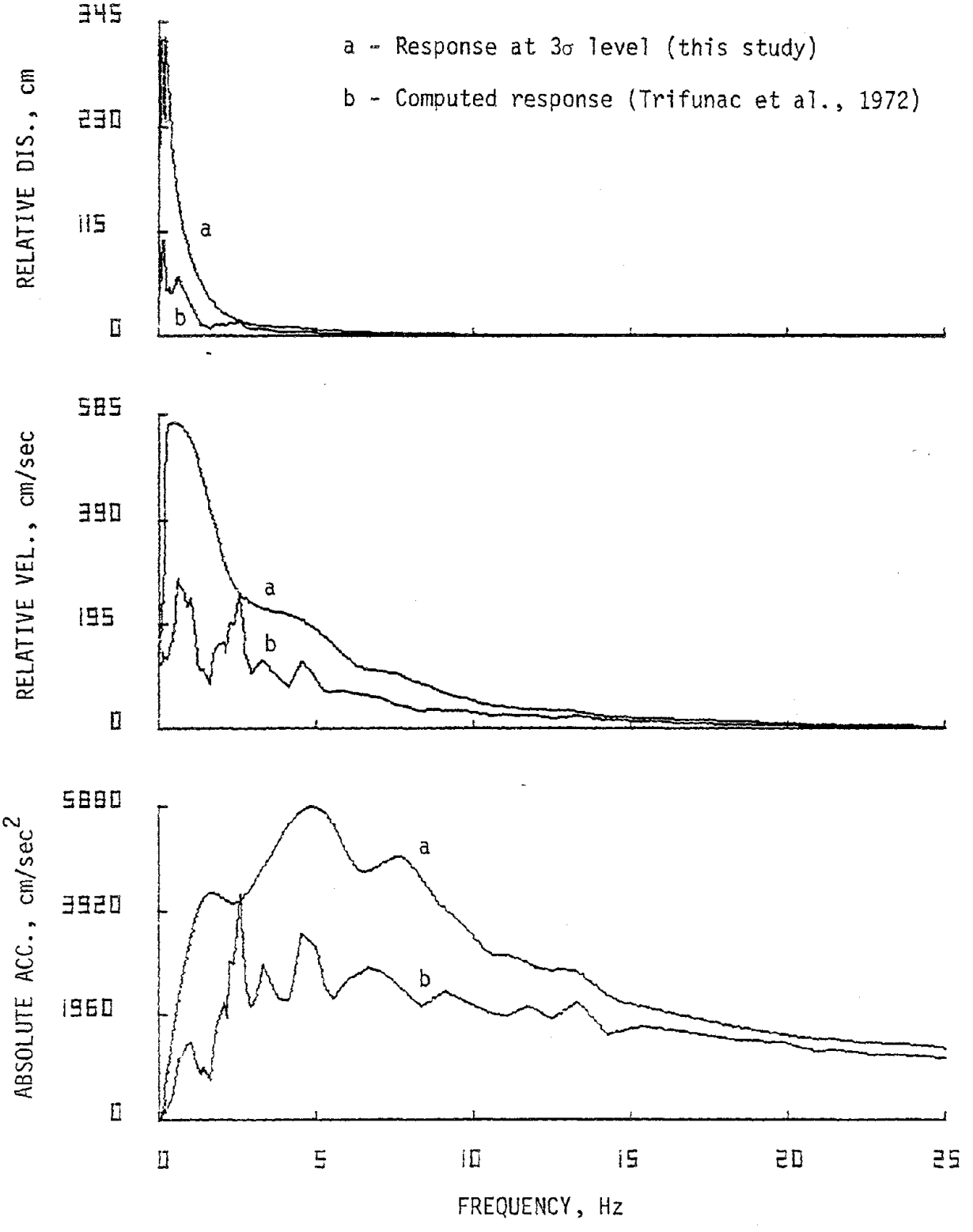

FIG. 5.33. Comparison of predicted response (hard) and computed response for 2 percent damping, Pacoima Dam, 1971--S15W.

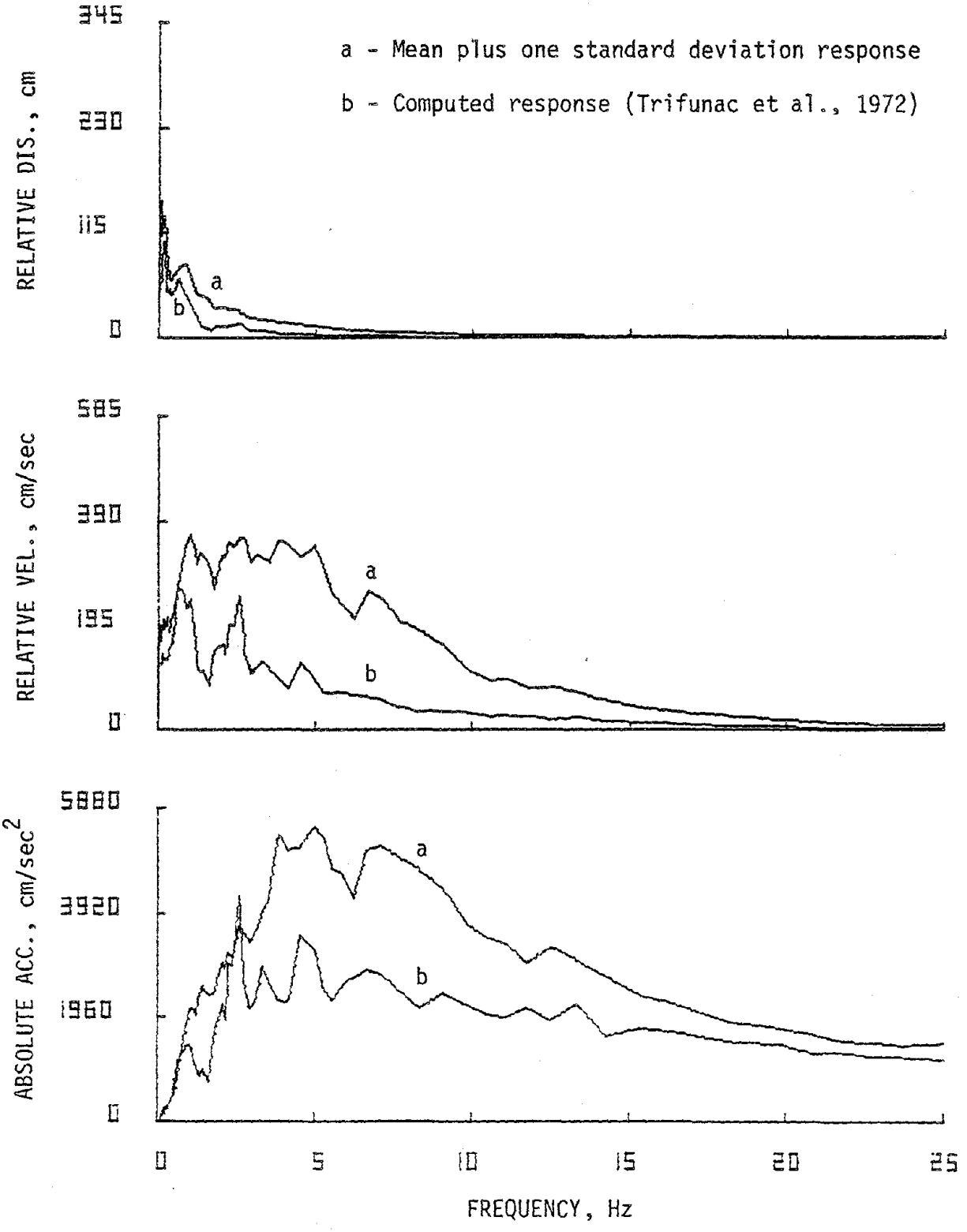

FIG. 5.34. Comparison of mean plus one standard deviation response (hard) and computed response for 2 percent damping, Pacoima Dam, 1971--S15W.

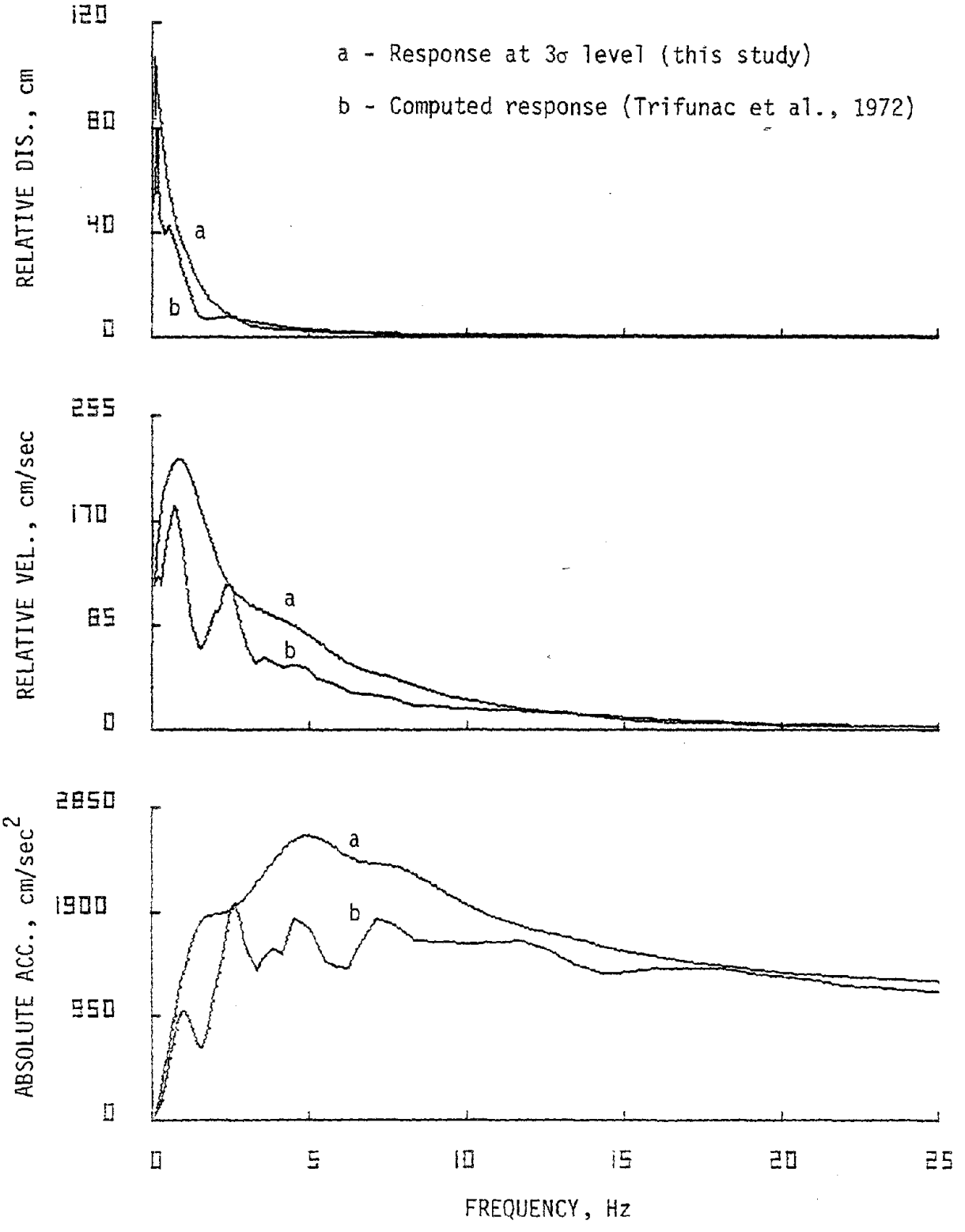

FIG. 5.35. Comparison of predicted response (hard) and computed response for 10 percent damping, Pacoima Dam, 1971--S15W.

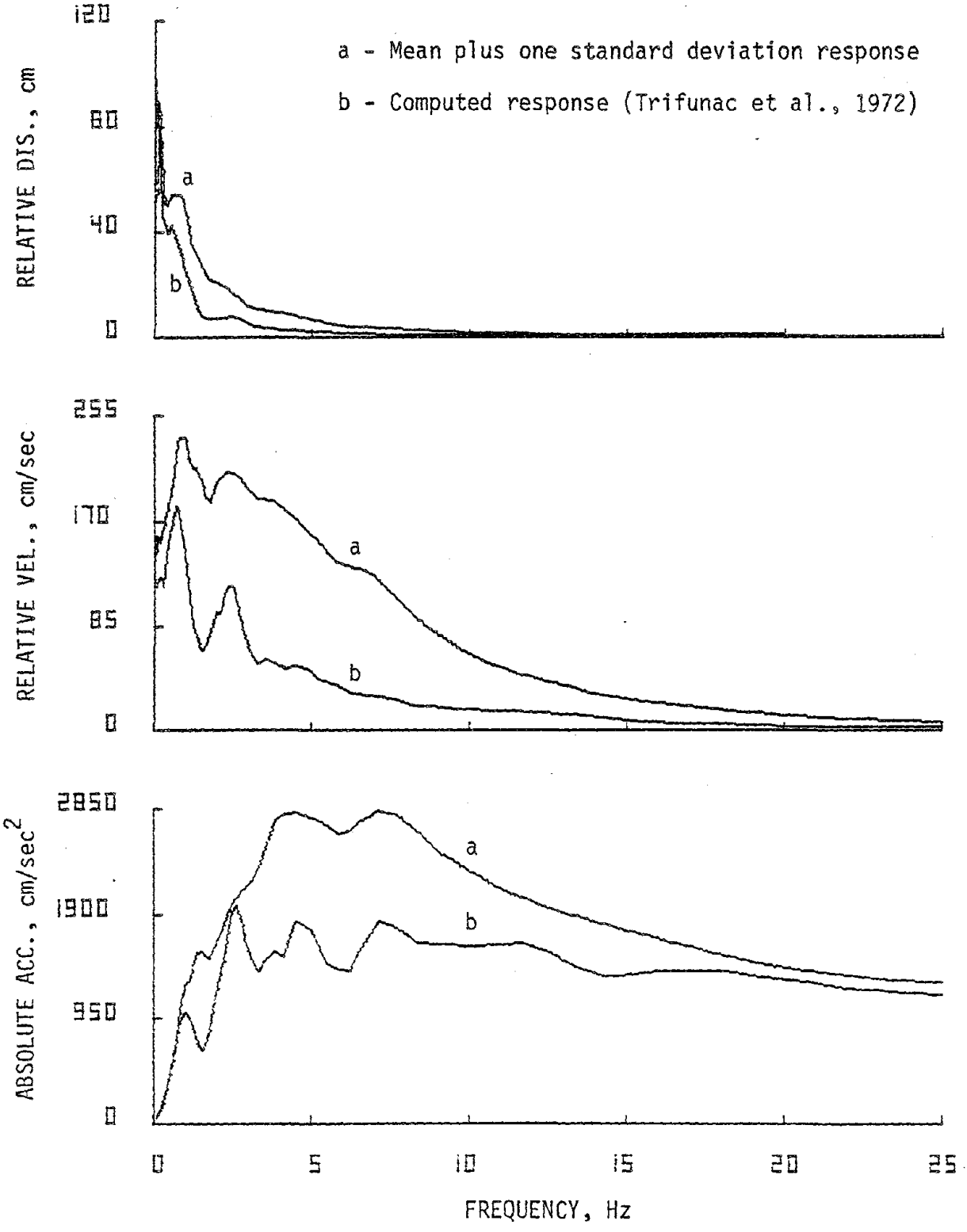

FIG. 5.36. Comparison of mean plus one standard deviation response (hard) and computed response for 10 percent damping, Pacoima Dam, 1971--S15W.

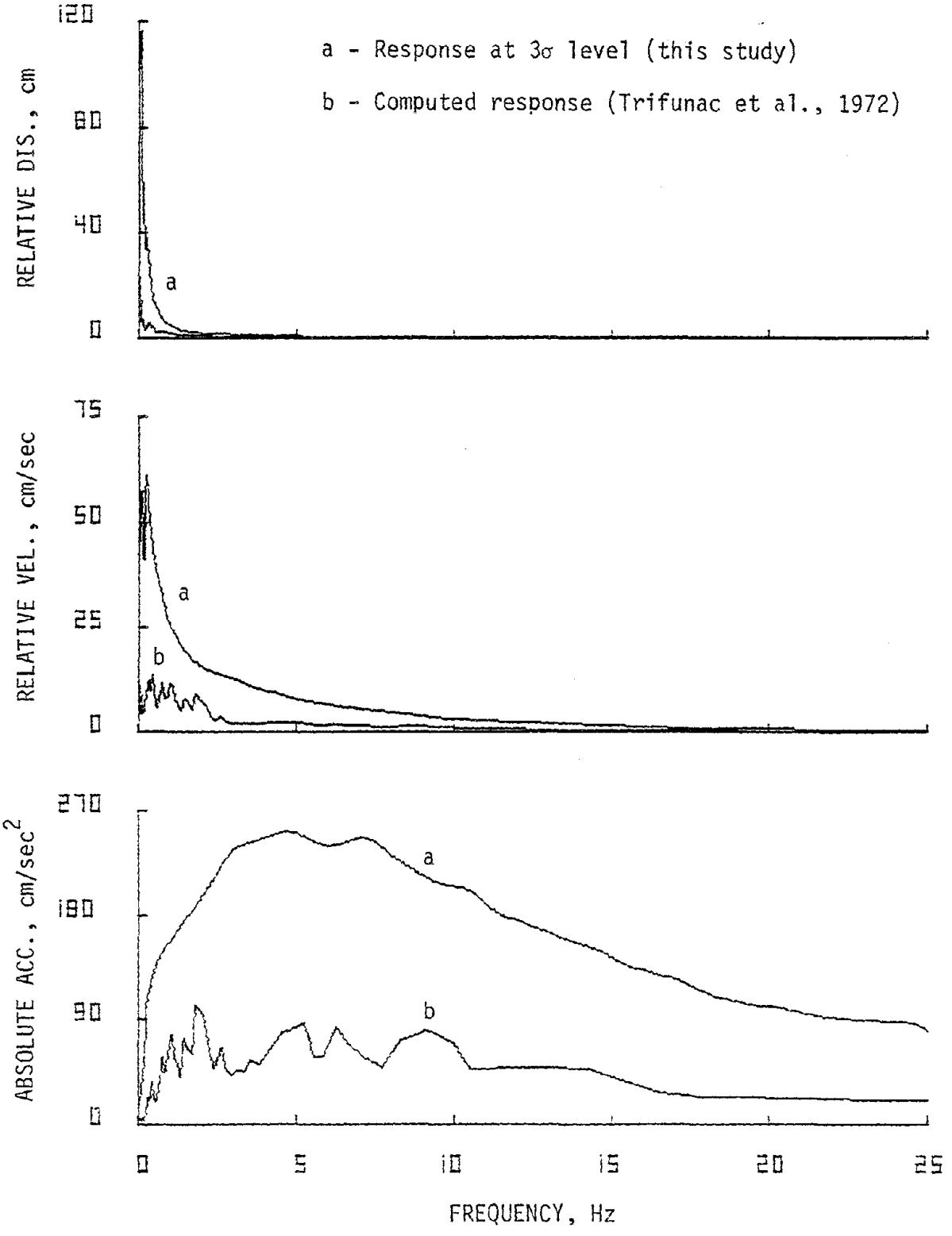

FIG. 5.37. Comparison of predicted response (soft) and computed response for 2 percent damping, Hollywood Storage P.E. lot, 1952--vertical.

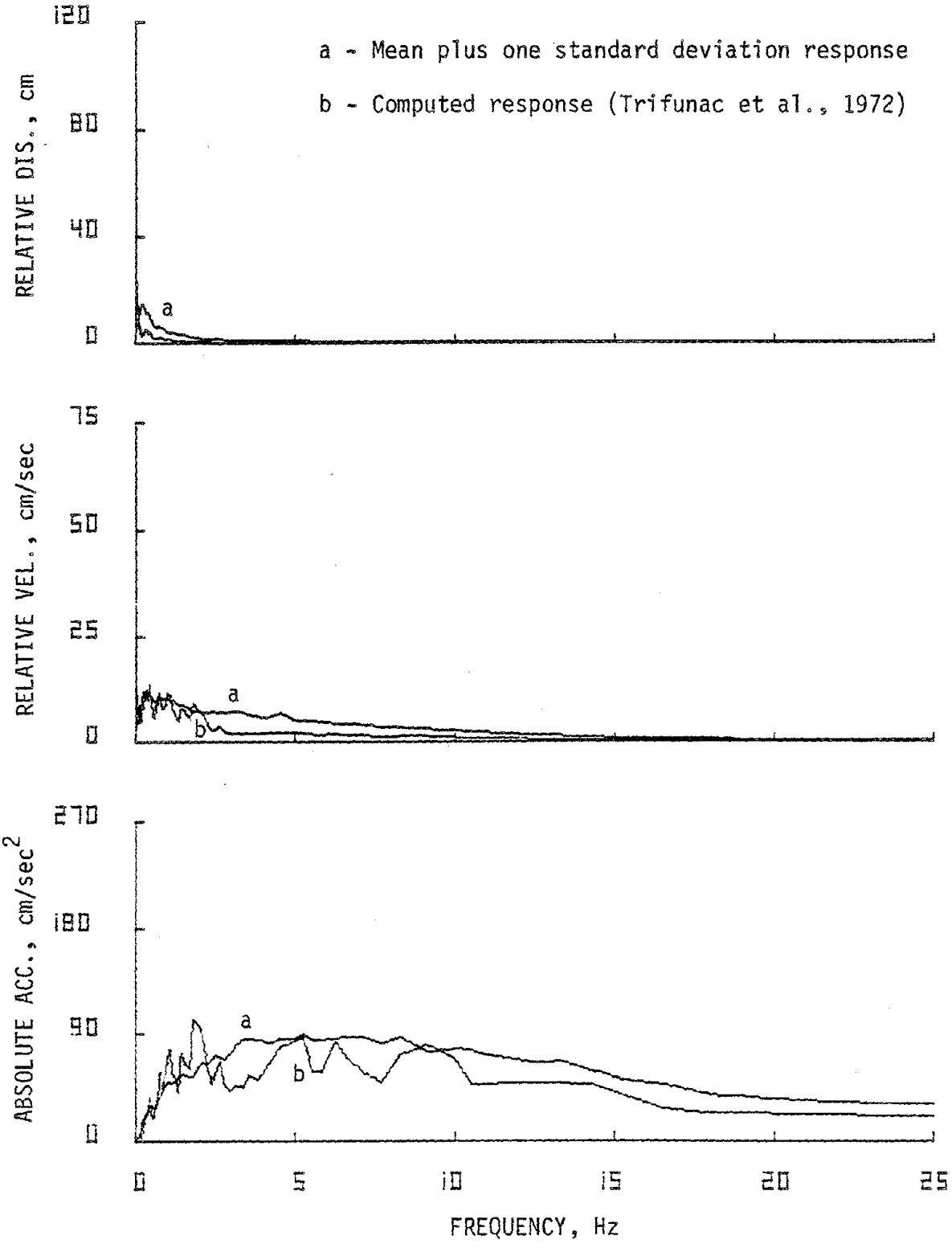

FIG. 5.38. Comparison of mean plus one standard deviation response (soft) and computed response for 2 percent damping, Hollywood Storage P.E. lot, 1952--vertical.

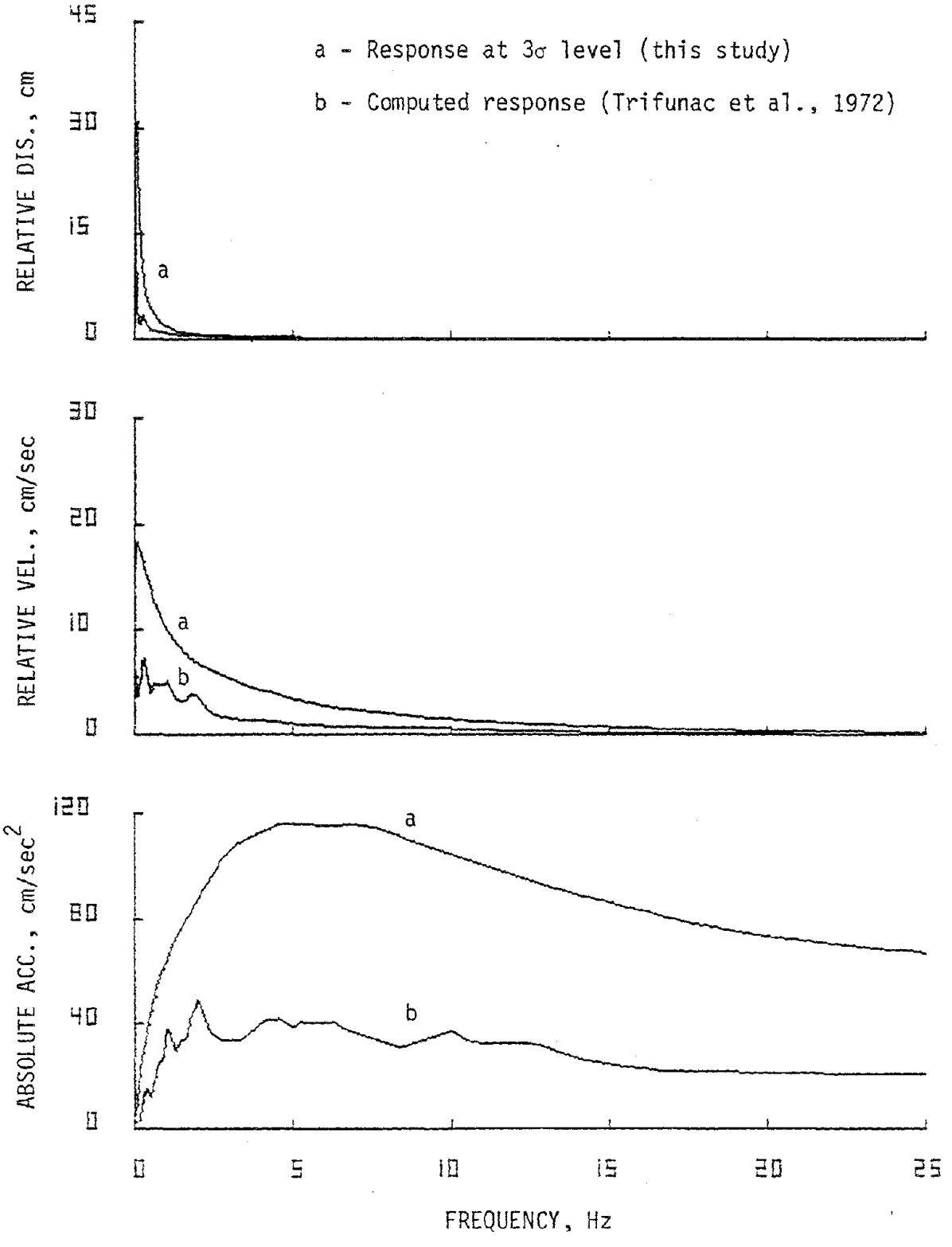

FIG. 5.39. Comparison of predicted response (soft) and computed response for 10 percent damping, Hollywood Storage P.E. lot, 1952--vertical.

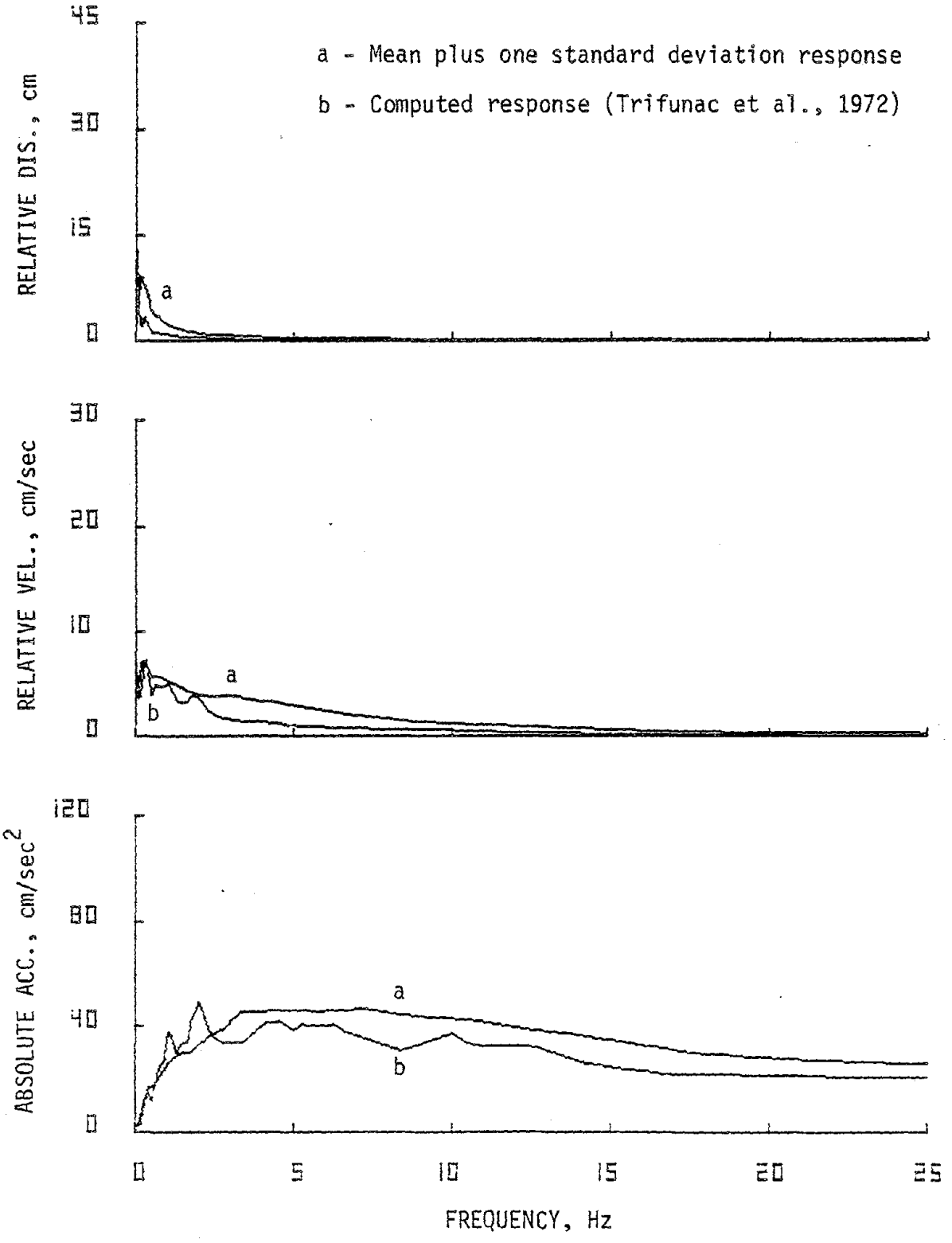

FIG. 5.40. Comparison of mean plus one standard deviation response (soft) and computed response for 10 percent damping, Hollywood Storage P.E. lot, 1952--vertical.

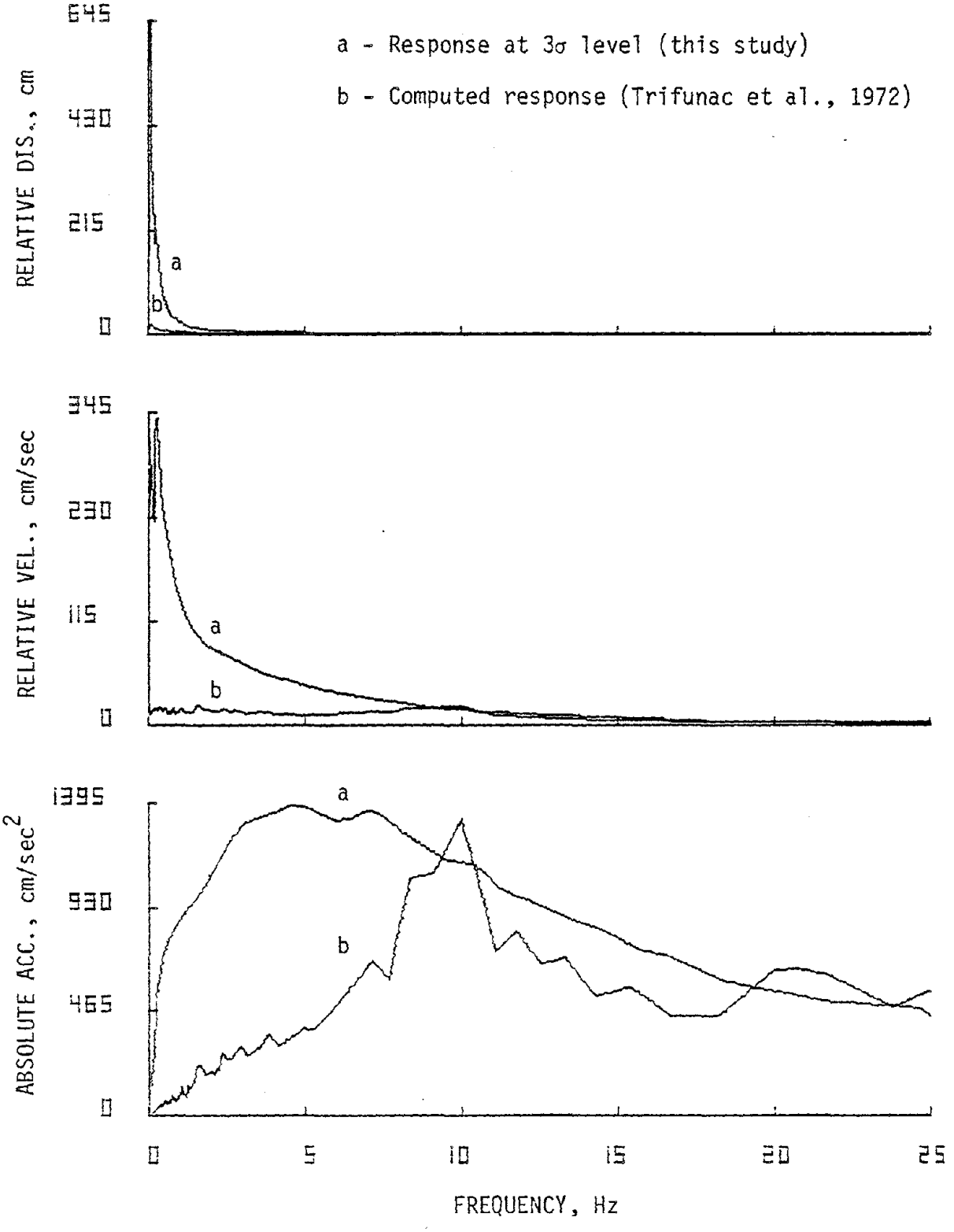

FIG. 5.41. Comparison of predicted response (soft) and computed response for 2 percent damping, El Centro, 1940--vertical.

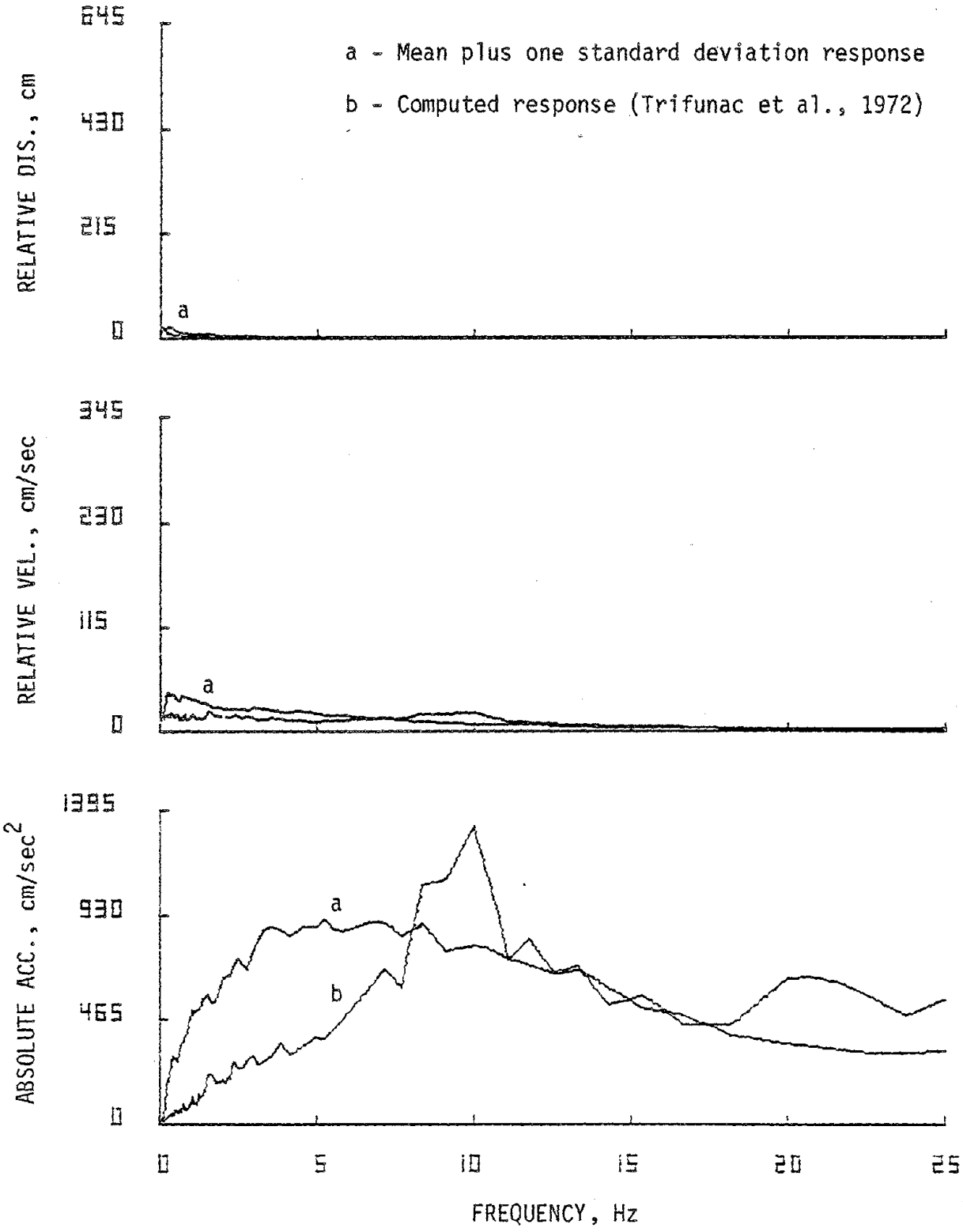

FIG. 5.42. Comparison of mean plus one standard deviation response (soft) and computed response for 2 percent damping, El Centro, 1940--vertical.

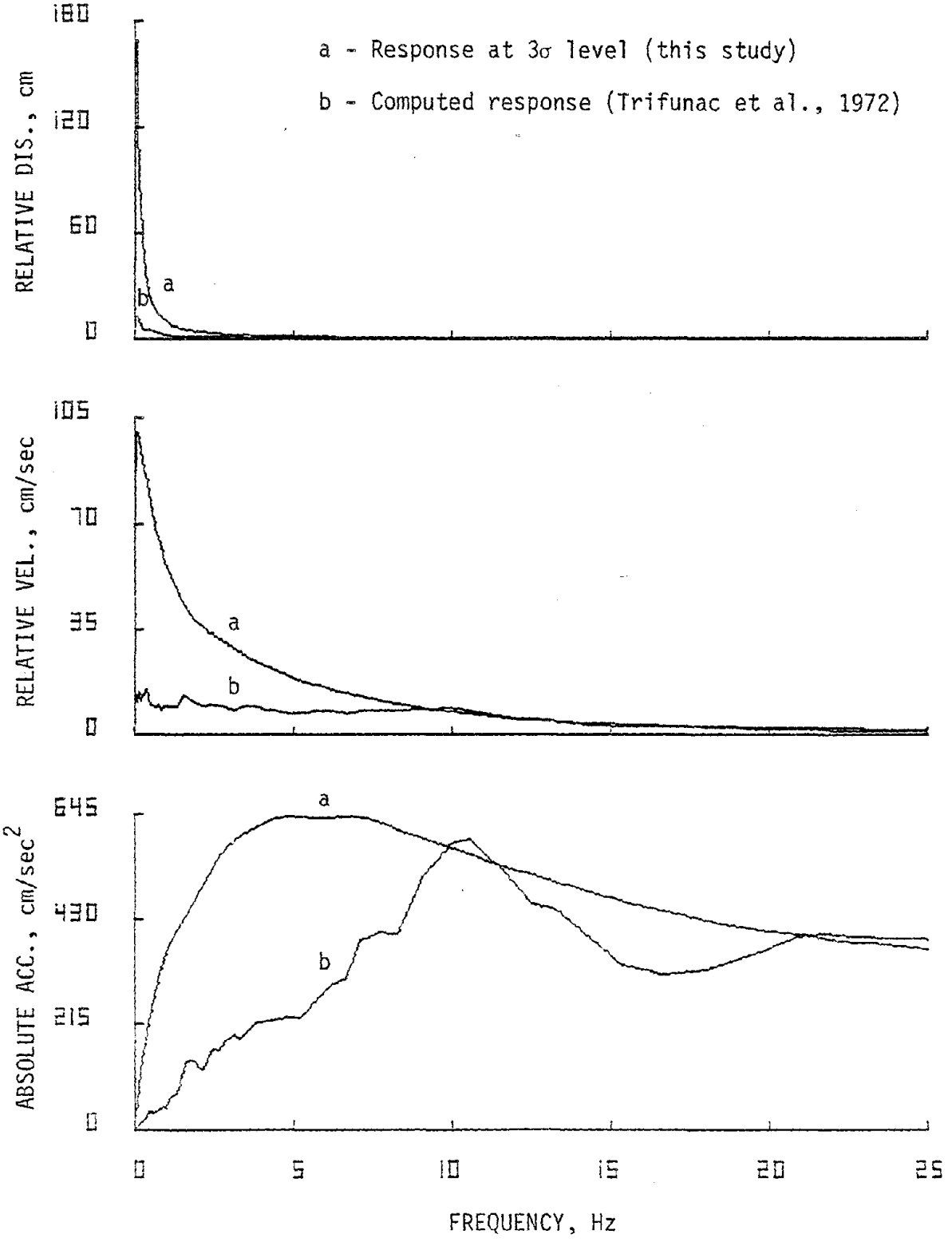

FIG. 5.43. Comparison of predicted response (soft) and computed response for 10 percent damping, El Centro, 1940--vertical.

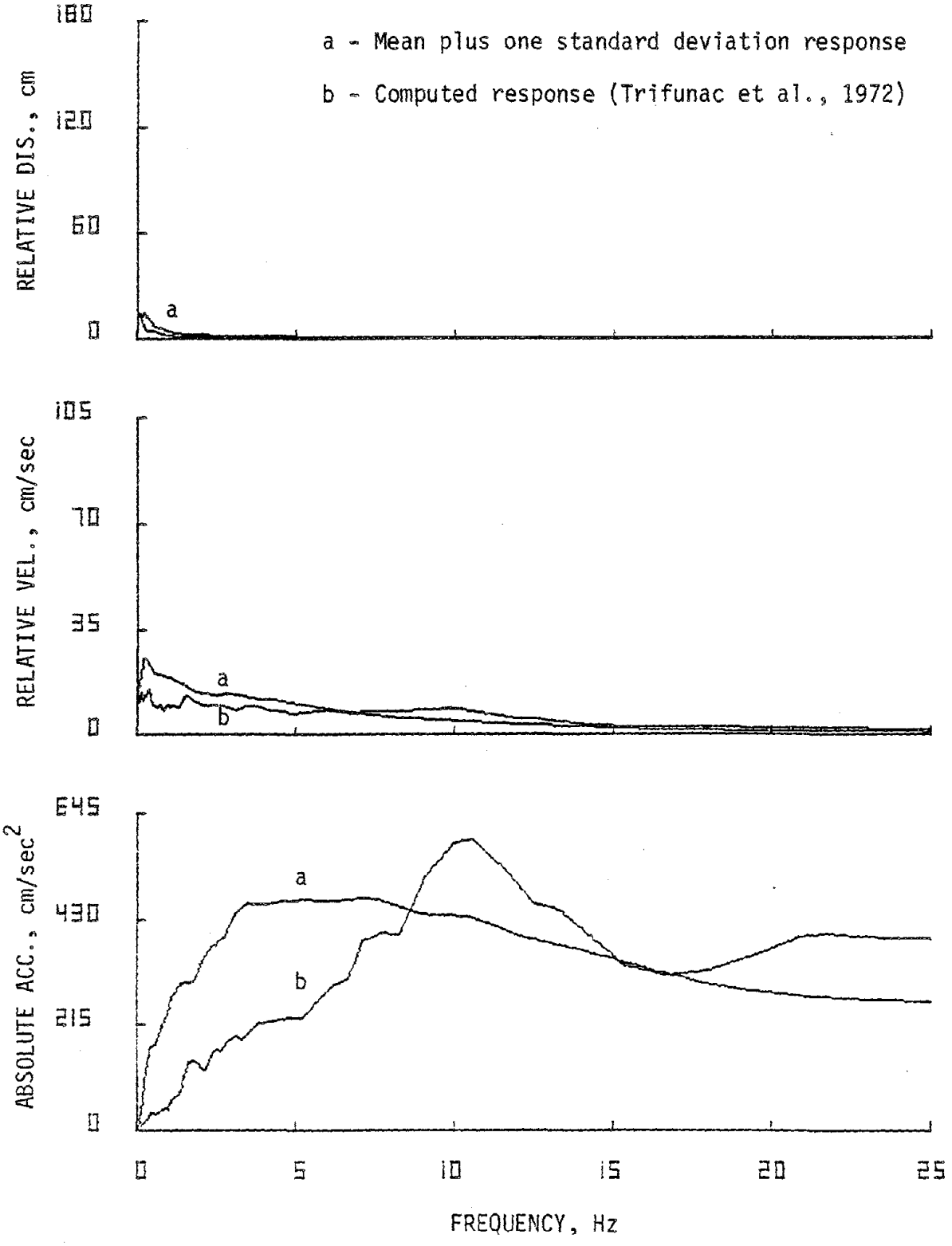

FIG. 5.44. Comparison of mean plus one standard deviation response (soft) and computed response for 10 percent damping, El Centro, 1940--vertical.

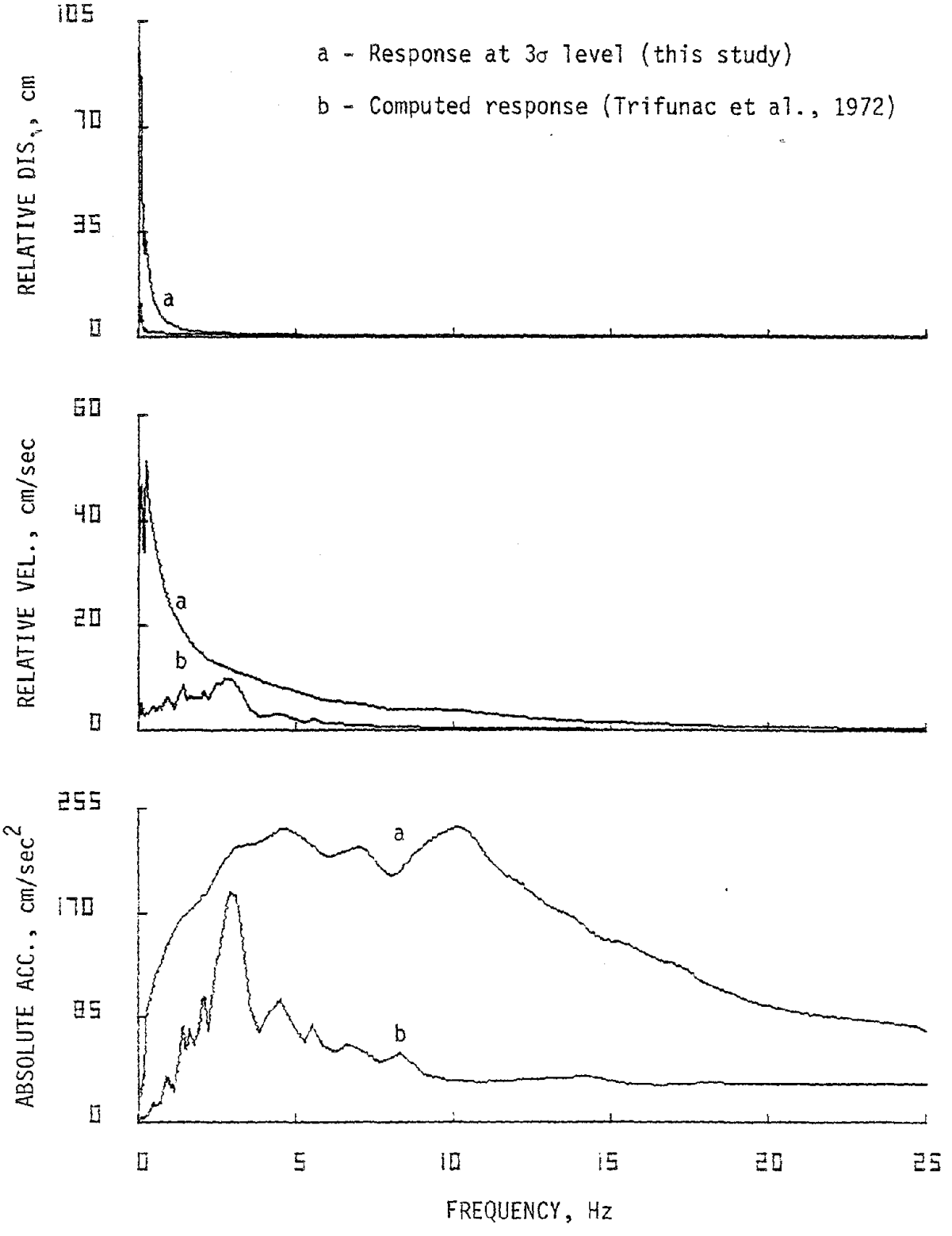

FIG. 5.45. Comparison of predicted response (intermediate) and computed response for 2 percent damping, Ferndale City Hall, 1952--vertical.

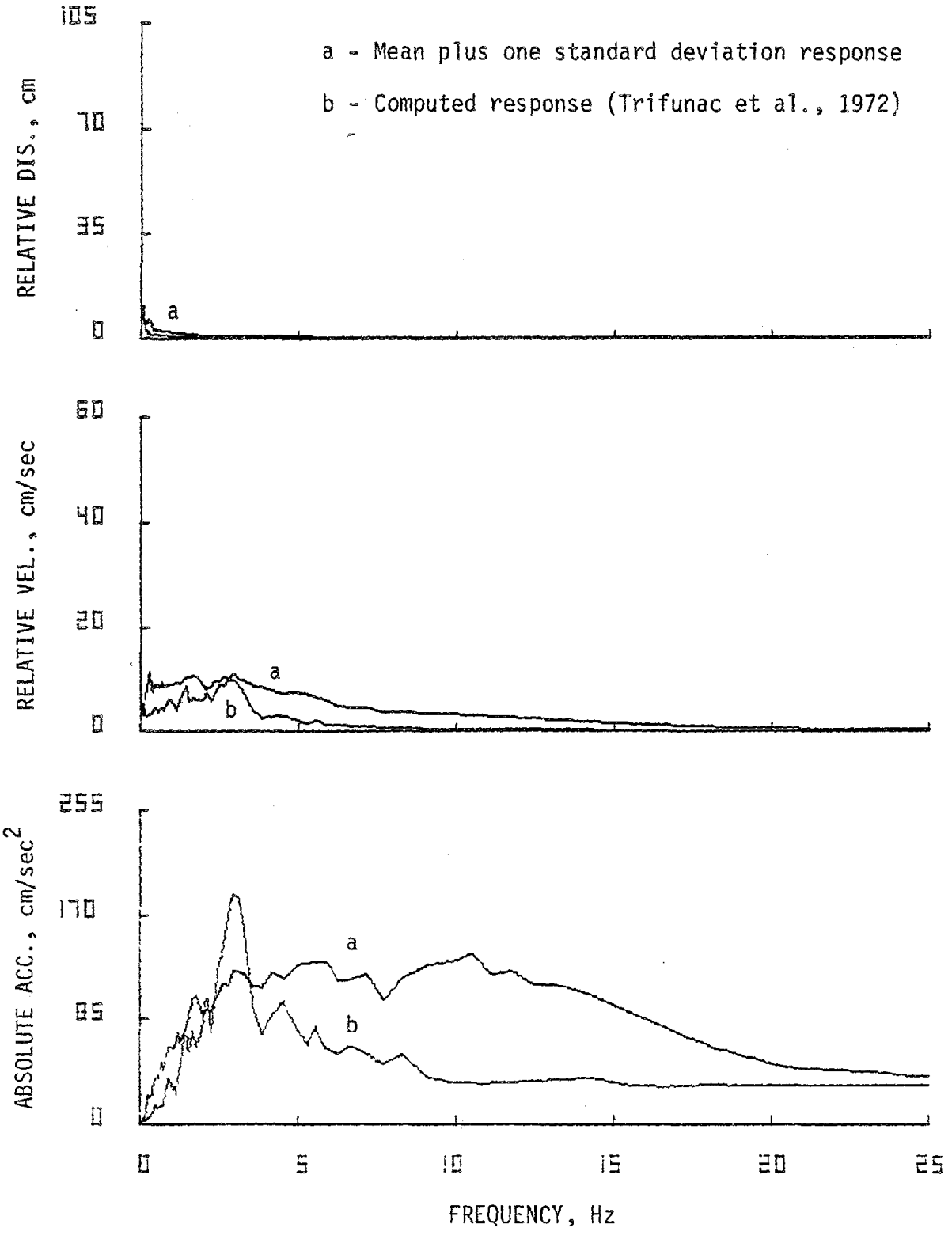

FIG. 5.46. Comparison of mean plus one standard deviation response (intermediate) and computed response for 2 percent damping, Ferndale City Hall, 1952--vertical.

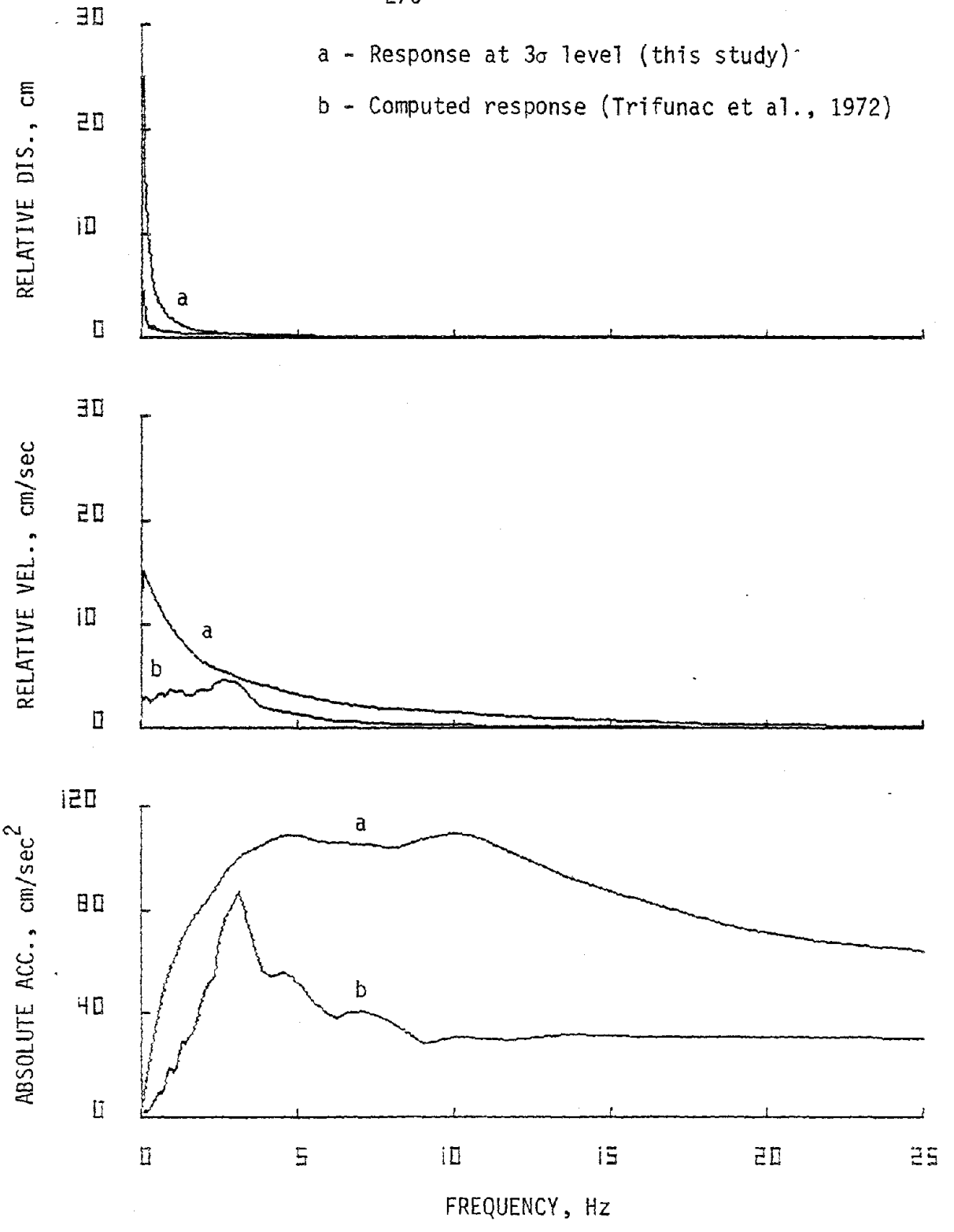

FIG. 5.47. Comparison of predicted response (intermediate) and computed response for 10 percent damping, Ferndale City Hall, 1952--vertical.

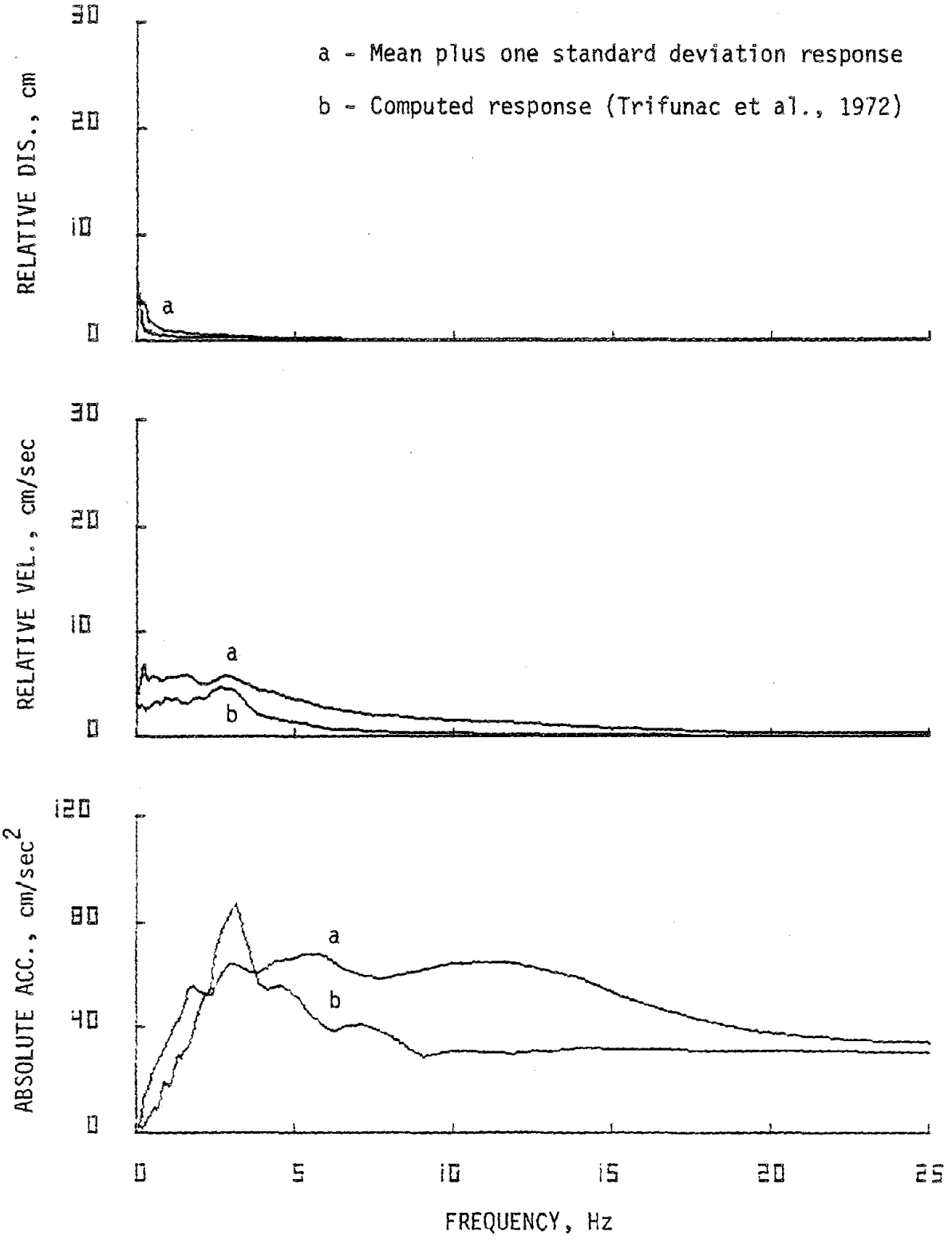

FIG. 5.48. Comparison of mean plus one standard deviation response (intermediate) and computed response for 10 percent damping, Ferndale City Hall, 1952--vertical.

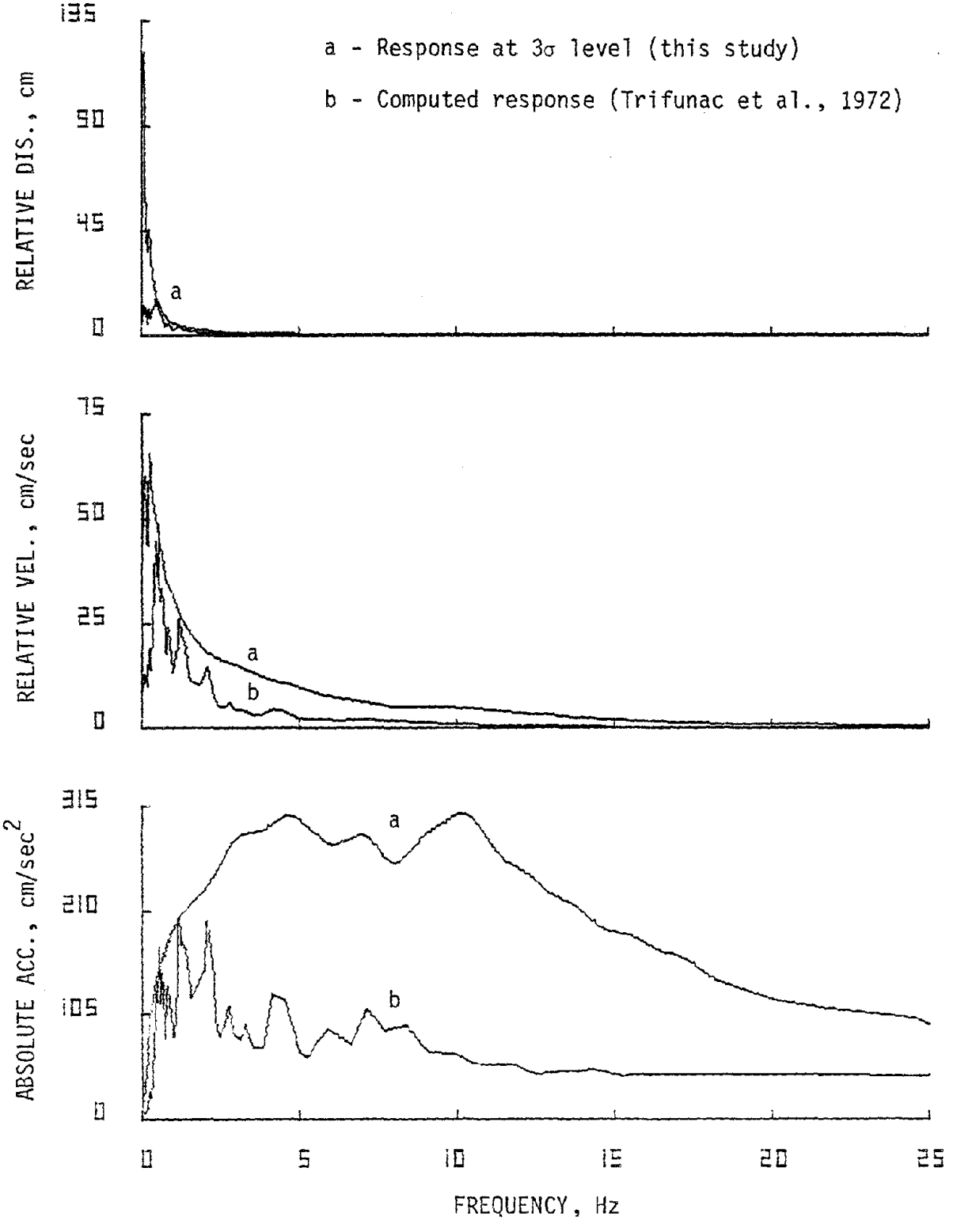

FIG. 5.49. Comparison of predicted response (intermediate) and computed response for 2 percent damping, Ferndale City Hall, 1954--vertical.

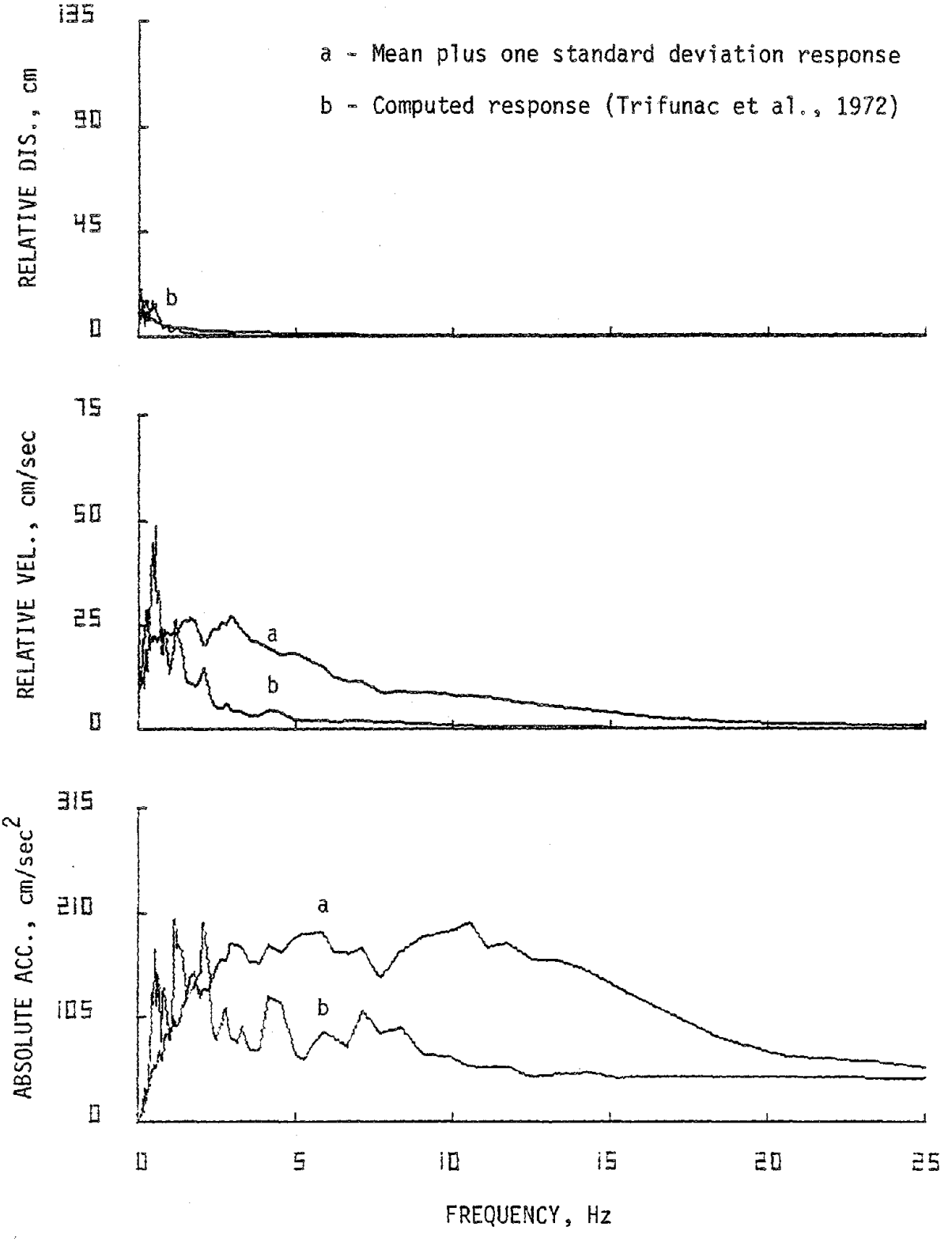

FIG. 5.50. Comparison of mean plus one standard deviation response (intermediate) and computed response for 2 percent damping, Ferndale City Hall, 1954--vertical.

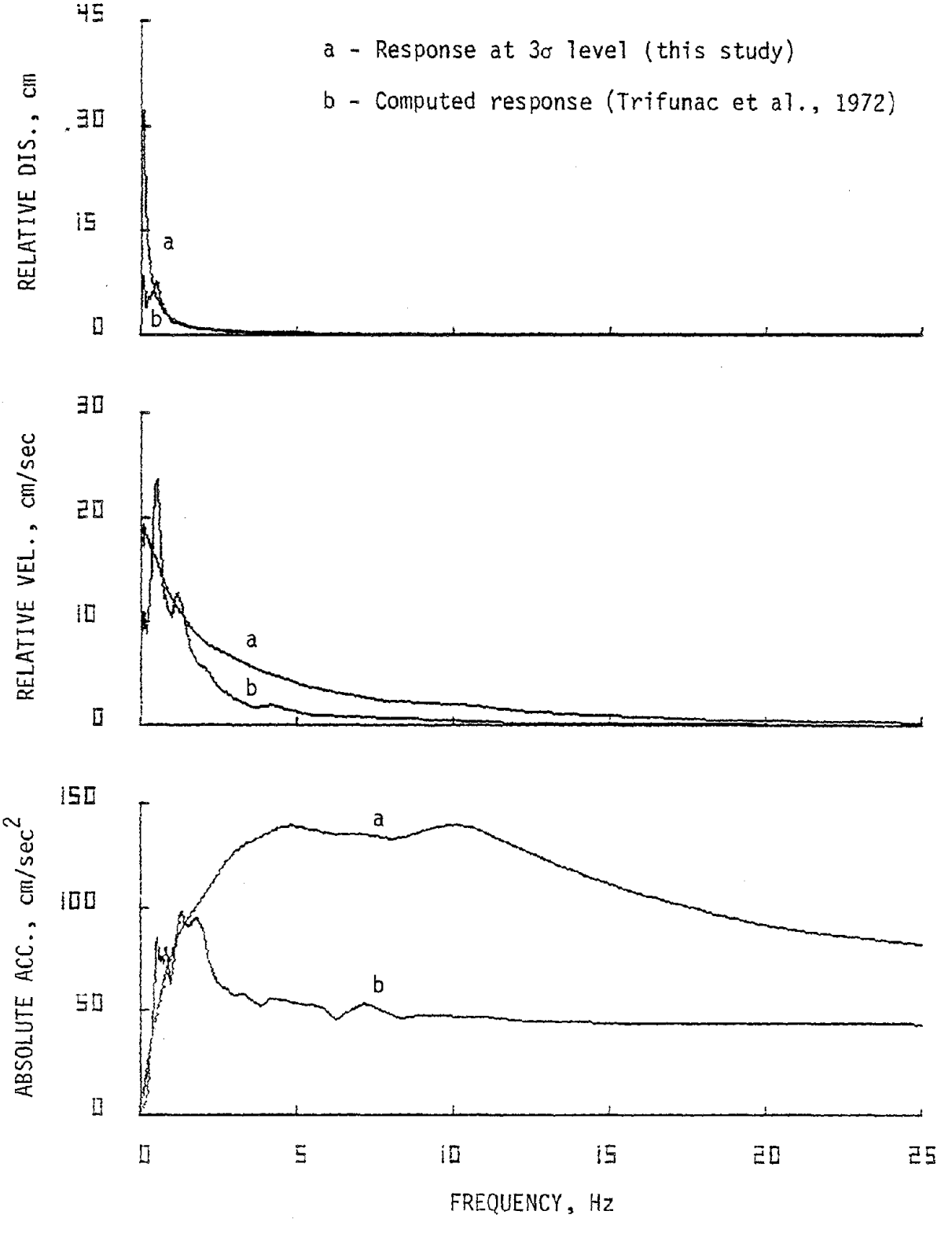

FIG. 5.51. Comparison of predicted response (intermediate) and computed response for 10 percent damping, Ferndale City Hall, 1954--vertical.

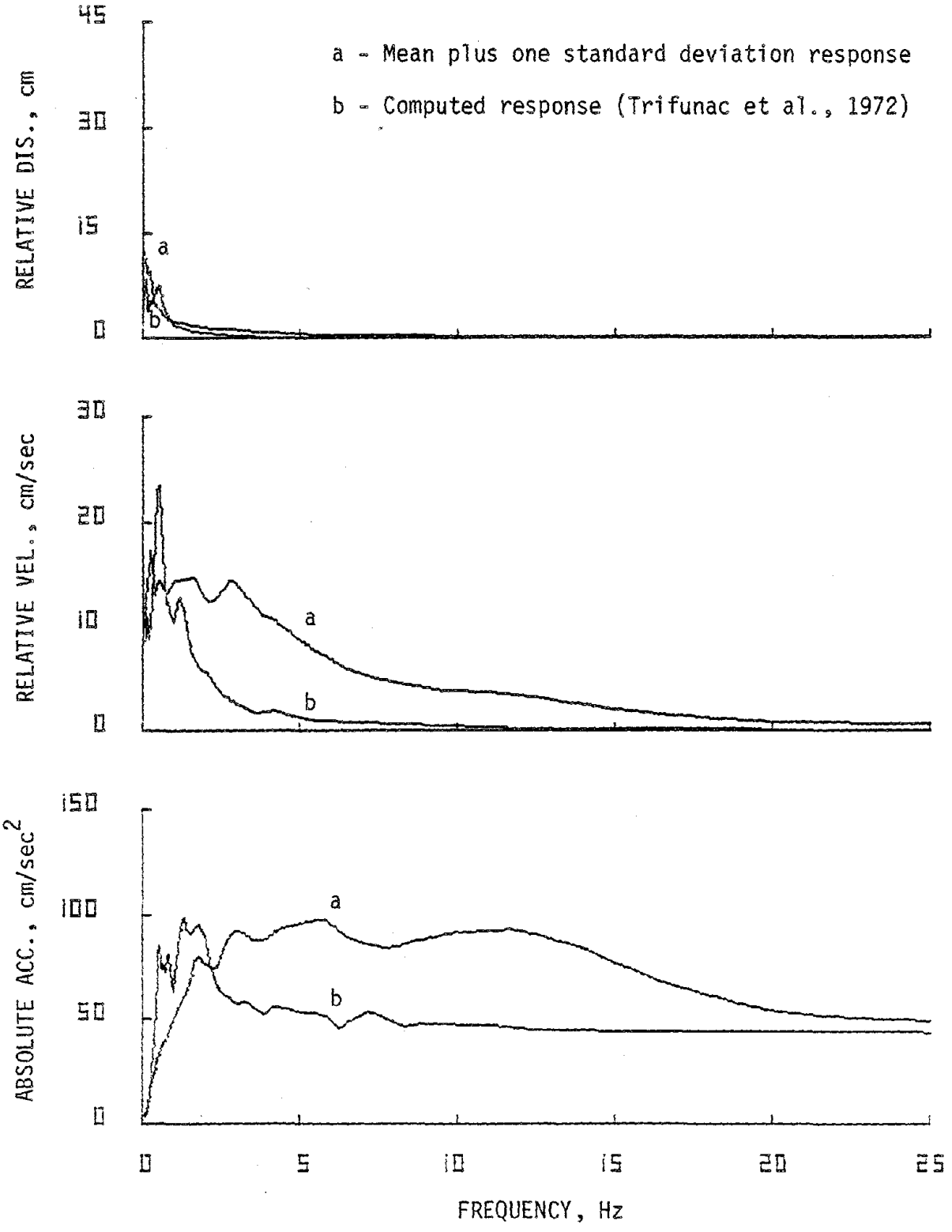

FIG. 5.52. Comparison of mean plus one standard deviation response (intermediate) and computed response for 10 percent damping, Ferndale City Hall, 1954--vertical.

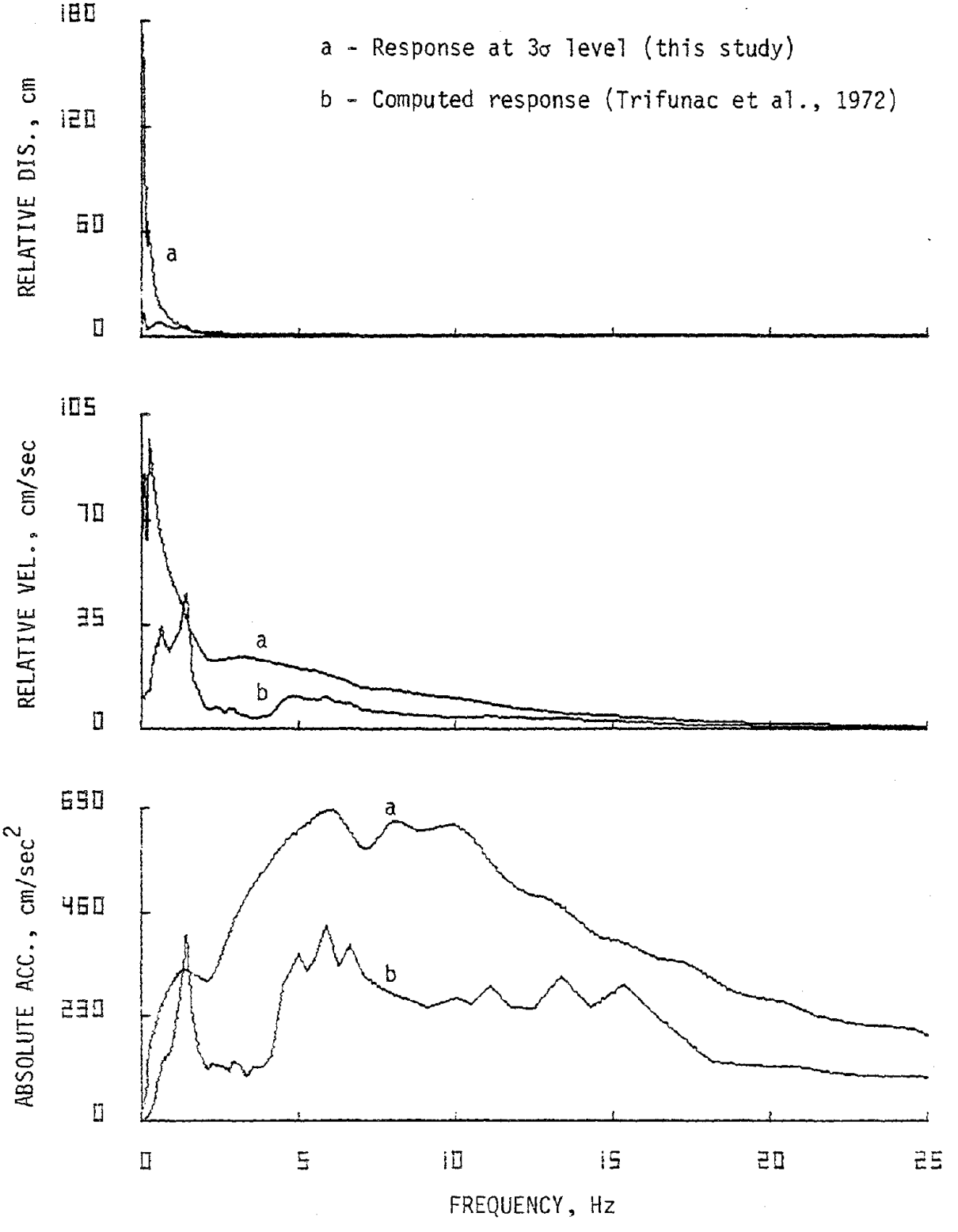

FIG. 5.53. Comparison of predicted response (hard) and computed response for 2 percent damping, Lake Hughes Station 1, 1971--vertical.

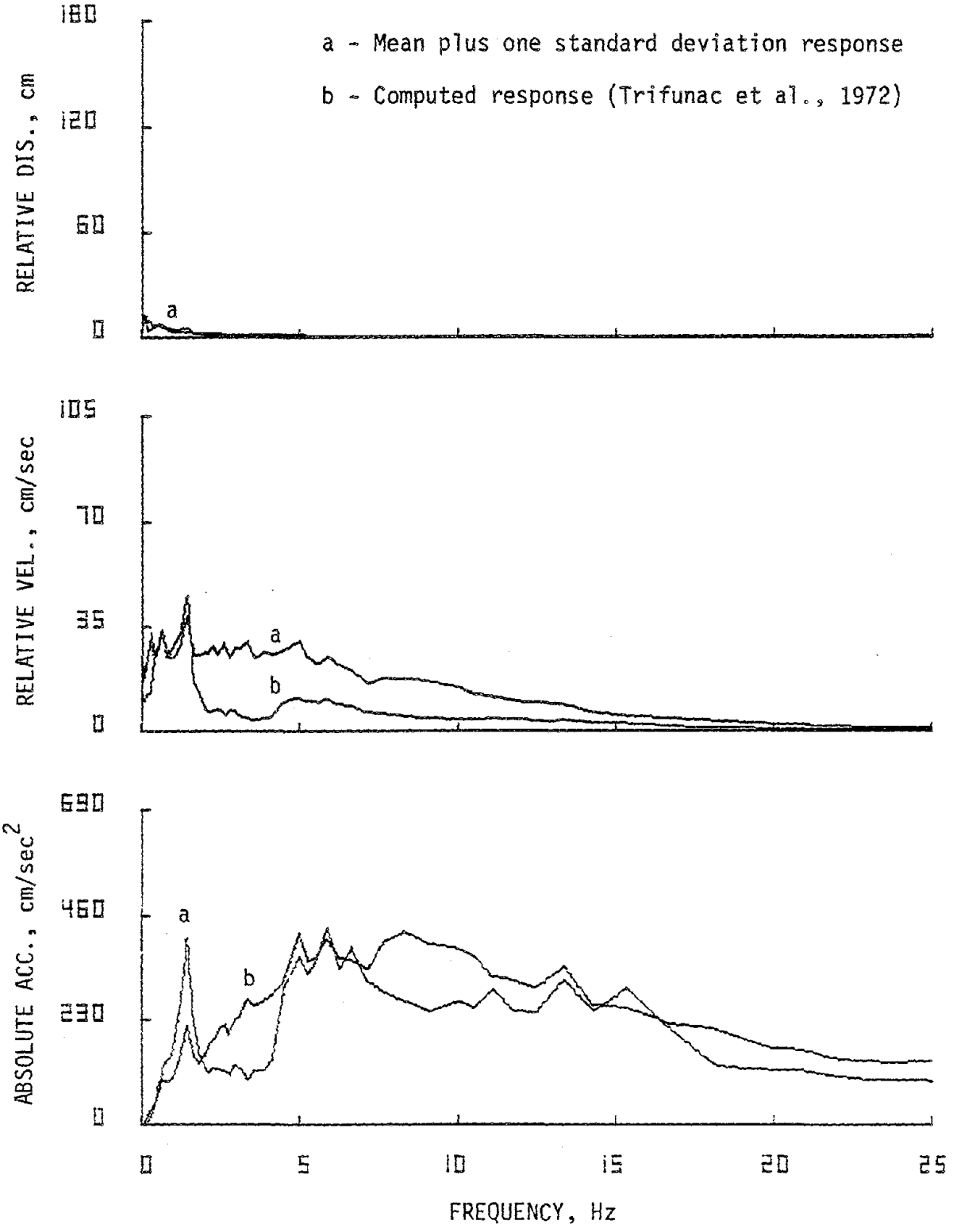

FIG. 5.54. Comparison of mean plus one standard deviation response (hard) and computed response for 2 percent damping, Lake Hughes Station 1, 1971--vertical.

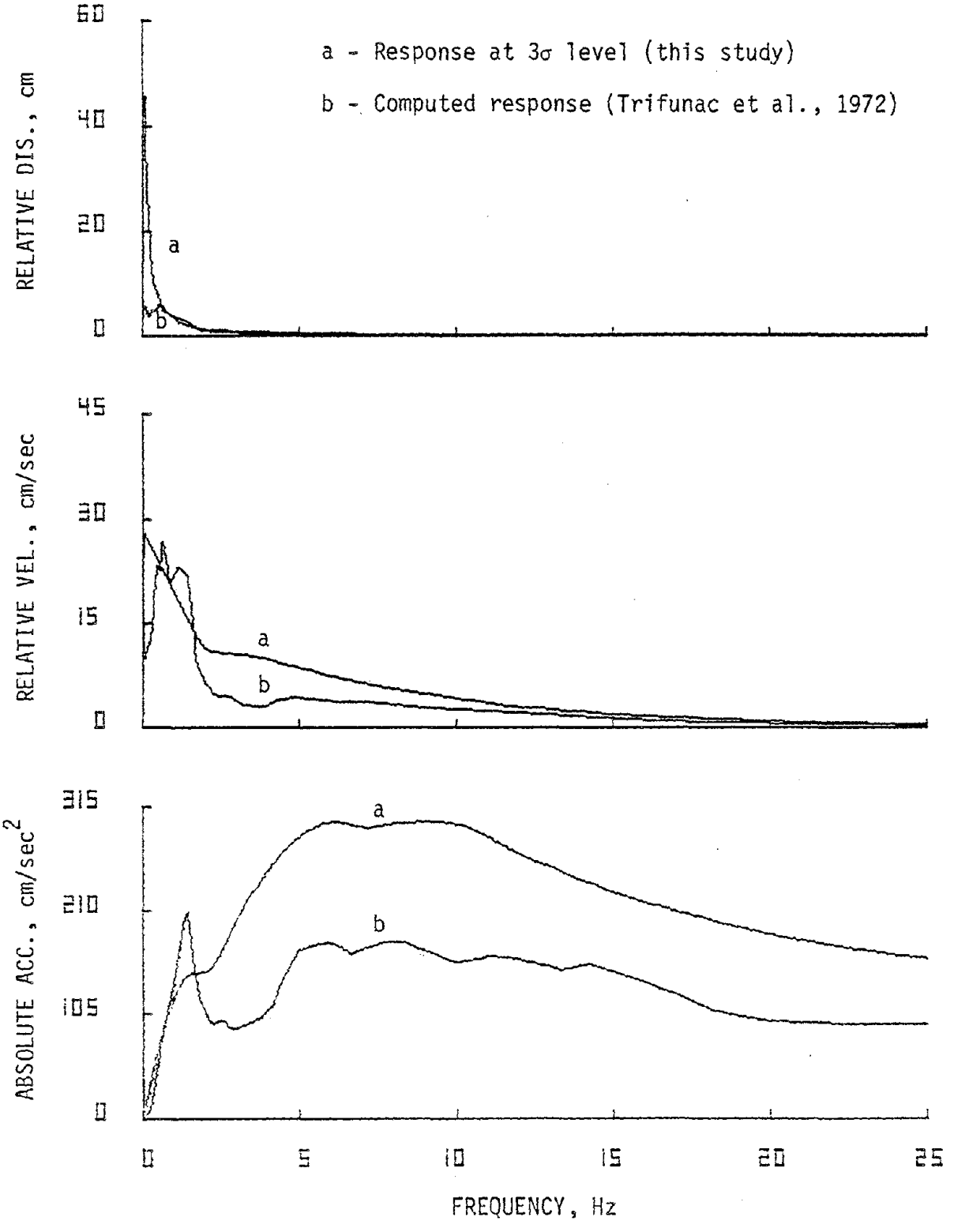

FIG. 5.55. Comparison of predicted response (hard) and computed response for 10 percent damping, Lake Hughes Station 1, 1971--vertical.

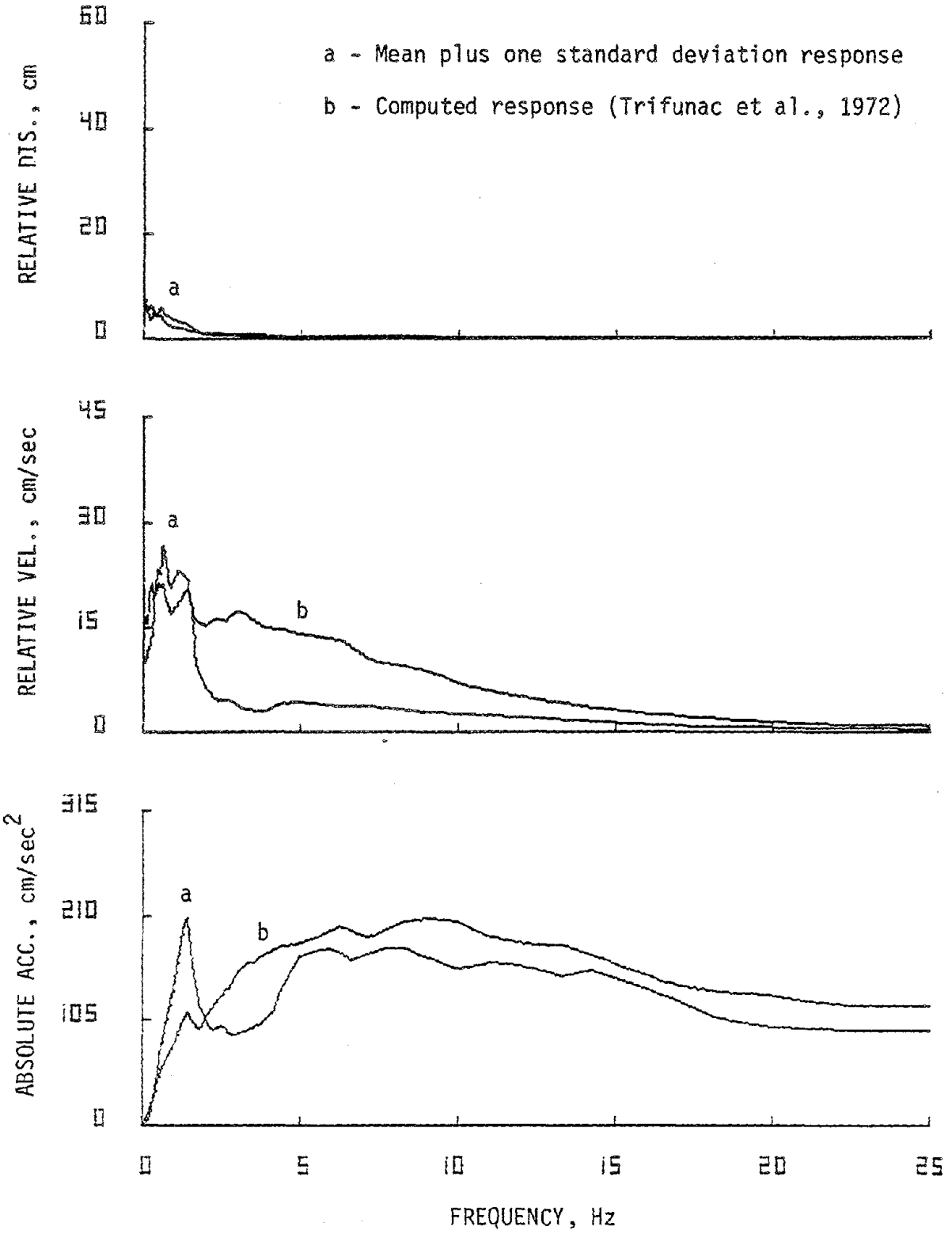

FIG. 5.56. Comparison of mean plus one standard deviation response (hard) and computed response for 10 percent damping, Lake Hughes Station 1, 1971--vertical.

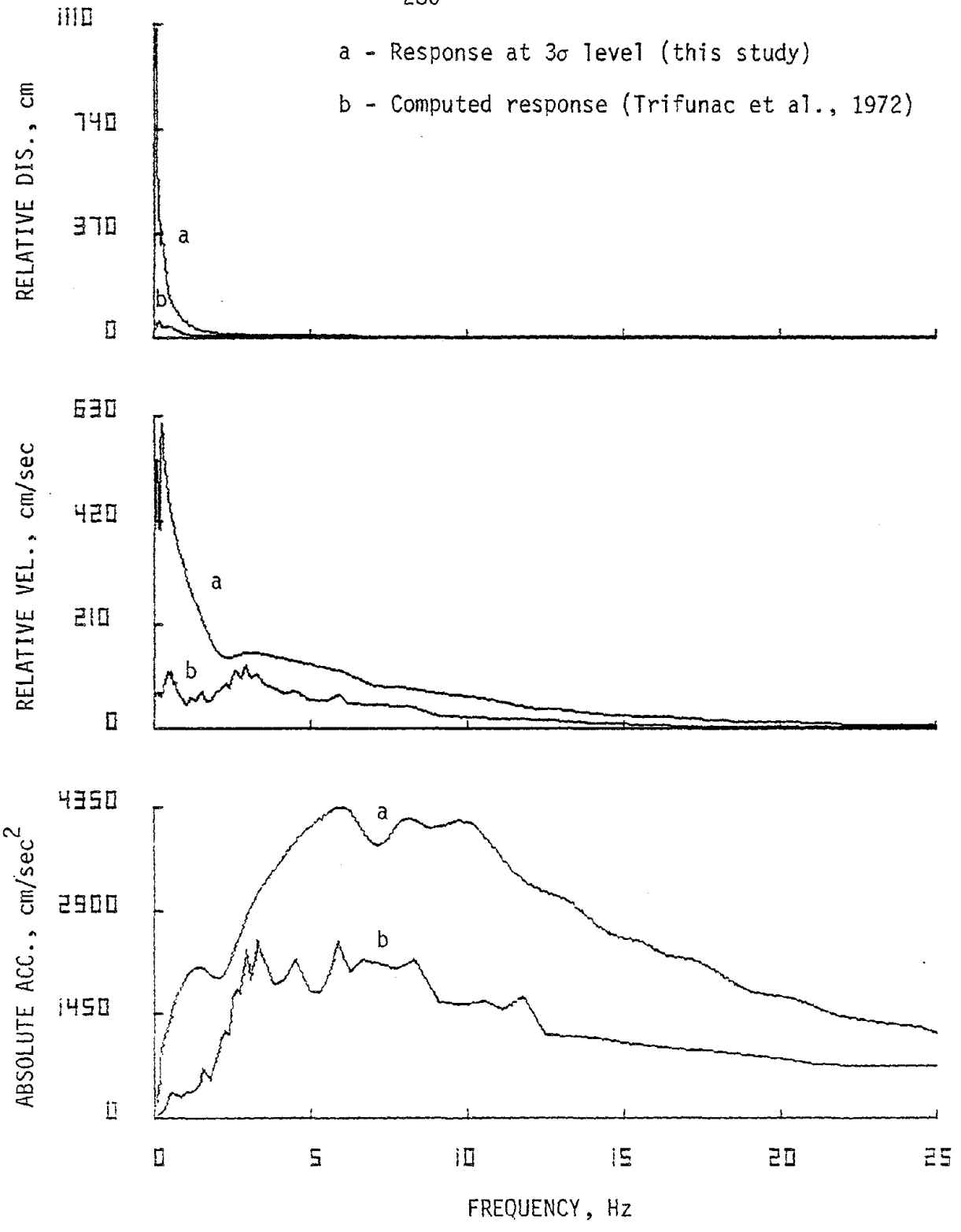

FIG. 5.57. Comparison of predicted response (hard) and computed response for 2 percent damping, Pacoima Dam, 1971--vertical.

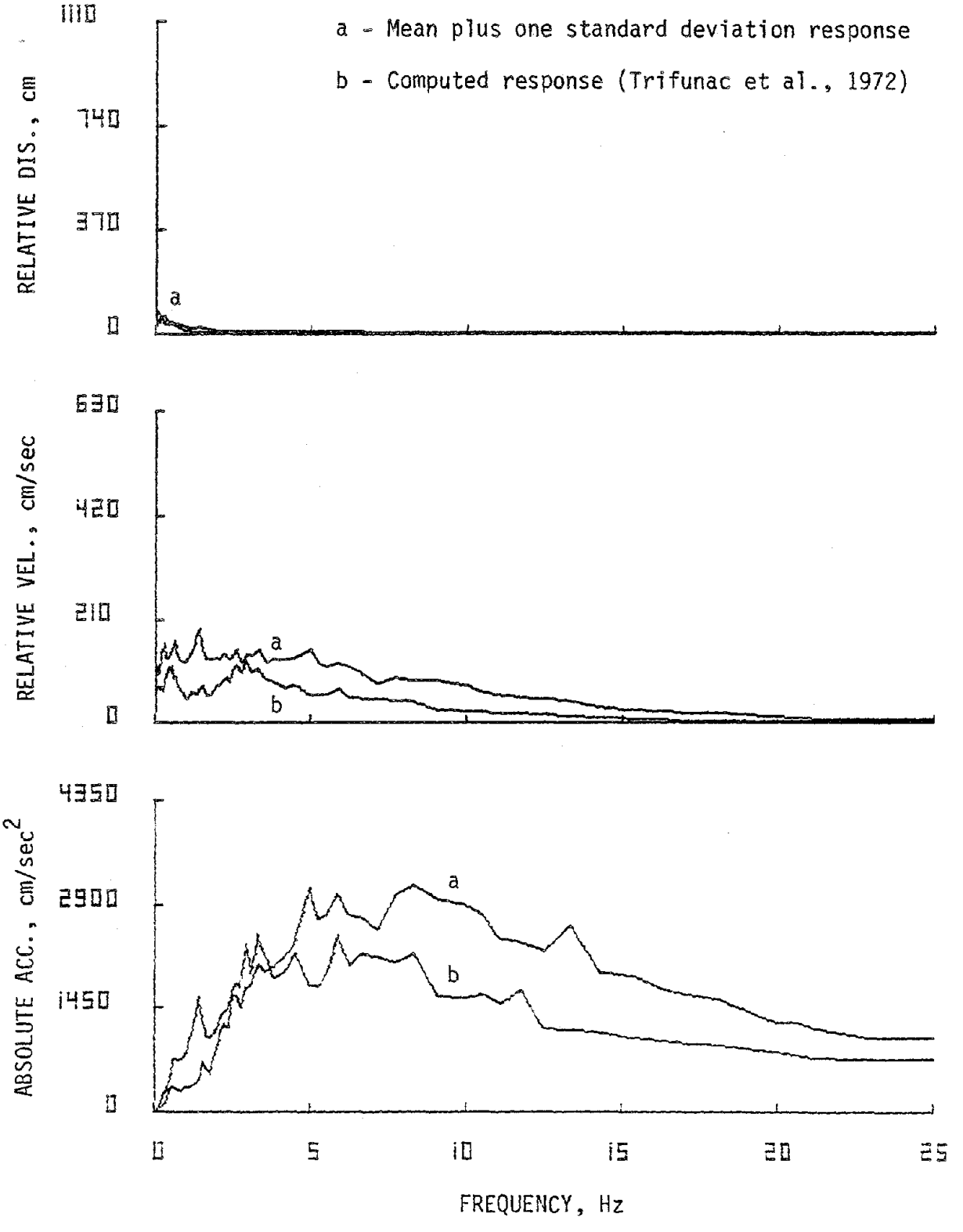

FIG. 5.58. Comparison of mean plus one standard deviation response (hard) and computed response for 2 percent damping, Pacoima Dam, 1971--vertical.

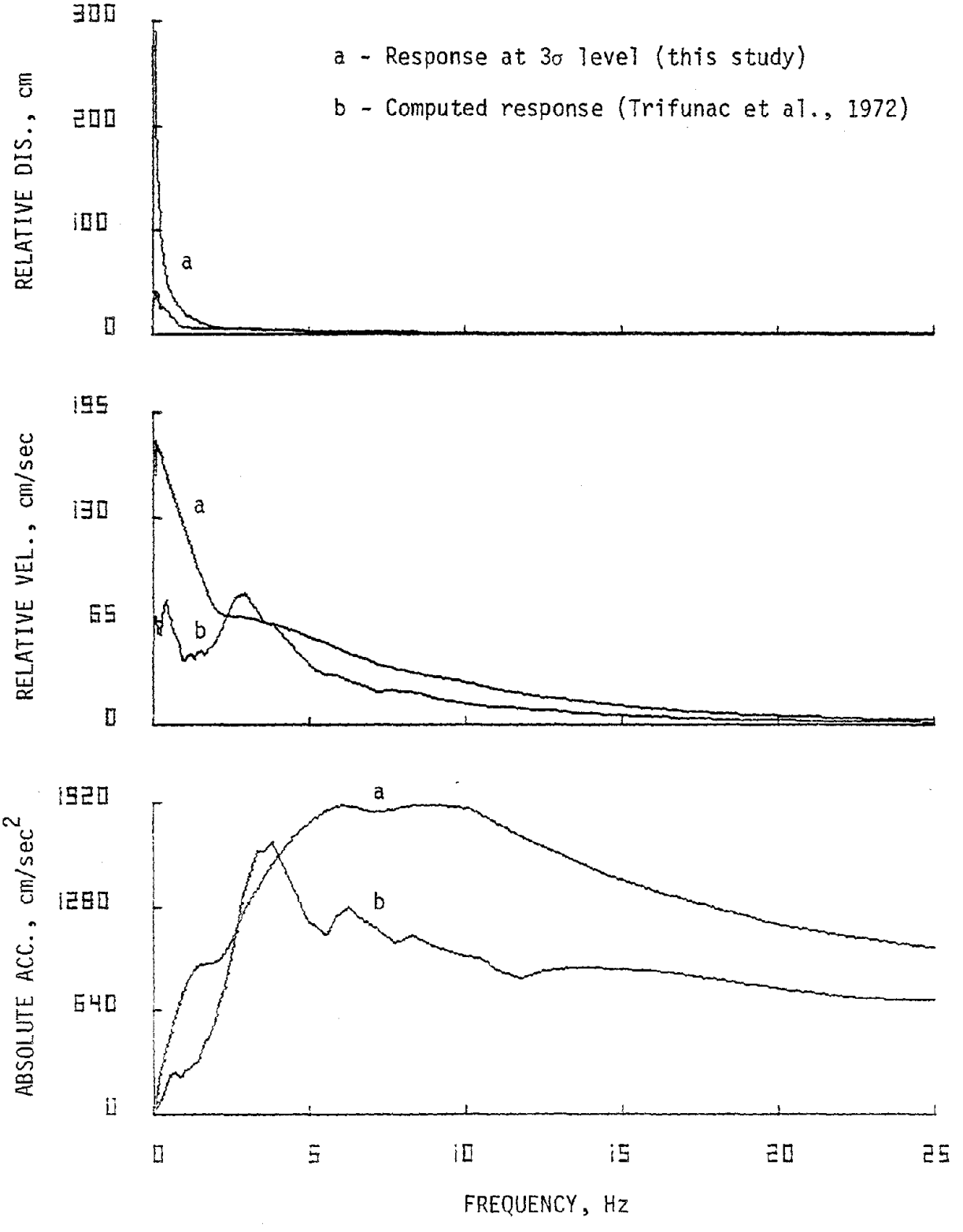

FIG. 5.59. Comparison of predicted response (hard) and computed response for 10 percent damping, Pacoima Dam, 1971--vertical.

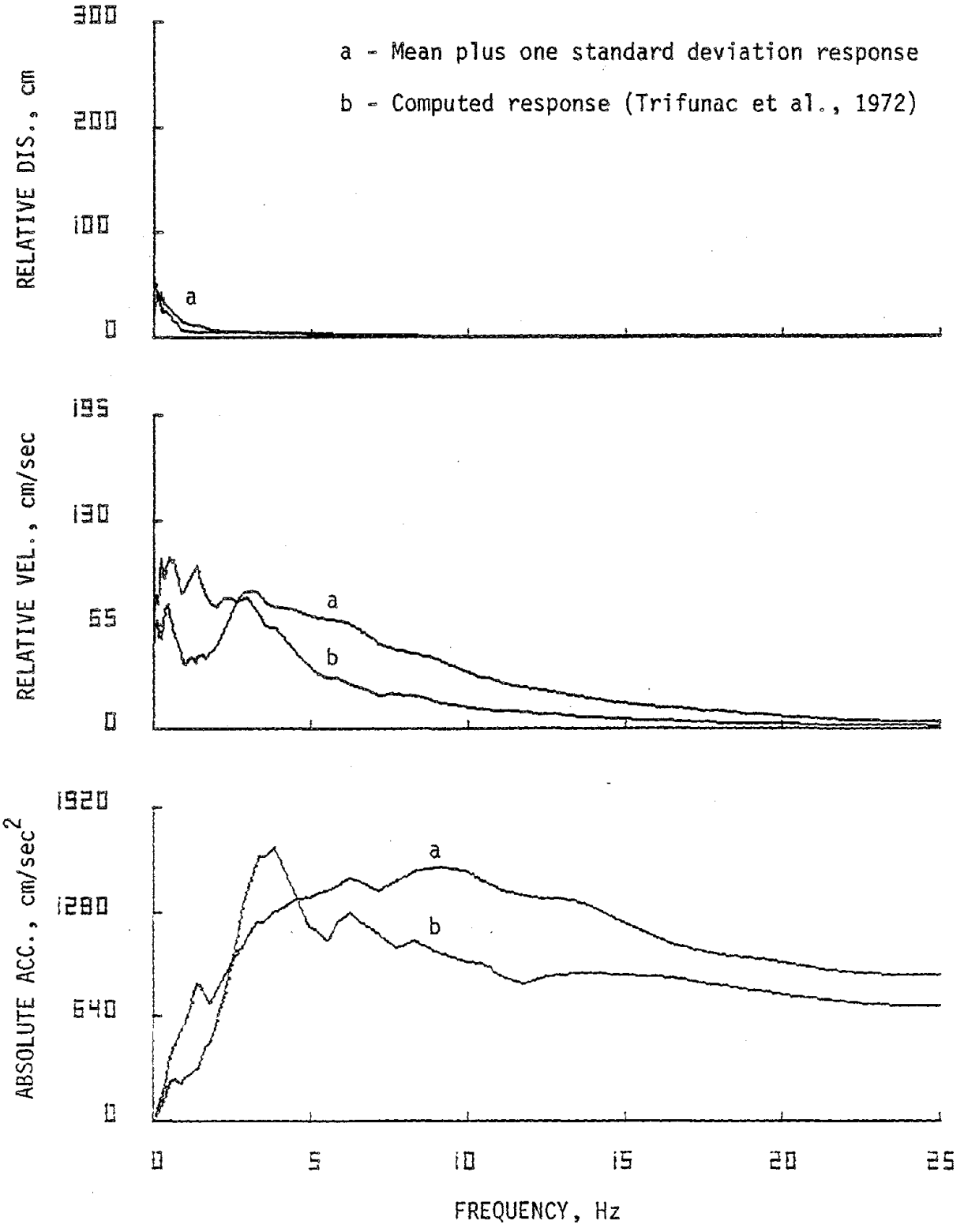

FIG. 5.60. Comparison of mean plus one standard deviation response (hard) and computed response for 10 percent damping, Pacoima Dam, 1971--vertical.

CHAPTER 6

SUMMARY AND CONCLUSIONS

6.1 SUMMARY

A statistical study is used to estimate a time-dependent power spectral density of recorded earthquake accelerograms. The study assumes that the strong motion segments of accelerograms form a locally stationary random process whose members exhibit a time-invariant frequency structure. In Chapter 3, in a pilot study, the validity of this assumption is examined. The pilot study shows that by selecting the strong motion segment of the record, the power spectral density estimates of the subsegments of that record exhibit shapes and frequency structures similar to that of the strong motion segment of the record itself. Using the strong motion segment of the records a time-dependent power spectral density is estimated which consists of three parts: a normalized power spectral density which describes the frequency structure of the ensemble and remains the same for the subsegments of records considered; a time-dependent scale factor which describes the variation of local mean square value; and finally the mean square value itself. Normalized power spectral densities and scale factors for horizontal and vertical components of accelerograms recorded on soft, intermediate and hard geology are presented in Chapter 5. Correlation of RMS values with a variable reflecting the four most commonly used design parameters, peak ground acceleration, earthquake magnitude, epicentral distance, and

the duration of strong motion are obtained and presented in Chapter 4. Such correlations will make it possible to estimate a power spectral density for a specific site and earthquake parameters. Correlations were obtained for several classifications of records; however, no significant changes on the correlation coefficients were observed due to site geology or component classification. The estimated power spectral densities are used to predict the response of a single degree of freedom system at several sites and the results are compared with spectral relative displacement, relative velocity, and absolute acceleration computed directly from the records.

The results of the study support the viability of using the random vibration theory in earthquake resistant design of structures. There are two features that make this study attractive for seismic analysis and design. First, the results can be used to predict the response of a system for a given probability that it may exceed a certain level, and second, the prediction incorporates site geology as well as earthquake magnitude, peak ground acceleration, epicentral distance and the duration of strong motion. Finally, the findings can be used in the study of artificially generated earthquake motion.

6.2 RECOMMENDATIONS FOR FURTHER STUDY

The following is a list of possible topics for future studies:

1. Inclusion of site geology in predicting the RMS values. Although correlations between RMS and peak acceleration, earthquake magnitude, epicentral distance and duration of strong motion are presented for different geological classifications in this study, the possibility

of obtaining a single correlation which would include the site geology should be investigated.

2. Expressions for power spectral densities and scale factors. Analytical expressions should be developed for power spectral densities and scale factors presented in Figs. 5.1-5.12. Such expressions together with the regression equations in Chapter 4 for estimating RMS values would be useful in seismic analysis and design of structures and equipments.

3. Generation of acceleration-time history from the power spectral densities. A procedure which is widely used in seismic analysis of complex structures is to subject the structure to an acceleration-time history to compute its response. Scaled acceleration-time histories from various seismic events as well as acceleration-time histories generated from design response spectra have been used for this purpose. Acceleration-time histories generated from the power spectral densities would be valuable to design engineers and should be considered.

4. Use of the entire acceleration-time history to estimate power spectral density. In this study we used the strong motion part of the records to obtain the power spectral densities. An extension of this study would be to consider the entire record length and estimate the power spectral density in which both the magnitude and frequency structure are time-dependent. One possible approach could be to estimate power spectral densities for different portions of the records.

REFERENCES

Amin, M. and H. -S. Ang (1968). Nonstationary stochastic model of earthquake motions, J. Eng. Mech. Div., ASCE 94, 559-583.

Amin, M., H. S. Tsao, and H. -S. Ang (1969). Significance of nonstationarity of earthquake motions, Proc. World Conf. Earthquake Eng. A-1, 4th, Santiago, Chile, 97-114.

Applied Technology Council, National Bureau of Standards, and the National Science Foundation (1978). Tentative provisions for the development of seismic regulations for buildings, ATC Publication ATC-3-06, NBS Special Publication 510, NSF Publication 78-8.

Barstein, M. F. (1960). Application of probability methods for design-the effect of seismic forces on engineering structures, Proc. World Conf. Earthquake Eng. A-2, 2nd, Tokyo & Kyoto, Japan, 1467-1482.

Bendat, J. S. and A. G. Piersol (1971). Random Data: Analysis and Measurement Procedures, Wiley-Interscience, New York.

Biot, M. A. (1941). A mechanical analyzer for prediction of earthquake stresses, Bull. Seism. Soc. Am. 31, 151-171.

Biot, M. A. (1942). Analytical and experimental methods in engineering seismology, Proc. Am. Soc. Civil Eng. 68, 49-69.

Blume, J. A., R. L. Sharpe and J. S. Dalal (1972). Recommendations for shape of earthquake response spectra, John A. Blume & Associates, San Francisco, California (AEC Report WASH-1254).

Bogdanoff, J. L., J. E. Goldberg, and M. C. Bernard (1961). Response of a single structure to a random earthquake-like disturbance, Bull. Seism. Soc. Am. 51, 293-310.

Bolotin, V. V. (1960). Statistical theory of the seismic design of structures, Proc. World Conf. Earthquake Eng. A-2, 2nd, Tokyo & Kyoto, Japan, 1365-1374.

Bolt, B. A. (1974). Duration of strong motion, Proc. World Conf. Earthquake Eng. 30, 4th, Santiago, Chile, 1304-1315.

Burridge, R., and L. Knopoff (1976). Model and theoretical seismicity, Bull. Seism. Soc. Am. 57, 341-371.

Bycroft, G. N. (1960). White noise representation of earthquakes, J. Eng. Mech. Div., ASCE 86, 1-16.

Caughy, T. K. and H. J. Stumpf (1961). Transient response of a dynamic system under excitation, J. Appl. Mech. 28, 563-566.

Clough, R. W. (1970). Earthquake response of structures, Chapter XII in Earthquake Engineering, R. L. Wiegel, Editor, Prentice-Hall, Englewood Cliffs, N. J.

Clough, R. W. and J. Penzien (1975). Dynamics of Structures, McGraw-Hill, New York.

Chopra, A. K. and O. A. Lopes (1979). Evaluation of simulated ground motion for predicting elastic response of long period structures and inelastic response of structures, Earthquake Eng. Struct. Dynamics 7, 383-402.

Cornell, C. A. (1960). Stochastic process model in structural engineering, Technical Report 34, Department of Civil Engineering, Stanford University, Stanford, California.

Crandall, S. H. and W. D. Mark (1963). Random Vibration in Mechanical Systems, Academic Press, New York.

DeBoor, C. (1978). A Practical Guide to Spline, Springer-Verlag, New York.

Esteva, L. (1976). Seismicity, Chapter 6 in Seismic Risk and Engineering Decision, C. Lomnitz and E. Rosenblueth, Editors, Elsevier Scientific Publishing Company, New York, New York.

Goto, H. and K. Toki (1969). Structural response to nonstationary random excitation, Proc. World Conf. Earthquake Eng. A-1, 4th, Santiago, Chile, 130-144.

Hammond, J. K. (1968). On the response of single and multidegree of freedom systems to non-stationary random excitations, J. Sound & Vibration 7, 393-416.

Housner, G. W. (1941). An investigation of the effects of earthquakes on buildings, Ph.D. Thesis, California Institute of Technology, Pasadena.

Housner, G. W. (1947). Characteristics of strong motion earthquakes, Bull. Seism. Soc. Am. 37, 19-37.

Housner, G. W. (1955). Properties of strong motion earthquakes, Bull. Seism. Soc. Am. 45, 197-218.

Housner, G. W. (1956). Limit design of structures to resist earthquakes, Proc. World Conf. Earthquake Eng., 1st, San Francisco, California.

Housner, G. W. (1959). Behavior of structure during earthquakes, J. Eng. Mech. Div., ASCE 85, 109-129.

Housner, G. W. and P. C. Jennings (1964). Generation of artificial earthquakes, J. Eng. Mech. Div., ASCE 90, 113-150.

Housner, G. W. (1970a). Strong ground motion, Chapter IV in Earthquake Engineering, R. L. Wiegel, Editor, Prentice-Hall, Englewood Cliffs, N. J.

Housner, G. W. (1970b). Design spectrum, Chapter V in Earthquake Engineering, R. L. Wiegel, Editor, Prentice-Hall, Englewood Cliffs, N. J.

Hudson, D. E. (Ed.) (1971). Strong motion instrumental data on the San Fernando earthquake of Feb. 9, 1971, Earthquake Engineering Research Laboratory, California Institute of Technology, Pasadena.

Hudson, D. E., A. G. Brady, M. D. Trifunac and A. Vijayaraghavan (1971-1975). Analysis of strong motion earthquake accelerograms--digitized and plotted data, Vol. II: Corrected Accelerograms and Integrated Ground Velocity and Displacement Curves, Parts A through Y, Earthquake Engineering Research Laboratory, California Institute of Technology, Pasadena.

Hsu, T. I. and M. C. Bernard (1978). A random process for earthquake simulation, Earthquake Eng. Struct. Dynamics 6, 347-363.

Hurty, W. C. and M. F. Rubinstein (1964). Dynamics of Structures, Prentice-Hall, Englewood Cliffs, N.J.

Iyengar, R. N. and K. T. Iyengar (1969). A nonstationary random process model for earthquake accelerogram, Bull. Seism. Soc. Am. 59, 1163-1188.

Iyengar, R. N. and P. N. Rao (1979). Generation of spectrum compatible accelerograms, Earthquake Eng. Struct. Dynamics 7, 253-263.

Jennings, P. C., G. W. Housner and N. C. Tsai (1968). Simulated earthquake motions, Earthquake Engineering Research Laboratory, EERL 68-10, California Institute of Technology, Pasadena.

Jennings, P. C., G. W. Housner and N. C. Tsai (1969). Simulated earthquake motion for design purposes, Proc. World Conf. Earthquake Eng. A-1, 4th, Santiago, Chile, 145-160.

Kanai, K. (1957). Semi-empirical formula for the seismic characteristics of the ground, Bull. Earthquake Research Institute 35, University of Tokyo, Tokyo, Japan.

Kubo, T. and J. Penzien (1976). Time and frequency domain analysis of three-dimensional ground motions, San Fernando earthquake, Earthquake Engineering Research Center, EERC 76-6, University of California, Berkeley.

Lin, Y. K. (1967). Probability Theory of Structural Dynamics, McGraw-Hill, New York.

Liu, S. C. (1970). Evolutionary power spectral density of strong motion earthquakes, Bull. Seism. Soc. Am. 60, 891-900.

McCann, Jr., W. M. and H. C. Shah (1979). Determining strong-motion duration of earthquakes, Bull. Seism. Soc. Am. 69, 1253-1265.

McCann, Jr., W. M. (1980). RMS acceleration and duration of strong ground motion, Department of Civil Engineering, Report 46, Stanford University, Stanford, California.

McGuire, R. K. (1974). Seismic structural response risk analysis incorporating peak response regressions on earthquake magnitude and distance, Structures Publication No. 399, Department of Civil Engineering, Massachusetts Institute of Technology, Cambridge, Massachusetts.

McGuire, R. K. (1978). A simple model for estimating fourier amplitude spectra of horizontal ground acceleration, Bull. Seism. Soc. Am. 68, 803-822.

McGuire, R. K. and T. C. Hanks (1980). RMS accelerations and spectral amplitudes of strong ground motion during the San Fernando, California, earthquake, Bull. Seism. Soc. Am. 70, 1907-1919.

Mohraz, B., W. J. Hall and N. M. Newmark (1972). Study of vertical and horizontal earthquake spectra, Nathan M. Newmark Consulting Engineering Services, Urbana, Illinois (AEC Report Wash-1255).

Mohraz, B. (1976). A study of earthquake response spectra for different geological conditions, Bull. Seism. Soc. Am. 66, 915-935.

Mohraz, B. (1978a). Comments on earthquake response spectra, Nuclear Eng. Design 45, No. 2.

Mohraz, B. (1978b). Influences of the magnitude of earthquakes and the duration of strong motion on earthquake response spectra, Proc. Central American Conf. Earthquake Eng., San Salvador.

Murakami, M. and J. Penzien (1975). Nonlinear response spectra for probabilistic seismic design and damage assessment of reinforced concrete structures, Earthquake Engineering Research Center, EERC 75-38, University of California, Berkeley.

Newmark, N. M., J. A. Blume and K. K. Kapur (1973). Seismic design criteria for nuclear power plants, J. Power Div., ASCE 99, 287-303.

Page, H. C. (1952). Instantaneous power spectra, J. Appl. Physics 23, 103-106.

Penzien, J. (1970). Application of random vibration theory, Chapter XIII in Earthquake Engineering, R. L. Wiegel, Editor, Prentice-Hall, Englewood Cliffs, N. J.

Power, D. V. (1969). Analysis of earth motions and seismic sources by power spectral density, Bull. Seism. Soc. Am. 59, 1071-1091.

Priestley, M. B. (1965). Evolutionary spectra and non-stationary processes. Royal Statistical Society Journal B, 27, No. 2, 204-237.

Priestly, M. B. (1967). Power spectral analysis of non-stationary random process, J. of Sound & Vibration 6, 86-97.

Ravara, A. (1965). Spectral analysis of seismic actions, Proc. World Conf. Earthquake Eng. A-1, 3rd, Auckland & Wellington, New Zealand, III-195-204.

Rosenblueth, E. and J. Bustamente (1962). Distribution of structure response to earthquakes, J. Eng. Mech. Div., ASCE 88, 75-106.

Ruiz, P. and J. Penzien (1969). Probabilistic study of the behavior of structure during earthquakes, Earthquake Engineering Research Center, EERC 69-3, University of California, Berkeley.

Sargoni, G. R. and G. C. Hart (1972). Nonstationary analysis and simulation of earthquake ground motion, Technical Report UCLA-ENG-7238, Mechanics & Structures Department, School of Engineering and Applied Science, University of California, Los Angeles.

Seed, H. B., C. Ugas and J. Lysmer (1976). Site-dependent spectra for earthquake resistance design, Bull. Seism. Soc. Am. 66, 221, 243

Shinozuka, M. and Y. Sato (1967). Simulation of nonstationary random process, J. Eng. Mech. Div., ASCE 93, 11-40.

Silverman, R. A. (1957). Locally stationary random process, IRE Transaction on Information Theory, 182-187.

Tajimi, H. (1960). A statistical method of determining the maximum response of a building structure during an earthquake, Proc. World Conf. Earthquake Eng. A-2, 2nd, Tokyo and Kyoto, Japan.

Thomson, W. T. (1959). Spectral aspect of earthquakes, Bull. Seism. Soc. Am. 49, 91-98.

Thomson, W. T. (1972). Theory of Vibration with Application, Prentice-Hall, Englewood Cliffs, N. J.

Trifunac, M. D. (1971a). Response envelope spectrum and interpretation of strong earthquake ground motion, Bull. Seism. Soc. Am. 61, 343-356.

Trifunac, M. D. (1971b). A method for synthesizing realistic strong ground motion, Bull. Seism. Soc. Am. 61, 1739-1753.

Trifunac, M. D., A. G. Brady and D. E. Hudson (1972-1975). Analysis of strong-motion earthquake accelerograms, Vol. III: Response Spectra, Parts A through Y, Earthquake Engineering Research Laboratory, California Institute of Technology, Pasadena.

Trifunac, M. D. and A. G. Brady (1975a). On the correlation of seismic intensity scales with the peak of recorded strong motion, Bull. Seism. Soc. Am. 65, 139-162.

Trifunac, M. D. and A. G. Brady (1975b). A study of the duration of strong earthquake ground motion, Bull. Seism. Soc. Am. 65, 581-626.

Trifunac, M. D. (1976). Preliminary empirical model for scaling fourier amplitude spectra of strong ground acceleration in terms of earthquake magnitude, source-to-station distance, and recorded site conditions, Bull. Seism. Soc. Am. 66, 1343-1373.

Walpal, R. E. and R. H. Myers (1978). Probability and Statistics for Engineers and Scientists, Macmillan Publishing Co., New York.

Wong, H. L. and M. D. Trifunac (1979). Generation of artificial strong motion accelerograms, Earthquake Eng. Struct. Dynamics 7, 509-527.